Cell wall synthesis in *Bacillus subtilis*

Jad Sassine

Centre for Bacterial Cell Biology

Institute for Cell and Molecular Biosciences

Thesis submitted for the degree of Doctor of Philosophy

Newcastle University

December 2016

Abstract

The peptidoglycan (PG) layer is responsible for maintaining cell shape and permitting cell division in almost all bacteria. Made of glycan chains connected by short peptides, PG forms a net-like structure surrounding the cytoplasmic membrane. Membrane-anchored PG synthases, called penicillin-binding proteins (PBPs), synthesize PG during cell growth and division by utilising the precursor lipid II but the molecular mechanism of these processes in *Bacillus subtilis* are largely unknown. The genetic and phenotypic analysis of *B. subtilis* has shown that PG synthesis and cell division are modulated by components of the central carbon metabolism (Weart *et al.,* 2007). In particular, UgtP, which synthesises the glucolipid precursor for the lipoteichoic acid, has been suggested to function as a metabolic sensor governing cell size. However, the mechanism by which UgtP impacts cell wall synthesis remained unknown.

Here we have constructed different *B. subtilis* strains with deletions in cell wall synthesis and/or carbon metabolism genes. Cells lacking the LTA precursor glucolipid grew with similar rate as wild type cells but were shorter and wider. The overexpression of *ugtP* caused filamentation, supporting the hypothesis that UgtP inhibits FtsZ polymerization (Weart *et al.,* 2007). The *ugtP* mutant had increased level of several PG precursors and mild alterations in PG composition suggesting an increased DL-endopeptidase activity. Combining *ugtP* deletion/depletion with deletions with several cell wall genes resulted in morphological effects. The deletion of the PBP1 gene and simultaneous depletion of *ugtP* resulted in thin and bent cells. The double deletion of *ugtP* and *lytE*, a hydrolase important for cell elongation, produced shorter bent cells with severe shape defects. These results suggest that the function of UgtP contributes to balanced cell wall synthesis and hydrolysis.

We also characterised several crucial cell wall enzymes. The depletion of the essential PBP2B caused cell division defects followed by lysis. Interestingly, cells expressing a catalytically inactive PBP2B were viable, but they required functional PBP3, a homologue of PBP2B that is dispensable in wild-type cells. PBP3 showed enhanced septal localisation in a strain with inactive PBP2B, but this strain produced aberrant septa. Biochemical assays were used to characterize for the first time the activities and interactions of PBP1, PBP2B, and PBP3. Novel interactions between these PBPs and with the lytic transglycosylase homologue YrrL were detected.

In summary, this work contributes to our understanding of the PG synthesis during cell division.

Acknowledgements

I would like to acknowledge Newcastle University, the Centre for Bacterial Cell Biology which is part of the Institute for Cell and Molecular Biosciences. I would like to thank Marie Skłodowska-Curie actions and the European Commission for the generous funding for my work during the last three years. Most of all I would like to thank my supervisors, Waldemar Vollmer and Richard Daniel for their excellent supervision, guidance and for being available and helpful whenever I faced a problem. I would like also to thank them for their support throughout my PhD, which I am very grateful for, and for allowing me to learn and improve to become a better scientist. It has been a great experience to work with my colleagues and friends. A big thank you for Alexander Egan who has helped me the most to acquire lab skills in addition to all the constructive discussions. It has been an honour to work with you. Big thanks for Master Jacob for helping me with the HPLC and the PG analysis. Daniela, our life in the lab wouldn't be the same without you, so thank you for being a great lab mother. I would like to thank Aurelie Guyet for her advice about cloning and for providing me with strains for my work. I would like to show appreciation to Manuel, Victor, Katherina, Christian, Hamish and Karzan for being great friends and colleagues and for any help you've showed me the last three years. I was lucky to be part of the CBCB community, where I was surrounded by supportive and loving friends and colleagues, making the centre an admirable place to work in.

I would like to express gratitude for Michael Lalk for hosting me in his lab in Greifswald, Germany, during which I gained knowledge in Metabolomics. I am very grateful for Joanna Sousa for her kindness and care, for being a great friend, and for teaching me everything I know about metabolomics. It has been a great experience!

I would like to thank Rick Lewis, Vincent Rao and Eefjan Breukink for their assistance in collaborative projects, which enhanced the significance of my work.

At last, I am most grateful for my father Fouad and my mother May, for your trust and continuous support during my career. Thank you for believing in me and this story wouldn't be the same without your aid. Carla, thank you for the love and care that kept me sane throughout.

Table of contents

Abbreviations

ABC	ATP binding cassette
Amp	Ampicillin
ATP	Adenosine-5'- triphosphate
BSA	Bovine serum albumin
CAA	casamino acids
cam	Chloranphenicol
CDP-DG	Cystidine diphosphate diacylglycerol
CPM	Counts per minute
C-terminal	Carboxy terminal
Da/KDa	Daltons/ Kilodaltons
DAPI	4,6-diamidino-2-phenylindole
dH_2O	deionised water
D-iGlu	D-isoglutamic acid
DNA	Deoxyribonucleic acid
DNase	Deoxyribonuclease
ECL	Enhanced chemiluminesence
EDTA	Ethylenediaminetetraacetic acid,
Erm	Erythromycin
et al,.	*et alii* (and others)
g	Acceleration due to gravity
GFP	Green fluorescent protein
Glc*N*Ac	*N*-acetylglucosamine
GTase	Glycosyltransferase
h	Hour
HEPES	2-[4-(2-hydroxyethyl)piperazin-1-yl]ethanesulfonic acid
His-	Hexahistidine tag (N-teminal)
HPLC	High pressure liquid chromatography
IEX	Ion exchange chromatography
IMAC	Immobilised metal affinity chromatography
IPTG	Isopropyl β-D-1-thiogalactopyranoside
IWZ	Inner wall zone
Kan	Kanamycin
LB	Luria Britani
LTA	Lipoteichoic acid
meso-Dap	*meso*-diaminopimelic acid
min	Minute
MM	Minimal medium
Mur*N*Ac	*N*-acetylmuramic acid
MW	Molecular weight
NA	Nutrient agar

Ni-NTA	$Nickel^{2+}$ – nitrilotriacetic acid
N-terminal	Amino-terminus
OWZ	Outer wall zone
PAB	Penassay broth
PAGE	Polyacrylamide gel electrophoresis
PGP	Phosphatidyl glycerol phosphate
PMSF	Phenylmethylsulfonyl fluoride
PBP	Penicillin-binding protein
PBS	Phosphate buffed saline solution
PCR	Polymerase chain reaction
PG	Peptidoglycan
RNA	Ribonucleic acid
rpm	Revolutions per minute
RT	Room temperature
SDS	Sodium dodecyl sulfate
SEC	Size exclusion chromatography
SMM	Spizizen minimal medium
Spc	Spectinomycin
SPR	Surface plasmon resonance
TAE	Tris-acetate-EDTA
TE	Tris-EDTA
TPase	transpeptidase
Tris	tris(hydroxymethyl)aminomethane
UV	Ultraviolet
WTA	Wall teichoic acid
w/v	Weight per volume
Xyl	Xylose
UDP	Uridine diphosphate

Index of Figures and tables

1 Introduction

1.1 *Bacillus subtilis* growth and morphology

Hans Christian Gram differentiated bacteria into Gram-positive and Gram-negative species using the Gram stain (Gram, 1884). In Gram-negative species, like proteobacteria, the cytoplasmic membrane is surrounded by a thin peptidoglycan (PG) of 3 – 6 nm thickness and an outer membrane. In Gram-positive species, such as firmicutes, the cell wall consists of a thick 10 – 60 nm PG with anionic polymers such as wall teichoic acid (WTA) and lipoteichoic acid (LTA) (Section 1.4). During the cell cycle, rod-shaped cells grow and elongate until they double in length and then divide forming two identical daughter cells. In parallel, the genomic DNA is duplicated and the sister chromosomes are segregated before the cell division machinery starts assembling.

Bacillus subtilis is a rod-shaped Gram-positive bacterium with the ability to form endospores allowing the microorganism to tolerate extreme environmental conditions (Errington, 2003). It is a non-pathogenic organism and is widely used as a model to study the growth and morphology of Gram-positive bacteria. *B. subtilis* cells sporulate by dividing asymmetrically, near one pole, resulting in a smaller cell called the forespore and a larger mother cell (Higgins and Dworkin, 2012). The cell shape of the bacterium is maintained by the cell wall surrounding the cytoplasmic membrane and is composed of major and minor components. The major components are the PG, the WTA and the LTA. The PG is essential to protect the cell from bursting due to the turgor while all three polymers are crucial for cell shape. The minor component is the minor teichoic acid and the absence of the latter has no effect on cell morphology or growth under laboratory conditions (Estrela *et al.*,1991). Maintaining structural integrity of the PG is crucial for cell survival during growth, thus understanding the process of PG synthesis during cell elongation and division is a fundamental but largely unanswered question in microbiology.

The PG in *B. subtilis* is a three dimensional mesh-like molecule referred to as the sacculus that is continuously synthesised, modified and hydrolysed to maintain the integrity of the cell and allow growth (Hayhurst *et al.,* 2008). The importance of the PG is exemplified by the variety of antibiotics, such as β-lactams and glycopeptides, which target its synthesis to kill the cell. In γ-proteobacteria, the PG is mostly single layered hence the tight coordination between the synthesis and hydrolysis of the PG. In Gram-positive bacteria the PG is multilayered, the mechanisms of PG synthesis is mostly unknown with limited information about the structure of the PG or the protein complexes involved in it synthesis.

On a different note, recent work in Petra Levin's lab showed that the size of the cell is coordinated by the presence of nutrients in the cytoplasm (Weart *et al.,* 2007). The UDP-glucose diacylglycerol glucosyltransferase, UgtP, was suggested to be a metabolic sensor that controls the timing of cell division by inhibiting Z-ring formation. However, the absence of UgtP causes wider cells providing questions whether UgtP has a more direct effect on cell wall synthesis.

1.2 Peptidoglycan synthesis

1.2.1 lipid II synthesis

PG precursor synthesis starts in the cytoplasm with the synthesis of the nucleotide precursors UDP-N-acetylglucosamine (Glc*N*Ac) and UDP-N-acetylmuramic acid (Mur*N*Ac) (Figure 1.1). Successive addition of L-Ala, D-Glu, diaminopimelic acid (DAP) and the dipeptide D-Ala-D-Ala to UDP-Mur*N*Ac is catalysed by four ligases MurC, MurD MurE and MurF, respectively (Barreteau *et al.,* 2008). Afterwards, the Mur*N*Ac-pentapeptide is transferred onto the membrane bound undecaprenyl phosphate molecule by MraY to form lipid I (Bouhss *et al.,* 2008). GlcNAc is added to lipid I by MurG forming lipid II, which is mostly amidated on the ε-carboxyl group of meso-A_2pm, followed by flipping across the cytoplasmic membrane by three transmembrane proteins RodA, FtsW and SpoVE (Miyao *et al.,* 1992). RodA is required for rod-shape during elongation by transporting cell wall precursors at the side wall, while FtsW presumably mediates lipid II flipping at the divisome (Henriques *et al.,*1998; Mohammadi *et al.,* 2011). RodA has been described recently to have a GTase activity (See section 1.3.4) (Meeske *et al.,*2016). SpoVE is 39.8% similar to FtsW, localises at the membrane surface of the emerging spore and is required for the synthesis of the spore PG (Ikeda *et al.,* 1989). It was recently published that the lipid II flippase in *E. coli* is MurJ (Ruiz, 2008; Sham *et al.,* 2014). A BLASTp-based analysis identified four MurJ homologs in *B. subtilis* called YtgP, SpoVB, YkvU and YabM (Fay and Dworkin, 2009). While MurJ was found to be essential for *E. coli* growth, the absence of the four homologs simultaneously in *B. subtilis* did not affect either the growth or the morphology of cells (Fay and Dworkin, 2009).

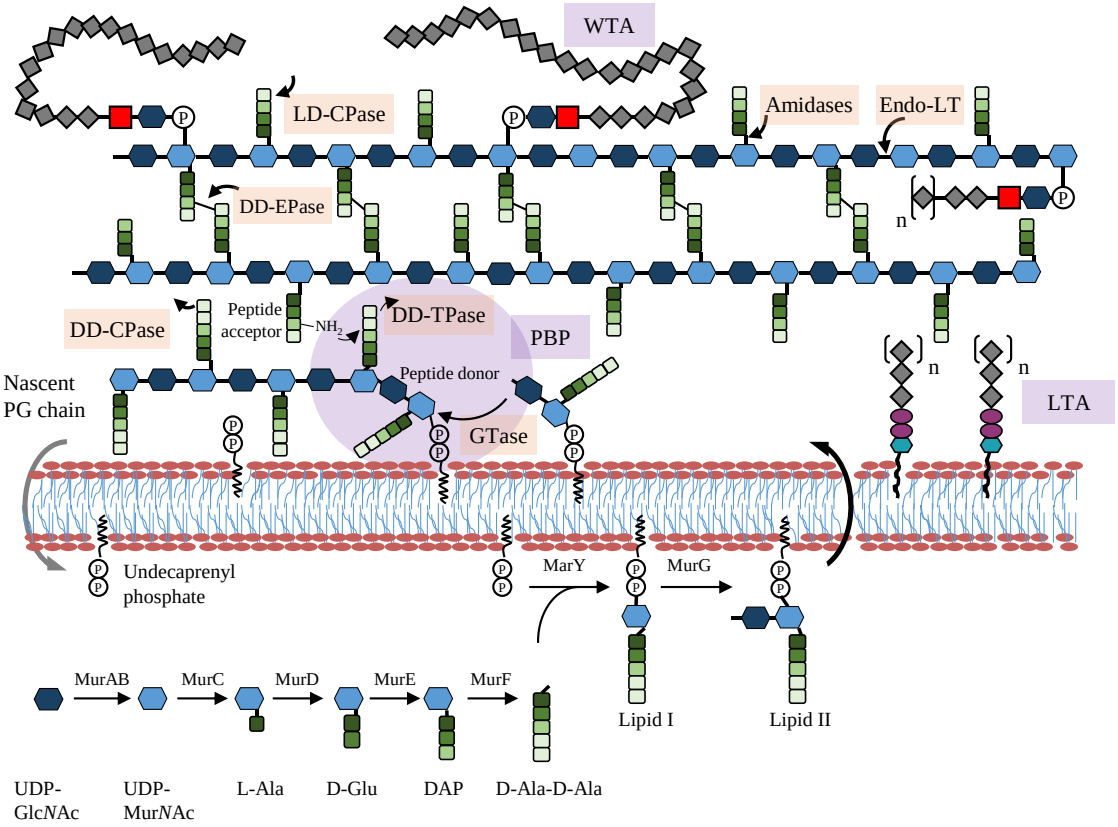

Figure 1.1 Peptidoglycan biosynthesis and components of the cell wall

Products of the *mur* operon, MraY and MurG catalyse the synthesis of the PG precursor lipid II from sugar nucleotide UDP-Glc*N*Ac in the cytoplasm. Lipid II is then flipped across the membrane and delivered to penicillin-binding proteins (PBPs). Lipid II is polymerised into glycan chains by GTase reaction and peptides are crosslinked by TPase reaction. Hydrolases modify the PG by cleaving various types of bonds. WTA is covalently bound to the Mur*N*Ac sugar. LTA is bound to the cell membrane via a diacylglycerol anchor. Both the WTA and LTA have the same glycerol-phosphate repeating unit. CPase, carboxypeptidase; Endo-LT, endo-lytic transglycosylase; EPase, endopeptidase; TPase, transpeptidase; GTase, glycosyltransferase.

1.2.2 Growth of the sacculus

The synthesis of peptidoglycan occurs extracellularly, by polymerizing the flipped lipid II into nascent glycan chains by a glycosyltransferase (GTase) reaction performed by monofunctional or bifunctional PG synthases (See section 1.3.1) (Barrett *et al.*,2007; Lovering *et al.*,2012). Recently, Meeske *et al.*, (2016) suggested that RodA from *Bacillus subtilis* is a PG polymerase (Section 1.3.4). The GTase reaction involves the formation of a β-1,4-glycosidic bond resulting in the release of the undecaprenyl pyrophosphate moiety (Van Heijenoort, 2001). In *B. subtilis*, as in Gram-negative bacteria, the glycan polymer terminates with a 1,6-anhydroMur*N*Ac residue formed by an intramolecular ring from C1 to C6 (Burmant and Park, 1983; Vollmer *et*

al., 2008). The peptide crosslink is achieved by the formation of an isopeptide bond between the fourth amino acid (D-Ala) of one stem with the third (*meso*-A_2pm-NH_2) of the other via a transpeptidase (TPase) reaction (Popham and Young, 2003). The TPase reaction is carried out by bi-functional (class A PBPs) or mono-functional penicillin-binding proteins (class B PBPs) to produce the net-like PG structure.

1.2.3 Structure of the sacculus

Understanding the architecture of the peptidoglycan is important to determine the mechanisms underlying sacculus growth during elongation and division. A few proposed models describe the possible structure for *B. subtilis* PG. First, the "scaffold" model in which the glycan strands run perpendicularly to the cytoplasmic membrane and the peptide in crosslinks run parallel to the cell long axis (Dmitriev *et al.*, 1999, 2005). Second, the "layered" topology where the glycan strands and the peptide crosslinks run horizontal to the membrane (Vollmer and Seligman, 2010). The development of the microscopic techniques in the last decade allowed a better visualization of the cell wall which helped in further characterising the architecture of the PG. The use of the cryo-transmission electron microscopy showed that the *B. subtilis* cell wall is 45 to 55 nm thick with two regions with distinct densities (Matias and Beveridge, 2005). The inner-wall zone (IWZ) was compared to the periplasmic space in Gram-negative bacteria and consisted of a low density zone with 22 nm thickness surrounding the plasma membrane. The outer-wall zone (OWZ) was suggested to contain the actual cell wall and had a thickness of up to 33 nm. The use of atomic force microscopy (AFM) supported a helical structure model where a number of glycan chains are polymerized and cross-linked to form a peptidoglycan "rope" (Hayhurst *et al.,* 2008). Subsequently, this rope acquires a helical structure with a 50 nm width, which is then crosslinked with two existing ropes and all are roughly oriented perpendicularly to the long axis of the cell. However, work done in Jensen's lab using electron cryotomography contradicted the helical model and proposed a uniformly dense cell wall model with a circumferentially oriented glycan strands (Beeby *et al.*, 2013). The IWZ observed previously was also contradicted by Beeby *et al.* and was suggested to be an artefact caused by the use of cryoprotectants. Beeby and colleagues also showed that the denaturation of PG using urea altered the secondary structure of linking peptides resulting in an increase in the length, but not the width, of the sacculus. This result is consistent with a circumferential model where the glycan strands are oriented perpendicularly to the long axis of the cell (Beeby *et al.,* 2013). Thus, despite significant progress made recently with the characterization of PG structure, many

components of the cell wall, such as the teichoic acids, haven't been considered or described in these models.

1.2.4 Role of the bacterial cytoskeleton

B. subtilis has three actin homologues, MreB, Mbl and MreBH, controlling its rod-shape (Section 1.3.4) (Jones *et al.*, 2001). The three homologues colocalised in a helical structure below the cytoplasmic membrane and along the cell length. MreB had a dynamic structure and formed small filamentous patches with a circumferential motion (Dominguez-Escobar *et al.*, 2011; Garner *et al.*, 2011). The growth and hydrolysis of the PG during cell elongation occurred in a helical-like configuration along the actin-like filaments, hence the hypothesis of interdependency between peptidoglycan synthesis and the actin homologues´ dynamic motion (Carballido-Lopez *et al.*, 2006; Daniel and Errington, 2003). These actin isoforms are engaged in different roles in *B. subtilis* and their absence leads to cell shape defects. Mbl is thought to direct the insertion of new PG material at the lateral cell wall (Daniel and Errington, 2003). MreBH is thought to control the autolytic activity at the lateral wall as it directed the localisation of the cell wall hydrolase LytE (Carballido-Lopez *et al.*, 2006). MreB maintains cell width and was also proposed to direct the assembly of the cell wall components (Kawai *et al.*, 2009). Recently, Kawai *et al.*, suggested that MreB coordinates not only PG insertion into the cell wall by controlling the localisation of PBP1 but also the binding of anionic polymer WTA to PG via TagTUV (Daniel and Errington, 2003; Kawai *et al.*, 2009, 2011).

FtsZ is another cytoskeletal element, required for cell division. It is a tubulin-like protein that polymerizes at midcell forming a dynamic ring called the Z ring (Bi and Lutkenhaus, 1991). During cell division the Z ring, which is used as a scaffold to recruit essential cell division proteins, is stabilized and tethered in the cytoplasmic membrane by EzrA, FtsA and SepF (Errington *et al.*,2003). In liposomes, FtsZ proteins polymerized causing membrane bending followed by constricted protrusions, indicating that FtsZ could probably generate force during cell division to separate daughter cells (Osawa and Erickson, 2013). Following Z-ring formation, PBP2B is the first protein to be recruited to midcell followed by PG synthases and hydrolases (Errington *et al.*, 2003; Scheffers *et al.*, 2004; Smith *et al.*, 1996; Daniel *et al.*, 2000). This divisome complex enables peptidoglycan synthesis, septum formation and cell separation for a complete cell division. Recently, a glucosyltransferase UgtP protein, involved in LTA synthesis, was shown to localise at midcell in nutrient-rich medium and to inhibit FtsZ

polymerization (Section 1.3.4). This metabolic sensor is suggested to coordinate growth rate with cell size (Weart *et al.,* 2007).

1.3 Peptidoglycan synthesis machinery

1.3.1 Class A and B penicillin-binding protein

PG is synthesised by high molecular weight (HMW) proteins called PBPs. All PBPs have a cytoplasmic region near their N-terminus, a short transmembrane region, and an extracytoplasmic part. PBPs are supposed to be involved in cell elongation and/or division due to their localisation and enzymatic activities and can be divided into 2 classes, class A bi-functional proteins and class B mono-functional PBPs (Table 1.1) (Bhavsar and Brown, 2006). *B. subtilis* Class A PBPs include PBP1, PBP2C, PBP4 and PBP2D and are capable of performing both GTase and TPase reactions. The absence of PBP2C, PBP4, or PBP2D had no effect on growth or cell morphology, whereas cells lacking PBP1 grew slower than wild type and they were thinner, bent and chaining (Murray *et al.,* 1998a). PBP1, PBP2C, PBP4 and PBP2D are thought to be involved in cell division due to their midcell localisation (Scheffers et al., 2004). PBP2C and PBP4 have a role in the spore PG synthesis (Driks and Popham, 2001). PBP1 was suggested to have an additional role in cell elongation due to its additional localisation at the cell periphery (Pedersen *et al.,* 1999; Scheffers *et al.,* 2004). *In vitro*, PBP1 polymerized the cell wall precursor lipid II into glycan chains and crosslinked amidated or non amidated peptides (Lebar *et al.,* 2014). Moreover, PBP1 exhibited a carboxypeptidase activity by removing the terminal D-Ala residue of the pentapeptide chain (Lebar *et al.,* 2014). PBP1 was recruited to the MreB helix at the lateral cell wall but thought to localise at the septum during the late stages of cell division (Claessen *et al.,* 2008; Kawai *et al.,* 2009). In addition, PBP1 was partially targeted to the division site and this localisation pattern was affected by several proteins such as GpsB, DivIB, DivIC and YvcK (Claessen *et al.,* 2008; Foulquier *et al.,* 2011; Pedersen *et al.,* 1999; Scheffers and Errington, 2004). The shuttling in PBP1 localisation between midcell and lateral wall is thought to be controlled by EzrA and GpsB via a direct interaction with the cytosolic N-terminus of PBP1 (Claessen *et al.,* 2008; Cleverley *et al.,* 2016). However, this interaction had no effect on the GTase or TPase activity of PBP1 *in vitro* (Cleverley *et al.,* 2016). McPherson and Popham were able to create a strain with deletions of the four Class A HMW PBP genes simultaneously (McPherson and Popham, 2003). Theoretically, this strain cannot polymerize new glycan strands due to the lack of GTase activity, however, they detected an unknown GTase activity in this quadruple mutant explaining

cell survival and growth (McPherson and Popham, 2003). Recently, Meeske *et al,*. suggested that RodA is not a lipid II flippase but has GTase activity and is responsible for PG synthesis in the quadruple mutant (Meeske *et al.,* 2016).

Class B PBPs includes PBP2A, PBP2B, PBP3, PBPH and YrrR, which have a non-catalytic domain and a transpeptidase domain (Table 1.1) (Bhavsar and Brown, 2006). The two mono-functional TPases, PBP2A and PBPH, are essentially redundant for lateral cell wall synthesis during cell elongation (Dominguez-Escobar *et al.,* 2011; Murray *et al.,* 1998b; Wei *et al.,* 2003). PBP2B is the only essential PBP in *B. subtilis* and it localised at midcell during exponential growth (Daniel *et al.,* 1996; Scheffers *et al.,* 2004). Midcell localisation of PBP2B is dependent on FtsZ, DivIB, DivIC and FtsL and it was suggested that PBP2B is required for initiation of septal PG synthesis and continued septal ingrowth (Daniel *et al.,* 2000). Little is known about the function of PBP3. The deletion of *pbpC* (PBP3 gene) had no effect on the growth rate, cell morphology or sporulation compared to wild type (Murray et al., 1996). In addition, the absence of PBP3 in the *ponA*, *pbpD* or *pbpF* single mutants had no additional effect on cell morphology, growth or sporulation efficiency (Murray et al., 1996). PBP3 has an enriched localisation at the septum but foci distributed along the cell periphery were also identified in vegetative cells (Scheffers *et al.,* 2004).

Table 1.1 List of *B. subtilis* high molecular weight PBPs

Gene	Protein	Role / Remarks
Class A PBPs (Bifunctional GTase/TPase)		
ponA	PBP1	Cell division, elongation and sporulation
pbpF	PBP2C	Cell division and later stages of sporulation
pbpD	PBP4	Cell division, elongation and sporulation
pbpG	PBP2D	Sporulation
Class B PBPs (Monofunctional TPase)		
pbpA	PBP2A	Cell elongation
pbpB†	PBP2B	Cell division and sporulation
pbpC	PBP3	Cell division
spoVD	SpoVD	Sporulation
phpH	PBPH	Cell elongation
yrrR	YrrR	Not known

†, gene essential for cell division

1.3.2 Peptidoglycan hydrolases

Hydrolases are essential for the insertion of new PG material into the sacculus without thickening the cell wall. They contribute to PG growth, cell division, and septum cleavage allowing the formation of two daughter cells (Blackman *et al.,* 1998). *B. subtilis* has as many as 35 PG hydrolases with redundant functions, which makes it difficult to understand the physiological role of each enzyme (Smith *et al.,* 1996, 2000; Vollmer, 2012).

Amidases hydrolyse the amide bond between the *N*-acetylmuramoyl residue and the L-Ala residue of PG (Hill, 1984). Several amidases such as LytC, CwlC, and CwlD cleave the septum during cell division allowing the separation of daughter cells (Blackman *et al.,*1998; Smith and Foster, 1995). *LytA*, *lytB* and *lytC* are all encoded in the same operon and LytA or LytB were suggested to be chaperons for LytC but their functions are still unclear (Lazarevic *et al.,* 1992). LytC localises at midcell as well as the cell periphery and in its absence a chaining cell morphology is exhibited (Margot and Karamata, 1992).

Endopeptidases cleave within peptides and are divided into 3 types, DD-peptidases, LD-peptidases and DL-peptidases (Smith *et al.,* 2000). LytF, a DL-endopeptidase, hydrolyses the linkage between the D-γ-Glu residue and the meso-diaminopimelic acid (Ohnishi *et al.,* 1999). Based on the sequence analysis of the *lytF* gene, the protein was suggested to have 5 LysM domains that are involved in PG binding (Yamamoto *et al.,* 2003). The absence of LytF caused cell chaining and localisation studies suggested that LytF has a role in cell separation due to its septal localisation (Ohnishi *et al.,* 1999; Yamamoto *et al.,* 2003). The localisation pattern and the expression of LytF was altered in cells lacking the LTA synthase LtaS (Kiriyama *et al.,* 2014). In the Δ*ugtP* mutant, the expression and the localisation of LytF was similar to wild type. However, in cells lacking the enzymes involved in the glucolipid synthesis pathway PgcA or GtaB, the expression level of LytF was lower compared to wild type cells for unknown reasons (Kiriyama *et al.,* 2014).

Another DL-endopeptidase, CwlO, localises at the cell periphery and is suggested to have a role in cell elongation (Yamamoto *et al.,* 2003). The absence of CwlO caused shorter and wider cells than wild type when grown in LB medium (Dominguez-Cuevas *et al.,* 2013). The ATP-binding cassette (ABC) transporter-like complex, FtsEX, regulates the activity of CwlO in the cell. CwlO interacts with FtsX *in vivo* and the absence of FtsX resulted in the release of CwlO in the culture supernatant (Figure 1.2) (Dominguez-Cuevas *et al.,* 2013). However, no interaction between the two proteins was detected *in vitro* (Meisner *et al.,* 2013).

Interestingly, the double deletion of two DL-endopeptidases, CwlO and LytE, is lethal in *B. subtilis* (Bisicchia *et al.,* 2007). LytE, like CwlO and LytF, has a DL-endopeptidase activity (Yamamoto *et al.,* 2003). LytE localised at midcell and in foci at the cell periphery during vegetative growth (Carballido-Lopez *et al.,* 2006; Yamamoto *et al.,* 2003). The absence of LytE caused bent cells and mild chaining suggesting a role in both cell division and elongation (Ohnishi *et al.,* 1999). In the *mreBH*-null mutant, the localisation of LytE at the cell periphery was diminished (Carballido-Lopez *et al.,* 2006). Additionally, a genomic screen for MreBH interaction partners identified LytE, hence the hypothesis of a transient interaction between the two proteins that positions LytE at the cell periphery prior to transport to the cell wall (Carballido-Lopez *et al.,* 2006).

The lethality of the *lytE cwlO* double deletion is caused by the lack of DL-endopeptidase activity at the cell periphery (Bisicchia *et al.,* 2007; Hashimoto *et al.,* 2012). This redundant essentiality of LytE and CwlO was used to identify regulators for both proteins. The lethality of the *mbl lytE* double mutant suggested a role for Mbl in controlling the function of CwlO via the FtsEX complex (Dominguez-Cuevas *et al.,* 2013). A similar lethality was observed for the *cwlO mreBH* or *ftsEX mreBH* double mutants hence the potential role of MreBH in the LytE system (Figure 1.2) (Dominguez-Cuevas *et al.,* 2013).

A σ^I –dependent increase in *lytE* expression was identified in the *ltaS* and *ugtP* mutants (Kasahara *et al.,* 2016). Likewise, the σ^I –dependent transcription of *mreBH* increased in the *ltaS* mutant cells (Matsuoka *et al.,* 2011a). Interestingly, LytE exhibited a midcell and lateral wall localisation in the *ltaS mreBH* mutant suggesting that the localisation of LytE in the *ltaS* mutant is independent of MreBH. Moreover, a *cwlO ltaS mreBH* triple mutant is viable and had a similar growth to the *cwlO ltaS* mutant suggesting that LytE is functional for lateral PG hydrolysis in the *ltaS* mutants and dispensable of MreBH (Kasahara *et al.,* 2016).

Endopeptidases and carboxypeptidases hydrolyse different amide bonds in the PG. Carboxypeptidases such as PBP5 and PBP4a remove the terminal D-Ala residue of the pentapeptide chain (Buchanan and Ling, 1992; Pedersen *et al.,*1998). Several hydrolases involved in different roles in bacteria like endospore formation and protein secretion were not mentioned above due to their irrelevance to this work at the moment (Lee and Huang, 2013).

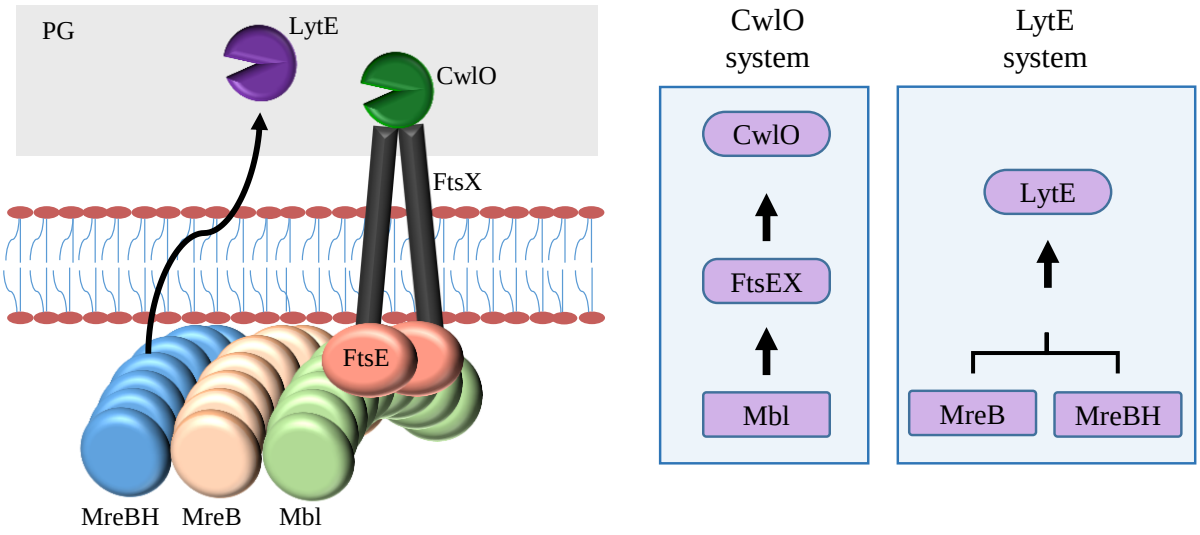

Figure 1.2 The control of hydrolases during cell elongation

(A) The actin cytoskeleton isoforms regulate the PG hydrolases CwlO and LytE required for cell elongation. MreBH ensures the localisation of LytE to the lateral wall via a transient interaction before LytE gets secreted into the extracellular domain. Mbl regulates the activity of CwlO via FtsEX by controlling the localisation of these proteins.
(B) The two proposed distinct pathways for the lateral PG hydrolysis during cell elongation (Dominguez-Cuevas *et al.*, 2013).

1.3.3 Lytic transglycosylase

Other hydrolases, such as CwlJ and SleB, are lytic transglycosylases (LT). These enzymes cleave the β1,4-glycosidic bond between Glc*N*Ac and Mur*N*Ac and catalyse the formation of the 1,6-anhydro bond between C1 and C6 of *N*-acetylmuramic acid (Höltje *et al.*, 1975). Pulse-chase studies indicated that the formation of the anhydroMur*N*Ac sugar occurs shortly after lipid II polymerization (Burman and Park, 1983; Glauner and Höltje, 1990). Recently, a synthetic lethal screen in *E. coli* cells lacking the PG synthase PBP1B identified the LT MltG (Yunck *et al.*, 2016). The overexpression of MtlG in the Δ*ponB* mutant lacking PBP1B resulted in spherical cells followed by lysis. MltG had sequence similarities in the catalytic cleft with SleB, an LT in *B. subtilis*. MltG exhibited activity against PG causing the release of sugar polymers capped by anhydroMur*N*Ac ends. MltG has a single α-helix that spans the cell membrane. The Δ*mltG* mutant had longer glycan strands and a 1.8 fold increase in the relative percentage of pentapeptides compared to wild type. Bacterial two-hybrid experiments indicated that MltG interacts with PBP1B but not PBP1A. Taken together, these results suggest that MltG has a weak endo-LT activity and presumably plays a role as a terminase during PG synthesis (Yunck *et al.*, 2016). A homologue for MltG was identified in *Streptococcus pneumoniae* (*Sp*MltG) (47% sequence similarity) (Tsui *et al.*, 2016). The absence of *Sp*MltG caused growth

defect and a spherical cell shape, suggesting a defect in peripheral PG synthesis. The growth of the *mltG* mutant was dependent on the increase in the WalRK regulon expression of PG hydrolases. Interestingly, the deletion of *mltG* rescued the lethality caused by the absence of essential proteins such as PBP2b, MreCD, RodZ or RodA. Moreover, the localisation pattern of *Sp*MltG relative to FtsZ was similar to that of PBP1a, PBP2b and MreC suggesting a role in cell elongation (Tsui *et al.*, 2016). *B. subtilis* has an MltG homologue called YrrL with an YceG-like superfamily domain. YrrL shows 32% amino acid sequence identity and 50% similarity with *E. coli* MltG extending over 356 amino acid residues. There is no information about the function or activity of YrrL in the published literature.

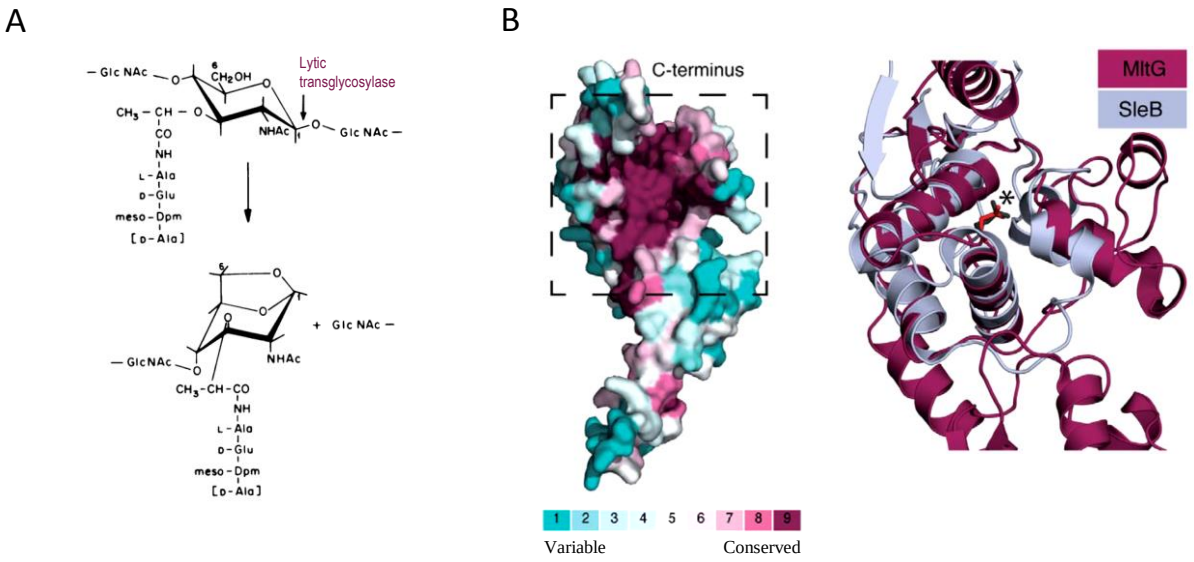

Figure 1.3 Lytic Transglycosylase

(A) The scheme adapted from Höltje et al. 1975 shows the conversion of the muramic acid moiety upon transglycosylase action.
(B) A space-filling model of the *E. coli* MltG structure with a highlight of the amino acid conservation. The ribbon diagram represents the structural alignment of the catalytic domain of the lytic transglycosylase SleB with the proposed catalytic region of MltG. The catalytic glutamate is shown in stick form and highlighted with an asterisk (Yunck *et al.*, 2016).

1.3.4 Elongasome

The actin-like MreB, Mbl or MreBH are required for lateral cell wall synthesis during cell growth. The synthesis and hydrolysis of the cell wall are presumably controlled by the MreB homologues through various protein-protein interactions which form the elongasome. MreB, Mbl, MreBH, MreC, MreD, RodZ, RodA, PBP2A, PBPH, PBP1, FtsEX, CwlO, LytE and TagGHO are all suggested to have roles in cell elongation (Figure 1.4) (Carballido-López and Formstone, 2007). The MreB isoforms, MreB, Mbl and MreBH, are soluble cytoplasmic

proteins required for cells to maintain their rod shape (Jones *et al.,* 2001; Varley and Stewart, 1992). *MreB* and *mbl* are essential for cell viability in the absence of magnesium ion supplements unlike *mreBH* which could be deleted resulting in helical shaped cells (Abhayawardhane and Stewart, 1995; Formstone and Errington, 2005; Jones *et al.,* 2001; Varley and Stewart, 1992). The depletion of MreB caused wider, rod-shaped cells while the depletion of Mbl caused the formation of small, bloated cells (Abhayawardhane and Stewart, 1995; Jones *et al.,* 2001). The differences in cell shape of the mutants suggest different functions for the MreB isoforms in the cell. The localisation of MreB, Mlb and MreBH showed extensive overlap between the three proteins that moved at similar speed and angle along the cell periphery, hence the suggestion that the MreB isoforms coexist in motile patches (Dominguez-Escobar *et al.,* 2011). A mutation in the MreB ATP binding site resulted in perturbed cell morphology but had no effect on the MreB motion, suggesting that the hydrolysis of ATP by MreB is essential for cell elongation (Garner *et al.,* 2011).

MreC and MreD are essential membrane bound proteins that play a role in cell elongation. The loss of MreC or MreD resulted in a round cell morphology (Defeu Soufo and Graumann, 2005). Fluorescence microscopy with high precision particle tracking showed colocalisation of MreC and MreD with the MreB homologues in the cell (Garner *et al.,* 2011). The localisation of MreC or MreD depended on the localisation of MreB and Mbl along the lateral wall and vice versa (Defeu Soufo and Graumann, 2005; Leaver and Errington, 2005). Thus, this interdependency between the MreB homologues, MreC and MreD suggests that these proteins coexist in the elongasome complex. Bacterial two-hybrid assays showed interaction between MreC and class A or B PBP2A, PBPH and PBP1 that are potentially playing a role in the PG synthesis at the lateral cell wall (Ent *et al.,* 2006). Consequently, MreC and MreD seem to link the scaffold proteins, the MreB homologues, to cell wall synthesis by interacting with and regulating both components during cell elongation.

RodZ is an essential membrane bound protein localising along the cell periphery in a spiral pattern similar to that of MreB (Garner *et al.,* 2011). The depletion of RodZ resulted in shorter and rounder cells and mislocalisation of FtsZ resulting in the formation of mini cells (Muchová *et al.,* 2013). The stability and localisation of RodZ are dependent on MreB and not Mbl or MreBH. RodZ interacted with MreD in bacterial two-hybrid assay and interacted with MreB, Mbl and MreBH in pull-down experiments (Muchová *et al.,* 2013). These results suggest that RodZ is a key player in PG synthesis during cell elongation, however, the role of RodZ in the cell remains unclear.

RodA, a member of the SEDS family (shape, elongation, division, spore), is an integral membrane protein required for cell elongation in *B. subtilis* (Henriques *et al.,* 1998). The depletion of RodA resulted in the loss of the side wall PG synthesis. Moreover, TEM imaging for cells lacking RodA showed a spherical morphology with no or impaired septation suggesting a role for RodA in cell division and cell elongation (Henriques *et al.,* 1998). RodA is presumably the lipid II flippase of the elongasome, responsible for the delivery of PG precursors to the synthases. Recently, RodA was suggested to be the missing glycosyltransferase in *B. subtilis* (Meeske *et al.,* 2016). The morphology and growth of cells lacking all class A PBPs (Δ4) were rescued by overexpressing RodA. The overexpression of RodA variants W105A or D280A did not rescue the Δ4 strain suggesting either of these amino acids to be the GTase active site. Partially purified RodA showed poor PG polymerization activity unlike RodA W105A or D280A that showed none. However, the purity of RodA purification was low which makes it unclear whether the detected activity is from RodA or a contaminant (Meeske *et al.,* 2016).

The synthesis of PG is performed by class A and B PBPs. PBP2A and PBPH are redundantly essential PBPs with TPase activities. The absence of both proteins caused round cell morphology (Wei *et al.,* 2003). PBP2A and PBPH colocalise with the elongation machinery (MreB, Mbl, MreBH, RodA, MreC and MreD) and their localisation pattern is dependent on the availability of the lipid II substrate (Dominguez-Escobar *et al.,* 2011; Garner *et al.,* 2011). The recruitment of the class A PBP1 to the elongasome is enabled by the cytosolic protein GpsB, which interacts with both PBP1 and MreC (Claessen *et al.,* 2008). Moreover, MreB interacts directly or in a complex with several PG synthases including PBP1, PBP2A and PBPH, and the bulging in the Δ*mreB* mutant was associated with the abnormal localisation of PBP1 (Kawai *et al.,* 2009). These results support the model in which the MreB homologues coordinate lateral cell wall synthesis during cell elongation.

PG hydrolysis is also controlled by cytoskeletal proteins, however there is no proof yet whether synthases and hydrolases in *B. subtilis* coexist in the same elongasome complex. The PG hydrolase LytE interacts with MreBH to ensure proper localisation at the lateral cell wall (Carballido-Lopez *et al.,* 2006), whereas the localisation and activity of CwlO are regulated by Mbl via the ABC-transporter like complex FtsEX (Section 1.3.2) (Dominguez-Cuevas *et al.,* 2013).

Interestingly, proteins involved in the WTA synthesis machinery such as TagGHO localised in a helical pattern at the lateral cell wall, and interacted with other elongasome proteins, MreC

and MreD (Formstone *et al.*, 2008). All these data support the model of a multiprotein complex controlling the synthesis of the PG and potentially WTA during cell elongation.

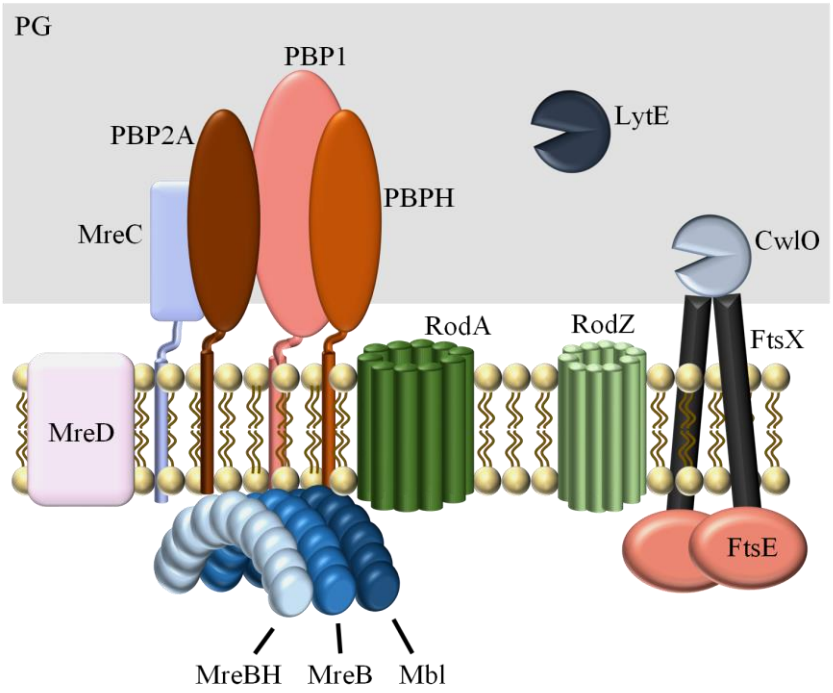

Figure 1.4 The elongasome

Schematic representation of proteins involved in PG synthesis, growth or maintenance during cell elongation. Proteins are represented with their structural features. The three actin homologues are proposed to be the scaffold for the PG synthesis machinery. RodA is presumably the lipid II flippase that delivers the PG substrate to the synthases. MreC and MreD are important in coordinating the intracellular and extracellular elongation machinery. PBP2A, PBPH and PBP1 represent the synthases involved in the PG synthesis during cell elongation. There is no proof for the coexistence of the hydrolases LytE and CwlO in the same complex as the PG synthesis machinery, however, at least one of these two hydrolases is essential for cell elongation and survival.

1.3.5 The initiation of divisome formation

Cell division is a dynamic process where several proteins assemble at midcell to synthesise and cleave the septal cell wall to produce the new poles of daughter cells. This process requires at least 12 proteins whose activities are tightly controlled (Errington *et al.*, 2003). The loss of any essential cell division protein causes the absence of septal formation resulting in filamentous cells and eventually lysis. The polymerization of a tubulin-like protein FtsZ into the Z-ring marks the initiation of cell division (Erickson *et al.*, 1996; Löwe and Amos, 1999; Mukherjee and Lutkenhaus, 1994). FtsZ polymerizes into filaments in a head to tail association dependent on GTP (Mukherjee and Lutkenhaus, 1998; Oliva *et al.*, 2004). FtsZ is a self-activating GTPase, and this activity depends on FtsZ polymerization (de Boer *et al.*, 1992; Mukherjee *et al.*, 1993;

RayChaudhuri and Park, 1992; Scheffers *et al.,* 2002). The polymerization of FtsZ is highly dynamic and takes 8-9 seconds to exchange FtsZ subunits (Stricker *et al.,* 2002). CryoEM tomography of *C. crescentus* FtsZ showed that the Z-ring is arranged in protofilaments rather than a continuous ring (Li *et al.,* 2007). The polymerization of FtsZ in liposomes caused convex bulging, which is presumably caused by the constrictive force generated by protofilaments (Li *et al.,* 2007; Osawa *et al.,* 2013).

To ensure midcell localisation of the Z-ring, the polymerization of FtsZ is positively and negatively regulated by several mechanisms which will be discussed below. The min system, which includes MinCDJ and DivIVA, prevents FtsZ assembly near the poles (Figure 1.5) (Bramkamp and Van Baarle, 2009). The absence of any component of the min system causes misplacement of the division site resulting in anucleated cells called mini cells (Adler *et al.,* 1967; Bramkamp *et al.,* 2008; Edwards and Errington, 1997; Reeve *et al.,* 1973). MinD is a membrane bound ATPase that belongs to the ParA/MinD family of proteins (Cordell and Löwe, 2001; Szeto *et al.,* 2003). MinD recruits MinC to the membrane, and the membrane association of the MinCD complex is essential for the inhibition of FtsZ polymerization (Gregory *et al.,* 2008). MinC also antagonizes the scaffolding of FtsZ by inhibiting its lateral interactions (Dajkovic *et al.,* 2008; Scheffers, 2008). MinC moves along the cell membrane and is presumed to rotate around the division site and accumulate at the cell poles, suggesting that MinCD acts at the new cell poles to prevent FtsZ re-polymering into the Z-ring (Gregory *et al.,* 2008). DivIVA localises at the assembling divisome and the cell poles, and is the topological determinant of MinCD (Edwards and Errington, 1997; Gamba *et al.,* 2009). DivIVA accumulates at negatively curved membranes without being able to impose curvature (Lenarcic *et al.,* 2009). MinJ has a transmembrane segment and interacts with MinD and DivIVA (Bramkamp *et al.,* 2008). MinJ is suggested to have an adaptor role linking the topology factor DivIVA to the inhibitory complex MinCD. MinJ also interacts with FtsL and the PG synthase PBP2B and facilitates the localisation of both proteins to midcell. This suggests another role for the min system in the regulation of membrane bound divisome components (Bramkamp *et al.,* 2008).

The second regulatory system for FtsZ polymerization is nucleoid occlusion (Figure 1.5). Noc prevents the polymerization if FtsZ into protofilaments over the nucleoid (Wu and Errington, 2004). Noc is a DNA dependent membrane binding protein. It has a highly conserved N-terminal domain responsible for Noc association to the cell membrane. The simultaneous binding of Noc to the DNA and the membrane is essential for nucleoid occlusion. This suggests that the mechanism by which Noc acts requires recruitment of DNA to the cell membrane

(Adams and Errington, 2009; Wu *et al.*, 2009). The overexpression of Noc blocked cell division in wild type cells but not in the *minCD* mutant (Wu and Errington, 2004). In cells lacking both the min and the nucleoid occlusion systems, FtsZ still preferentially polymerized at midcell between the nucleoids suggesting the presence of another regulatory factor (Rodrigues and Harry, 2012; Wu and Errington, 2004). It was also proposed that the role of both systems is to ensure efficient utilization of the division site by positioning the Z-ring at midcell. Such a hypothesis suggests the presence of an as yet unknown mechanism by which FtsZ identifies the division site (Rodrigues and Harry, 2012).

A third element that influences FtsZ polymerization at midcell is the glucolipid transferase UgtP (Weart *et al.*, 2007). UgtP was described as a metabolic sensor that coordinates cell size with cell division. The role of UgtP and the mechanism of such regulation are discussed in section 1.5.1.

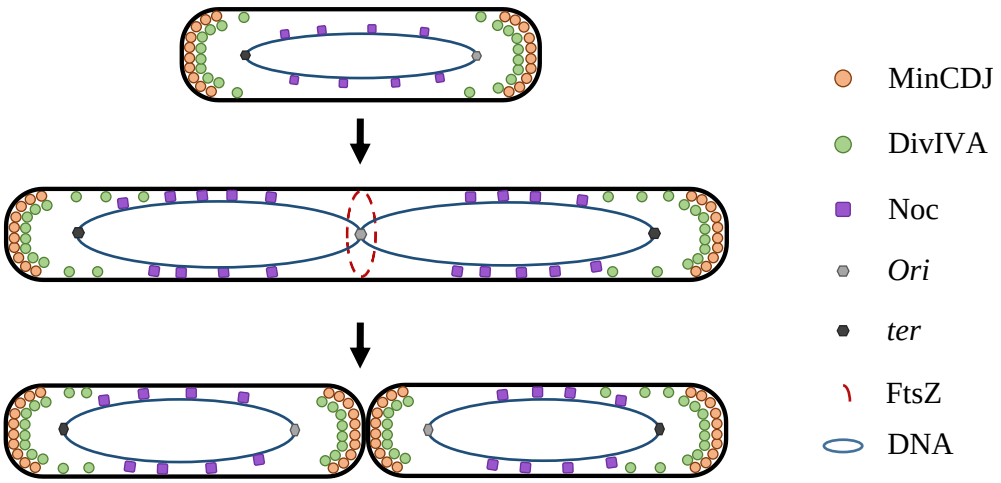

Figure 1.5 The selection of the division site

The polymerization of FtsZ at midcell is regulated by the Min system and the nucleoid occlusion system. The Min system including MinCDJ and DivIVA, prevents the polymerization of FtsZ at the cell poles. MinC inhibits FtsZ polymerization while MinDJ and DivIVA control the activity and the localisation of MinC. The nucleoid system, Noc, prevents Z-ring formation over the nucleoid. The binding of Noc to the DNA and to the membrane simultaneously is essential for nucleoid occlusion.

1.3.6 The assembly of the divisome

In *E. coli*, the divisome assembles in a sequential manner by the hierarchical recruitment of cell division proteins to midcell (Goehring *et al.,* 2006). Conversely, *B. subtilis* appears to have a two-step assembly dynamics of the divisome where division proteins are recruited in a cooperative rather than a sequential manner (Gamba *et al.,* 2009). In this system, FtsZ, FtsA, EzrA and ZapA are recruited to the assembling divisome in the first 25% of the cell cycle followed by the recruitment of PBP2B, FtsL, DivIB, DivIVA and FtsW with a delay of at least 20% of the cell cycle (Figure 1.6) (Gamba *et al.,* 2009). The Z-ring is stabilized at midcell by its positive regulators including FtsA, ZapA and SepF. FtsA has an actin-like structure and an ATP-binding site, however, the oligomerization of FtsA is ATP independent (van den Ent and Löwe, 2000; Feucht *et al.*, 2001; Shiomi and Margolin, 2007; Singh *et al.*, 2013; Yim *et al.*, 2000). *E. coli* FtsA interacts with the cell membrane via an amphipathic helix. Also, FtsA interacts with FtsZ and enables its anchoring to the cytoplasmic membrane (Wang *et al.*, 1997). The ratio of FtsZ to FtsA in the cell is 5 to 1 and as such the balance between the two proteins must be maintained for correct cell division (Feucht *et al.,* 2001).

SepF, like FtsA, interacts directly with FtsZ and promotes Z-ring formation and bundling (Duman *et al.,* 2013; Singh *et al.,* 2008). SepF binds to lipid membranes and is proposed to function as a cell membrane anchor for the Z-ring (Duman *et al.*, 2013). *SepF*-null cells, like *ftsA*-null cells, are elongated and have distorted and abnormally thick septa, hence the potential role of SepF in modulating septal PG synthesis or constriction (Hamoen *et al.,* 2006). The overexpression of SepF complements the *ftsA*-null phenotype suggesting partial redundancy between the two proteins (Ishikawa *et al.,* 2006).

ZapA, which is recruited at the early stages of cell division, interacts with FtsZ and promotes FtsZ polymerization into protofilaments (Gueiros-Filho and Losick, 2002). In addition, ZapA inhibits the GTPase activity of FtsZ resulting in increased stability and rigidity of FtsZ protofilaments (Gueiros-Filho and Losick, 2002; Low *et al.*, 2004; Small *et al.*, 2007).

EzrA, a membrane bound protein, negatively regulates Z-ring formation by inhibiting FtsZ polymerization (Chung *et al.,* 2007; Cleverley *et al.,* 2014; Haeusser *et al.,* 2004; Land *et al.*, 2014; Levin *et al.,* 1999; Singh *et al.,* 2007). EzrA localises at midcell and the cell periphery, and the *ezrA* mutant has polar Z-rings in addition to thin cell morphology (Levin *et al.,* 1999). These results suggest a role for EzrA not only in cell division but also in cell elongation. However, it is still unclear why a negative regulator of FtsZ assembly is recruited at the early stages of the cell division. Moreover, EzrA interacts directly with GpsB and coordinates the

recruitment of PBP1 to the division site (Claessen *et al.,* 2008; Tavares *et al.,* 2008). The absence of both EzrA and GpsB resulted in the delocalisation of the cell wall synthesis machinery and impaired septal PG synthesis (Claessen *et al.,* 2008). In addition, cells lacking both SepF and EzrA do not recruit the essential PG synthase PBP2B to the divisome leading to cell death (Hamoen *et al.,* 2006). These results provide evidence for the importance of these proteins not only in regulating FtsZ polymerization but also in recruiting PG synthases during cell division.

The second step in divisome assembly involves the recruitment of several proteins such as FtsL, DivIB, DivIC, FtsW, PBP2B, GpsB and PBP1 to midcell (Figure 1.6) (Gamba *et al.,* 2009). Each of these proteins has a unique role during cell division that will be discussed below. FtsL is essential for cell viability and has a N-terminal cytoplasmic domain, a transmembrane segment and a C-terminal extracellular domain (Bramkamp *et al.,* 2006; Daniel *et al.,* 1996, 1998). The cytosolic region of FtsL is important for the stability of the protein but is dispensable for division (Bramkamp *et al.,* 2006). FtsL formed a trimeric complex with cell division proteins DivIB and DivIC in yeast three-hybrid assays (Daniel *et al.,* 2006; Robichon *et al.,* 2008). Furthermore, the marked instability of FtsL in the absence of the essential cell division proteins DivIB, DivIC and PBP2B presumably made it a key control point in cell division (Daniel *et al.,* 2006; Wadenpohl and Bramkamp, 2010).

DivIC is an essential cell division protein with a similar topology to FtsL (Katis *et al.,* 1997). DivIC has dispensable cytoplasmic and transmembrane regions and an essential extracellular domain for function and midcell localisation (Katis *et al.,* 1997). The stability and turnover of DivIC depends on DivIB in wild-type cells or the Δ*ftsL* mutant (Daniel *et al.,* 1998, 2006). DivIB is a membrane bound cell division protein not essential for viability at 30˚C (Beall and Lutkenhaus, 1989, 1992; Harry and Wake, 1989). The overexpression of FtsL supresses the *divIB*-null lethality at high temperature suggesting either an overlap in divIB and FtsL functions or the division defect in *divIB*-null resulted from FtsL degradation (Daniel and Errington, 2000). Moreover, DivIB is important for the synthesis of the polar septum during sporulation suggesting an additional sporulation-specific role (Rowland *et al.,* 1997; Thompson *et al.,* 2006).

FtsW is an essential protein that belongs to the SEDS family of proteins (Boyle *et al.,* 1997; Ikeda *et al.,* 1989). The deletion of *ftsW* resulted in long filamentous cells and PBP2B mislocalisation suggesting a block in cell division (Boyle *et al.,* 1997; Gamba *et al.,* 2016). The FtsW homologue from *E. coli* has ten transmembrane segments and functions as a lipid II

flippase that transfers lipid II from the cytoplasm to the extracellular region where it is delivered to PBPs (Höltje, 1998; Mohammadi *et al.*, 2011, 2014).

PBP2B is the first PBP to be recruited to the assembling divisome and is crucial for septal PG synthesis (Daniel *et al.*, 1996). The depletion of FtsL, DivIB, DivIC or FtsW causes mislocalisation of PBP2B from midcell, which results in a block in cell division (Daniel *et al.*, 2000; Gamba *et al.*, 2016). More information about PBP2B can be found in section 1.3.1.

The localisation of the synthase PBP1 to the lateral cell wall during cell elongation is controlled by GpsB (Section 1.3.4). However, PBP1 is also involved in septal PG synthesis and the recruitment of the synthase to midcell is coordinated by EzrA (Claessen *et al.*, 2008). Thus, the shuttling of PBP1 between midcell and the cell periphery is presumably controlling the cell elongation-division cycle. Moreover, GpsB is essential in absence of EzrA suggesting a partial redundancy in the control of PBP1 localisation (Tavares *et al.*, 2008).

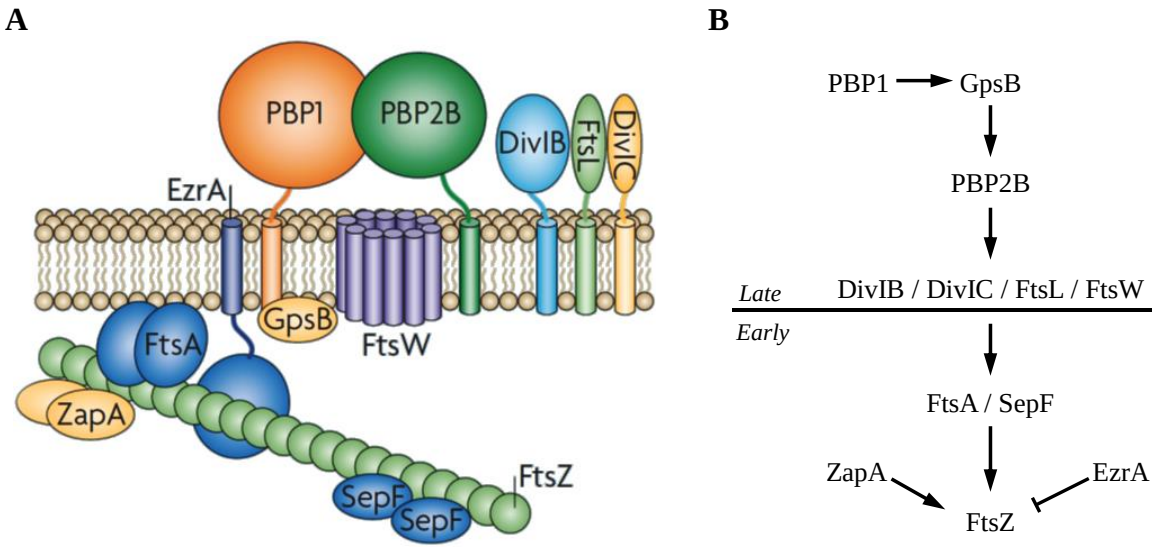

Figure 1.6 The assembly of the divisome

(A) Schematic representation of proteins involved in cell division (Adams and Errington, 2009). Proteins are represented with their structural features. The tubulin-like protein FtsZ works as scaffold for the PG synthesis machinery. ZapA and Ezra are positive and negative regulators for FtsZ polymerization, respectively. FtsA and SepF stabilize the Z-ring and tether it to the membrane. FtsW is presumably the lipid II flippase that delivers the PG substrate to the synthases. DivIB, DivIC and FtsL are essential for cell division but their roles are unclear. PBP2B is the first PG synthase recruited to the assembling divisome. PBP1 is involved in PG synthesis during cell division and its localisation to the septum is regulated by GpsB and EzrA.

(B) The scheme represents the two-step assembly process of the divisome. During the early step, FtsZ polymerize into a ring at midcell. This polymerization is regulated by ZapA, SepF, FtsA and EzrA. The late step of the divisome assembly is the step during which DivIB, DivIC, FtsL and FtsW are co-recruited to the assembling divisome. The absence of any of the later proteins causes a destabilization of the divisome. PBP2B is the first synthase recruited to the divisome for septal PG synthesis followed by PBP1 and the rest of the unmentioned cell division machinery.

1.4 Anionic cell wall polymers

1.4.1 Wall teichoic acid WTA

WTA accounts for up to 60% of the mass of the cell wall (Ellwood, 1970). It is an anionic polymer composed of a disaccharide linkage unit and a chain of glycerol-phosphate residues (Figure 1.7). WTA is covalently linked to PG by a phosphodiester bond to the C6 hydroxyl group of the *N*-acetyl muramic acid sugars (Araki and Ito, 1989; Yokoyama *et al.*,1986). In *B. subtilis*, WTA is synthesised by *tag* (teichoic acid glycerol) gene products. The synthesis starts at the cytoplasmic face of the cellular membrane on an undecaprenyl-phosphate lipid anchor. TagO catalyses the transfer of Glc*N*Ac-1-P from UDP-Glc*N*Ac to undecaprenyl phosphate (Soldo *et al.*, 2002), followed by the addition of *N*-acetylmannosamine (Man*N*Ac) catalysed by TagA (Ginsberg *et al.*, 2006). The glycerolphosphotransferase TagB catalyses the addition of *sn*-glycerol-3-phosphate unit to Man*N*Ac (Bhavsar *et al.*, 2005; Ginsberg *et al.*, 2006). These three steps are required for the synthesis of the disaccharide linkage unit and they are highly conserved among all *B. subtilis* strains characterized so far. Once the synthesis of the linkage unit is complete, TagF catalyses the addition of up to 60 glycerol phosphate Gro-P units to *sn*-glycerol-3-phosphate to assemble the polymer (Schertzer and Brown, 2003). The transfer of the polymer across the membrane is performed by an ABC-transport system, TagGH (Lazarevic and Karamata, 1995). Once at the outer leaflet, the polymer is D-alanylated by the products of the *dltABCD* operon then transferred to the PG where it covalently binds Mur*N*Ac (Araki and Ito, 1989; Coley *et al.*, 1978; Perego *et al.*, 1995). This transfer from the undecaprenylphosphate to the PG is done by 3 redundant enzymes TagT, TagU and TagV (Kawai *et al.*,2011).

WTA polymers have numerous roles in cell morphology and growth but the molecular details of their function are still not well understood. *B. subtilis* cells lacking WTA grew slower than wild type cells and they had cell wall abnormalities, thick PG layer with an increase in cell size and aberrant cell division (Cole *et al.*, 1970; D'Elia *et al.*, 2006). WTA also has a role in regulating the activities of autolytic enzymes in the cell wall in addition to an increase in antibiotic resistance (Brown *et al.*, 2013).

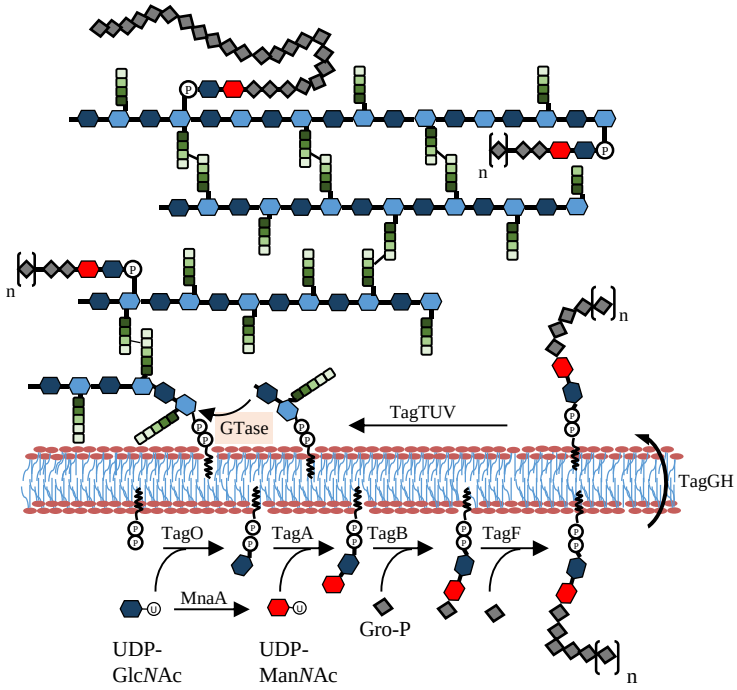

Figure 1.7 Wall teichoic acid biosynthesis

Products of the tag operon catalyses the synthesis of the WTA from the sugar nucleotide UDP-Glc*N*Ac. The lipid anchor undecaprenyl-pyrophosphate is used as a carrier molecule. TagGH are suggested to catalyse the transfer of the precursor from the cytoplasm to the extracellular domain. TagTUV suggested to be involved in the transfer of the WTA from the undecaprenyl-pyrophosphate to the PG.

1.4.2 Lipoteichoic acid LTA

A second anionic polymer in *B. subtilis* is lipoteichoic acid (LTA). It is composed of a membrane anchored glycolipid and glycerol-phosphate repeats (Figure 1.8). The synthesis of LTA starts at the cytoplasmic side of the cell membrane where cytidine diphosphate diacylglycerol (CDP-DG) is first synthesised from phosphatidic acid PA by a phosphatidate cytidylyltransferase CdsA (Figure 1.9) (Gaillard *et al.*, 1983). The phosphatidylglycerophosphate synthase PgsA catalyses the synthesis of phosphatidylglycerol phosphate (PGP) from CDP-DG (Miyazaki *et al.*, 1985). PGP is then dephosphorylated producing phosphatidylglycerol. UDP-glucose diacylglycerol glucosyltransferase UgtP transfers two glucose molecules from UDP-glucose to the phosphatidylglycerol anchor which is then transported across the membrane by a transmembrane protein LtaA (Grundling and Schneewind, 2007)**.** At the extra-cellular membrane the lipoteichoic acid synthases polymerise the addition of Gro-P repeats to the glycolipid molecule. *B. subtilis* has four synthase isoforms encoded by *ltaS, yfnI, yqgS* and *yvgJ* (Schirner *et al.*, 2009). The LTA is D-alanylated at the outer leaflet in the same way as the WTA by the products of the *dltABCD* operon. The lack of the D-alanyl-ester in LTA and WTA has no effect on the cell shape. However, an increase in autolysis activity and an increase in susceptibility to antimicrobial peptides has been detected

in such cells (Perego *et al.,* 1995; Wecke *et al.,* 1997; Wecke *et al.,* 1996). CryoEM studies indicated a continuous layer of LTA along the membrane (Matias and Beveridge, 2008). Such a distribution of LTA suggests a role for this polymer in the overall structural organisation of the cell envelope (Matias and Beveridge, 2008). LtaS and its homologue YqgS both localised predominantly at midcell in vegetative cells (Schirner *et al.,* 2009). The Δ*ltaS* mutant exhibited a reduction in cell diameter, cell bending in addition to cell division defects described by the presence of long aseptate regions and aberrant septa (Schirner *et al.,* 2009). The absence of the LTA synthase LtaS suppressed the magnesium dependency of the Δ*mbl* and Δ*mreB* mutants (Schirner *et al.,* 2009). The Δ*ltaS* mutant exhibited bigger LTA size suggesting an alteration of the LTA structure. Interestingly, the synthase quadruple mutant was viable, but cells grew slower than wild-type and with cell division defects (Schirner *et al.,* 2009). No LTA was found in this quadruple mutant, meaning the lipoteichoic acid synthases were required for LTA synthesis, along with CdsA and PgsA (Wormann *et al.,* 2011). The Δ*ltaS* mutant exhibited an increase in total phosphatidic acid and CDP-DG levels in the cell. Cells lacking LtaS also had an 8-fold decrease in the diglucosyldiacylglycerol (DGDG) level, which is synthesised by UgtP (Section 1.4.3) (Hashimoto *et al.,* 2013). The transcription of *sigM* increased up to 8-fold in the Δ*ltaS* and the Δ*ugtP* mutant, suggesting that the SigM upregulation response in the Δ*ltaS* or the Δ*ugtP* mutants could be caused by the low levels or absence of the diacylglucose moiety, respectively (Hashimoto *et al.,* 2013; Seki *et al.,* 2015). In *Bacillus anthracis*, the absence of the LTA synthases LtaS1 and LtsS2 exhibited rough cell surfaces compared to wild type cells suggesting increased PG hydrolase activity (Garufi *et al.,* 2012).

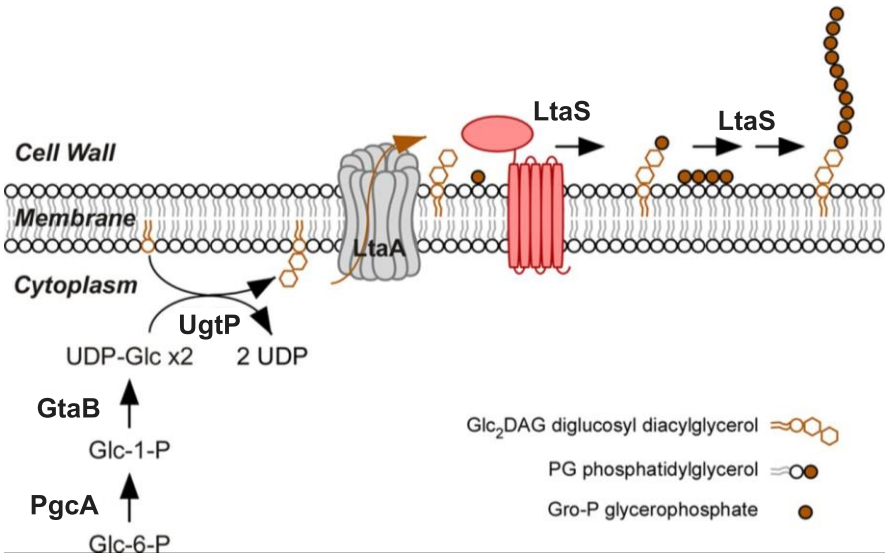

Figure 1.8 LTA biosynthesis

Schematic representation of LTA synthesis in *B. subtilis* adopted and modified from (Schneewind and Missiakas, 2014)**.** PgcA and GtaB synthesise glucose-1-P and UDP-glucose, respectively. Two glucose residues are transferred successively from UDP-glucose to diacylglycerol by UgtP to synthesise Glc_2DAG. This latter is flipped across the cytoplasmic membrane by LtaA. Subsequently, LtaS catalyses the addition of the Gro-P repeats to Glc_2DAG to synthesise LTA.

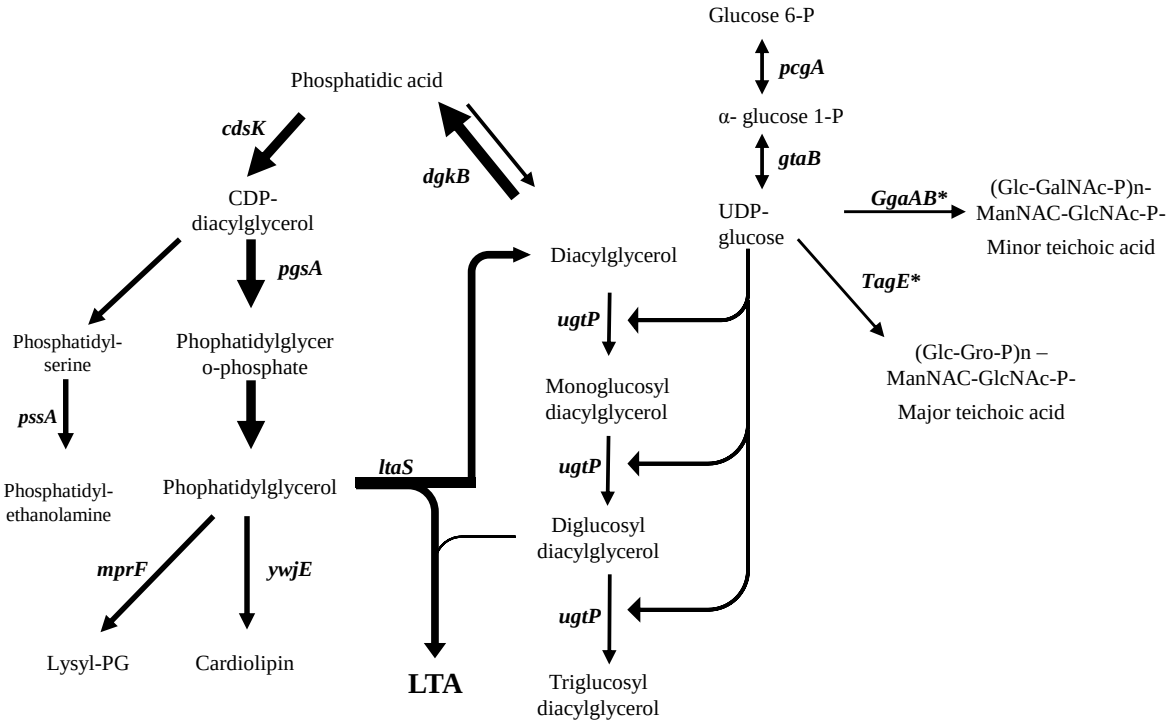

Figure 1.9 Phospholipids, glycolipids and LTA biosynthesis pathways in *B. subtilis*

Thick arrows on the left side of the figure represent the diacylglycerol cycle for lipoteichoic acid synthesis (Jerga *et al.*, 2007). The right side of the diagram represents the pathway for glucolipid biosynthesis (Yasbin *et al.*, 1976).

1.4.3 Glucolipid biosynthesis

Glucolipids constitute one of the components used for LTA synthesis. Their production start by transforming glucose-6 phosphate to α-glucose-1 phosphate by the α-phosphoglucomutase PgcA, followed by the synthesis of UDP-glucose by α-glucose-1-phosphate uridylyltransferase GtaB (Figure 1.8 and 1.9) (Yasbin *et al.*,1976). UDP-glucose is used as a precursor for the synthesis of three teichoic acids: the minor teichoic acid (GlcGal*N*Ac1-P)$_n$-Man*N*Ac-Glc*N*Ac-P by two sugar transferases GgaA and GgaB (Freymond *et al.,* 2006), the major teichoic acid (Glc-Gro-P)$_n$-Man*N*Ac-Glc*N*Ac-P by the glucosyltransferase TagE (Mauel *et al.*,1991) and the LTA (Figure 1.9). The diacylglycerol glucosyltransferase UgtP catalyses three consecutive transfers of glucose residues to a membrane anchored diacylglycerol (Jorasch *et al.*,1998). *B. subtilis* has monoglucosyldiacylglycerol (MGDG), diglucosyldiacylglycerol (DGDG) and triglucosyldiacylglycerol (TGDG), forming 1.2%, 9.8% and 0.3% of the total membrane lipids, respectively (Kawai *et al.*,2006). In *S. aureus*, MGDG is flipped across the membrane by multi-transmembrane spanning protein LtaA to be used for LTA synthesis (Grundling and Schneewind, 2007).

1.5 UgtP, a metabolic sensor for cell size homeostasis

1.5.1 Cell growth coordinates cell division

Bacteria are significantly larger in nutrient rich media than in nutrient poor medium. Therefore, the coordination between cell size and growth rate is important for cells to be at the appropriate size to face a given environment. It was suggested that the glycolipid pathway functions as a metabolic sensor to control cell size in *B. subtilis* in addition to its role in teichoic acid synthesis (Weart *et al.*,2007). Transposon-based screen searching for FtsZ assembly inhibitors identified the α-phosphoglucomutase PgcA (Weart *et al.,* 2007). *PgcA, gtaB* and *ugtP* mutants exhibited short cell morphologies and were able to suppress the cell division block associated with MinCD overexpression. The expression level of FtsZ in the *pgcA* mutant was similar to wild type suggesting that PgcA modulates the assembly dynamics and not the expression level of FtsZ (Weart *et al.*,2007). The absence of PgcA or GtaB did not affect the expression level of UgtP in the cell but it interfered with the midcell localisation of UgtP in vegetative cells in nutrient rich medium (Nishibori *et al.,* 2005; Weart *et al.,* 2007). For cells grown in minimal sorbitol medium, UgtP was randomly distributed in foci and the level of UgtP expression decreased 6-fold compared to wild type. These results suggested that PgcA and GtaB modulated FtsZ assembly by controlling UDP-glucose availability in nutrient rich conditions. The

overexpression of UgtP caused 22% increase in cell length (Weart *et al.,* 2007). *In vitro*, UgtP inhibited FtsZ assembly in a concentration dependent manner and destabilized the lateral interactions between FtsZ protofilaments (Chien *et al.*,2012). In the presence of UDP-glucose, UgtP had a higher affinity for FtsZ than for itself (Chien *et al.*, 2012). Thus a shift from the UgtP-UgtP complex to the UgtP-FtsZ complex is presumably dependent on the increased levels of UDP-glucose, hence the stimulation of the UgtP-mediated inhibition of FtsZ assembly. Taken together these results suggests that nutrient availability altered both the expression and localisation of UgtP, thus ensuring that the inhibition of Z-ring formation is coupled to growth rate (Chien *et al.*, 2012; Weart *et al.*, 2007).

1.5.2 The effect of glycolipids on bacterial actin homologues

Matsuoka *el at.,* (2011) studied the effect of UgtP on the actin polymers. They tested the actin-homologs´ expression levels by *lacZ* transcriptional fusion in *B. subtilis ugtP* mutant cells. The *mreB* operon has 2 promoters, a $P_{upstream\ mreB}$ and a P_{mreB} (Tseng and Shaw, 2008). In *ugtP* mutants, *mreB* ($P_{upstream\ mreB}$) and *mreBH* transcription levels were 4.3 and 2.3 times higher than wild type, respectively (Matsuoka *et al.*,2011). However, *mbl* expression was not affected. Strains lacking both MreB and UgtP were viable and cells had an oval shape (Matsuoka *et al.*,2011). The absence of UgtP altered MreB localisation during exponential growth but not during stationary phase. The levels of MreB decreased significantly during exponential phase in the absence of UgtP, however, the addition of 10 mM $MgSO_4$ supressed the abnormal localisation and level of MreB in the *ugtP* mutant. No interaction has been identified between MreB and UgtP by bacterial two-hybrid experiments, suggesting that glycolipids stabilise MreB polymerization or protect it from proteolysis (Matsuoka *et al.*, 2011).

1.5.3 The effect of glycolipids on the cell wall

UgtP catalyses the transfer of glucose residues to a membrane anchored diacylglycerol during LTA synthesis. The absence of UgtP caused a significant decrease in the levels of glucolipids in the cell membrane (Salzberg and Helmann, 2008). In *B. subtilis*, Δ*ugtP*, Δ*pgcA* and Δ*gtaB* mutants had similar LTA content to wild type cells (Matsuoka *et al.*, 2011b). However, in *S. aureus* the *ypfP*-null (UgtP homologue) and the *ltaS*-null both exhibited a bigger LTA size compared to wild type suggesting an alteration in the LTA structure (Reichmann *et al.*, 2014).

In addition, YpfP interacted directly or indirectly with the LTA synthesis machinery LtaA and LtaS by bacterial two-hybrid assays (Reichmann *et al.,* 2014).

Extracytoplasmic function sigma factors were another element studied in the *ugtP* mutant to understand the changes in cell morphology. In the Δ*ugtP* mutant, the promoter activity of σ^M, σ^V and σ^X increased 6.9, 3.4, and 1.5 folds, respectively (Hashimoto *et al.,* 2013; Seki *et al.,* 2015). σ^M is involved in cell wall synthesis and cell shape maintenance by its regulation of several genes such as *murBF, ponA* and *rodA* (Cao *et al.,* 2002; Jervis *et al.,* 2007). In the 168 Marburg strain, cells lacking SigM had wild type shape while cells lacking UgtP were thick, filamentous and bent during exponential phase. However, cells lacking both SigM and UgtP had an oval shape and lysed (Matsuoka *et al.,* 2011a). In addition, a microarray analysis for the PY79Δ*ugtP* mutant showed up to 30% of the genes in the SigM, SigK and SigG regulons had increased transcription levels compared to wild type (Salzberg and Helmann, 2008).

Furthermore, the absence of GtaB or PgcA but not UgtP diminished biofilm formation, however, the Δ*ugtP* mutant showed flatter and matte biofilm compared to wild-type cells (Lazarevic *et al.,* 2005; Salzberg and Helmann, 2008).

The effect of UgtP on PG synthesis is still poorly characterized. The treatment of the Δ*ugtP* mutant with fluorescently-labelled vancomycin showed a similar staining pattern to wild type cells suggesting that PG synthesis and lipid II incorporation were mostly unimpaired (Salzberg and Helmann, 2008). Moreover, the *S. aureus* YpfP interacted directly or indirectly with the divisome members DivIB, DivIC, FtsL, FtsW and PBP1 by bacterial two-hybrid experiments (Reichmann *et al.,* 2014). These results suggest that UgtP might have an effect not only on FtsZ polymerization but also on other cell division proteins. The expression of LytE increased up to two fold in cells lacking LtaS, UgtP, PgcA or GtaB compared to wild type, however, the localisation of LytE in the latter mutants was unaffected (Kasahara *et al.,* 2016). The reasons behind this increase in LytE expression in cells with defective LTA synthesis is not clear.

1.6 Aims of the project

Changes in the concentrations of glucose or magnesium ions in culture media helped several mutants to recover from defective aspects of the cell wall (Murray *et al.*, 1998; Formstone and Errington, 2005). However, the mechanisms behind such recovery and how the metabolism of the cell impacts PG synthesis is unclear. Moreover, the mechanism of peptidoglycan synthesis in *B. subtilis* is mostly uncharacterized. Therefore, the following questions were investigated in this work:

1. How does the absence of glucolipids in the cell impact the cell wall synthesis?
2. How does PBP3 complement the lack of the TPase activity of PBP2B? What are the roles of PBP1, PBP2B and PBP3 in the synthesis of PG during cell division?
3. What is the role of YrrL, a lytic transglycosylase homologue, in *B. subtilis*?

2 Methods

2.1 Strains and plasmids

Table 2.1 List of *B. subtilis* strains used in this study

Strain	Genotype	Reference/Source
168CA	*trpC2*	Laboratory collection
2083	*trpC2 ponA::(*P_{xyl} *gfp-ponA cat)*	(Claessen *et al.*, 2008)
3105	*trpC2 pbpC*::pSG5045 (*cat* P_{xyl} *gfp-pbpC*)	Laboratory collection
4001	*trpC2 pbpB*$^{(S309A)}$	Laboratory collection
4015	*trpC2 pbpC*::*cat*	Laboratory collection
BGSC1	*yrrL::erm*	BGSC
BGSC2	*yocA::erm*	BGSC
BGSC3	*sigM::erm*	BGSC
KS53	*trpC2 amyE::(spc* P_{spac} *pbpC*$^{(S410A)}$*)*	Laboratory collection
PG237	*trpC2 ugtP*::*neo*	Laboratory collection
PDC463	*trpC2 cwlO*::*spc*	(Dominguez-Cuevas *et al.*, 2013)
PDC464	*trpC2 lytE*::*cat*	(Dominguez-Cuevas *et al.*, 2013)
PS2062	*trpC2 ponA::spc*	(Popham and Setlow, 1995)
SSB122	*trpC2 pgcA*::*tet*	(Weart *et al.*, 2007)
JS07	*trpC2 gtaB::erm*	This work
JS45	*trpC2 yrrL::erm*	168CA transformed with BGSC1 DNA
JS46	*trpC2 yocA::erm*	168CA transformed with BGSC2 DNA
JS48	*trpC2 sigM::erm*	168CA transformed with BGSC3 DNA
JS55	*trpC2 ugtP*::*neo ponA::cat*	PG237 transformed with JS06 DNA

JS60	*trpC2 ΔyrrL*	This work
JS62	*trpC2 ΔyrrL yocA::erm*	JS60 transformed with JS46 DNA
KS10	*lytABC::neo*	Kenneth Seistrup, unpublished
KS07	*lytF::spc*	Kenneth Seistrup, unpublished
BSB1	Autotroph	Nicolas *et al.*, 2012
JS03	BSB1 *ugtP::neo*	BSB1 transformed with PG237 DNA
JS04	BSB1 *pgcA*::*tet*	BSB1 transformed with SSB122 DNA
JS05	BSB1 *ugtP*::*neo amyE*::(spc P_{spank} *ugtP)*	JS03 transformed with pJS01
JS06	BSB1 *ponA*::*cat*	This work
JS07	BSB1 *pgcA*::*tet aprE*::(spc P_{spac} *pgcA)*	JS04 transformed with pJS02
JS09	BSB1 *gtaB::erm*	This work
JS12	BSB1 *gtaB*::*erm aprE*::(spc P_{spac} *gtaB)*	JS09 transformed with pJS03
JS13	BSB1 *ugtP::neo cwlo::spc*	JS03 transformed with PDC463 DNA
JS14	BSB1 *ugtP::neo lytE::cat amyE*::(P_{spank} *ugtP spc)*	JS05 transformed with PDC464 DNA
JS15	BSB1 *ugtP*::*neo ponA::cat amyE*::(*spc* P_{spank} *ugtP)*	JS05 transformed with JS06 DNA
JS17	BSB1 *gtaB::erm lytABC::neo*	JS09 transformed with KS10 DNA
JS19	BSB1 *pgcA::tet lytF::spc*	JS04 transformed with KS07 DNA
JS20	BSB1 *lytABC::neo*	BSB1 transformed with KS10 DNA
JS21	BSB1 *lytF::spc*	BSB1 transformed with KS07 DNA

JS23	BSB1 *lytF::spc ugtP::neo*	JS03 transformed with KS07 DNA
JS32	BSB1 *S827*::*erm*	This work
JS36	BSB1 *gtaB*::*erm ponA::cat aprE*::(*spc* P_{spac} *gtaB)*	JS12 transformed with JS06 DNA
JS38	BSB1 *pgcA::tet ponA::(*P_{xyl} *gfp-ponA cat)*	JS04 transformed with 2083 DNA
JS39	BSB1 *ugtP::neo ponA::*(P_{xyl} *gfp-ponA cat)*	JS03 transformed with 2083 DNA
JS40	BSB1 *ponA::(*P_{xyl} *gfp-ponA cat)*	BSB1 transformed with 2083 DNA
JS41	BSB1 *ugtP*::*neo amyE*::(spc P_{spank} *ugtP*-S827*)*	JS03 transformed with pJS04
JS42	BSB1 *cwlO::spc*	BSB1 transformed with PDC463 DNA
JS43	BSB1 *lytE::cat*	BSB1 transformed with PDC464 DNA
JS44	BSB1 *ugtP::neo lytE::cat*	JS03 transformed with PDC464 DNA
JS49	BSB1 *ugtP::neo lytE::cat sigM::erm*	JS44 transformed with BGSC3 DNA
JS52	BSB1 *ugtP::neo lytE::cat ponA::spc*	JS44 transformed with JS06 DNA
JS54	BSB1 *lytE::cat ugtP::neo amyE*::(*spc* P_{spank} *ugtP)*	JS05 transformed with JS43 DNA
JS56	BSB1 *ugtP*::*neo ponA::Cm amyE*::(*spc* P_{spank} *ugtP*-S827*)*	JS41 transformed with JS06 DNA
DH5α	*E. coli* F^- φ*80lacZΔM15,* Δ(*lacZYArgF*)*U196, recA1, endA1, hsdR17,* (r_{k-}, m_{k+})*, phoA, supE44,* λ^-*, thi-1, gyrA96, relA1*	Invitrogen
BL21(DE3)	*E. coli* B F^- *ompT gal dcm lon hsdS*$_B$($r_B^-m_B^-$) λ(DE3 [*lacI lacUV5-T7p07 ind1 sam7 nin5*]) [*malB*$^+$]$_{K\text{-}12}$(λ^S)	

Table 2.2 List of plasmids used in this study

Plasmid	Characteristics	Reference/Source
pAPNC213	*bla aprE' spc lacI* P_{spac}*' aprE*	Morimoto *et al.*, 2002
pDR111	*bla amyE' spc lacI* P_{spank}*' amyE*	David Rudner, Harvard University
PcotC-GFP	*bla cat* P_{cotC} *cotC-gfp*	Veening *et al.*, 2006
pET-28a(+)	*kan* P_{T7} *lacI*	This work
pET28-28a(+)::*ponA*	*kan* P_{T7} *ponA lacI*	Cleverley *et al.*, 2016; Rismondo *et al.*, 2016
pMUTIN	*erm* P_{spac} *lacZ lacI*	Vagner *et al.*, 1998
pJS01	*bla amyE' spc lacI* P_{spank} *ugtP' amyE*	This work
pJS02	*bla aprE' spc lacI* P_{spac} *pgcA' aprE*	This work
pJS03	*bla aprE' spc lacI* P_{spac} *gtaB' aprE*	This work
pJS04	*bla amyE' spc lacI* P_{spank} *ugtP*-S827*' amyE*	This work
pJS05	*kan* P_{T7} *pbpC lacI*	This work
pJS06	*kan* P_{T7} $pbpC^{(17\text{-}668)}$ *lacI*	This work
pJS07	*kan* P_{T7} *pbpB lacI*	This work
pJS08	*kan* P_{T7} $pbpB^{(24\text{-}716)}$ *lacI*	This work
pJS09	*kan* P_{T7} $pbpB^{(S309A)}$*lacI*	This work
pJS10	*kan* P_{T7} $pbpC^{(S410A)}$ *lacI*	This work
pJS11	*kan* P_{T7} *yrrL lacI*	This work

2.2 Growth and Media

2.2.1 Media supplements and antibiotics

Table 2.3 List of media supplements

Supplements	Final concentration
Chloramphenicol (dissolved in 100% ethanol)	5 µg/ml
Erythromycin (dissolved in 50% ethanol)	1 µg/ml
Ampicillin	5 µg/ml
Kanamycin for *B. subtilis*	2-5 µg/ml
Kanamycin for *E. coli*	25 µg/ml
Tetracycline	10 µg/ml
Xylose	0.5%
IPTG	0.1-1 mM
$MgCl_2$	20 mM

2.2.3 Bacterial growth and storage

B. subtilis or E. coli cells were cultivated in Luria Britani (LB), Difco antibiotic medium no. 3 (PAB), competence medium or M9 medium (Kleijn *et al.*, 2010) depending on the experiments' requirements. Fresh cultures were inoculated with overnight culture and grown at 30 or 37˚C with continuous shaking. For growth curves the OD_{600} was recorded every 15 min when cells were grown in nutrient rich medium and every 30 min when grown in minimal medium. For solid media, 1% agar (Bacteriological agar no. 1, Oxoid) was added in addition to the appropriate amount of supplements (Table 2.3). For short term growth and selection, nutrient agar (Oxoid) plates were used. For long term storage, liquid cultures (in LB) were grown to OD 0.4 to 0.6 and mixed with sterile glycerol to a final concentration of 20% glycerol, frozen in liquid nitrogen and stored at -80˚C.

2.3 DNA methods

2.3.1 Polymerase chain reaction (PCR)

Q5 High-Fidelity DNA Polymerase (NEB, UK) was used for gene amplification during cloning and a Gotaq Flexi DNA Polymerase (Promega, USA) was used for confirming DNA modifications and/or gene deletions. Reactions (20 to 100 µl) were prepared as per the manufacturer's instruction including 0.3 µM forward and reverse primers, 0.2 mM dNTPs, reaction buffer, DNA template and polymerase. The PCR amplification steps consisted of an initial denaturation (98°C, 2 min), 30 amplification cycles and a final oligonucleotides extension step (72°C for 4 min). Each amplification cycle consisted of denaturation (98°C, 10 s), annealing (2°C lower than the oligonucleotides melting temperatures, 30 s) and oligonucleotide extension (72°C, 30 s/kb).

2.3.2 Isolation of plasmid DNA

E. coli DH5α cells carrying the plasmid were grown overnight in 5 ml LB with appropriate antibiotics at 37°C. Cells were pelleted by centrifugation (3893 *g*/ 5 min) and plasmids were purified by using a QIAprep Spin Miniprep Kit (Qiagen) as per the manufacturer's instructions.

2.3.3 Purification of DNA products

PCR amplified DNA or plasmid DNA digested with restriction endonucleases were purified using QIAquick PCR Purification Kit (Qiagen, Germany) as per the manufacturer's instructions.

2.3.4 Agarose gel electrophoresis of DNA fragments

DNA loading dye (phenol red) was mixed with DNA fragments at a 1:3 ratio and loaded to a 1% agarose gel made with TAE buffer (2 M Tris/HCl pH 8.3, 5.7% acetate, 50 mM sodium acetate). A constant voltage (100 V) was applied for 1 h followed by the immersion of the gel in a TAE buffer with 0.75 µg/ml ethidium bromide for 15 min. Bands were visualised with a UV transilluminator and pictures were taken using a lumenera USB 2.0 camera.

2.3.5 Restriction endonuclease (RE) digestion

Restriction enzymes were obtained from Roche, New England, Biolabs or Promega and they were used as per the manufacturer's instructions. Samples contained DNA, the manufacturer's recommended buffer and enzymes and were incubated for 3 h at 37˚C. Enzymes were deactivated by incubation at 65˚C or 80˚C for 20 min. alternatively, with heat stable enzymes, a PCR cleanup kit was used to stop the reaction.

2.3.6 DNA dephosphorylation reaction

Restriction digested plasmids were dephosphorylated using shrimp alkaline phosphatase (SAP, Usb). The reaction was performed directly in the restriction endonuclease buffer with the addition of phosphatase (1 µl) and incubating at 37˚C for 1h.

2.3.7 Ligation of DNA

DNA fragments with compatible ends were ligated using a T4 DNA ligase (Roche, Switzerland) as per the manufacturer's instructions. The reaction consisted of DNA fragments, a provided ligation buffer and 1 unit of T4 ligase. Samples were incubated overnight at 4˚C then heated at 80˚C for 15 min followed by a transformation into *E. coli* or *B. subtilis* cells.

2.4 *Bacillus subtilis* methods

2.4.1 *Bacillus subtilis* transformation

The method was performed as published (Anagnostopoulos and Spizizen, 1961) with modifications (Hamoen *et al.*,2002). Competence medium (5 ml) (Table 2.5) was inoculated with *B. subtilis* strains and incubated overnight at 30°C with agitation. Fresh competence medium (5 ml) was inoculated with 500 µl of the overnight culture and incubated for 3 h at 37°C with shaking. Pre-warmed starvation medium (5 ml) (Table 2.6) was added to the previous culture and cells were incubated at 37°C for another 2 h with shacking (cells are competent). DNA (1-3 ng/ml) was added to competent cells (900 µl) and incubated at 37°C for 1 h. Cells were plated on nutrient agar plates with appropriate antibiotics and incubated overnight at 37°C.

Table 2.4 SMM medium composition

SMM medium	concentration
Ammonium sulphate	0.2%
Dipotassium phosphate	1.4%
Potassium dihydrogen phosphate	0.6%
Sodium citrate dihydrate	0.1%
Magnesium sulphate	0.02%

The pH was adjusted to 7.5

Table 2.5 Competence medium composition

Competence medium	Volume
SMM medium	10 ml
Glucose (40%)	125 µl
Tryptophan solution 2 mg/ml	100 µl
1 M $MgSO_4$	60 µl
Casamino acid (20%)	10 µl
Fe-NH_4-citrate (0.22%)	5 µl

Table 2.6 Starvation medium composition

Starvation medium	Volume
SMM medium	10 ml
Glucose (40%)	125 µl
1 M $MgSO_4$	60 µl

2.4.2 Purification of chromosomal DNA

Luria Broth (LB) medium (5 ml) was inoculated with cells from an overnight culture and incubated for 5 h at 37˚C. Cells were pelleted (3893 *g/* 5 min) and resuspended with 100 µl EDTA (50 mM). Lysozyme [3 µl of a 10 mg/ml stock prepared in TES buffer (0.2 M Tris/HCl, 5 mM EDTA, 100 mM NaCl, pH 7.5)] and RNase (3 µl of a 10 mg/ml stock in TES buffer) were added to the suspension and samples were incubated for 1 h at 37˚C. Nuclei lysis solution (Promega) (500 µl) was added and cells were incubated for 5 min at 80°C then cooled down to room temperature (25°C). Protein precipitation solution (200 µl) was added and the mixture and vortexed for 20 s at high speed. Cells were incubated afterwards on ice for 10 min then centrifuged for 10 min at 13000 *g*. The supernatant was transferred to a clean microfuge tube containing 600 µl of isopropanol (Sigma, Germany), mixed gently then centrifuged (13000 *g*/10 min/ 4°C). The supernatant was discarded and 600 µl of 70% ethanol was added to the pellet. Samples were centrifuged as before, the supernatant was discarded carefully and the tubes were left to dry. DNA was resuspended in distilled water (100 µl) and incubated at 65°C for 15 min.

2.5 *Escherichia coli* methods

2.5.1 Generation of competent cells

DH5α or BL21(DE3) cells were grown in 10 ml LB for overnight at 37˚C. LB medium (50 ml) was inoculated with 500 µl of the overnight culture and cells were grown at 37°C to OD_{600} 0.5. Cells were pelleted by centrifugation (3893 *g/* 10 min/ 4˚C) and resuspended in cold TFB1 solution (100 mM RbCl, 50 mM $MnCl_2$, 30 mM potassium acetate, 10 mM $CaCl_2$, 15% glycerol, pH 5.8). The suspension was incubated on ice for 90 min then pelleted again as before in 2 ml cold TFB2 solution (10 mM MOPS, 10 mM RbCl, 75 mM $CaCl_2$, 15% glycerol, pH 6.8). Aliquots of 100 µl of the previous suspension were transferred into sterile tubes then stored immediately at -80°C.

2.5.2 Transformation of competent cells

Cells were thawed on ice for 10 min and the DNA (600 ng/ml) was added and incubated on ice for 15 min. Cells were heat-shocked for 60 s at 42°C in a water bath, then transferred back on ice for 5 min. Cells were plated on nutrient agar plates with appropriate antibiotics and incubated overnight at 37°C.

2.6 Cloning

2.6.1 Ligase free cloning

This experiment was adopted from (Richardson *et al.*, 2016) and requires two sets of primers, the first and second sets were used to amplify the plasmid and the insert, respectively (Figure 2.1). The 5' end of the insert primers should include one homologue and one complementary sequence to the plasmid primers. The plasmid and the insert were amplified using standard conditions (Section 2.3.1). PCR products were analysed using agarose gels. Products were then mixed at a 1:1 ratio (30 µl total volume) and heated to 98°C for 2 minutes in a heat block. The mixed products were then incubated at RT for 2 minutes. This heating/cooling step was repeated twice. On the last cooling step the mixture was left in the heat block to cool down slowly to a temperature of 45°C. Restriction enzyme buffer was added to the mix in addition to the restriction endonuclease DpnI (1 µl) and incubated for 3 h at 37˚C, followed by transformation into *E. coli* DH5α (Section 2.5.2)

2.6.2 Construction of plasmids

Two methods were used for the insertion of DNA fragments into plasmids. All constructed plasmids were transformed into *E. coli* DH5α cells.

The first was the ligase free method which required 4 sets of primers and 2 DNA templates, plasmid DNA and genomic DNA (section 2.6.1). pET-28a(+) plasmid was amplified using JS98-JS99 primers, and *pbpC**, *pbpB**, and *yrrL* were amplified using the oligonucleotides JS130-JS131, JS132-JS133 and JS134-JS135, respectively (Table S1).

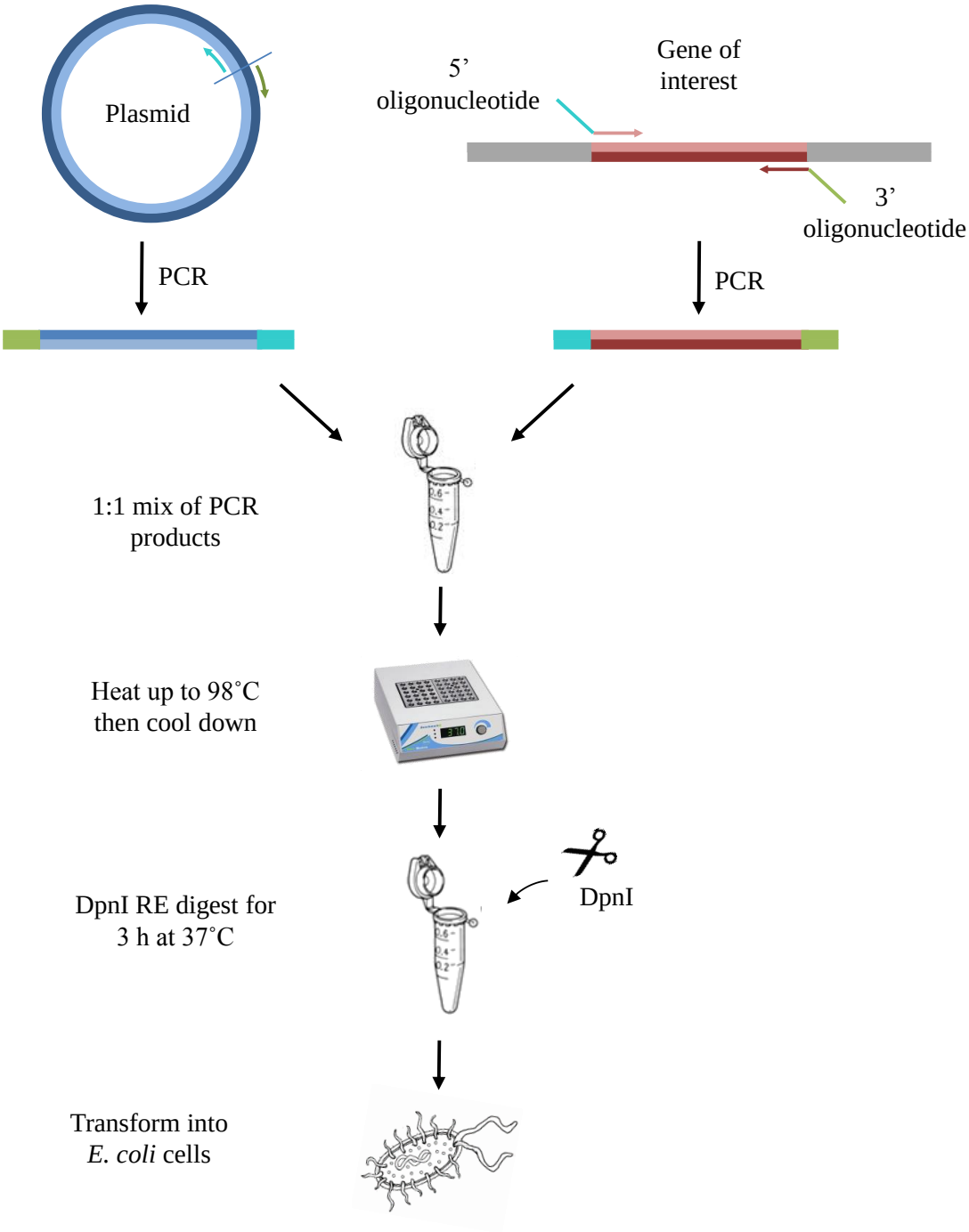

Figure 2.1 Ligase free cloning diagram

Diagram showing the steps of the ligase free cloning experiment. DNA amplification for the plasmid and gene of interest using PCR. DNA products were mixed at a 1 to 1 ratio and heated up to 98˚C for 2 min. Afterwards, Samples were cooled down for 2 min. the heating/ cooling step was repeated 3 times followed by the addition of the RE DpnI to digest the DNA templates. Three hours later, *E. coli* competent cells were transformed with the whole mix. Microfuge tube image was adopted from StarLab webpage. The heat-block picture adopted from Benchmark Scientific webpage. The bacteria clipart was adapted from pinterest.co.uk

For the second method, plasmid DNA and PCR fragments were digested with the same RE enzymes and ligated as previously described (Section 2.3.5 and 2.3.7). The plasmid pDR111 was used for the construction of strains JS01 and JS04. The plasmid pAPNC213 was used for the construction of strains JS02 and JS03. The oligonucleotides used to amplify the DNA fragments mentioned above can be found in Table S1.

Table 2.7 Oligonucleotides and restriction enzymes used for the construction of plasmids

Plasmids	Restriction enzymes	oligonucleotides	Description/comments
pJS01	SalI	JS05	5' *ugtP*
	SphI	JS06	3' *ugtP*
pJS02	BamHI	JS07	5' *pgcA*
	SacI	JS08	3' *pgcA*
pJS03	SalI	JS09	5' *gtaB*
	EcoRI	JS10	3' *gtaB*
pJS04	SalI	JS05	5' *ugtP*
	SphI	JS104	3' *ugtP* S827
pJS05	NdeI	JS59	5' *pbpC*
	BamHI	JS60	3' *pbpC*
pJS06	NdeI	JS63	5' *pbpC*
	BamHI	JS60	3' *pbpC*
pJS07	NheI	JS84	5' *pbpB*
	BamHI	JS85	3' *pbpB*
pJS08	NheI	JS94	5' *pbpB*
	BamHI	JS85	3' *pbpB*

2.6.3 Construction of strains

Gene knockouts were achieved by replacing the gene coding sequence with an antibiotic resistance cassette (Fabret *et al.*, 2002). The sequence upstream and downstream (2 kb) of the gene of interest were amplified by PCR. Restriction sites were introduced in the 3' end of the upstream amplicon and the 5' end of the downstream amplicon. A resistance cassette was amplified with the same restriction sites aforementioned. The products were digested and ligated with equimolar concentrations (1.5 µg of each) then transformed into *B. subtilis* competent cells. Successful transformants grew on plates with antibiotics and a further PCR check was performed for the confirmation of mutants in addition to sequencing if necessary. BSB1 or 168CA genomic DNA were used for the amplification of *B. subtilis* coding sequences.

The plasmids pMUTIN4 and pCotC-GFP were used for the amplification of erythromycin and chloramphenicol cassettes, respectively.

JS03 was transformed with pJS01 creating the strain JS05. JS04 was transformed with pJS02 creating the strain JS07. JS09 was transformed with pJS03 creating the strain JS12. To confirm double cross-over insertion, cells were grown on nutrient agar plates with starch and exposed to iodine. Cells with a double crossover cannot digest starch due to AmyE inactivation and failed to produce a halo around the colonies when exposed for 2 min to iodine vapour.

Table 2.8 Oligonucleotides and restriction enzymes used for the construction of strains

Strains	Restriction enzymes	Oligonucleotides	Description/comments
168CA *gtaB::erm*	-	JS43	5' *gtaB* upstream
	XbaI	JS69	3' *gtaB* upstream
	XbaI	JS67	5' *Erm*
	EcoRI	JS68	3' *Erm*
	EcoRI	JS70	5' *gtaB* downstream
	-	JS046	3' *gtaB* downstream
BSB1 S827*::erm*	-	JS101	5' S827 upstream
	XbaI	JS102	3' S827 upstream
	XbaI	JS67	5' *Erm* F
	EcoRI	JS100	3' *Erm* R
	EcoRI	JS103	5' S827 downstream
	-	JS93	3' S827 downstream
BSB1 *ponA::cat*	-	JS35	5' *ponA* upstream
	XbaI	JS57	3' *ponA* upstream
	XbaI	JS51	5' *Cm* F
	EcoRI	JS53	3' *Cm* R
	EcoRI	JS56	5' *ponA* downstream
	-	JS36	3' *ponA* downstream

2.7 Microscopy

2.7.1 Microscopic imaging

Microscopic images were taken using inverted Nikon eclipse Ti microscope coupled to a Sony Cool-Snap HQ2 CCD camera (Roper scientific) operated by Metamorph 6 imaging software (Universal imaging). Cell were grown in LB media and images were taken during exponential phase (OD_{600} 0.5) unless otherwise mentioned. Samples (0.5 µl) were mounted on 1% agarose and imaging was performed with brightfield illumination with 300 ms exposure time. For membrane or nucleoid staining, cells were mounted on agarose with Nile red dye (1 µg/ml, Molecular Probes) or DAPI (1 µg/ml, Sigma), respectively (Figure 2.2). All images were analysed with ImageJ (Schneider *et al.,* 2012).

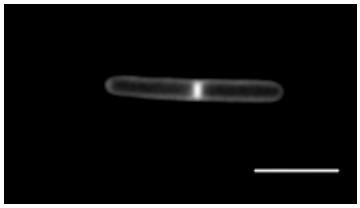

Figure 2.2 Nile red membrane dye for BSB1 cell.
Fluorescent microscope for BSB1 cells with membrane dye during exponential phase. Bar = 4 µm.

2.7.2 Immunofluorescence

Microscopic images were taken using a spinning disk microscope coupled to a Sony Cool-Snap HQ2 CCD camera operated by Metamorph 6 imaging software (Universal imaging). Cells were grown to OD_{600} 0.5 followed by the addition of an equal volume of fix buffer (5% paraformaldehyde in PBS). The mixture was cooled down on ice for at least 30 min. Cells were washed 3 × in PBS and resuspended in GTE buffer (50 mM glucose, 25 mM Tris/HCl, 10 mM EDTA, pH 8.0). Cells were spotted on a dry multiwell slide and allowed to stand for up to 5 min. The solution was aspirated off and the slide left to dry. Polylysine (0.01%) was spotted onto the cells for 2 min, aspirated off and cells were allowed to dry. Cell spots were treated with lysozyme (10 mg/ml), washed with PBS, and allowed to dry. Cells were rehydrated with PBS for 2 min then blocked with PBS buffer with 2% BSA for 15 min. The primary antibody was added to the cells and left for overnight at 4°C. Cell spots were washed 10 × with PBS. The secondary antibody was added and the slide was incubated at room temperature in the dark for 1.5 h. Cells washed 10 × with PBS, DAPI (0.2 µg/ml in antifade) was added, and slides were

ready for imaging. All images were analysed with Metamorph 6 imaging software. Fluorescence data were sorted using Python7 and Heat maps were created using ImageJ.

2.7.3 Transmission electron microscopy

A Philips CM 100 Compustage (FEI) Transmission Electron Microscope coupled to an AMT CCD camera (Deben) was used to collect images for several mutant cells. The growth and fixation of cells and the imaging were done by myself, whereas the dehydration and the processing of the samples were done by Kathryn White at the electron microscopy unit at Newcastle University. Cells were grown in LB media to OD_{600} 0.5 at 37˚C, mixed in a 1:1 ratio with fix buffer I (2% glutaraldehyde, 0.1 M sodium cacodylate) and incubated at 4˚C for overnight. Cells were pelleted then washed with 0.1 M sodium cacodylate buffer followed by a secondary fixation step with 1% osmium tetroxide in water for 1 h. Cells were dehydrated using graded acetone (25%, 50%, 75% and 100%). Subsequently, cells were impregnated sequentially in 25%, 50%, 75% and 100% resin (in methanol). A final embed was performed in 100% resin at 60˚C for 24 to 36 h. to check if cells were not present, sections of 0.5 µm thickness were cut and stained with 1% toluidine blue in 1% borax. Ultrathin sections of 70 nm were then cut with a diamond knife using a Leica EM UC7 ultramicrotome. Sections were stretched with chloroform to eliminate compression, transferred to a Pioloform-filmed copper grids and stained on a Leica EM AC20 automatic staining machine with 2% aqueous uranyl acetate 3% lead citrate.

2.8 Protein Methods

2.8.1 Sodium dodecyl sulphate-polyacrylamide gel electrophoresis (SDS-PAGE)

SDS-PAGE was used to estimate the molecular weight of the proteins and their purity. It was used in protein purifications, western blots, and bocillin assays. BIO-RAD equipment was used with 12% acrylamide gels submerged in Tris buffer (20 mM Tris/HCl, 192 mM glycine, 0.1% SDS, pH 8.3). Protein samples (20 µl) were mixed with 10 µl of the loading buffer, boiled for 10 min at 100˚C and centrifuged for 30 s at 18000 *g*. The supernatant (20 µl) was loaded to the gel wells and the gel was run at 100 V to completion. Gels were stained with Coomassie brilliant blue for 8 min on a shaker, then destained with (30% ethanol, 60% H_2O, 10% acetic acid) for 8 min. Sufficiently destained gels were scanned using an EPSON perfection V350 scanner and the accompanying software.

2.8.2 Western Blot

A BIO-RAD wet-blot system was used for this experiment. Proteins were separated by SDS-PAGE and transferred to a nitrocellulose membrane. The transfer was done in buffer I (20 mM Tris/HCl, 192 mM glycine, 0.1% SDS, 10% methanol, pH 8.3) with a current of 0.35 A for 1 h. The membrane was submerged in Tris-buffered saline (TBS, 10 mM Tris/HCl, 0.09% NaCl, pH 7.4) supplemented with 0.5% casein (blocking buffer) overnight and stored at 4˚C. The buffer was discarded and the membrane was submerged in 10 ml TBS with a protein specific antibody and incubated at room temperature for 90 min. The membrane was washed with 3 × 10 ml TBST buffer (10 mM Tris/HCl, 0.09% NaCl, 0.08% Tween, pH 7.4) for 10 min. TBS buffer (10 ml) containing a secondary antibody was added to the membrane followed by incubation for 90 min at RT. Another membrane wash using 3 × 10 ml TBST buffer was performed for 10 min/wash and an enhanced chemiluminescence ECL Prime kit (GE Healthcare) was used for antibody labelling as per the manufacturer's instruction. Blots were visualized using ImageQuant LAS4000mini biomolecular imager (GE Healthcare) with accompanying software.

2.8.3 Determination of protein concentration in solution

The concentration of proteins in buffers containing Triton X-100 were measured using a BCA protein assay kit (Thermo scientific) as per the manufacturer's instruction. Concentrations of soluble proteins were measured using a Nano-drop spectrophotometer with ND1000 V3.7.1 software.

2.9 Protein purification methods

2.9.1 Purification of PBP1

The PBP1 purification protocol was adopted from (Rismondo *et al.,* 2016) and modified. BL21(DE3) pET28a (+)::*ponA* cells were grown in 2 × 50 ml LB for 4 h at 37˚C. LB medium (5 × 1 l) with 50 µg/ml kanamycin and 20 ml/l auto-induction medium (250 mg/l glycerol, 100 g/L α-lactose and 25 g/L glucose) was inoculated with 50 ml of the previous culture and cells were grown at 30˚C for 18 h. Cells were harvested then resuspended in 130 mL lysis buffer (50 mM Hepes/NaOH, 500 mM NaCl, 3 mM $MgCl_2$, 0.3 mM DTT, pH 7.5) and supplemented with 1/1000 protease inhibitor cocktail (PIC), phenylmethylsulfonylfluoride (PMSF, 100 mM stock)

and desiccated DNase (≈ 1 mg). Cells were sonicated for 3 × 20 seconds at 5, 16, 22, 33, 44 and 60 W. Cell membranes were pelleted by ultracentrifuge at 133907 *g* for 1 h at 4˚C. Membrane pellets were resuspended in 120 ml resuspension buffer (50 mM Hepes/NaOH, 500 mM NaCl, 3 mM $MgCl_2$, 2% Triton X-100, 15% glycerol, 10 mM β-mercaptoethanol, pH 7.5) supplemented with PIC and PMSF as before and stirred for 3 h at 4˚C. Membrane extracts were ultracentrifuged at 100000 *g* for 1 h at 4°C and the supernatant was supplied with 20 mM imidazole. The first purification step was done with a 5 ml HisTrap HP column by using an ÄKTAprime plus FPLC. The column was equilibrated with 50 ml running buffer (50 mM Hepes/NaOH, 500 mM NaCl, 3 mM $MgCl_2$, 0.2% reduced Triton X-100, 15% glycerol, 20 mM imidazole, pH 7.5). The protein mixture was loaded to the column via a 50 ml superloop at a flow rate of 1 ml/min, followed by column washing with the same running buffer. Proteins were eluted at a flow rate of 1 ml/min with elution buffer (same as running buffer with 250 mM imidazole). Protein samples were mixed with restriction grade thrombin and dialysed overnight at 4˚C against 3 × 1 l dialysis buffer (25 mM Hepes/NaOH, 300 mM NaCl, 10% glycerol, 0.2% Triton X-100, pH 8.5). Afterwards, an ion exchange chromatography was performed using Äkta Prime FPLC with a HiTrap SP HP column. The column was washed with 50 ml distilled water followed by 50 ml of dialysis buffer supplemented with 0.2% Triton X-100 (buffer I). The dialysed protein samples were injected into the column at a 1 ml/min flow rate. The column was washed with 30 ml buffer I and proteins were eluted in a 200 ml gradient with buffer II (10 mM Hepes/NaOH, 1 M NaCl, 3 mM $MgCl_2$, 0.2% Triton X-100, 12% glycerol, pH 7.5). The third purification step consisted of a size exclusion chromatography using a Superdex 75 HR16/60 ml column that was washed with water and then equilibrated with SEC buffer (10 mM Hepes/NaOH, 300 mM NaCl, 3 mM $MgCl_2$, 0.2% Triton X-100, 12% glycerol, pH 7.5). Protein samples were injected into the column at 0.5 ml/min flow rate and 4 ml fractions were collected. Collected samples were analysed by SDS-PAGE.

2.9.2 Purification of PBP2B

BL21(DE3) pET28a (+)::*pbpB* cells were grown in 2 × 50 ml LB overnight at 30˚C. Fresh LB medium (3 × 1 l) with 50 µg/ml kanamycin was inoculated with 30 ml of the overnight culture and cells were grown at 37˚C to an OD_{578} of 0.5. The expression of PBP2B was induced with 1 mM IPTG for 3 h at 30˚C. Cells were pelleted by centrifugation (6371 *g* / 4˚C/ 15 min) and resuspended in 40 ml buffer I (25 mM Tris/HCl, 10 mM $MgCl_2$, 1 M NaCl, pH 7.5). 1/1000 PIC and PMSF were added and desiccated DNase (≈ 1 mg). Cells were sonicated for 3 × 20 s at 5, 16, 22, 33, 44 and 60 W. Membrane proteins were pelleted by ultracentrifuge (133907 *g* /

4˚C/1 h) and the soluble fraction was discarded. The pellet was resuspended in 50 ml running buffer (25 mM Tris/HCl, 10 mM $MgCl_2$, 1 M NaCl, 20 mM imidazol, 10% glycerol, 2% Triton X-100, pH 7.5). Nickel beads were washed with 30 ml distilled water and 30 ml running buffer. Solubilised proteins were added to the equilibrated beads and mixed gently for 24 hr at 4˚C. The mixture was applied to a gravity column where unbound protein flowed through the filter. The beads were washed with 40 ml running buffer. Bound proteins were eluted using elution buffer (25 mM Tris/HCl, 10 mM $MgCl_2$, 400 mM imidazole, 1 M NaCl, 0.2% Triton X-100, pH 7.5) and 3 ml fractions were collected. Restriction grade thrombin (1 µl per 1 ml protein) was added to the appropriate elution fractions that were dialysed against 2 × 2 L of dialysis buffer I (25 mM Tris/HCl, 500 mM NaCl, pH 6.0) and 2 × 2 l of dialysis buffer II (25 mM Tris/HCl, 100 mM NaCl, pH 6) overnight at 4˚C. Ion exchange chromatography was performed using an Äkta Prime FPLC with a HiTrap SP HP column, which was washed with 50 ml distilled water followed by 50 ml of buffer I (25 mM Tris/HCl, 100 mM NaCl, 0.2% Triton X-100, pH 6). The dialysed proteins were injected into the column and bound proteins were eluted in a gradient buffer II (25 mM Tris/HCl, 1 M NaCl, 0.2% Triton X-100, pH 7.5). Collected samples were analysed for purity by SDS-PAGE.

2.9.3 Purification PBP2B(S309A)

BL21(DE3) pET28a (+)::$pbpB^{(S309A)}$ cells were grown in 2 × 50 ml LB for overnight at 30˚C. LB medium (5 × 1 l) with 50 µg/ml kanamycin was inoculated with 30 ml of the overnight culture and cells were grown at 37˚C to OD_{578} of 0.5. The expression of $pbpB^{(S309A)}$ (*pbpB**) was induced with 1 mM IPTG for 3.5 h at 30˚C. Cells were pelleted by centrifugation (6371 *g* / 4˚C/ 15 min), and resuspended in 80 ml buffer I (25 mM Tris/HCl, 10 mM $MgCl_2$, 1 M NaCl, pH 7.5). 1/1000 PIC and PMSF were added and desiccated DNase (≈ 1 mg). Cells were sonicated for 3 × 20 s at 5, 16, 22, 33, 44 and 60 W. Membrane proteins were pelleted by ultracentrifuge (133907 *g* / 4˚C/1 h) and the soluble fraction was discarded. The pellet was resuspended in 100 ml running buffer (25 mM Tris/HCl, 10 mM $MgCl_2$, 1 M NaCl, 20 mM imidazole, 10% glycerol, 2% Triton X-100, pH 7.5). The subsequent steps consisted of affinity chromatography using nickel beads (1.5 ml) and ion exchange chromatography using a HiTrap SP HP column. The two chromatography experiments were performed as described in section 2.9.2.

2.9.4 Purification of PBP3

BL21(DE3) pET28a (+)::*pbpC* cells were grown in 50 ml LB for overnight at 30˚C. LB medium (3×1 l) with 50 μg/ml kanamycin was inoculated with 30 ml of the overnight culture and cells were grown at 37˚C to an OD_{578} of 0.5. The expression of *pbpC* was induced with 1 mM IPTG for 3 h at 30˚C. Cells were pelleted by centrifugation (6371 *g* / 4˚C/ 15 min), and resuspended in 40 ml buffer I (25 mM Tris/HCl, 10 mM $MgCl_2$, 1 M NaCl, pH 7.5). 1/1000 PIC and PMSF were added and desiccated DNase (≈ 1 mg). Cells were sonicated for 3 × 20 s at 5, 16, 22, 33, 44 and 60 W. Membrane proteins were pelleted by ultracentrifuge (133907 *g* / 4˚C/1 h) and the soluble fraction was discarded. The pellet was resuspended in the appropriate amount of running buffer (25 mM Tris/HCl, 10 mM $MgCl_2$, 1 M NaCl, 20 mM imidazol, 10% glycerol, 2% Triton X-100, pH 7.5). Nickel beads (3 ml) were washed with 30 ml distilled water and 30 ml running buffer. Solubilised proteins were added to the equilibrated beads and mixed gently for 24 h at 4˚C. The mixture was applied to a gravity column where unbound protein flowed through the filter. The beads were washed with 40 ml running buffer. Bound proteins were eluted using elution buffer (25 mM Tris/HCl, 10 mM $MgCl_2$, 400 mM imidazole, 1 M NaCl, 0.2% Triton X-100, pH 7.5) and 3 ml fractions were collected. Restriction grade thrombin was added to the appropriate elution fractions that were dialysed against 2 × 2 l of dialysis buffer I (25 mM Tris/HCl, 500 mM NaCl, pH 8.3) and 2 × 2 l of dialysis buffer II (25 mM Tris/HCl, 100 mM NaCl, pH 8.3) overnight at 4˚C. Ion exchange chromatography was then performed using an Äkta Prime FPLC with a HiTrap monoQ column, which was washed with 50 ml distilled water followed by 50 ml of buffer I (25 mM Tris/HCl, 100 mM NaCl, 0.2% Triton X-100, pH 6). Dialysed protein was injected into the column and bound proteins were eluted in a 200 ml gradient buffer II (25 mM Tris/HCl, 1 M NaCl, 0.2% Triton X-100, pH 6). Collected samples were analysed by SDS-PAGE.

2.9.5 Purification of PBP3(17-668)

BL21(DE3) pET28(a)+ *pbpC*Δ1-51 cells were grown in 20 ml LB for overnight at 30˚C. LB medium (3×1 l) with 50 μg/ml kanamycin was inoculated with 30 ml of the overnight culture and cells were grown at 37˚C to an OD_{578} of 0.5. Plasmid expression was induced with 1 mM IPTG for 3 h at 30˚C. Cells were harvested by centrifugation (6371 *g*/ 15 min/ 4˚C) and resuspended in 40 ml of buffer I (25 mM Tris/HCl, 10 mM $MgCl_2$, 1 M NaCl, pH 7.5). 1/1000 PIC and PMSF were added and desiccated DNase (≈ 1 mg). Cells were sonicated for 3 × 20 s at 5, 16, 22, 33, 44 and 60 W. Cell membranes were pelleted by ultracentrifuge (133907 *g*/ 1 h/ 4˚C). Nickel beads were washed with 30 ml distilled water and 30 ml running buffer (25 mM

Tris/HCl, 20 mM imidazole, 10 mM $MgCl_2$, 1 M NaCl, pH 7.5). The soluble fraction of the pelleted cell membrane was mixed with the equilibrated beads. Imidazole was added to the mix to a final concentration of 20 mM and the mixture was gently mixed for 24 h at 4˚C. The mixture was applied to a gravity column where unbound protein flowed through the filter. The beads were washed with 40 ml running buffer. Bound proteins were eluted using elution buffer (25 mM Tris/HCl, 400 mM imidazole, 10 mM $MgCl_2$, 1 M NaCl, pH 7.5) and 3 ml fractions were collected. Restriction grade thrombin was added to the appropriate elution fractions that were dialysed against 2 × 2 l of dialysis buffer (25 mM Tris/HCl, 100 mM NaCl, pH 8.3) overnight at 4˚C. Ion exchange chromatography was then performed using an Äkta Prime FPLC with a HiTrap monoQ column, which was washed with 50 ml distilled water followed by 50 ml of buffer I (25 mM Tris/HCl, pH 8.3, 100 mM NaCl). The dialysed protein sample was injected into the column. The protein didn't bind to the column and was collected in the flow through. The column was washed with Buffer II (25 mM Tris/HCl, pH 7.5, 1 M NaCl). PBP3 containing samples were concentrated to a volume < 5 ml by centrifugation (3893 *g*/ 4˚C / 15 min). The third purification step consisted of a size exclusion chromatography using a superdex 75 16/60 ml column that was washed with water and then equilibrated with SEC buffer (25 mM Tris/HCl, 500 mM NaCl, pH 7.5). Protein samples were injected into the column and 4 ml fractions were collected. Collected samples were analysed for purity by SDS-PAGE.

2.9.6 Purification of PBP3(S410A)

PBP3(S410A) (PBP3*) was purified according to the PBP3 purification protocol using BL21(DE3) pET28a+::*pbpC** cells. The difference was that PBP3* was dialysed to pH 8.5 instead 8.3, allowing the binding of the protein to the HiTrap monoQ column followed by the elution of PBP3* using a gradient of buffer II (25 mM Tris/HCl, 1 M NaCl, 0.2% Triton X-100, pH 7.5).

2.9.7 Purification of YrrL

YrrL was purified following the same protocol for the purification of PBP2B.

2.9.8 Purification of PBP3 antibody

Affinity chromatography was performed for the purification of antibodies from serum with immobilised antigen. The purification consisted of 2 steps:

Step 1.

CNBr-activated sepharose beads (desiccated) (0.8 g) were placed into a gravity column and washed with 200 ml of 1 mM HCl for 15 min. PBP3 protein, diluted to 0.5 mg/ml using coupling buffer (100 mM $NaHCO_3$, 10 mM $MgCl_2$, 500 mM NaCl, 0.1% Triton X-100, pH 8.3), was applied to the sepharose beads and incubated overnight at 4˚C with mixing. The beads were washed with 25 ml coupling buffer. The remaining active groups of the beads were blocked with 10 ml blocking buffer (200 mM Tris/HCl, 500 mM NaCl, 10 mM $MgCl_2$, 0.1% Triton X-100, pH 8.0). The mix was incubated overnight at 4˚C with mixing. The gravity column was washed 3 × 20 ml with acetate buffer (100 mM sodium acetate, 500 mM NaCl, 10 mM $MgCl_2$, 0.1% Triton X-100, pH 4.8) and blocking buffer. The beads were washed with 5 ml binding buffer (10 mM Tris/HCl, 10 mM $MgCl_2$, 50 mM NaCl, 0.1% Triton X-100, pH 6.8) and stored in 5 ml binding buffer ready for use.

Step 2.

The beads were first washed with 1 × 5 ml elution buffer I (100 mM glycine/HCl, 0.1% Triton X-100, pH 2.0). then washed with 30 ml buffer I (10 mM Tris/HCl, 10 mM $MgCl_2$, 1 M NaCl, 0.1% Triton X-100, pH 7.2). The serum (10 ml) was diluted with 35 ml diluent (10 mM Tris/HCl, 0.1% Triton X-100, pH 7.4) and centrifuged (4500 *rpm* / 4˚C / 10 min). The supernatant was then incubated with the PBP3-sepharose material for 20 hours at 4°C with gentle mixing. The mixture was transferred back to the gravity column, the solution flowed through, and the bead material was collected. Beads were washed with 20 ml buffer I followed by 20 ml buffer II (10 mM Tris/HCl, 10 mM $MgCl_2$, 150 mM NaCl, 0.1% Triton X-100, pH 7.2). Bound antibodies were eluted with 10 × 1 ml of elution buffer I (100 mM glycine/HCl, 0.1% Triton X-100, pH 2.0) into tubes containing 200 µl of elution buffer II (2 M Tris/HCl, pH 8.0). Glycerol (300 µl) was added to each 1.2 ml sample, which was analysed by SDS-PAGE and stored at -80˚C.

2.10 Other protein methods

2.10.1 *In vitro* cross-linking pulldown assay

This method was adapted from (Egan *et al.,* 2015). Proteins (1 µM) were mixed in 200 µl binding buffer (10 mM Hepes/NaOH, 10 mM $MgCl_2$, 150 mM NaCl, 0.05% Triton X-100, pH 7.5). Samples were incubated for 10 min at room temperature followed by the addition of 0.2% w/v formaldehyde (Sigma, USA) and further incubation at 37˚C for 10 min. Blocking buffer (100 mM Tris/HCl, pH 7.5) was added to block the excess cross-linker and samples were incubated for 10 min at room temperature. Samples were applied to 100 µl of washed and equilibrated Ni-NTA superflow beads (Qiagen, The Netherlands) and incubated overnight at 4˚C with gentle mixing. In the absence of cross-linker, proteins were mixed straight away with the Ni-NTA beads. The beads were then washed with 8 × 1 ml wash buffer (10 mM Hepes/NaOH, 10 mM $MgCl_2$, 500 mM NaCl, 50 mM imidazole, 0.05% Triton X-100, pH 7.5) and boiled in SDS–PAGE loading buffer. Beads were then pelleted by centrifugation and samples analysed by SDS–PAGE. Gels were stained with Coomassie brilliant blue (Roth, Germany).

2.10.2 Surface Plasmon Resonance (SPR) assay

Immobilization of PBPs to ampicillin-coated sensor chips.

This method was adapted from (Vollmer *et al.,* 1999). A ProteOn XPR36 system and associated software (BioRad) were used for this experiment. Ampicillin has a free amino group in the side chain that was immobilised to a GLC sensor chip via amino coupling following the standard N-ethyl-N9-(3-dimethylaminopropyl)-carbodimide hydrochloride/N-hydroxysuccinimide procedure recommended by BioRad. The chip temperature was set to 35˚C then initialised with air or glycerol. Buffer lines were put in immobilization buffer (10 mM Tris/maleate, 150 mM NaCl, 0.05% Triton X-100, pH 7.5) and the chip was preconditioned by injecting 0.5% SDS, 50 mM NaOH then 100 mM HCl. The chip was activated by injecting 70 µl of a 1:1 mixture of 400 mM N-ethyl-N9-(3-dimethylaminopropyl)-carbodimide hydrochloride and 100 mM N-hydroxysuccinimide. Ampicillin solution (10 mg/ml in 100 mM sodium acetate buffer, pH 4.6) was applied for 5 min and immobilized to the chip surface giving a response of approximately 80 to 120 RU. Ethanolamine (1 M) was used to block the free remaining activated functional groups on the chip surface. PBPs were injected at optimum µg/ml concentration to the ampicillin matrix (optimal response signal is 1000 to 2000 RUs) at a rate of 30 µl/min for 5 min. As a control, immobilisation buffer with no protein was injected onto the ampicillin

surface. The surface was then rinsed with regeneration buffer (10 mM Tris/maleate, 1 M NaCl, 2% Triton X-100, pH 6.8). β-lactamase solution (0.1 unit/µl, Merck) was injected at to digest the remaining free ampicillin.

Protein-protein interaction studies

Binding assays were performed at 25˚C in running buffer (10 mM Tris/Maleate, 250 mM NaCl, 0.05% Triton X-100, pH 7.5). Proteins to be injected (analyte) were dialysed into 2 × 1 l of dialysis buffer (10 mM Tris/Maleate, 250 mM NaCl, pH 7.5) then centrifuged using a Beckman TLA120.2 rotor (90000 rpm, 30 min, 4˚C) to remove aggregates. The concentration of the protein was measured again and the analytes were diluted in running buffer to 6 concentration ranges from 0 to 2 µM. It was important to make sure the Triton X-100 level in the analyte was as close to the running buffer as possible. Immobilized protein surfaces were regenerated with regeneration buffer (10 mM Tris/maleate, 1 M NaCl, 2% Triton X-100 and pH 7.5) injected for 3 min at 100 µl/min.

Estimation of kinetic parameters

SigmaPlot software (windows version 13.0) was used for kinetic calculations. Several repeats (at least 3) were required across a range of analyte concentrations. The K_D (nM) of ligand binding was based on the assumption of a one site saturation with the use of the equation $y = \frac{Bmax \times x}{(Kd+x)}$ where y is the response (RU) for an analyte concentration in (nM), and B_{max} is the maximum response recorded (RU).

2.10.3 *In vitro* glycosyltransferase activity assay

This method was performed as published with modifications (Banzhaf *et al.,* 2012; Offant *et al.,* 2010; Schwartz *et al.,* 2002) (Figure 2.3). The experiment was performed in a FLUOstar OPTIMA microplate reader (BMG Labtech, Offenburg, Germany) using a medium-binding black 96-well microplate (Greiner Bio-One ref. 655076, Freickenhausen, Germany). Samples (60 µl each) consisted of 0.5 µM of each protein and lysine-dansylated lipid II (10 µM) in 50 mM Hepes/NaOH, 10 mM $CaCl_2$, 20 mM NaCl, 0.5 µg/µl cellosyl, 0.02% Triton X-100 pH 7.5. Samples were prepared without the addition of lipid II, transferred to the microplate and incubated at 30˚C for 3 min. Reactions were initiated by adding lipid II (dissolved in H_2O) to

samples and the GTase activity was measured over the time course of 20 min at 30˚C. The fluorophore was excited with 340 nm wavelength and the emission was recorded at a wavelength of 520 nm. The experiment consisted of 60 cycles of 20 s with orbital shaking. The data shown represent the mean florescence presented as a percentage of initial fluorescence at a given time-point. The gradient of the curve at its steepest point correspond to the rate of reaction.

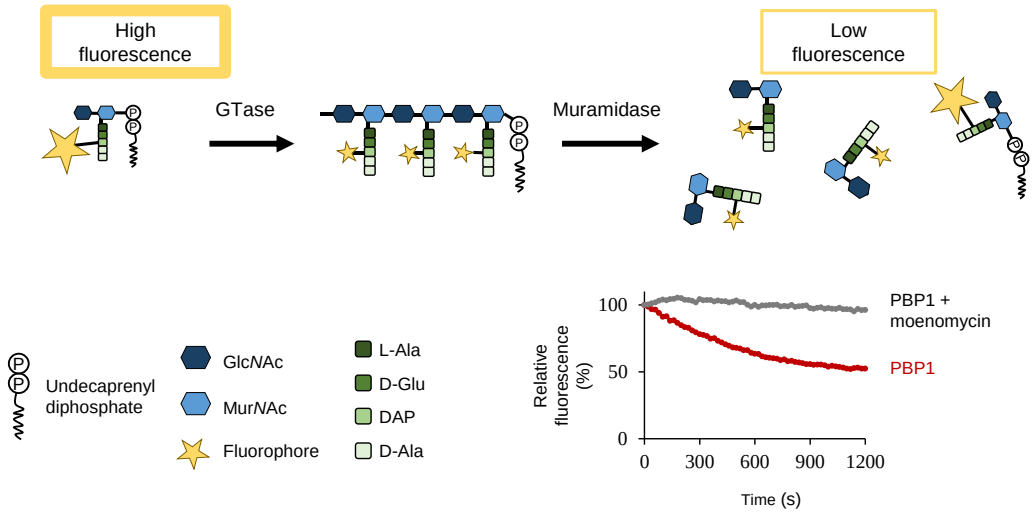

Figure 2.3 *In vitro* glycosyltransferase assay

Fluorescently labelled lipid II is used to monitor the GTase activity of PBPs *in vitro*. In the presence of GTase activity lipid II is polymerised into glycan chains, which are digested by muramidases into muropeptides. Labelled muropeptides has lower level of fluorescence than labelled lipid II. Such decrease in the levels of fluorescence is monitored over time and the data is presented as a percentage of the initial fluorescence.

2.10.4 *In vitro* peptidoglycan synthesis assay

This method was adapted from (Bertsche *et al.*, 2005) (Figure 2.4). The reaction was performed in standard buffer condition (10 mM Hepes/NaOH, 10 mM $CaCl_2$, 20 mM NaCl, 0.02% Triton X-100, pH 7.5). Appropriate amount of [^{14}C]-Glc*N*Ac labelled mDap Lipid II was used to obtain a final concentration of 15 µM in 100 µl. A volume of Lipid II was first dried then resuspended in 5 µl on 0.1% Triton X-100. Protein solution (95 µl total volume) was prepared in a standard buffer condition and left on ice for 10 min. Lipid II was then added to the protein mix which was briefly vortexed and incubated at 37˚C with shaking (850 rpm) in a thermomixer for 1 h. Samples were heated for 4 min at 100˚C to stop the reaction before digestion with muramidase to produce muropeptides for HPLC analysis (Section 2.11.3).

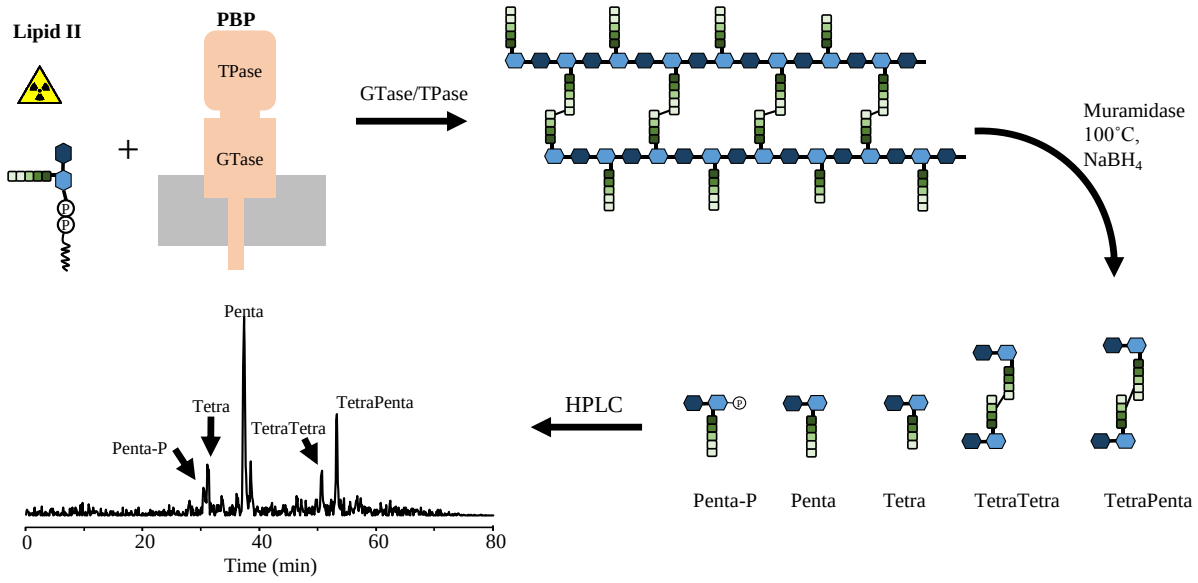

Figure 2.4 *In vitro* peptidoglycan synthesis assays

Radio labelled lipid II is used to test the GTase and TPase activities of PBPs *in vitro*. Lipid II is polymerised into glycan chains by GTase activity and peptides are crosslinked by TPase activity. After 1 hour, the reaction is stopped by boiling followed by digestion of the PG with muramidase generating muropeptides that are subsequently reduced and analysed by HPLC.

2.10.5 Bocillin binding assay

This assay was used to test the binding of β-lactams to the TPase domain of PBPs. The method was adopted from a published protocol (Zhao *et al.,* 1999) with minor modification. PBPs (10 µg) were mixed with 1 ng/µl of the fluorescently labelled β-lactam bocillin (Molecular Probes, Life Technologies, UK) and incubated for 10 min at 37˚C. As a control, the same amount of PBPs were mixed with 1 ng/µl penicillin G and incubated at 37˚C for 10 min prior to the addition of bocillin. Samples were analysed by SDS-PAGE and the final gel was scanned with a Typhoon scanner using a blue FAM channel at 488 nm.

2.11 Cell wall analysis methods

2.11.1 Cell wall purification

This method was adopted from (Atrih *et al.*, 1999) and modified as per (Bisicchia *et al.*, 2011). Culture (1 l) of *B. subtilis* cells was grown to OD600 0.5 then cooled down in an ice bath to 4˚C. Cells were pelleted (10,000 *g*/ 4˚C/ 15 min) then resuspended in 30 ml ice-cold 50 mM

Tris/HCl, pH 7. Cell suspension was dropped into 120 ml of slightly boiling 5% SDS, left to boil for an additional 15 min, and then the lysate was cooled down at room temperature overnight. Lysates were transferred to PPCO Nalgene 50 ml round bottom tubes and centrifuged (12000 *g*/ 30 min/ room temperature). The supernatant was discarded, and the pellet was resuspended in 20 ml of 1 M NaCl. The lysate was centrifuged again as above with 1 M NaCl and then with H_2O_{MilliQ} until the suspension was free of SDS (6 to 8 times). The pellet was resuspended in H_2O_{MilliQ} (6 ml) and transferred to 2 ml screw cap tubes filled to 1/3 with glass beads. Cells were broken down using a bead beater (Thermo FastPrep FP120) with 12 cycles of 3 × 6.5 pulse speed for 20 s. After each cycle the tubes were cooled on ice for a few minutes before the subsequent cycle starts. The broken cells were filtered through a glass frit to remove the glass beads, which were washed with 10 ml H_2O_{MilliQ}. The filtrate was then transferred to a 50 ml Falcon tube and centrifuged (2000 *g*/ 5 min/ room temperature). The supernatant was transferred to a PPCO Nalgene tube while the pellet was resuspended in 25 ml $H_2O_{MilliQ,}$ centrifuged as before and the supernatant was added to the PPCO Nalgene tube, which was centrifuged for 30 min at 25000 *g*. The pellet was resuspended in 10 ml Tris buffer (100 mM Tris/HCl, 20 mM $MgSO_4$, pH 7.5) to which DNase I (10 µg/ml [Sigma]) and RNase (50 µg/ml [Sigma]) were added. The sample was stirred at 37˚C for 2 h followed by the addition of $CaCl_2$ (10 mM) and trypsin (Novagen/Merck), porcine pancreas (100 µg/ml) and stirred for another 18h at 37˚C. 20 ml of 1% SDS was added and the tube was incubated for 15 min at 80˚C in a water bath. The mix was then centrifuged (25000 *g*/ 30 min/ room temperature) and the pellet was resuspended in 10 ml LiCl (8 M). The sample was incubated for 15 min at 37˚C then Centrifuged as above. The pellet was resuspended in 10 ml EDTA (100 mM and pH 7.0), incubated for 15 min at 37˚C then centrifuged as above. The pellet was washed, resuspended and centrifuged twice with 30 ml H_2O MilliQ, then centrifuged and resuspended in 3 ml H_2O MilliQ. The suspension was transferred to a glass container and frozen at -80˚C for at least 1 h then lyophilized for 2 days using an Alpha 1-2 freeze dryer (Biopharma).

2.11.2 Isolation of peptidoglycan from cell wall

Cell wall (5 mg) was transferred to a polyallomer tube for the 100.3 rotor (desktop-UZ) and dissolved in 3 ml hydrofluoric acid at 4˚C for 48 h with stirring. Next, the tube was centrifuged in a precooled TL 100 rotor (90000 *rpm*, 4˚C, and 30 min). The supernatant was discarded and the pellet was washed, resuspended and centrifuged twice with 3 ml with ice-cold H_2O MilliQ, once with 3 ml with ice-cold 100 mM Tris/HCl pH 7.0 and twice with 3 ml with ice-cold H_2O_{MilliQ}, respectively. After washing, the murein was resuspended in 500 µl of ice-cold

H_2O_{MilliQ} and transferred to a 2 ml screw-cap tube. Sodium azide (0.05%) was added and samples were kept at 4˚C.

2.11.3 Muropeptide preparation and analysis

Muropeptides were generated from the digestion of peptidoglycan with cellosyl (Hoechst, Germany) following an established protocol (Glauner *et al.*, 1988). Peptidoglycan was either isolated from cells (Section 2.11.1) or produced in the *in vitro* peptidoglycan synthesis assay (Section 2.10.4). Cellosyl buffer (80 mM NaH_2PO_4, pH 4.8) was added to samples for a final concentration of 20 mM NaH_2PO_4 with 8 µg of cellosyl. Samples were incubated for 2 h at 37°C with shaking (850 *rpm*) for *in vitro* synthesised PG, or overnight for isolated sacculi. Samples were incubated at 100°C for 7 min and centrifuged at 14,000 *rpm* for 10 min. An equal volume of sodium borate (0.5 M, pH 9.0) was added to samples in addition to a full small spatula of solid sodium borohydride and centrifuged at 4000 *rpm* for 30 min. The pH was adjusted between 3 and 4 with 20% phosphoric acid and the sample was transferred to HPLC tubes ready for analysis.

The HPLC analysis was performed using Agilent Technologies Series 1200 HPLC system with a reverse phase column (Prontosil 120-3-C18-AQ 3 µM, Bischoff). For PG isolated from *B. subtilis* cells a linear gradient was used from 100% solvent A (40 mM sodium phosphate pH 4.5 + 0.0003% NaN_3) to 100% solvent B (40 mM sodium phosphate, 20% methanol, pH 4.0) at 55˚C, for 5 h. For PG isolated from the *in vitro* peptidoglycan synthesis assay a linear gradient was used from 100% solvent A (50 mM sodium phosphate pH 4.31 + 0.0002% NaN_3) to 100% solvent B (75 mM sodium phosphate, 15% methanol, pH 4.75) at 55˚C, for 90 min. Muropeptides were detected by a UV detector at 205 nm and [^{14}C]-labelled muropeptides were detected by an online scintillation counter (Agilent Technologies). Laura software v4.1.7.70 (LabLogic Systems Ltd) was used for the data analysis. The detected muropeptides are shown in figure S2. The levels of peptides in crosslink (x) was calculated using the formula x = 100 - (%TetraTetra + %TetraPenta).

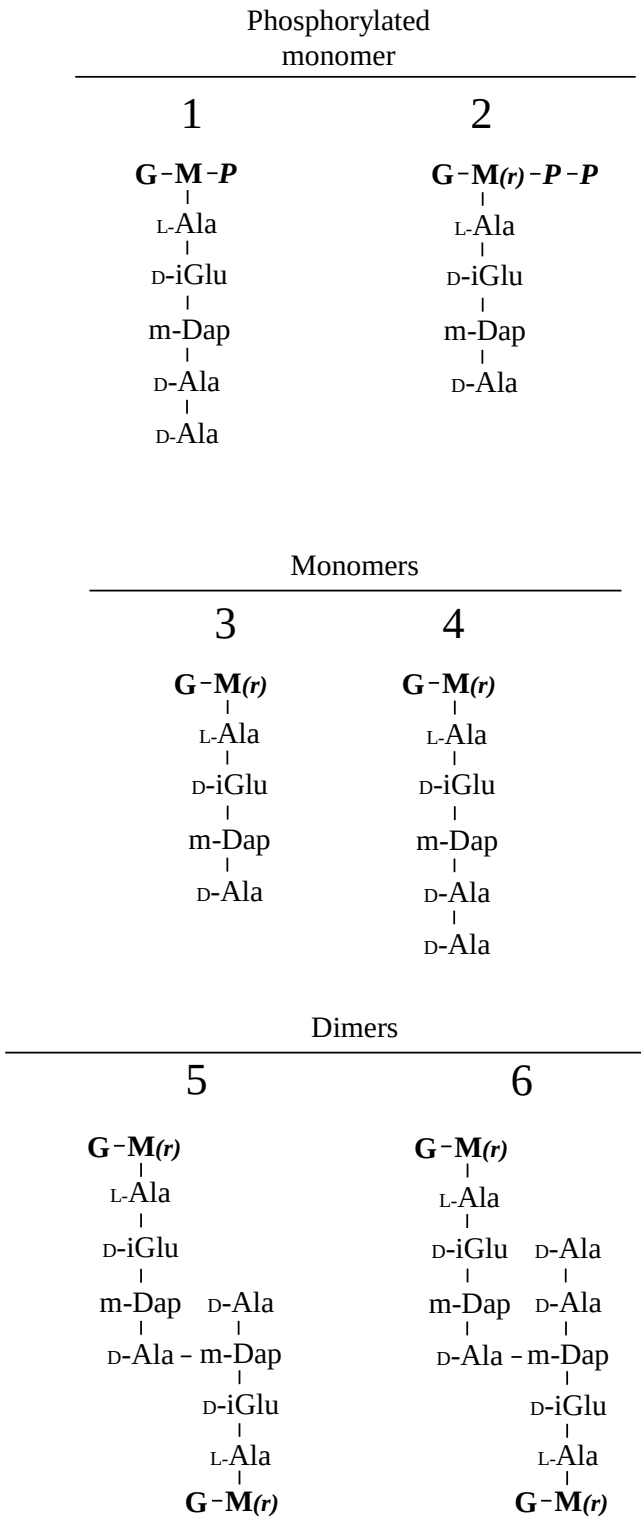

Figure 2.5 Chemical structure of muropeptides detected by HPLC

The chemical structures of muropeptides from *in vitro* PG synthesis assays. 1, Penta-P, the product of glycan chain ends and/or unreacted substrate. 2, Penta-P-P, produced after boiling lipid II for a prolonged time. 3, Tetra-peptide, the product of both GTase and the CPase activities. 4, Penta-peptide, the product of GTase alone. 5, TetraTetra-, the product of GTase, TPase and CPase activities. 6, TetraPenta-, product of GTase and TPase activities.

Results

3 The impact of carbon metabolism on the synthesis of PG

3.1 Effects of glucolipid absence on cell growth and morphology

3.1.1 Introduction

Changes in the glucose and magnesium ion concentrations of the culture medium ameliorated the growth of several mutants with cell wall defects probably by changing their metabolic status (Formstone and Errington, 2005; Murray *et al*., 1998a). The focus of this part of the work was to study the effect of carbon metabolism on cell wall synthesis in *B. subtilis*. It was suggested that proteins involved in the synthesis of the LTA glucolipid anchor, such as UgtP, PgcA and GtaB, link nutrient availability to cell division, however, the impact of these proteins on the cell wall is still unclear (Weart et al., 2007). In this work, we studied the effect of the absence of UgtP, PgcA or GtaB on cell growth and morphology. We also studied the effect of glucolipid absence on PG synthesis. As part of the AMBER-ITN consortium, we used the BSB1 strain as the wild type for these experiments (Nicolas *et al.,* 2012).

3.1.2 Strains with single deletions in *ugtP, gtaB* and *pgcA* do no exhibit growth defects

To study the effect of the absence of UgtP, GtaB or PgcA on cell growth and morphology, we replaced the coding sequence of these genes with neomycin, tetracycline and erythromycin resistance cassettes, respectively. Copies of the deleted genes were introduced in the *amyE* or *aprE* loci to create complementation strains (Section 2.6.3). For Δ*ugtP* complementation, a copy of the *ugtP* gene was introduced in the *amyE* locus under the control of a hyper-*spank* IPTG inducible promoter. For Δ*pgcA* or Δ*gtaB* complementation, a copy of the gene was introduced in the *aprE* locus under a P_{spac} IPTG inducible promoter. The growth and morphology of strains with single deletions in *ugtP*, *gtaB* and *pgcA* were studied and compared to wild type. Complementation strains were characterised in presence or absence of inducer. The *ugtP*, *gtaB* and *pgcA* mutants in addition to the complementation strains showed similar growth curves to wild-type cell (Figure 3.1).

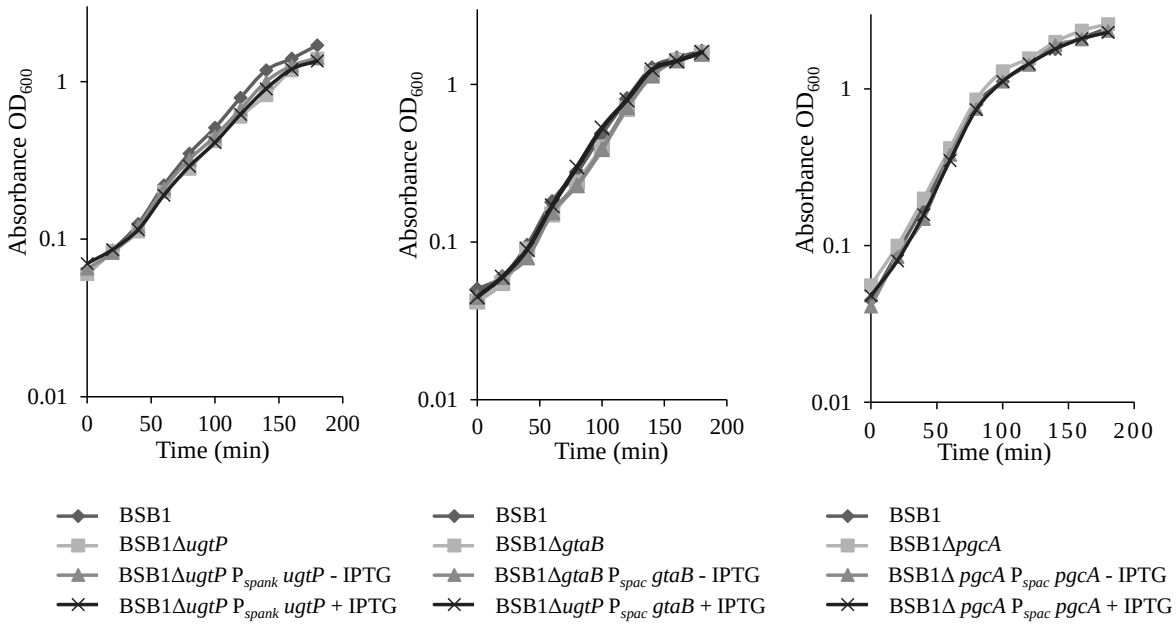

Figure 3.1 Growth curves for the *ugtP, gtaB, pgcA* mutants and complementation strains

The growth curves for mutants and corresponding complemented strains in LB media at 37˚C. *UgtP*, *gtaB* or *pgcA* complementation strains were grown in the presence or absence of IPTG. All mutants had similar growth curves to BSB1.

3.1.3 The absence of UgtP, GtaB or PgcA causes short cells

The morphology of cells lacking UgtP, GtaB or PgcA during exponential phase was studied using fluorescence microscopy and Nile red membrane dye was used to visualise possible cell membrane defects (section 2.7.1). The white spots that were observed at the cell periphery (in <1% of the cells) are artefacts of the dye. The cell widths and cell lengths for all mutants were quantified using ImageJ. The absence of UgtP caused shorter and wider cells than wild type (Figure 3.2). The *ugtP* complementation strain showed longer cells than the *ugtP* mutant in the absence of inducer which was probably due to the leaky expression of the ectopic *ugtP*. The presence of 0.1 mM IPTG was sufficient to cause longer and thinner cells than wild type, in addition to a chaining morphology (Figure 3.2 and 3.5). Septum mislocalisation was also observed occasionally (≈ 5% of cells had septal mislocalisation), and the frequency of such mislocalisation increased in presence of 1 mM IPTG (≈ 20%). This morphology was probably caused by the inhibition of FtsZ polymerization by UgtP (Weart *et al.*, 2007).

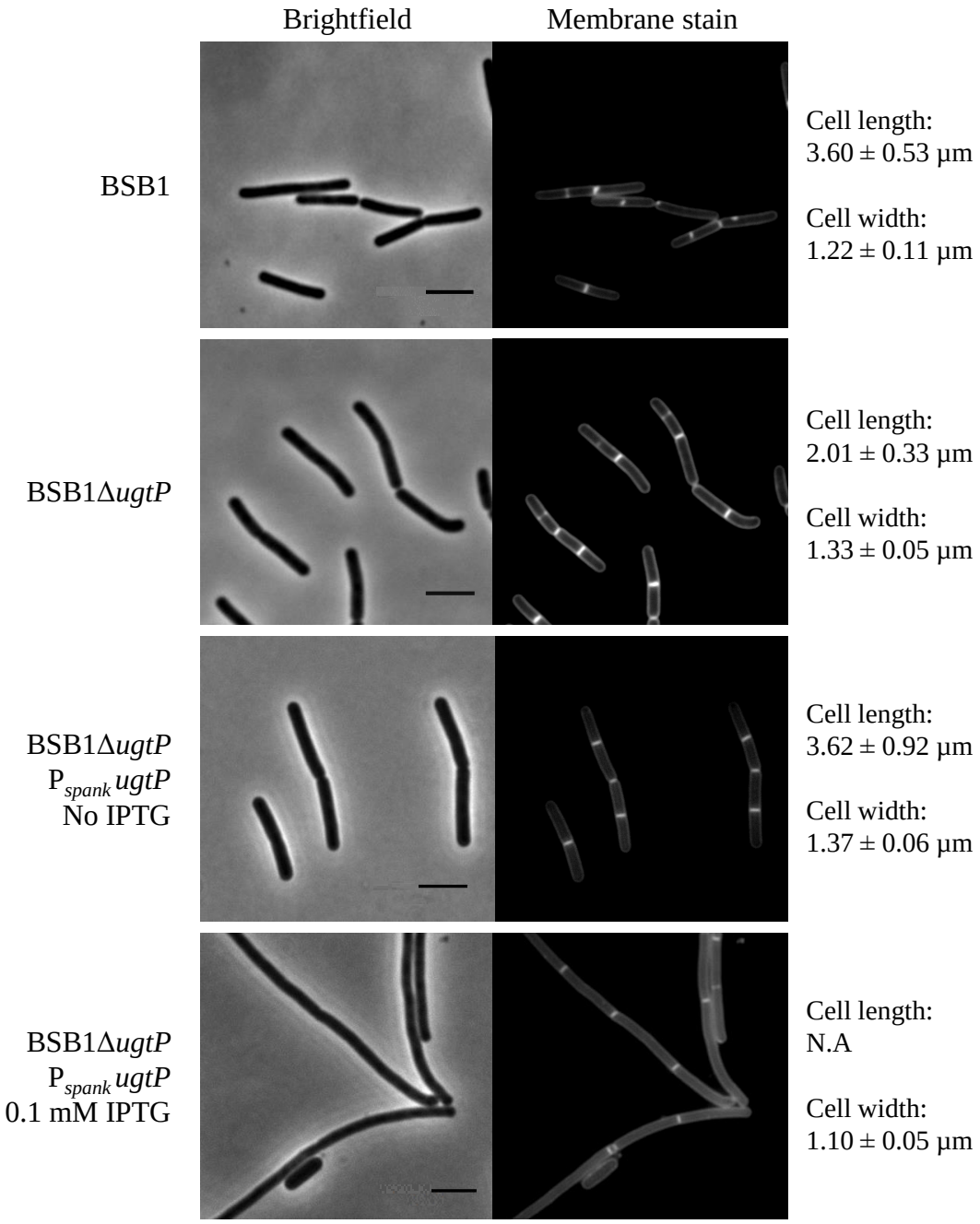

Figure 3.2 Morphology and complementation of cells lacking UgtP

Phase contrast and cell membrane stained images of BSB1, BSB1Δ*ugtP,* and BSB1Δ*ugtP* P$_{spank}$ *ugtP* mutants. The *ugtP* complementation mutant was grown in the presence or absence of IPTG. Cell dimensions represent the mean cell length ± standard deviation of 100 cells. The lack of UgtP caused short and wide cells. The overexpression of *ugtP* resulted in long and chained cells. NA, not assigned due to the high variations in cell length caused by septum mislocalisation. Scale bars: 4 µm.

The absence of GtaB caused similar cell morphology to the absence of UgtP. Microscopic analysis of the *gtaB* mutant showed shorter and slightly wider cells during exponential phase when grown in nutrient rich medium (Figure 3.3 and 3.5). The complementation of *gtaB* restored the cell length and decreased the cell width almost back to wild type values.

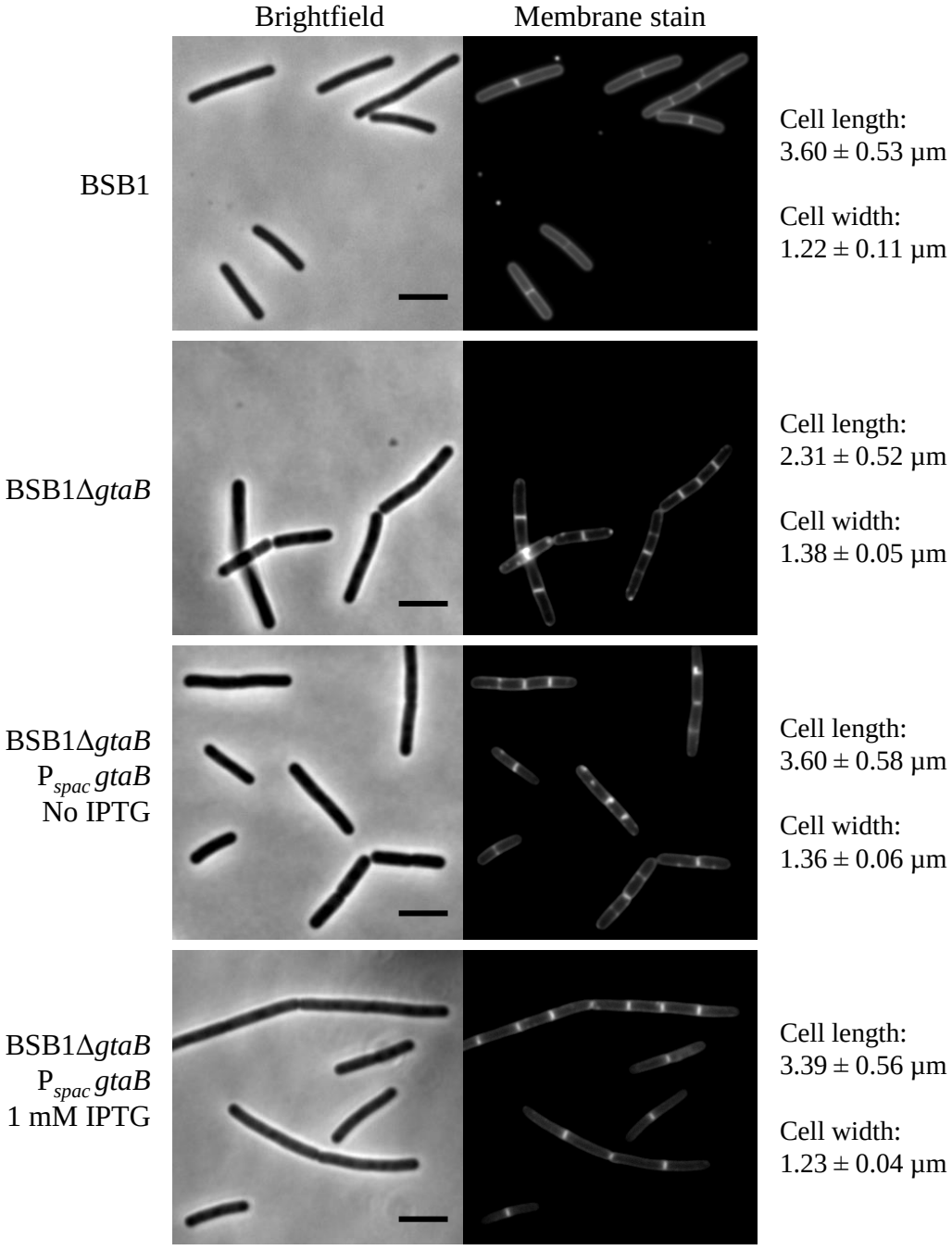

Figure 3.3 Morphology and complementation of cells lacking GtaB

Phase contrast and cell membrane stained images of BSB1, BSB1Δ*gtaB*, and BSB1Δ*gtaB* P$_{spac}$ *gtaB* cells. The *gtaB* complementation mutant was grown in the presence or absence of IPTG. Cell dimensions represent the mean cell length or width ± standard deviation of 100 cells. The lack of GtaB caused short cells. The complementation of GtaB increased the cell length and decreased the cell width. Scale bars: 4 µm.

The replacement of the *pgcA* gene with a tetracycline resistance cassette resulted in short and chained cell morphology during exponential phase in nutrient rich medium (Figure 3.4 and 3.5). The lack of PgcA also caused slightly wider cells than wild type, a similar morphology to the *gtaB* mutant. The complementation of *pgcA* increased the length and decreased the width of the cells almost back to wild type values. The chaining effect was not seen in either *ugtP* or *gtaB* mutant cells suggesting that PgcA may have an additional unknown function in BSB1.

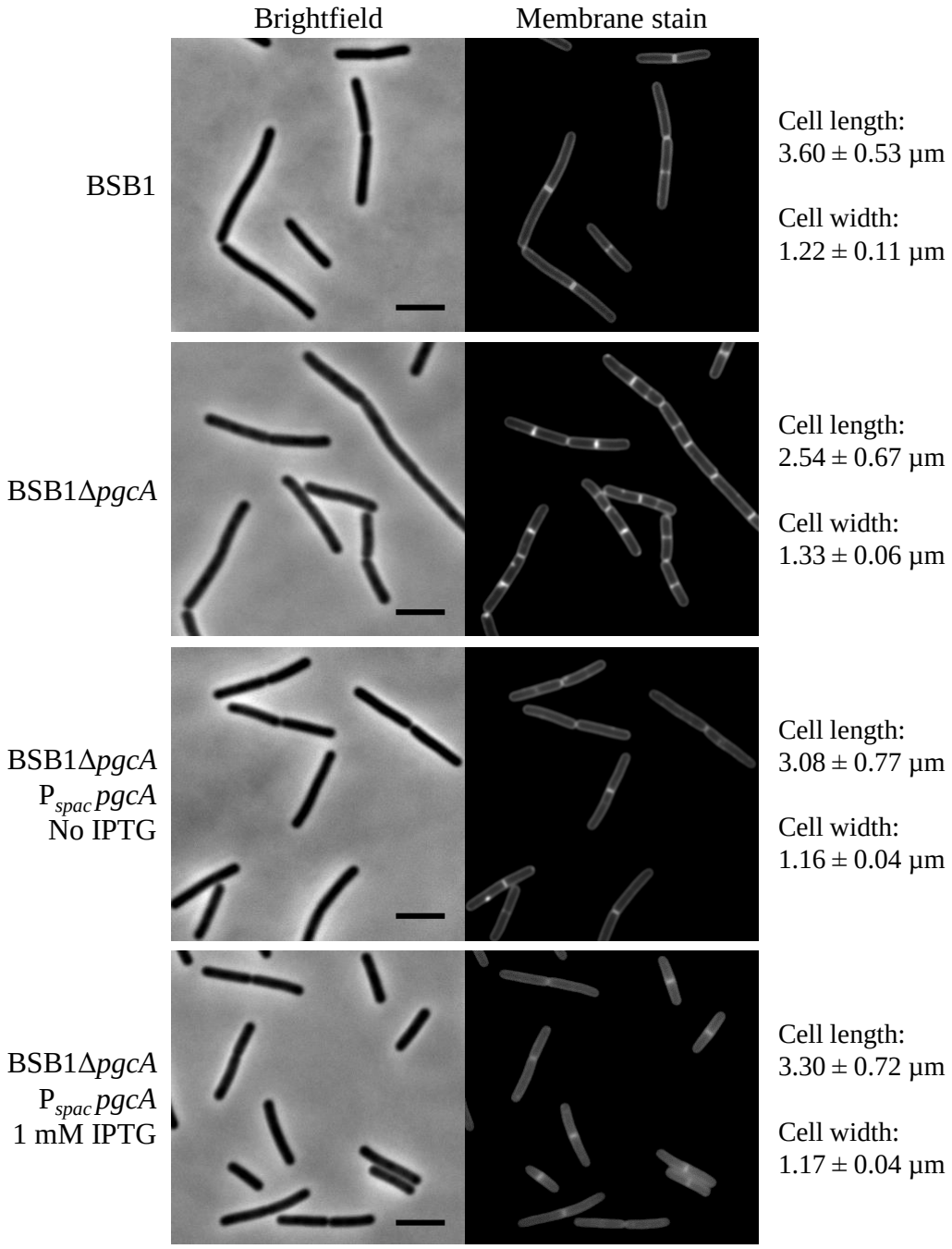

Figure 3.4 Morphology and complementation of cells lacking PgcA

Phase contrast and cell membrane stained images of BSB1, BSB1ΔpgcA, and BSB1ΔpgcA P_{spac} pgcA cells. The *pgcA* complementation mutant was grown in the presence or absence of 1 mM IPTG. Cell dimensions represent the mean cell length and width ± standard deviation of 100 cells. The lack of PgcA caused shorter and wider cells than BSB1. The complementation of PgcA increased cell length and decreased cell width. Scale bars: 4 µm.

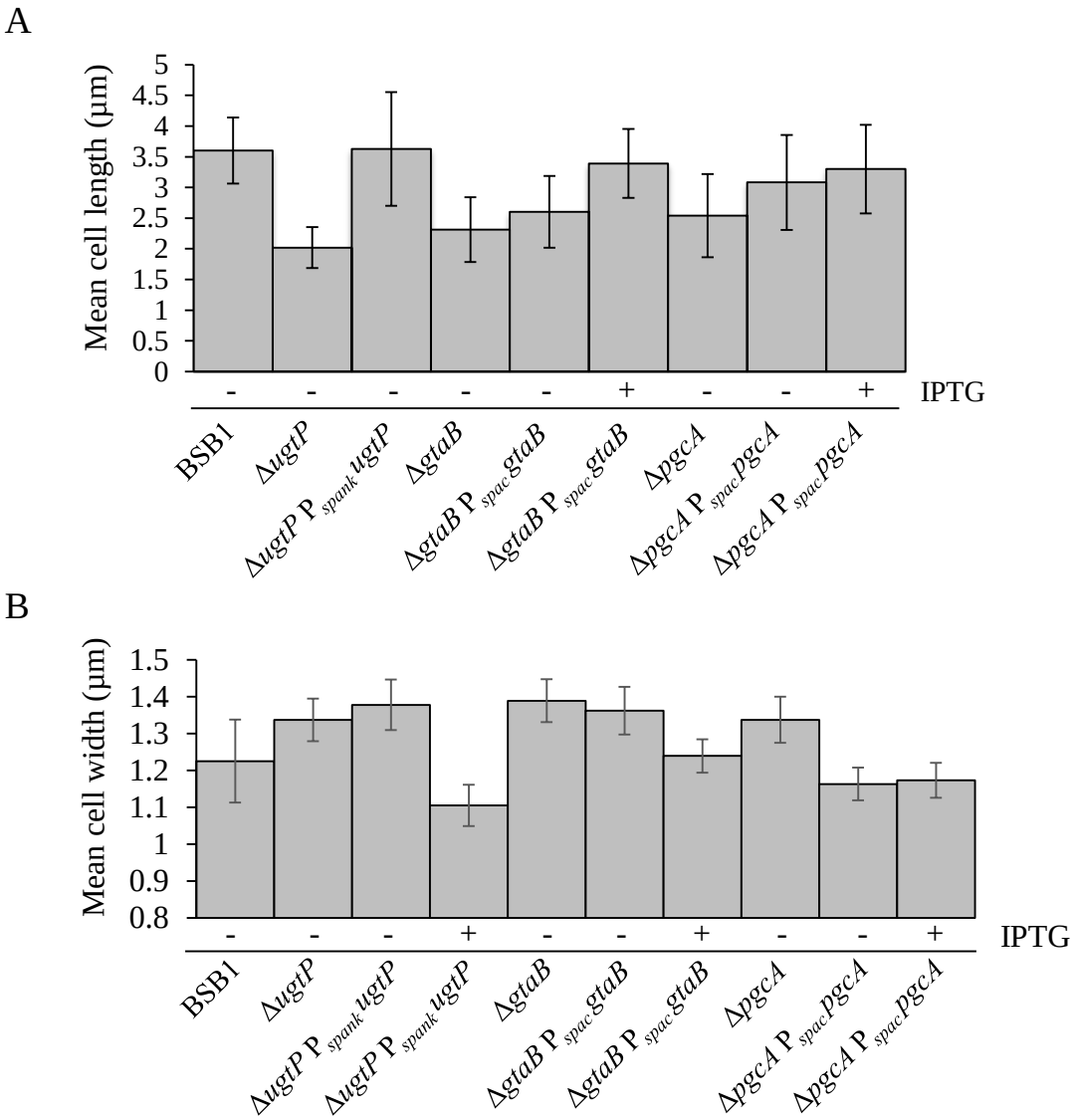

Figure 3.5 Summary of cell dimensions for wild type and mutant cells

The diagrams represent the cell length (A) or cell width (B) of wild-type and mutant cells. The dimensions for the *ugtP*, *gtaB* or *pgcA* complementation strains were quantified when cells were grown with or without IPTG. Each column represents the mean cell length or width ± standard deviation of 100 cell. All values significantly differed to that of BSB1 with $P<0.01$.

3.1.4 The absence of the PG synthase PBP1 in *ugtP* mutant causes thin and chained cells

Morphological studies of cells lacking UgtP, GtaB or PgcA showed changes in cell dimensions compared to wild type. To investigate the effects of these deletions on cell wall synthesis, the levels of cell wall precursors were quantified by Joana Sousa at the University of Greifswald using LC-MS. In Δ*ugtP*, Δ*gtaB* or Δ*pgcA* cells, the levels of LTA or WTA precursors such as UDP-glucose, glycerol-phosphate or CDP-glycerol were similar to wild type. Interestingly, the levels of several cytosolic PG precursors were higher in Δ*ugtP*, Δ*gtaB* and Δ*pgcA* mutants compared to wild type (Figure 3.6). The level of precursors increased up to 3-fold for these mutant cells compared to BSB1; the highest precursor level was present in cells lacking UgtP, suggesting an upregulation of PG synthesis. To further investigate this hypothesis, PG synthesis in Δ*ugtP*, Δ*gtaB* or Δ*pgcA* cells was disrupted and the growth and morphology of these strains were characterized. *Bacillus subtilis* has 4 bi-functional PBPs, PBP1, PBP2C, PBP4 and PBP2D (Bhavsar and Brown, 2006). PBP1, encoded by *ponA*, is the highest expressed PBP and plays an important role in PG synthesis during cell division (Pedersen *et al.*, 1999). Cells lacking PBP1 were thinner and grew more slowly than BSB1 in nutrient rich medium (Popham and Setlow, 1995). The deletion of PBP1 in the BSB1Δ*ugtP* mutant was lethal, however, it was possible to delete *ponA* in the *ugtP* complementation strain (BSB1Δ*ugtP* P_{spank} *ugtP*). All mutants grew on NA plates with or without IPTG at 37˚C, however, the Δ*ponA* mutant and the Δ*ponA* Δ*ugtP* P_{spank} *ugtP* mutant did not grow on PAB plates in the absence of IPTG at 37˚C (Figure 3.7). Interestingly, the Δ*ponA* mutant recovered the growth defect on PAB plates when incubated at 45˚C but the Δ*ponA* Δ*ugtP* P_{spank} *ugtP* mutant did not when grown in the absence of IPTG. The reasons behind these different phenotypes are unclear due to the unknown effects of high temperature on cell wall synthesis. Nevertheless, these results show that the partial complementation of *ugtP* was sufficient to rescue cell growth.

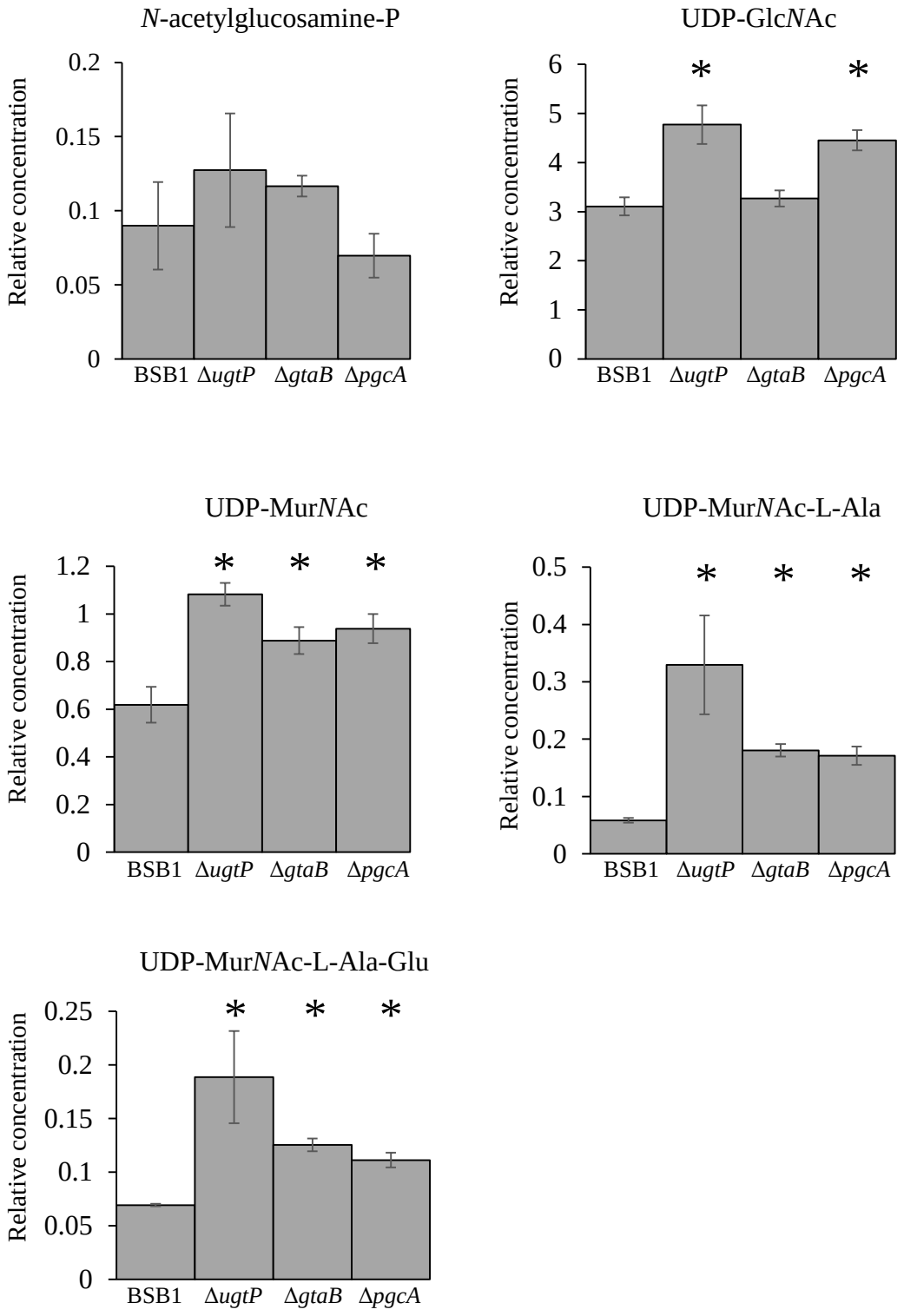

Figure 3.6 Quantification of peptidoglycan precursors

Relative quantification of cell wall precursors using LC-MS. The bars represent the mean ± standard deviation of three independent experiments. Δ*ugtP*, Δ*gtaB* or Δ*pgcA* mutants showed higher levels of peptidoglycan precursors compared to wild type cells. *, values significantly differed to that of BSB1 with $P<0.01$

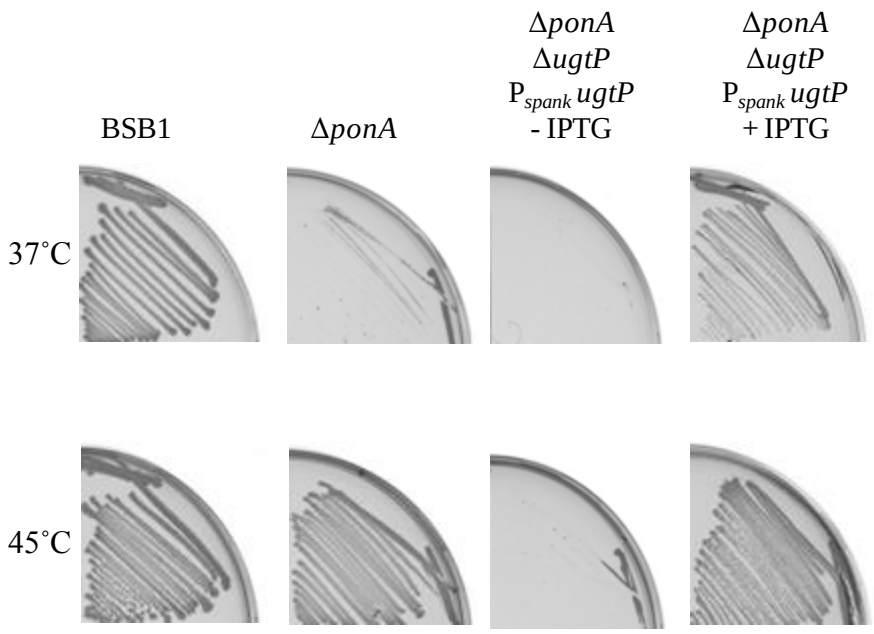

Figure 3.7 Growth of several mutants lacking the PG synthase PBP1 on PAB plates

PAB plates showing the growth of several mutants at 37 or 45˚C. The Δ*ponA* mutant and the Δ*ponA* Δ*ugtP* P_{spank} *ugtP* mutant showed grow at 37˚C on PAB plates in the absence of IPTG. At 45˚C, the Δ*ponA* mutant grew sufficiently on PAB plates whereas the Δ*ponA* Δ*ugtP* P_{spank} *ugtP* mutant was not able to grow in the absence of inducer.

The Δ*ponA* Δ*ugtP* P_{spank} *ugtP* mutant grown without IPTG exhibited cell chains that were thinner than the *ponA* mutant and longer than the *ugtP* mutant (Figure 3.8 and 3.9). The addition of 0.1 mM IPTG had no significant effect on the cell shape. The increase in IPTG concentration did not increase the width of the cells (Figure 3.9) and caused the formation of spots along the cell periphery (data not shown). These results suggest that the complementation is partial upon *ugtP* induction.

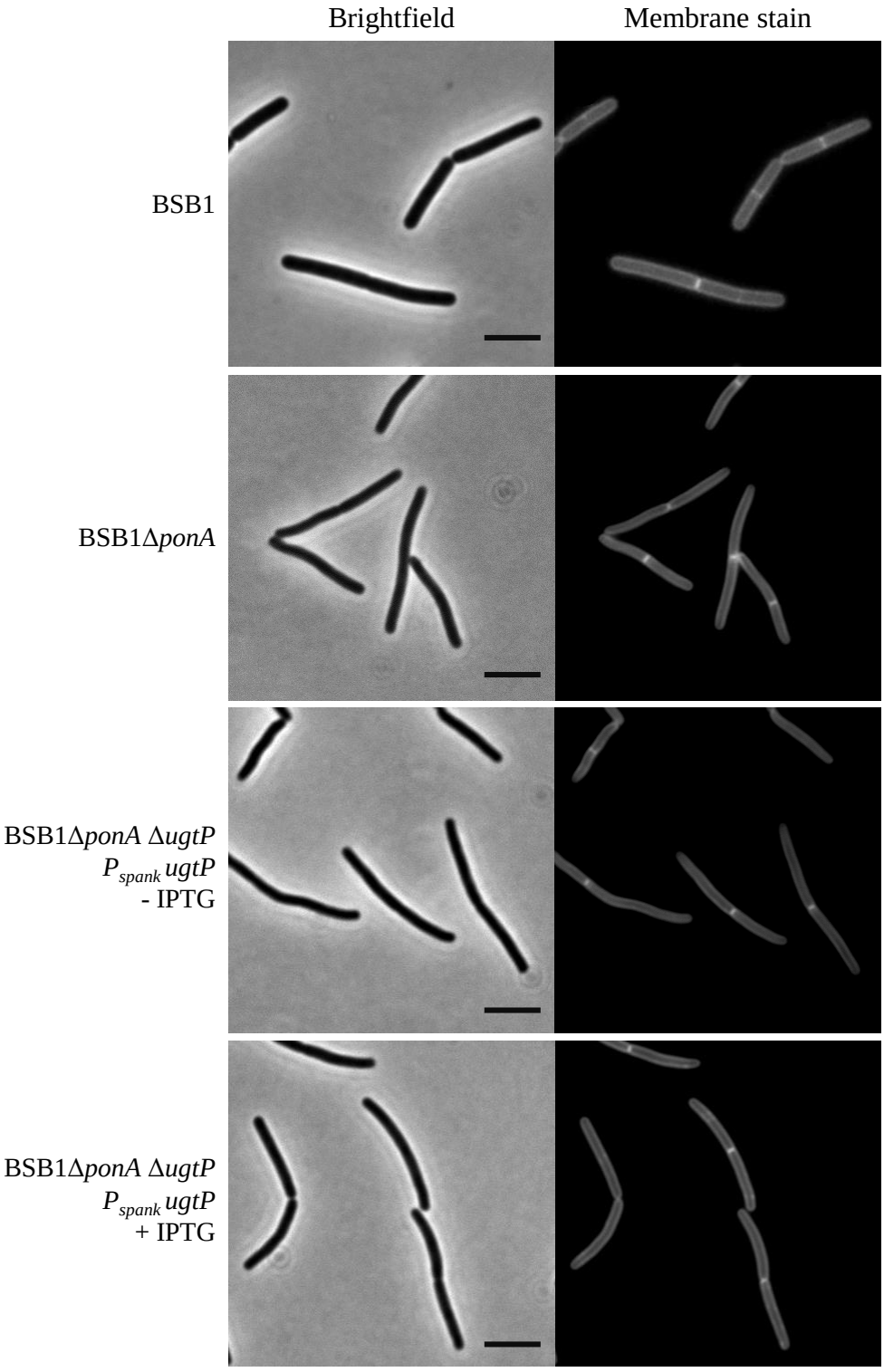

Figure 3.8 Morphology of BSB1Δ*ugtP* cells lacking the PG synthase PBP1

Phase contrast and cell membrane stained images for vegetative cells grown in LB media. BSB1Δ*ponA* and BSB1Δ*ugtP* Δ*ponA* P_{spank} *ugtP* mutants had thin cell morphology in the absence of IPTG. The addition of IPTG had no effect on the cell shape. Scale bars: 4 µm.

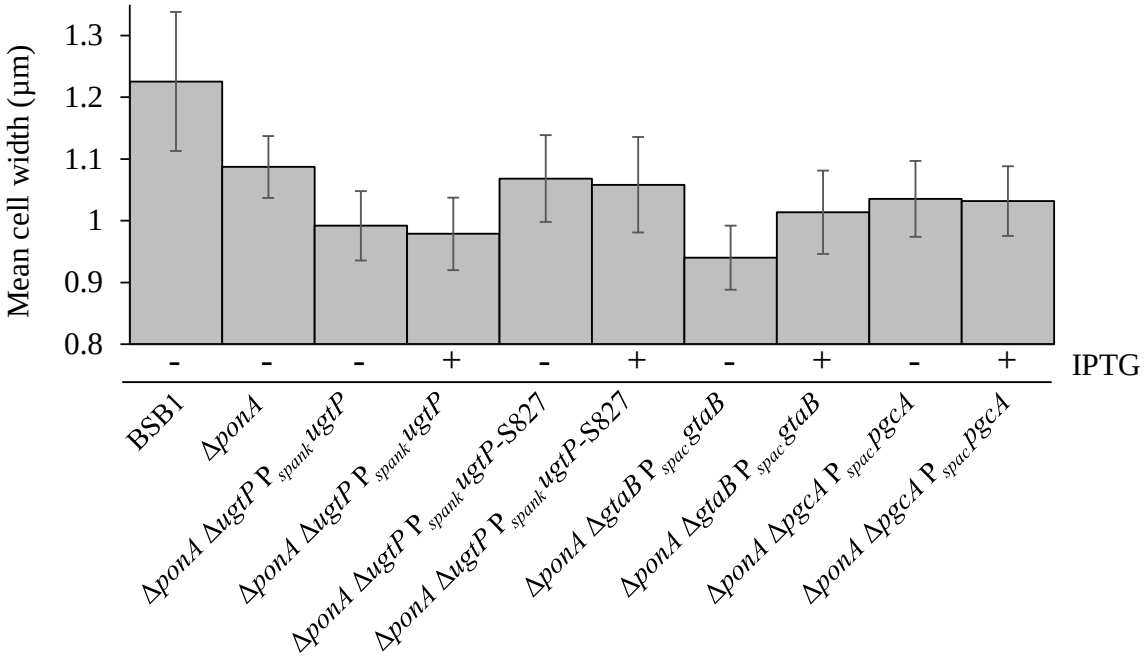

Figure 3.9 Cell width of mutant cells

The diagram represents the mean cell width of several mutants. The Δ*ugtP* Δ*ponA* P_{spank} *ugtP* mutant was shorter than both BSB1 and the Δ*ponA* mutant. The complementation of UgtP did not recover the cell width. Complementation of the S827 antisense RNA caused wider cells than Δ*ugtP* Δ*ponA* P_{spank} *ugtP* mutants. The ectopic expression of GtaB in Δ*ponA* Δ*gtaB* P_{spac} *gtaB* mutant resulted in wider cells but not as wide as the Δ*ponA* mutant. The complementation of PgcA in Δ*ponA* Δ*pgcA* P_{spac} *pgcA* mutant had no effect on the cell width. Each column represents the mean cell width ± standard deviation of 100 cells. All values significantly differed to that of BSB1 with $P<0.01$.

3.1.5 The effect of the S827 RNA on the cell width

Based on the microarray data published by (Nicolas *et al.*, 2012), the Subtiwiki web server (http://subtiwiki.uni-goettingen.de) suggested the presence of an anti-sense transcript called S827 that overlaps with the *ugtP* locus (Figure 3.10). In the BSB1Δ*ugtP* mutant as well as in all published *ugtP* mutants the S827 transcript was disrupted (Matsuoka et al., 2011a; Salzberg and Helmann, 2008; Weart et al., 2007). In order to investigate if the S827 RNA is a reason for the partial complementation of *ugtP*, the S827 RNA was included in the ectopic expression of *ugtP*. Hence, *ugtP* was inserted into the *amyE* locus under the expression of an IPTG inducible promoter and the 3' end of *ugtP* was extended to include the S827 RNA and its putative promoter. The complementation of S827 in BSB1Δ*ugtP* Δ*ponA* P_{spank} *ugtP* did not support cell growth on PAB plates at 37˚C or 45˚C (Figure 3.11 A), but it resulted in wider cells in the presence or absence of the inducer (Figure 3.9 and 3.11 B). These results suggest that the complementation of S827 did not rescue the growth of the BSB1Δ*ugtP* Δ*ponA* P_{spank} *ugtP*

mutant at high temperature but the RNA is probably partially responsible for the thin cell morphology of the latter mutant. The promoter sequence of the RNA was replaced with an erythromycin cassette to investigate the effect of S827 on cell growth and morphology. However, cells lacking S827 had similar growth and morphology to BSB1 indicating that the RNA dispensable for growth and morphology in wild-type cells.

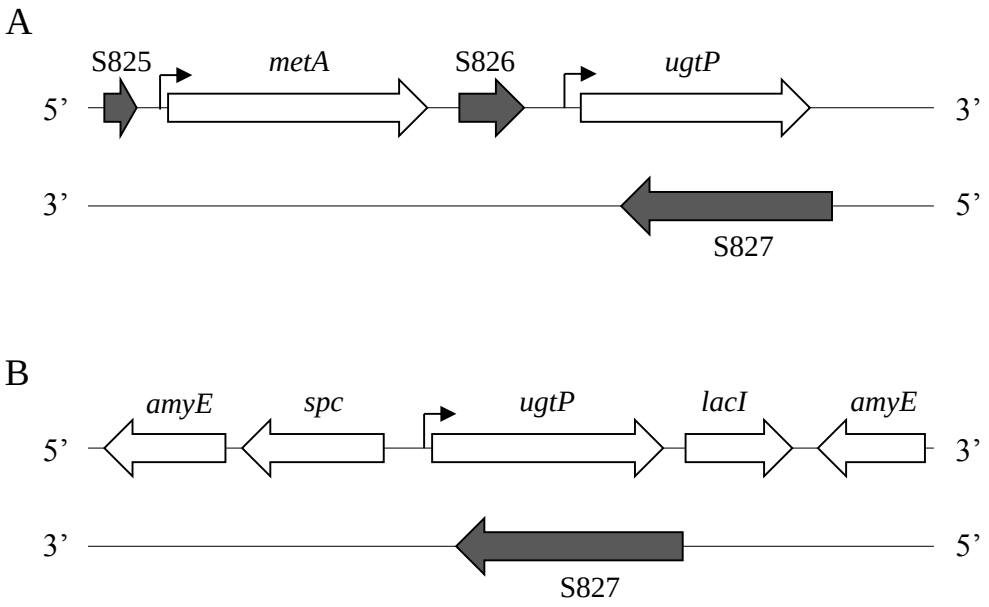

Figure 3.10 Transcriptome data for *ugtP* and S827

(A) The diagram represent microarray results adopted from (Nicolas *et al.*, 2012). The diagram shows the double stranded DNA for the operon that *ugtP* is part of.

(B) Gene mapping for *ugtP* and S827 RNA complementation construct.

The coding genes and the RNA genes are represented as white or grey arrows, respectively. The direction of the arrows indicates the direction of the transcription. The small arrow bars in black represent the promoters.

A

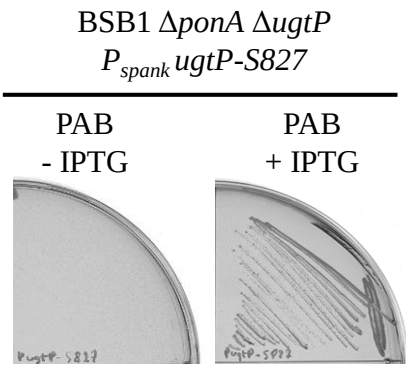

B

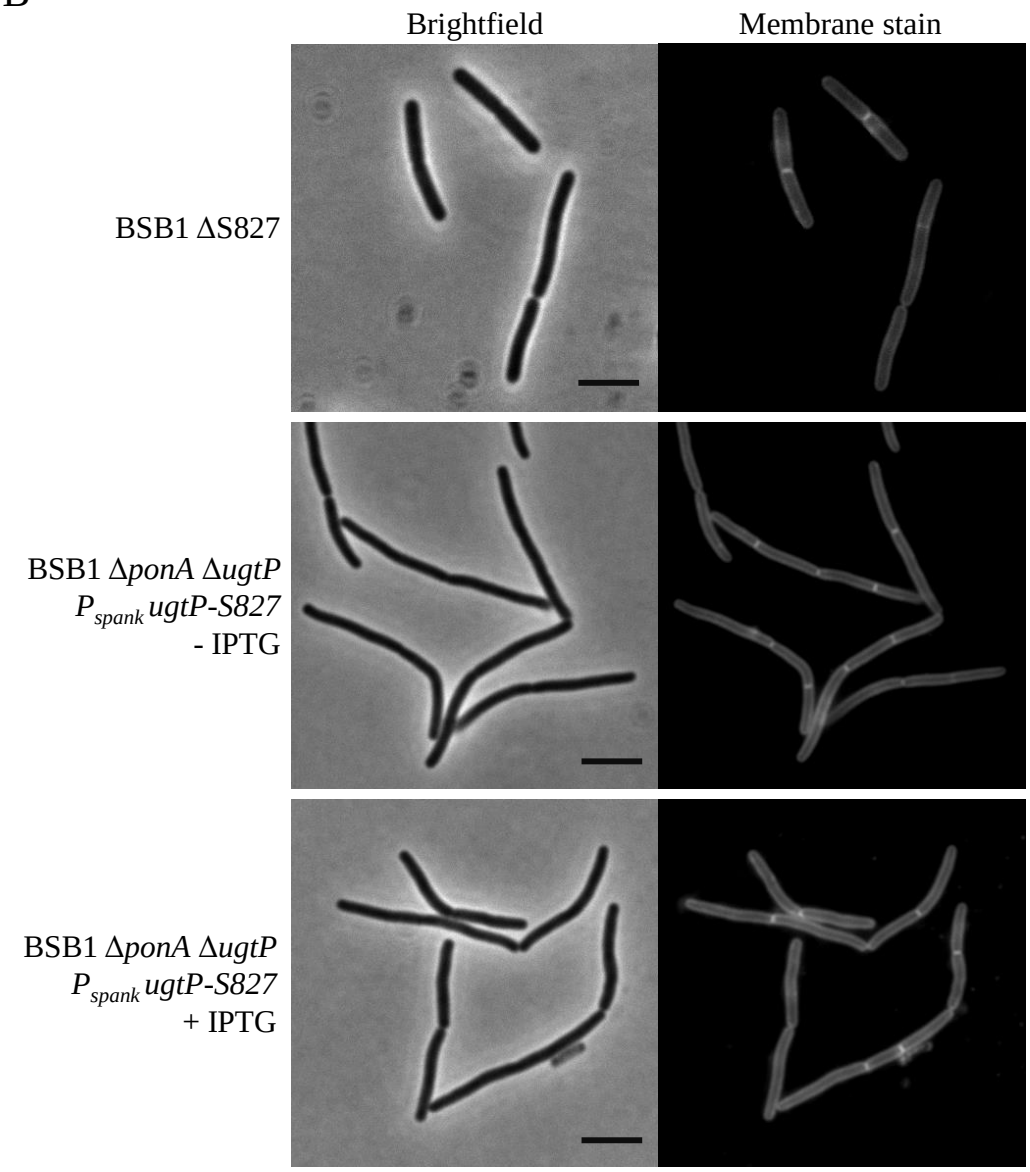

Figure 3.11 Complementation of the S827 RNA in the Δ*ugtP* Δ*ponA* P$_{spank}$ *ugtP* mutant

Phase contrast and cell membrane stained images for vegetative cells grown in LB media. The BSB1ΔS827 mutant exhibited similar cell morphology to wild type cells. Cells with complemented *ugtP* and S827 had similar growth (A) and cell morphology (B) to the Δ*ugtP* Δ*ponA* P$_{spank}$ *ugtP* mutant. Scale bar: 4 µm.

3.1.6 The absence of PBP1 in *gtaB* mutant causes thin and chained cells

GtaB produces UDP-glucose which is a constituent of the LTA and WTA in the cell. UgtP catalyses the transfer of UDP-glucose to diacylglycerol. Thus the absence of GtaB should presumably have the same effect on the LTA structure/composition as the absence of UgtP. Furthermore, the absence of GtaB altered the localisation of UgtP from midcell during exponential phase (Weart *et al.,* 2007). Thus GtaB is assumed to regulate cell growth and division by controlling substrate availability for UgtP (Weart *et al.,* 2007). The double deletion of *gtaB* and *ponA* (PBP1 gene) was lethal, suggesting that the LTA glucolipid precursor is crucial for cells lacking PBP1. The deletion of *ponA* in the *gtaB* complementation mutant was viable and cells grew sufficiently in the presence or absence of IPTG. This mutant allowed us to further investigate whether the S827 RNA has a role in the partial complementation of the cell width in the BSB1Δ*ponA* Δ*ugtP* P_{spank} *ugtP* mutant since the BSB1Δ*ponA* Δ*gtaB* P_{spac} *gtaB* mutant contains UgtP and S827 but lacks the LTA glucolipids and PBP1. Interestingly, the BSB1Δ*ponA* Δ*gtaB* P_{spac} *gtaB* mutant was able to grow on PAB plates at 37˚C or 45˚C in the presence or absence of inducer (Figure 3.12 A). The Δ*ponA* Δ*gtaB* P_{spac} *gtaB* mutant was thinner than the BSB1Δ*ponA* Δ*ugtP* P_{spank} *ugtP* mutant in the absence of inducer and the complementation of GtaB increased the cell width by 7% (Figure 3.9 and 3.12 B). The cell width measurements were also obtained for the BSB1Δ*ponA* Δ*pgcA* P_{spac} *pgcA* mutant grown in LB with or without IPTG (Figure 3.9). These measurements showed that BSB1Δ*ponA* Δ*pgcA* P_{spac} *pgcA* cells were wider than BSB1Δ*ponA* Δ*ugtP* P_{spank} *ugtP* cells and almost as wide as BSB1Δ*ponA*. These results suggested that the S827 RNA has a role in controlling the cell width, but the mechanism of this regulation is unclear. Next, we studied the localisation of PBP1 in cells lacking UgtP or PgcA.

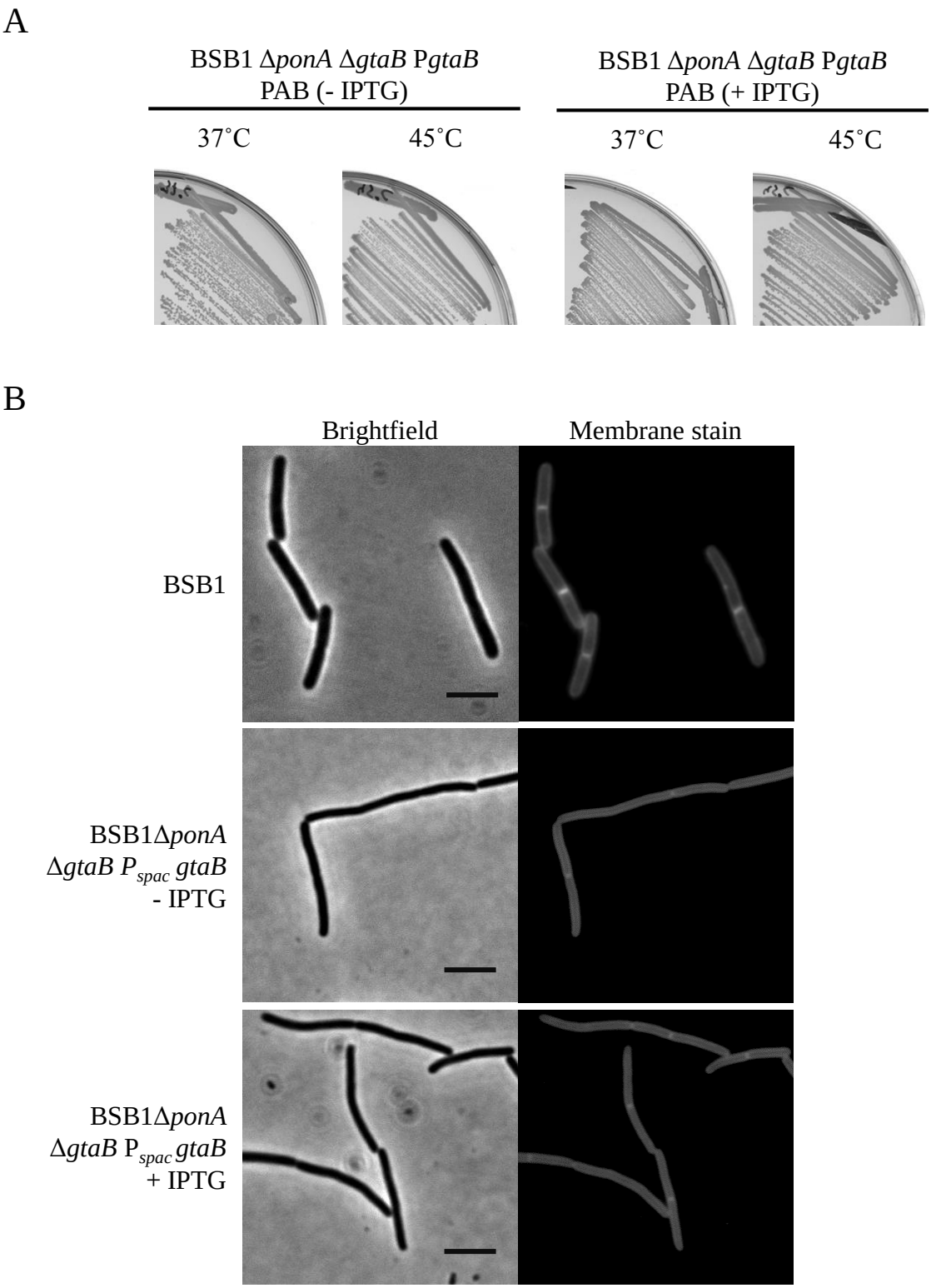

Figure 3.12 Growth and Morphology of BSB1Δ*gtaB* cells lacking the PG synthase PBP1

(A) The BSB1Δ*ponA* Δ*gtaB* P_{spac} *gtaB* mutant grown on PAB plates in the presence or absence of IPTG at 37 or 45˚C. The growth of the latter mutant was independent of the temperature or the inducer.

(B) Phase contrast and cell membrane stained images for BSB1 and the Δ*ponA* Δ*gtaB* P_{spac} *gtaB* mutant grown in LB with or without IPTG. The latter mutant exhibited thin and chained cell morphology independent of the presence of IPTG. Scale bar: 4 µm.

3.1.7 The localisation PBP1 in the *ugtP* mutant is similar to wild-type

The localisation of PBP1 was studied in BSB1, Δ*ugtP* and Δ*pgcA* mutants. A *gfp* gene under the control of a xylose inducible promotor was introduced at the 5' end of the native *ponA* locus in BSB1, Δ*ugtP* and Δ*pgcA* mutants. Cells were grown in LB with 0.5% xylose and the localisation of PBP1 was studied using fluorescence microscopy. The localisation pattern in both mutants was similar to wild type cells where PBP1 seemed to be localised at the septum during vegetative growth and occasionally at the cell periphery (Figure 3.13). These results suggests that the absence of LTA glucolipids has no effect on the localisation of Gfp-PBP1 in the cell.

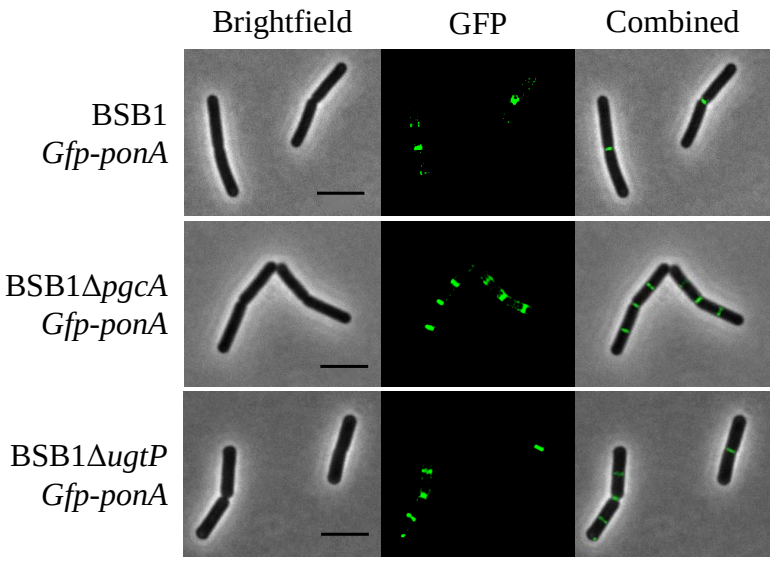

Figure 3.13 Localisation of PBP1 in *ugtP* or *pgcA* mutant cells

BSB1 *ponA::*(P_{xyl} *gfp-ponA*), BSB1Δ*pgcA ponA*::(P_{xyl} *gfp-ponA*) and BSB1Δ*ugtP ponA*::(P_{xyl} *gfp-ponA)* mutants were grown in LB media in the presence of 0.5% xylose. Phase contrast and GFP fluorescence images showed similar localisation pattern for PBP1 in BSB1, Δ*ugtP* and Δ*pgcA* mutants. Scale bars: 4 µm.

3.1.8 TEM images indicated altered cell wall structure for the *ugtP* mutant

Cells lacking LTA glucolipids exhibit higher sensitivity to lysozyme and salt compared to wild type cells (Fedtke *et al.,* 2007; Matsuoka *et al.,* 2011a). Fluorescence microscopy allowed us to study the morphology of the strains, but high resolution images were required to better characterize the cell wall. Therefore, Δ*ponA*, Δ*ugtP* and Δ*ugtP* Δ*ponA* P_{spank} *ugtP* mutants were analyzed by transmission electron microscopy (TEM), at the electron microscopy facility, Newcastle University. The effect of *ponA* deletion on the cell morphology was previously described as thin cells with membrane invaginations and occasional aberrant septa (Pedersen *et al.*,1999). However, TEM analysis for the BSB1Δ*ponA* mutant indicated thin cells with normal septa (Figure 3.14). Interestingly, BSB1Δ*ponA* cells had thinner cell walls (CW) than BSB1 cells (≈ 15% thinner). The absence of UgtP caused rough cell surfaces compared to wild type cells but had no effect on the thickness of the CW. The BSB1Δ*ugtP* Δ*ponA* P_{spank} *ugtP* mutant had thinner cell walls compared to both the parent BSB1 and the Δ*ponA* mutant (≈ 30% thinner than wild type) in addition to a similar rough cell wall structure to the *ugtP* mutant. Consequently, the altered cell wall structure might be a reason behind the higher susceptibility of the *ugtP*-null mutant to lysozyme.

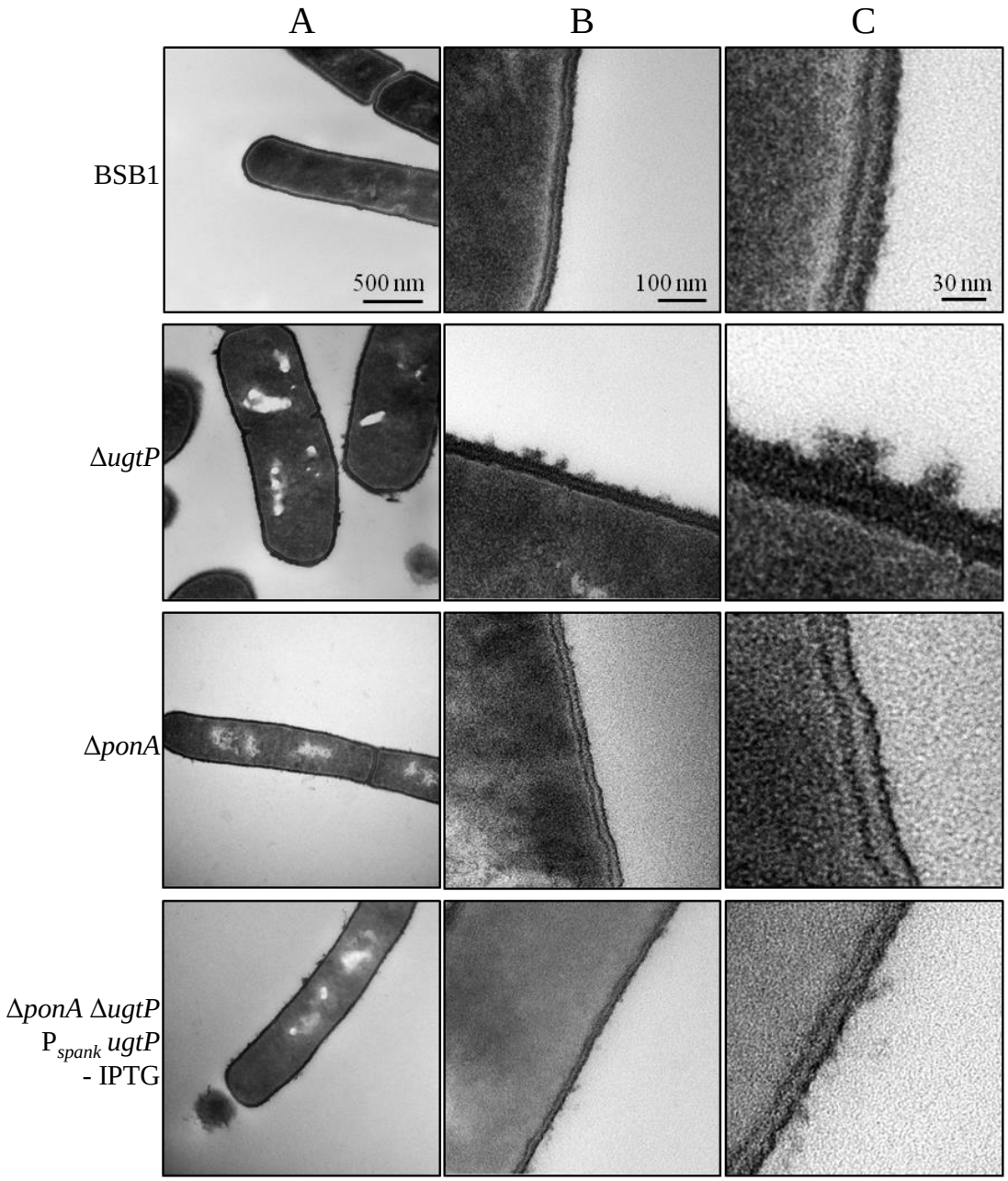

Figure 3.14 TEM analysis for several mutants

TEM images for BSB1, Δ*ponA*, Δ*ugtP* and Δ*ugtP* Δ*ponA* P_{spank} *ugtP* mutants during exponential phase using three different magnifications. The *ugtP* mutant had altered cell wall structure. The Δ*ponA* and Δ*ponA* Δ*ugtP* P_{spank} *ugtP* mutants had thinner cell wall than BSB1 cells. Scale bars: (A) 500 nm, (B) 100 nm and (C) 30 nm

3.2 The role of the PG hydrolases in *ugtP*, *gtaB* or *pgcA* mutants

3.2.1 Introduction

Cells lacking UgtP had LTA with longer glycerol-phosphate chains (Aurelie Guyet, unpublished data). Changes in the LTA structure were implicated with higher susceptibility to antimicrobial peptides and an increase in the autolysis activity in the cells (Perego *et al.*, 1995; Wecke *et al.*, 1997; Wecke *et al.*, 1996). TEM images for cells lacking UgtP showed rough cell wall structure suggesting higher or uncontrolled PG hydrolase activity. To investigate this phenomenon, we quantified muropeptides from BSB1, Δ*ugtP* and Δ*pgcA* cells. Subsequently, we constructed mutants lacking UgtP, GtaB or PgcA and cell wall hydrolases and the morphology of these mutants was analysed by fluorescence microscopy.

3.2.2 Quantification of muropeptides from *ugtP* or *pgcA* mutants

To test if the absence of UgtP or PgcA had any effect on peptidoglycan structure or composition, we analysed the muropeptide profiles for the Δ*ugtP* and Δ*pgcA* single mutants. First, the PG of these strains was purified (Section 2.11.2), digested with cellosyl to muropeptides and analysed by HPLC using a reversed phase column (Section 2.11.3). The HPLC chromatograms for the Δ*ugtP* and Δ*pgcA* mutants were comparable to that of BSB1 (Figure 3.15). However, looking at more subtle differences, it was evident that both Δ*pgcA* and Δ*ugtP* mutants had increased levels of "Di" (peak 5) and "Tri-Ala-mDap $(NH_2)_2$" (peak 8) (Table 3.1). Such an increase in these two muropeptides was reported previously in strains where higher autolytic enzymes activity was present, specifically CwlO or LytE activities (Bisicchia *et al.*, 2007). The percentages of Di or Tri-Ala-mDap$(NH_2)_2$ were 30% or 37% higher in the Δ*ugtP* mutant compared to BSB1, respectively (Table 3.1) (Figure 3.16). The Δ*pgcA* mutant had an increase of 43% and 51% in the Di or Tri-Ala-mDap$(NH_2)_2$ MP compared to BSB1, respectively. The percentage of the other muropeptides did not change with the loss of UgtP or PgcA compared to BSB1. Thus there is a strong suggestion that CwlO or LytE are either upregulated or have higher activity in cells lacking UgtP or PgcA.

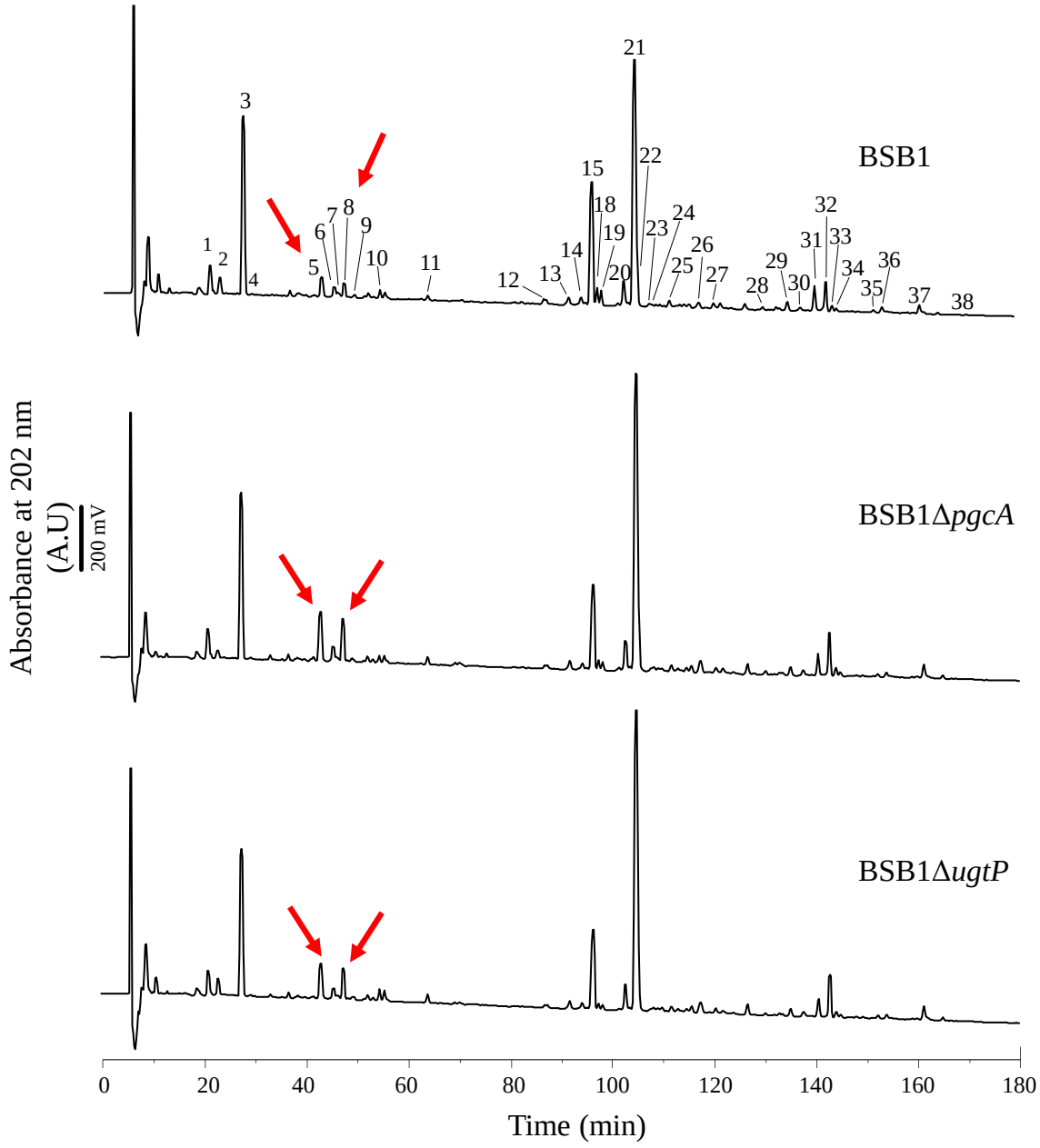

Figure 3.15 RP-HPLC analysis of muropeptides from BSB1, Δ*ugtP* and Δ*pgcA* mutants

The peaks 1-38 have been assigned according to Bisicchia *et al.*,2011. BSB1, Δ*ugtP* or Δ*pgcA* mutants showed comparable muropeptide profiles except that the peaks number 5 and 8 (red arrows) corresponding to the levels of the muropeptides Di- and Tri-Ala-mDap$(NH_2)_2$, respectively, were bigger in the Δ*ugtP* and Δ*pgcA* mutants compared to BSB1.

Muropeptides [1]	Peak no	Peak area (%)		
		BSB1	*pgcA*	*ugtP*
Tri	1	2.2 ± 0.2	1.9 ± 0.0	1.8 ± 0.1
Tri (NH_2) (PO_4)	2	1.0 ± 0.3	0.7 ± 0.2	1.0 ± 0.3
Tri (NH_2)	3	14.2 ± 1.4	11.8 ± 0.5	12.1 ± 0.9
Tri (NH_2) (deAc)	4	0.0 ± 0.0	0.1 ± 0.1	0.1 ± 0.0
Di	5	2.3 ± 0.3	4.0 ± 0.2	3.2 ± 0.2
Tri-Ala-mDap (NH_2)	6	1.4 ± 0.4	1.5 ± 0.2	1.2 ± 0.2
tetra (NH_2)	7	0.5 ± 0.2	0.3 ± 0.0	0.2 ± 0.0
Tri-Ala-mDap $(NH_2)_2$	8	1.4 ± 0.2	2.9 ± 0.2	2.2 ± 0.3
penta (Gly5) (NH_2)	9	0.3 ± 0.0	0.3 ± 0.0	0.2 ± 0.0
TriTetra (-GM) $(NH_2)_2$	10	0.6 ± 0.1	0.6 ± 0.1	0.7 ± 0.3
penta (NH_2)	11	0.4 ± 0.0	0.6 ± 0.1	0.6 ± 0.2
TriTetra (-G)	12	0.7 ± 0.2	0.4 ± 0.1	0.4 ± 0.1
TriTetra (NH_2) (PO_4)	13	0.8 ± 0.4	1.5 ± 0.6	1.6 ± 0.7
TetraTetra (-GM) $(NH_2)_2$	14	1.4 ± 0.4	0.6 ± 0.1	0.7 ± 0.0
TriTetra (NH_2)	15	13.5 ± 1.9	10.9 ± 3.0	11.3 ± 3.0
TriTetra (NH_2) (deAc)	18	2.1 ± 0.6	1.1 ± 0.2	1.1 ± 0.5
TriTetra (NH_2) (deAc)	19	1.7 ± 0.5	0.8 ± 0.2	0.9 ± 0.4
TriTetra (NH_2)	20	3.0 ± 0.5	2.8 ± 0.0	2.7 ± 0.1
TriTetra $(NH_2)_2$	21	26.0 ± 0.1	28.3 ± 0.9	29.2 ± 2.2
TriTetra $(NH_2)_2$ (deAc)	22	0.2 ± 0.2	0.1 ± 0.1	0.1 ± 0.1
TriTetra $(NH_2)_2$ (deAc)	23	0.4 ± 0.0	0.3 ± 0.1	0.2 ± 0.0
Penta (Gly5) Tetra	24	0.3 ± 0.1	0.6 ± 0.0	0.5 ± 0.1
Penta (Gly5) Tetra $(NH_2)_2$	25	0.7 ± 0.3	0.7 ± 0.0	0.6 ± 0.0
TetraTetra $(NH_2)_2$	26	0.6 ± 0.2	1.4 ± 0.0	1.3 ± 0.2
PentaTetra $(NH_2)_2$	27	0.6 ± 0.1	0.5 ± 0.2	0.4 ± 0.1
TriTetraTetra $(NH_2)_2$	28	0.4 ± 0.1	0.4 ± 0.1	0.3 ± 0.1
TriTetraTetra (-G)	29	1.1 ± 0.1	1.0 ± 0.2	1.0 ± 0.3
TriTetraTetra $(NH_2)_2$	30	0.5 ± 0.1	0.7 ± 0.0	0.7 ± 0.1
TriTetraTetra $(NH_2)_3$	31	2.6 ± 0.4	2.5 ± 0.6	2.3 ± 0.6
TriTetraTetra $(NH_2)_3$ (deAc)	32	2.5 ± 0.1	3.3 ± 0.2	3.3 ± 0.4
TriTetraTetra $(NH_2)_3$ (deAc)	33	0.6 ± 0.0	0.6 ± 0.2	0.6 ± 0.1
Penta(Gly5)TetraTetra $(NH_2)_{2-3}$	34	0.3 ± 0.0	0.3 ± 0.1	0.3 ± 0.0
TriTetraTetraTetra $(NH_2)_{2-3}$	35	0.3 ± 0.1	0.4 ± 0.1	0.3 ± 0.0
TriTetra(Anh) $(NH_2)_2$	36	0.7 ± 0.1	0.8 ± 0.3	0.7 ± 0.3
TriTetraTetraTetra $(NH_2)_4$	37	0.9 ± 0.0	1.4 ± 0.0	1.5 ± 0.2
TriTetraTetra(Anh) $(NH_2)_2$	38	0.0 ± 0.0	0.0 ± 0.0	0.0 ± 0.0
Sum monomers		25.9 ± 0.3	24.8 ± 0.8	23.9 ± 0.3
Sum dimers		61.8 ± 0.4	59.6 ± 1.1	61.4 ± 0.8
Sum trimers		9.3 ± 0.1	10.2 ± 0.2	9.9 ± 0.2
Sum tetramers		1.4 ± 0.0	2.1 ± 0.0	2.1 ± 0.3
Sum dipeptides		2.6 ± 0.2	4.7 ± 0.4	3.8 ± 0.3
Sum tripeptides		56.0 ± 0.4	53.9 ± 0.4	54.4 ± 0.5
Sum tetrapeptides		39.2 ± 0.3	38.8 ± 0.5	39.7 ± 0.1
Sum pentapeptides		1.9 ± 0.3	2.3 ± 0.4	1.9 ± 0.3
Degree of Crosslinkage [2]		38.1 ± 0.3	38.1 ± 0.6	38.9 ± 0.3
% Peptides in Crosslinkage [3]		74.1 ± 0.3	75.2 ± 0.8	76.1 ± 0.3

Table 3.1 Muropeptide identities and quantification for BSB1, Δ*ugtP* and Δ*pgcA* mutants

BSB1, Δ*ugtP* and Δ*pgcA* mutants had similar muropeptide levels except that the muropeptides Di and Tri-Ala-mDap $(NH_2)_2$ from *pgcA* or *ugtP* mutants were higher compared to BSB1, respectively. The chemical structure for the identified muropeptides are presented in Figure 3.16. Values represent the mean ± standard deviation from two independent PG preparations.

[1] Nomenclature of muropeptides according to Glauner *et al*., (1988)

[2] calculated according to Glauner *et al.*, (1988)

[3] calculated as 100% - % monomers.

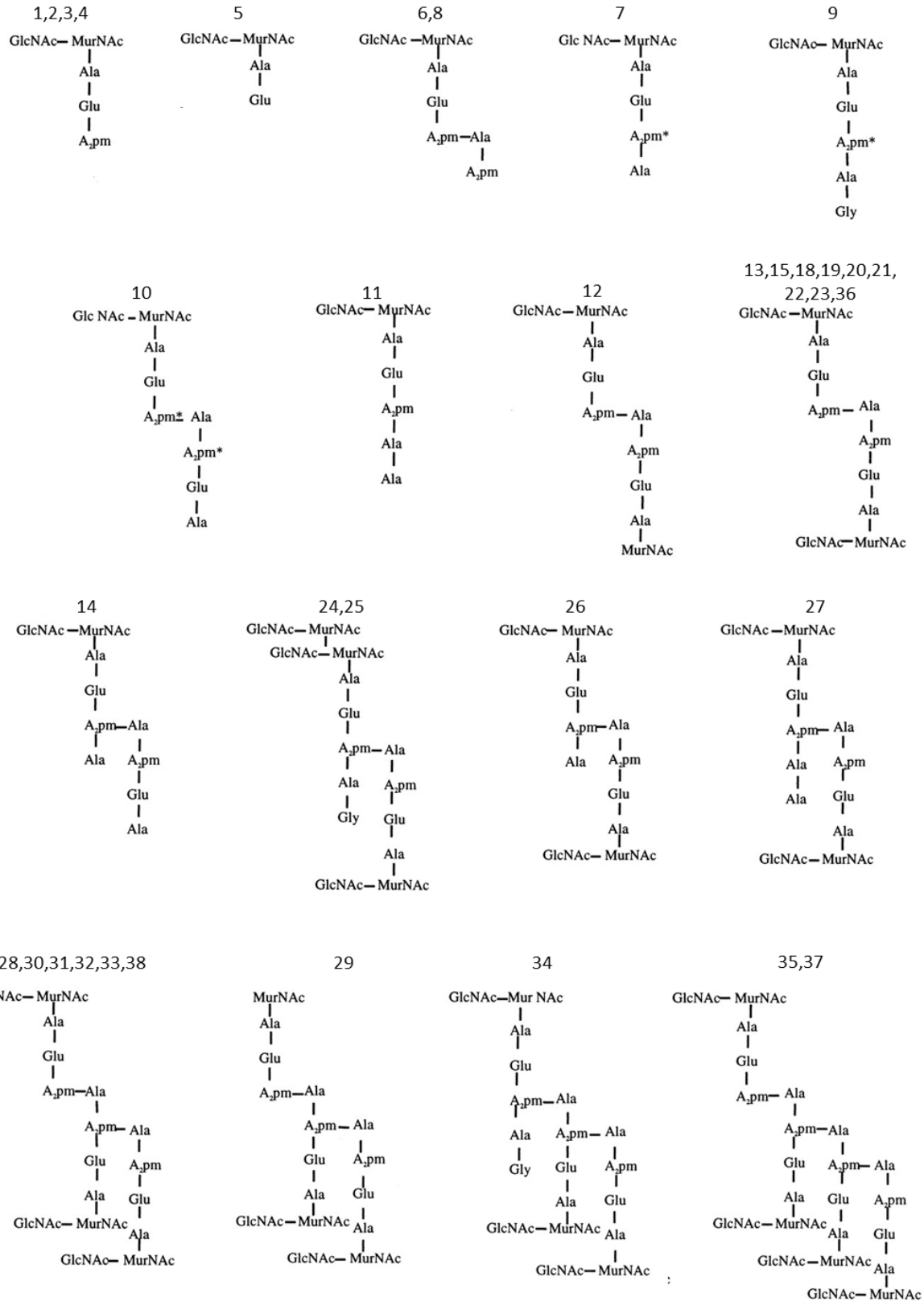

Figure 3.16 Chemical structure of identified muropeptides

Proposed basic structure for muropeptides from *B. subtilis* according to (Atrih *et al.*, 1999). Numbers refer to peaks in table 3.1.

3.2.3 The deletion of *lytE* in cells lacking UgtP causes sever growth and shape defects

The analysis of muropeptides form Δ*ugtP* or Δ*pgcA* mutants suggested that the levels or activities of CwlO or LytE might be affected. Furthermore, *ugtP*, *pgcA* and *ltaS* mutants have higher levels of LytE and not CwlO (Kasahara *et al.,* 2016). LytE and CwlO both have DL-endopeptidase activity. LytE is suggested to be involved in cell elongation and division due to its localisation at the septum and the lateral cell wall (Kasahara *et al.*,2016; Yamamoto *et al.,* 2003), whereas, CwlO is suggested to be more involved in cell elongation based on its lateral cell wall localisation (Hashimoto *et al.,* 2012). To better understand the roles of these DL-endopeptidases in the absence of LTA glucolipids, BSB1Δ*ugtP* Δ*lytE* and BSB1Δ*ugtP* Δ*cwlO* mutants were constructed and characterised. Since the absence of CwlO or LytE has not been described before in the BSB1 background, these strains were also constructed as controls.

The loss of LytE in BSB1 cells did not have an effect on cell growth on PAB plates at 37˚C or 45˚C. However, Δ*ugtP* cells lacking LytE showed smaller colonies than BSB1 on both PAB and NA plates at 37˚C suggesting slower growth. No growth was observed for the Δ*ugtP* Δ*lytE* double mutant on PAB plates at 45˚C suggesting lethality at permissive temperature (Figure 3.17 A). The morphology of the mutants was studied using fluorescence microscopy. BSB1 cells lacking LytE were bent slightly when grown in LB media (Figure 3.17 B). The Δ*ugtP* Δ*lytE* mutant cells had severe shape defects featuring short bent cells with a high number of mini cells. These results suggest that LytE may have an important role in maintaining the rod shape in cells lacking UgtP.

The *lytE* gene was also deleted in the *ugtP* complementation mutant, subsequently the growth and morphology of the constructed mutant were characterized in the presence or absence of inducer. Δ*ugtP* Δ*lytE* P_{spank} *ugtP* cells grew on PAB at 45˚C with or without IPTG, suggesting that the leaky expression of the ectopic *ugtP* was sufficient to support growth (Figure 3.17 A). Δ*ugtP* Δ*lytE* P_{spank} *ugtP* colonies were smaller when grown on PAB without IPTG. However, in the presence of IPTG, the latter mutant had similar growth to BSB1. In the absence of IPTG, the mutant partially recovered the rod morphology and fewer mini cells were observed (Figure 3.17 B). However, the cells were shorter than wild type and bent. In the presence of IPTG, the cells completely recovered their rod shape and no bending was observed. However, mini cells and mislocalisation of the septum were still present (Figure 3.17 B).

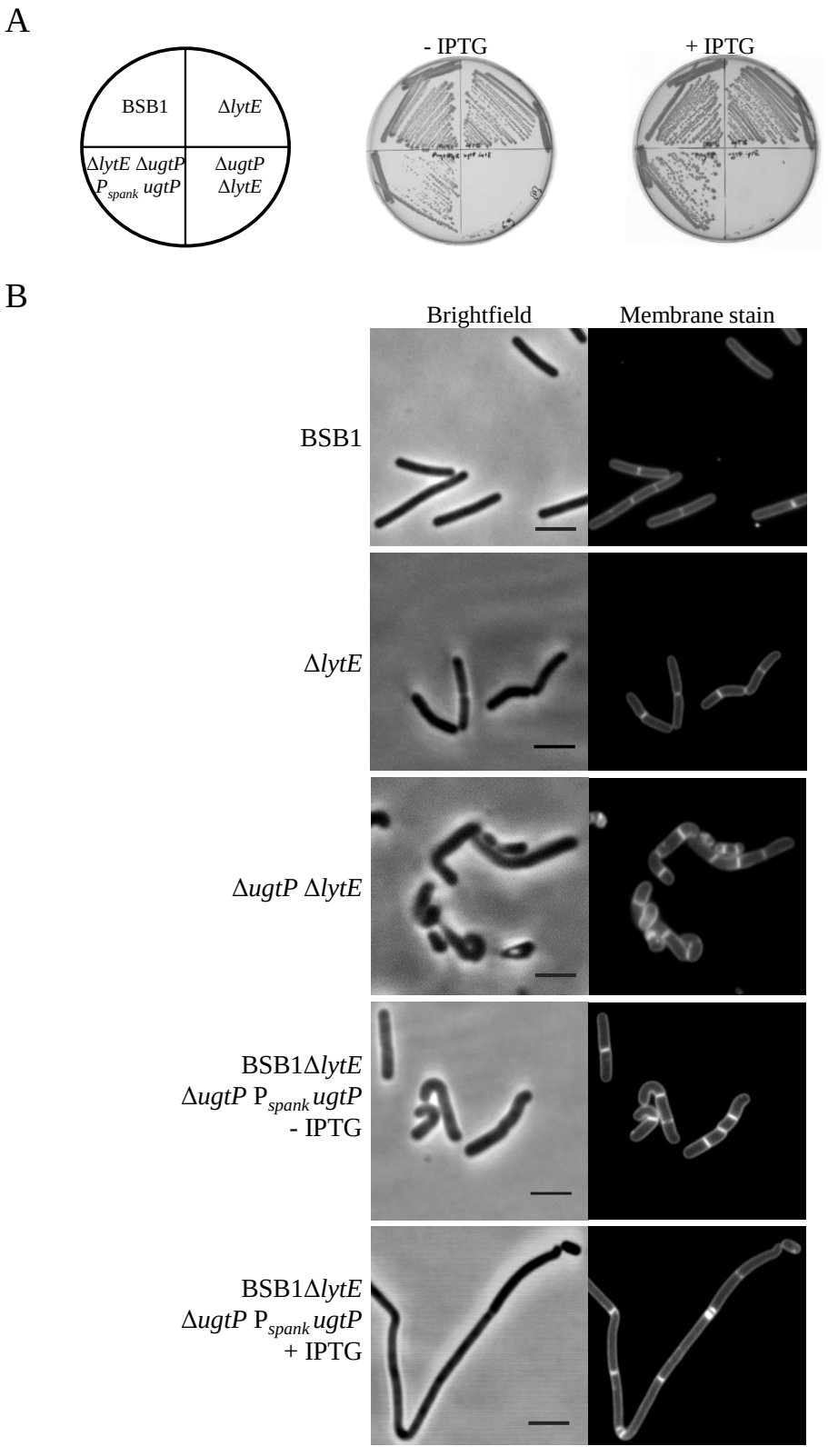

Figure 3.17 Growth and morphology of BSB1Δ*ugtP* cells lacking the DL-endopeptidase LytE

(A) Growth of BSB1, Δ*lytE*, Δ*ugtP* Δ*lytE* and Δ*ugtP* Δ*lytE* P_{spank} *ugtP* cells on PAB plates with or without IPTG at 45˚C.

(B) Phase contrast or membrane stained images for Δ*lytE*, Δ*ugtP* Δ*lytE* or Δ*ugtP* Δ*lytE* P_{spank} *ugtP* mutants. The Δ*ugtP* Δ*lytE* mutant had severe shape defects compared to the Δ*lytE* mutant. The complementation of *ugtP* partially rescued the Δ*ugtP* Δ*lytE* morphological defect. Scale bars: 4 µm.

3.2.4 The deletion of *cwlO* in cells lacking UgtP causes short and wide cells

The absence of LytE in the Δ*ugtP* mutant caused a severe shape defect. CwlO and LytE have the same enzymatic activity and they both play a role in cell elongation (Bisicchia *et al.,* 2007; Hashimoto *et al.,* 2012). The absence of CwlO in BSB1 or Δ*ugtP* mutants had no effect on cell growth. Fluorescence microscopy analysis for BSB1Δ*cwlO* showed shorter and wider cells than BSB1 (Figure 3.18). Interestingly, the Δ*ugtP* Δ*cwlO* mutant was wider than *cwlO* or *ugtP* single mutants and had a similar short cell morphology to Δ*ugtP* cells. These results show that the Δ*ugtP* Δ*cwlO* mutant had worse morphological defect compared to the Δ*ugtP* mutant, however, LytE seems to have a greater contribution in maintaining proper cell morphology than CwlO in cells lacking UgtP.

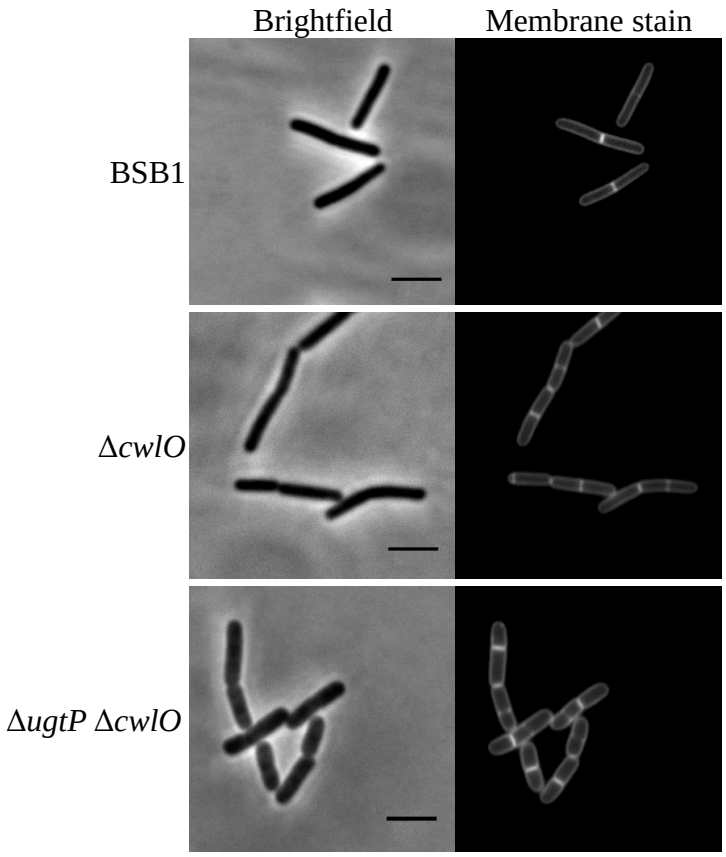

Figure 3.18 Morphology of BSB1Δ*ugtP* strains lacking the DL-endopeptidase CwlO

Phase contrast or cell membrane stained images for BSB1, Δ*cwlO* or Δ*ugtP* Δ*cwlO* mutants grown in LB media at 37˚C. Δ*cwlO* mutant had shorter and wider cells than BSB1. Δ*ugtP* Δ*cwlO* mutant had shorter and wider cells than both BSB1 and the Δ*cwlO* mutant. Scale bars: 4 µm.

3.2.5 The deletion of *lytF* in cells lacking UgtP causes chaining and shorter cells

Cells lacking LytE but not CwlO showed severe growth and shape defects. Unlike CwlO that is involved in cell elongation only, LytE is assumed to play a role in both cell elongation and division. LytF, a DL-endopeptidase, has a role in PG hydrolysis during cell division (Yamamoto *et al.,* 2003). BSB1Δ*ugtP* Δ*lytF* was constructed and characterised to test if this DL-endopeptidase is as important as LytE in the absence of UgtP. BSB1Δ*lytF* was also constructed and studied as a control. BSB1Δ*lytF* and BSB1Δ*ugtP* Δ*lytF* had similar growth as BSB1 on NA plates (data not shown). Fluorescence microscopy analysis for the Δ*lytF* mutant cells showed chain formation that is probably caused by delay in cell separation (Figure 3.19). Cells lacking both UgtP and LytF were shorter than wild-type cells and formed chains. This morphology is a combination of those of the single mutants, suggesting that LytE has a bigger role in maintaining rod shape than LytF in the *ugtP* mutant.

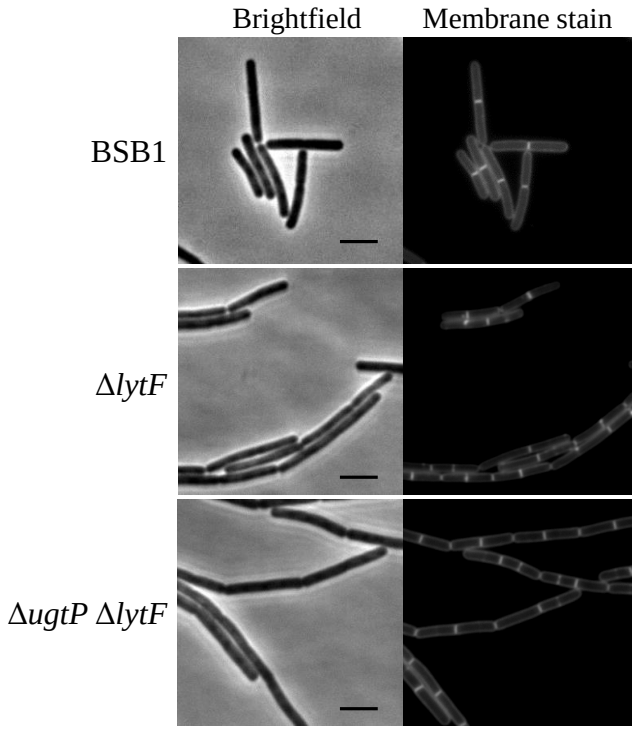

Figure 3.19 Morphology of the *ugtP* mutant lacking the DL-endopeptidase LytF

Phase contrast and cell membrane stained images for BSB1, Δ*lytF* and Δ*ugtP* Δ*lytF* mutants grown in LB at 37˚C. The deletion of *lytF* in BSB1 or the Δ*ugtP* mutant caused similar chaining morphology. Scale bars: 4 µm.

3.2.6 The deletion of *lytABC* in cells lacking GtaB causes chaining and short cells

We initially considered to construct a strain lacking the LTA glucolipid precursor and the amidase LytC using the available strains. LytC is involved in cell separation by hydrolysing the bond between the N-acetylmuramic acid and the L-Ala of PG (Rogers *et al.,* 1984). *lytC* is encoded in the *lytABC* operon where LytA and LytB are suggested to be chaperons for LytC (Lazarevic *et al.*,1992), hence the use of the *lytABC* mutant. Both the *lytABC* and *ugtP* mutants available have neomycin cassettes, thus the strategy was changed to construct a strain lacking *lytC* and *gtaB*. The double deletion of *gtaB* and *lytABC* had no effect on growth. The morphology of Δ*lytABC* and Δ*gtaB* Δ*lytABC* mutants was studied using fluorescence microscopy. The Δ*LytABC* mutant cells formed chains suggesting a delay in cell separation whereas the Δ*gtaB* Δ*lytABC* mutant cells were short and chaining (Figure 3.20). The latter morphology is a combination of those of the single mutants. These results suggest that LytE contributes more to the cell morphology than LytABC in cells lacking LTA glucolipids. Thus, LytE seems to have an unknown important role in cells lacking UgtP. Subsequently, TEM

analysis was performed for several mutant to acquire high resolution images in order to better understand the effects of these mutations on the cell wall.

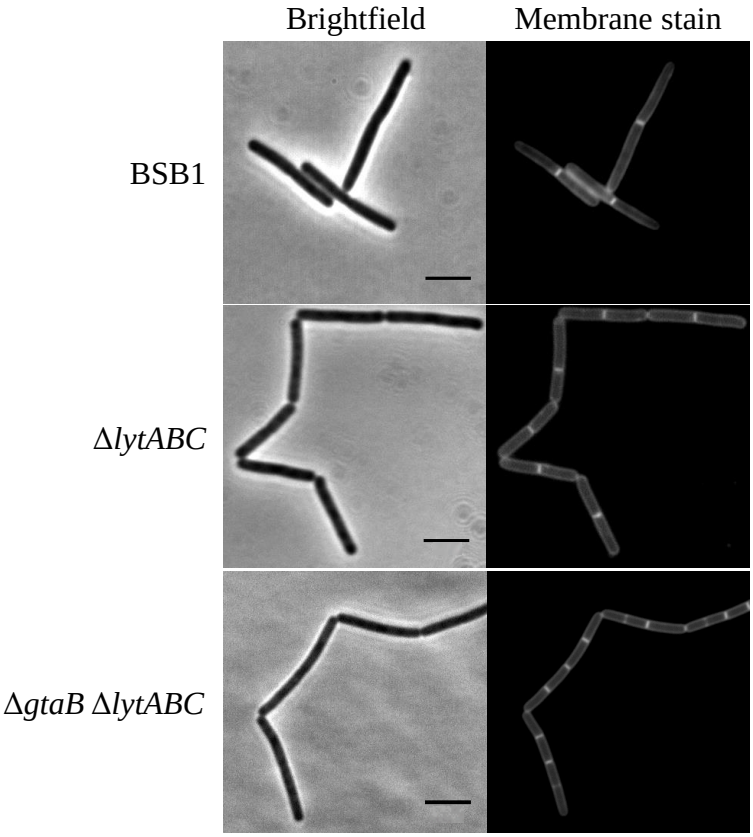

Figure 3.20 Morphology of Δ*gtaB* mutants lacking the *lytABC* operon

Phase contrast and cell membrane stained images for BSB1, Δ*lytABC* and Δg*taB* Δ*lytABC* mutants grown in LB media. The absence of LytABC resulted in chained cells whereas the absence of both LytABC and GtaB resulted in short and chained cells. Scale bars: 4 µm.

3.2.7 TEM imaging for the *ugtP lytE* and *ugtP cwlO* mutants

The absence of UgtP caused rough cell surface (Figure 3.14). The absence of LytE or CwlO in the *ugtP* mutant worsen the morphology of the cells. Using fluorescence microscopy with or without membrane dye was insufficient to observe changes in cell wall morphology, therefore, mutants were analysed by TEM to obtain high resolution images. The deletion of both *cwlO* and *ugtP* caused wider cells, as seen by fluorescence microscopy (Figure 3.18), and a rougher cell surface than the Δ*ugtP* mutant (Figure 3.21). The BSB1Δ*LytE* mutant had similar cell wall morphology to wild type cells while the Δ*lytE ΔugtP* mutant had severe shape defect with the loss of rod shape, formation of bulges and loss of cell wall integrity (Figure 3.17 and 3.21). The cell wall morphology of the Δ*ugtP* Δ*lytE* mutant adds evidence to demonstrate the importance

of LytE in maintaining shape in the absence of UgtP. This suggests that the DL-endopeptidase LytE contributes to CW hydrolysis in the Δ*ugtP* mutant and such activity is required for cells to maintain the rod shape.

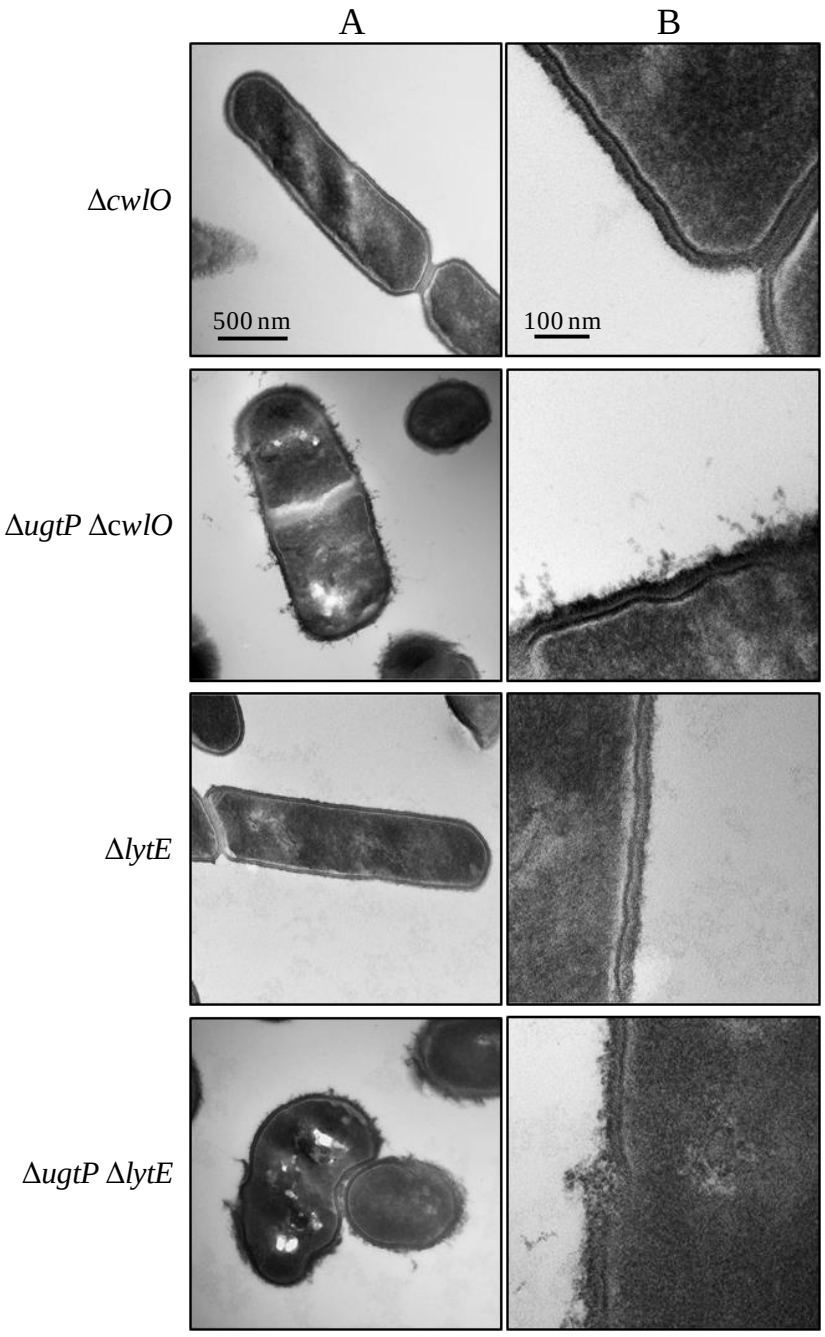

Figure 3.21 TEM images for Δ*cwlO*, Δ*ugtP* Δ*cwlO*, Δ*lytE* and Δ*ugtP* Δ*lytF* mutants

The Δ*cwlO* Δ*ugtP* mutant had wide cells and rough cell wall structure compared to both BSB1 and Δ*cwlO* cells. The Δ*lytE* Δ*ugtP* mutant had a severe shape defect with loss of cell wall integrity. Scale bars: (A) 500 nm, (B) 100 nm.

3.2.8 Growth and morphology of the *ugtP lytE ponA* and *ugtP lytE sigM* mutants

The Δ*ugtP* mutant exhibited an altered cell wall structure probably caused by high PG hydrolase activity in addition to increased levels of cell wall precursors suggesting an upregulation of PG synthesis. Thus, the deletion of *ponA* or σ^M genes could rescue the Δ*ugtP* Δ*lytE* phenotype by balancing the PG synthesis and hydrolysis. σ^M is an ECF sigma factor involved in cell wall synthesis and cell shape maintenance through upregulation of genes involved in cell wall synthesis (Cao *et al.*, 2002; Jervis *et al.*, 2007).

The deletion of *ponA* in the *ugtP* mutant was lethal (Section 3.1.4), however, the deletion of *ponA* in the Δ*ugtP* Δ*lytE* double mutant was viable. The triple mutant grew at 37˚C on NA or PAB plates but it was not able to grow at 45˚C on PAB plates (Figure 3.22 A). Fluorescence microscopy analysis showed that the Δ*ugtP* Δ*lytE* Δ*ponA* mutant had a comparable morphology to the Δ*ponA* mutant (Figure 3.8), in addition to the formation of chained cells (Figure 3.22 B).

The deletion of *sigM* in the Δ*ugtP* Δ*lytE* mutants did not rescue the lethal phenotype of cell growth on PAB at 45˚C (Figure 3.22 A). However, the deletion of *sigM* partially rescued the shape defect caused by the deletion of *ugtP* and *lytE* (Figure 3.22 B). The triple mutant cells were shorter and wider than wild type cells, formed chains, and had occasional (≈ 5%) mislocalisation of the septum. These results show that deleting *ponA* or *sigM*, rescues the morphological defect of the *ugtP lytE* double knockout.

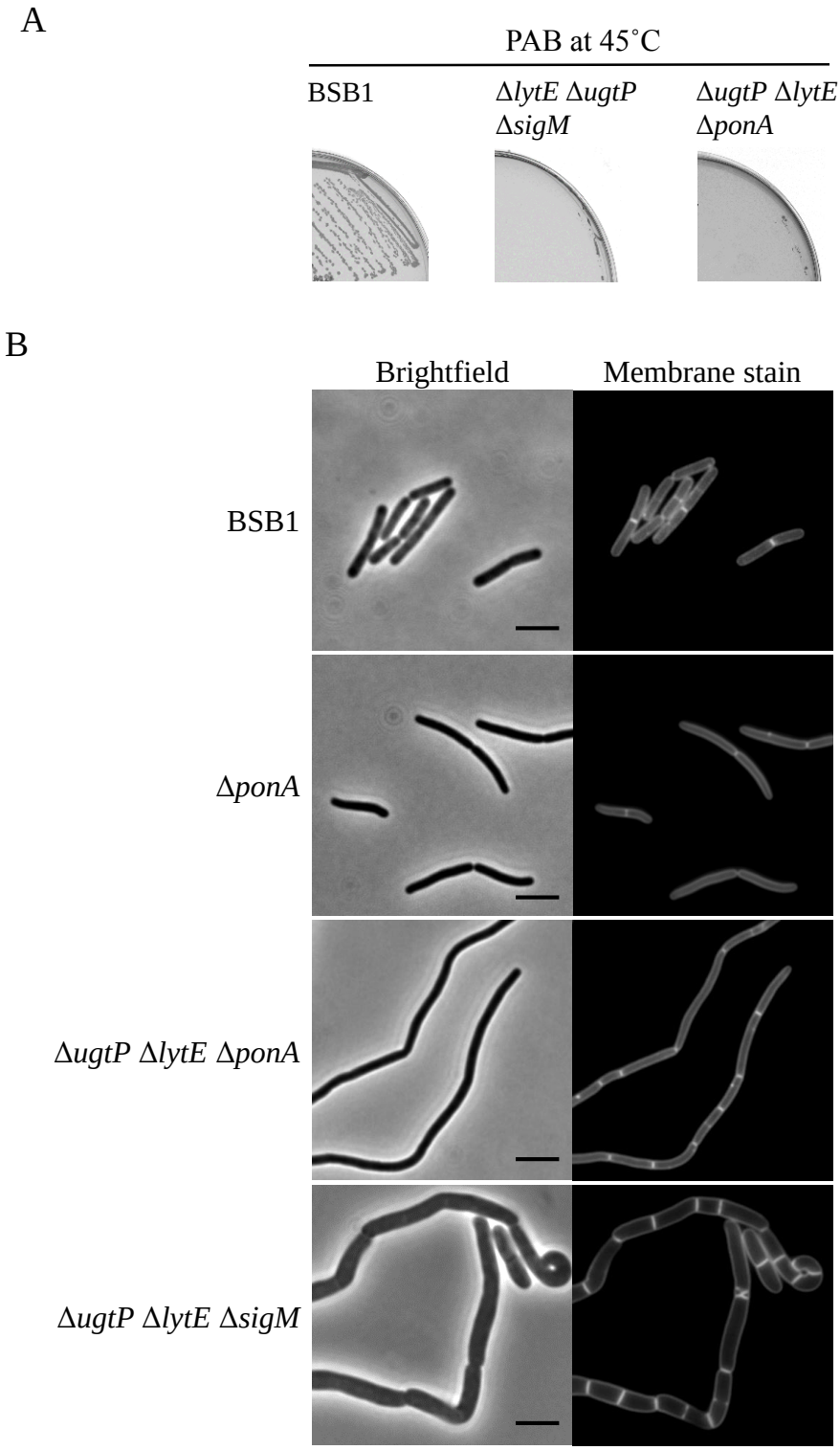

Figure 3.22 Growth and morphology of BSB1Δ*ugtP* Δ*lytE* strains lacking SigM or PBP1

(A) BSB1Δ*ugtP* Δ*lytE* Δ*ponA* or BSB1Δ*ugtP* Δ*lytE* Δ*sigM* mutant cells did not grow on PAB plates at 45˚C.

(B) Phase contrast and cell membrane stained images for BSB1, Δ*ponA*, Δ*ugtP* Δ*lytE* Δ*ponA* and Δ*ugtP* Δ*lytE* Δ*sigM* mutants grown in LB at 37˚C. BSB1Δ*ugtP* Δ*lytE* Δ*ponA* cells had thin and chained cell morphology. The Δ*ugtP* Δ*lytE* Δ*sigM* mutant had wide, short and chained cell morphology in addition to occasional mislocalisation of the septum. Scale bar: 4 µm.

3.3 Conclusions and discussion

The BSB1Δ*ugtP*, Δ*gtaB* or Δ*pgcA* mutants grew similarly to wild-type cells but exhibited a short and wide cell morphology. UgtP coordinates cell size to growth rate in a nutrient rich environment by regulating the polymerization of FtsZ (Chien *et al.*, 2012b; Weart *et al.*, 2007). Thus, the overexpression of *ugtP* in the BSB1Δ*ugtP* P_{spank} *ugtP* strain resulted in increased cell length and occasional septal mislocalisation (≈20%) which correlates with the function of UgtP as an inhibitor of FtsZ polymerization (Weart *et al.*, 2007).

Microarray experiments for the *ugtP* mutant indicated an increase in the transcription levels of several genes with unknown functions (Salzberg and Helmann, 2008). However, microarray studies only reveal the relative amounts of mRNAs in the cell, which might not correlate with the expression levels of the gene, or with the activity of the corresponding proteins. Thus, metabolomics analysis for the *ugtP* mutant performed by our collaborators determined the levels of several PG precursors were increased up to three fold suggesting upregulation of PG synthesis. The double deletion of *ugtP*, *gtaB* or *pgcA* and *ponA*, encoding the class A PG synthase PBP1, was lethal. However, the deletion of *ponA* in the complementation strain was viable even in absence of inducer suggesting that a minimal amount of UDP-glucose is sufficient for cell survival in the absence of the PBP1.

Both Δ*ponA* and Δ*ponA* Δ*ugtP* P_{spank} *ugtP* mutants grew poorly at 37˚C on PAB plates without magnesium ion supplements. Interestingly, the growth of the Δ*ponA* but not the Δ*ponA* Δ*ugtP* P_{spank} *ugtP* mutant was improved when cells were grown at 45˚C. The sigma factor SigI, required for cell growth at high temperature, responds to heat stress by upregulating the expression of *lytE*, *mreBH*, *bcrC* and *rsgI* (Schirner and Errington, 2009; Tseng and Shaw, 2008; Tseng *et al*., 2011). BcrC is an undecaprenyl phosphate phosphatase that produces the carrier lipid for cell wall synthesis. Thus, the increase in the expression of *bcrC* at high temperature might be responsible for the alleviated growth of the *ponA* mutant by increasing the availability of lipid II. However, the inability for the cells lacking UgtP and PBP1 to grow at 45˚C suggest that the upregulation of the SigI controlled genes are insufficient to support the Δ*ponA* mutant growth in the absence of LTA glucolipids.

The absence of the PG synthase PBP1 caused thin cell morphology. MreB is an actin homolog and a shape-determining factor in rod-shaped bacteria (Daniel and Errington, 2003). Previously published data proposed that MreB provides a scaffold that organizes the peptidoglycan synthesis machinery during cell elongation and thereby directing the lateral cell wall growth (Dominguez-Escobar *et al.*, 2011; Garner *et al.*, 2011). *E. coli* cells expressing MreB with a

substitution in the ATP binding domain (MreBD165A/E) exhibited thin cell morphology similar to the *ponA* mutant (Kruse *et al.,* 2003). Moreover, cells with different MreB alleles exhibited variations in cell width dimensions which correlated with the MreB helical pitch angle and the MreB polymer length (Ouzounov *et al.,* 2016). These results suggests that MreB is a key determinant of cell diameter. Therefore, since PBP1 is part of the elongation machinery, the absence of the synthase might alter the dynamics of the elongasome complex leading to a change in the MreB helical conformation and resulting in thin cell morphology. Additionally, the deletion of *ugtP* resulted in increased expression of MreB and MreBH (Matsuoka *et al.,* 2011). Therefore, cells lacking both UgtP-S827 and PBP1 might be subject to additional stress caused by increased MreB expression and altered cytoskeleton dynamics resulting in thinner cell width than the Δ*ponA* mutant.

Defects in UgtP reduced the size of the cell by 20% during growth in a nutrient rich medium, however, the absence of UgtP had no effect on growth when cells were grown in minimal medium (Weart *et al.,* 2007). Since cells lacking UgtP had similar growth and viability to wild-type cells, the defects resulting from the absence of UgtP are probably due to abnormal cell size homeostasis (Weart *et al.,* 2007). *B. subtilis* coordinates cell size with nutrient availability but why they do so is unclear. It was suggested that UgtP inhibits FtsZ polymerization when cells are grown in nutrient-rich medium resulting in an increase in the cell size which permits the accommodation of the extra DNA generated by multifork replication (Chien *et al.,* 2012a). The absence of both UgtP and PBP1 caused thin cells but had no significant effect on the cell length (Section 3.1.4). These results suggests that the role of UgtP is dispensable in the absence of PBP1 even when cells are grown in nutrient rich medium. Thus, we propose that the decrease in the dimensions of cells lacking UgtP and PBP1 resulted in a smaller cytoplasm, in which case the min and the nucleoid occlusion systems are sufficient to regulate Z–ring polymerization thereby cell size (Section 1.3.4).

Alteration in the LTA structure or composition causes cell shape defects in addition to increased autolysis activity and susceptibility to antimicrobial peptides (Matias and Beveridge, 2008; Perego *et al.,* 1995; Schirner *et al.,* 2009; Wecke *et al.,* 1996, 1997). UgtP synthesises the LTA glucolipid precursor, and the absence of UgtP or the LTA synthase LtaS in *S. aureus* cells resulted in longer LTA strands (Reichmann *et al.,* 2014). TEM analysis for cells lacking UgtP showed an altered cell surface suggesting high or uncontrolled hydrolase activity. This observation is consistent with previously published data showing increased levels of the endopeptidase LytE in cells grown at high temperature or in the absence of UgtP (Kasahara *et al.,* 2016). Moreover, the absence of the LtaS2 in *B. anthracis* resulted in a similar rough cell

surface to the *B. subtilis ugtP* mutant suggesting that the altered LTA structure is responsible for the increased autolytic activity in the cells (Garufi *et al.*, 2012). These modifications in cell wall structure or composition might be one of the reasons for the increased susceptibility to lysozymes and antimicrobials and for the induction of the stress response sigma factors *sigM*, *sigV* and *sigX* (Hashimoto *et al.*, 2013; Matsuoka *et al.*, 2011; Salzberg and Helmann, 2008). The TEM analysis also showed a decrease in cell wall thickness for cells lacking PBP1 and a further decrease in thickness for cells lacking both PBP1 and UgtP in addition to a rough cell surface. Therefore, the thin cell wall structure and the increased hydrolase activity might be creating weak points in the cell wall structure leading to cell lysis which might explain the lethality of the *ponA ugtP* double deletions.

PG analysis for the *ugtP* and *pgcA* mutants showed increased levels of Di- and Tri-Ala-mDap(NH_2)$_2$ muropeptides suggesting an increased DL-endopeptidase activity. *B. subtilis* has two redundantly essential lateral cell wall endopeptidases LytE and CwlO, important for cell elongation (Bisicchia *et al.*, 2007; Hashimoto *et al.*, 2012). The absence of both UgtP and LytE resulted in severe growth and shape defects whereby cells were short and twisted with a high number of mini-cells. The *ugtP cwlO* mutant showed shorter and wider cells than the *cwlO* single mutant suggesting that the loss of UgtP aggravates the shape defect caused by the absence of CwlO due to the increased cell requirement for DL-endopeptidase activity at the lateral wall (Hashimoto *et al.*, 2012). The depletion of CwlO in the *lytE* mutant resulted in similar twisted cell morphology to the *ugtP lytE* double mutant. In addition, the labelling of cells lacking both CwlO and LytE with fluorescent vancomycin showed no fluorescence along the cell periphery suggesting a halt in lateral wall PG synthesis (Bisicchia *et al.*, 2007). Therefore, we hypothesised that either CwlO is only partially active in cells lacking the LTA glucolipids making LytE essential for cell survival or that LytE has a crucial unknown role in cells lacking UgtP.

The expression of *lytE*, which is controlled by SigI, significantly increased in cells either lacking UgtP or grown at high temperatures (Kasahara *et al.*, 2016; Zuber *et al.*, 2001). Moreover, the overexpression of *lytE* in the absence of *sigI* rescued cell growth at high temperature (Tseng *et al.*, 2011). However, cells lacking both UgtP and LytE were viable at 37˚C but were not able to grow at 45˚C probably due to the lack of LytE activity.

The absence of *ugtP* resulted in increased autolysin activity and an upregulation of PG synthesis. The combined deletion of *ugtP* with *lytE* or *ponA* caused severe shape defects or lethality, respectively. Interestingly, cells with triple deletions in *ugtP*, *lytE* and *ponA* exhibited normal rod shape cells with a moderate chaining morphology. Moreover, the absence of SigM,

which responds to cell wall defects by upregulating genes involved in cell wall synthesis, in the *ugtP lytE sigM* triple mutant recovered the rod morphology but cells were short, wide and chaining (Cao *et al.,* 2002; Jervis *et al.,* 2007). The morphology of both triple mutants suggests that alteration in PG synthesis in the *ugtP lytE* mutant helps the cells to partially recover their rod shape. Taken together, these results suggest that a balanced PG synthesis and hydrolysis is important in cells lacking the LTA glucolipid precursor.

These results provided evidence for the importance of LytE in cells lacking the LTA glucolipids, however, the reasons behind the upregulation of this endopeptidase or the PG synthesis are not clear. Hence, the isolation of mutants that suppress the growth and shape defects of the *ugtP lytE* mutant might be helpful to further understand the role of LTA in the cell.

The impact of LTA on PG synthesis and hydrolysis

In rod-shaped bacteria and in *B. subtilis* in particular, the elongation of the cell wall occurs by the homogenous incorporation of newly synthesised PG in the lateral surface of the sacculus (den Blaauwen *et al.,* 2008; Daniel and Errington, 2003). The PG is also continuously modified and hydrolysed to maintain integrity and avoid thickening (Hayhurst *et al.,* 2008). Therefore, the activity of both synthases and hydrolases must be coordinated during synthesis to avoid weak points in the sacculus that might lead to bursting by turgor. UgtP was suggested to play a role in modulating cell size by regulating the assembly of the master regulator for cell division FtsZ (Chien *et al.,* 2012; Weart *et al.,* 2007). UgtP is also responsible for the synthesis of the LTA glucolipid precursor (Jorasch *et al.,* 1998). In *S. aureus*, the deletion of *ugtP* or *ltaS* resulted in increased LTA size suggesting longer glycerol phosphate chains (Reichmann *et al.,* 2014). Such changes in the LTA structure was coupled with increased LytE levels which was shown in this work to be important for cell growth and morphology in absence of glucolipids (Kasahara *et al.,* 2016). The increased *lytE* expression in the *ugtP* mutant was paralleled with rough cell surface and altered muropeptide composition suggesting high DL-endopeptidase activity. These modification in the cell wall structure are probably one of the reasons causing the induction of the extracellular sigma factor SigM, which responds to cell wall synthesis and cell shape maintenance (Cao *et al.,* 2002; Jervis *et al.,* 2007; Matsuoka *et al.,* 2011a). Interestingly, the loss of SigM or PBP1 was lethal in the absence of UgtP but not in the absence of both UgtP and LytE. Moreover, the *ugtP lytE sigM* and the *ugtP lytE ponA* mutants partially recovered the normal rod morphology. These results show that several dispensable proteins in

wild-type cells involved in PG synthesis, such as SigM and PBP1, seem to be crucial in the absence of UgtP when uncontrolled hydrolase activity occurs. Consequently, maintaining balanced PG synthesis and hydrolysis is essential for cells with altered LTA structure. Considering the above, this work enhanced our knowledge about the impact of *ugtP* deletion not only on FtsZ polymerization but also on PG synthesis (Figure 3.23). However, the reasons for the *lytE* upregulation in the cell with altered LTA structure is still unclear and the generation of suppressor mutants for the *ugtP lytE* phenotype might help in understanding the causes behind these complex genetic interactions.

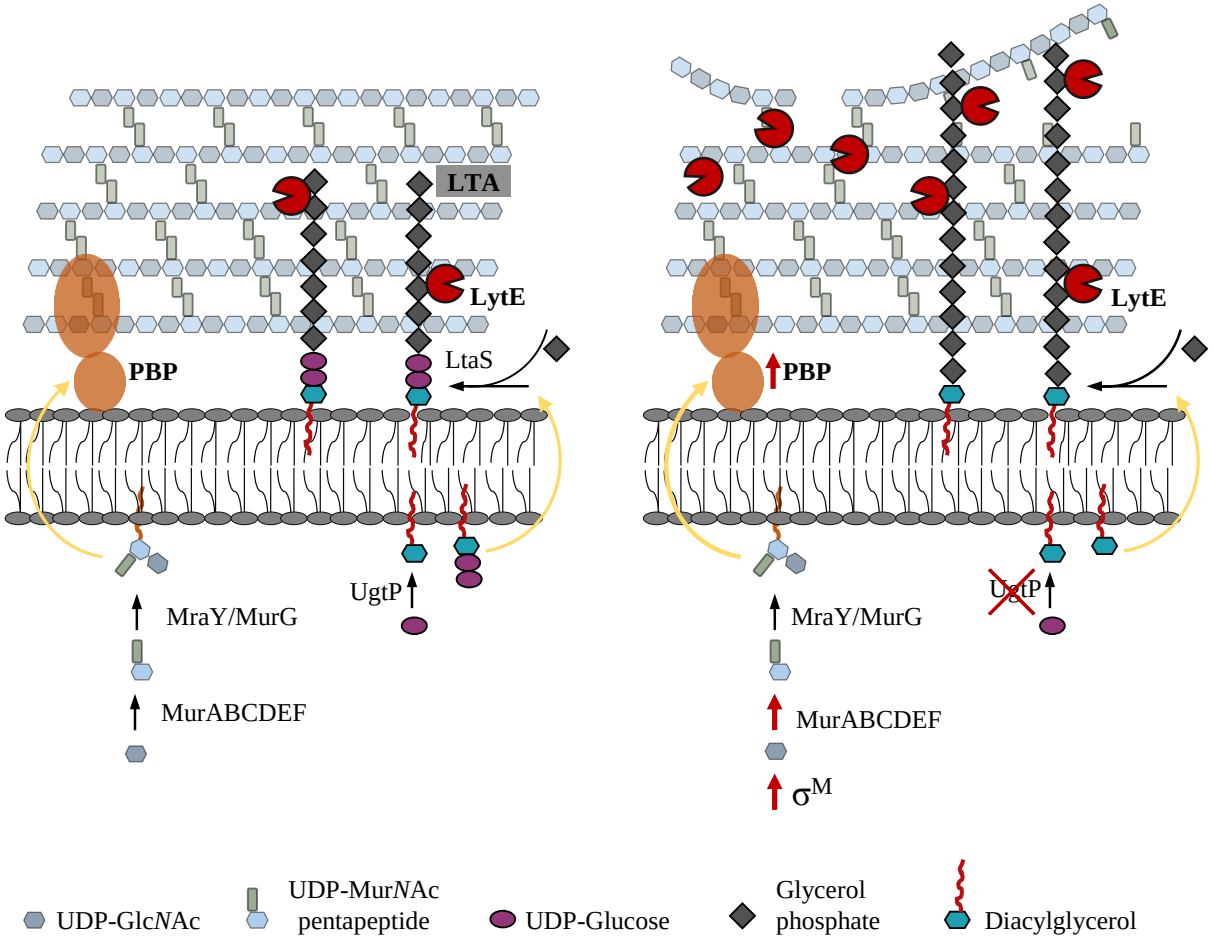

Figure 3.23 Simplified scheme showing the effects of *ugtP* deletion on the cell wall

To the left, the cartoon represents the synthesis and the structure of the PG and LTA in wild-type cells. To the right, the deletion of *ugtP* causes in the loss of the LTA UDP-Glucose resulting in longer LTA structure. The latter changes in the LTA resulted in higher LytE expression leading to altered cell wall structure. The absence of UDP-Glucose also caused increased expression of the extracellular sigma factor σ^M, which is probably resulting in the upregulation of PG synthesis.

4 Coordination of peptidoglycan synthesis during cell division

4.1 *In vitro* and *in vivo* characterization of the role of PBP3 in PG synthesis

4.1.1 Introduction

B. subtilis has 16 PBPs but only PBP2B (encoded by *pbpB*) is essential for cell division. PBP2B is a class B PBP with a catalytic TPase domain and a non-catalytic domain. Interestingly, in cells expressing PBP2B with a substitution of the TPase active site serine to an alanine residue (PBP2B*), PBP3, which is a non-essential PBP2B homologue, becomes essential (Richard Daniel, unpublished data). Further work showed that the inactivation of the TPase domain of PBP3 is lethal in the *pbpB** mutant suggesting enzymatic redundancy. In this work, the role of PBP3 in the *pbpB** mutants was characterized by studying the localisation of both PBPs using immunofluorescence microscopy. The effect of the PBP2B* mutation on the cell morphology was investigated using TEM. Interactions and activities of PBP2B and PBP3 were characterised *in vitro* in assays with the class A PBP1.

4.1.2 Similar localisation of PBP3 in 168CA and PBP2B* mutant cells

Previously, the localisation of PBP3 was studied using a GFP-PBP3 construct (Scheffers *et al.*, 2004). In wild-type cells GFP-PBP3 predominantly localised in dots or foci at the cell periphery and more frequently at the cell poles after division was completed, but with relatively little enrichment at the division site (Scheffers *et al.*, 2004). In the PBP2B* mutant, the localisation pattern of GFP-PBP3 was similar to that in the wild type cells. An alternative approach was also used to study the localisation of PBP3 by using immunofluorescence microscopy (IFM) (section 2.7.2). Full length PBP3 was purified and used to produce α-PBP3 antibodies from guinea pigs. Subsequently, affinity chromatography was used with immobilised PBP3 to purify the antibody from the serum (section 2.9.8). Western blot analysis using the α-PBP3 antibody for cells expressing GFP-PBP3 (168CA *pbpC*::(P_{xyl} *gfp-pbpC*) showed two strong and two weak bands. The upper strong band correspond to GFP-PBP3 whereas the lower strong one correspond to PBP3. The weak bands presumably correspond to degradation products. This result suggests that the GFP was removed from the N-terminal of some GFP-PBP3 molecules (Figure 3.24). Immunofluorescence microscopy (IFM) with the α-PBP3 antibody was used to localise PBP3 in 168CA and PBP2B* cells. The α-PBP2B antibody from Daniel *et al.*, (2000) was used for the localisation of PBP2B in 168CA or PBP2B* cells as a control and the DNA was stained with DAPI. The localisation pattern of PBP3 in the PBP2B* mutant was comparable to that in 168CA cells, with PBP3 being slightly more enriched at the septum and

the cell poles (Figure 3.25). The differences in PBP3 localisation between wild-type cells and the PBP2B* mutant were difficult to quantify, thus an alternative method was required to investigate possible localisation differences.

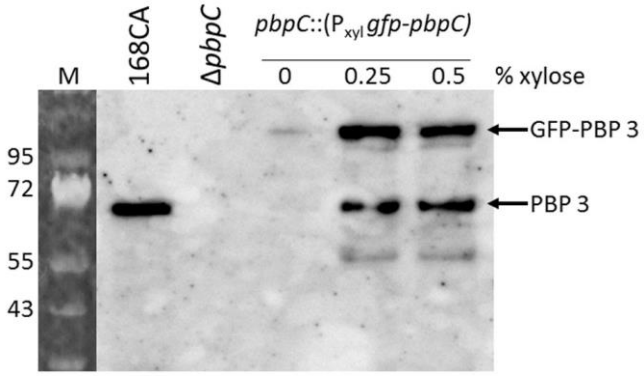

Figure 3.24 Cellular level of PBP3 (encoded by *pbpC* gene)

Western blot using α-PBP3 antibody for 168CA, the *pbpC* and the *pbpC*::(P_{xyl} *gfp-pbpC*) mutants grown in LB with or without xylose. The blot shows 2 bands that correspond to PBP3 and GFP-PBP3 in addition to degradation products, suggesting the removal of the GFP from some of the PBP3 molecules.

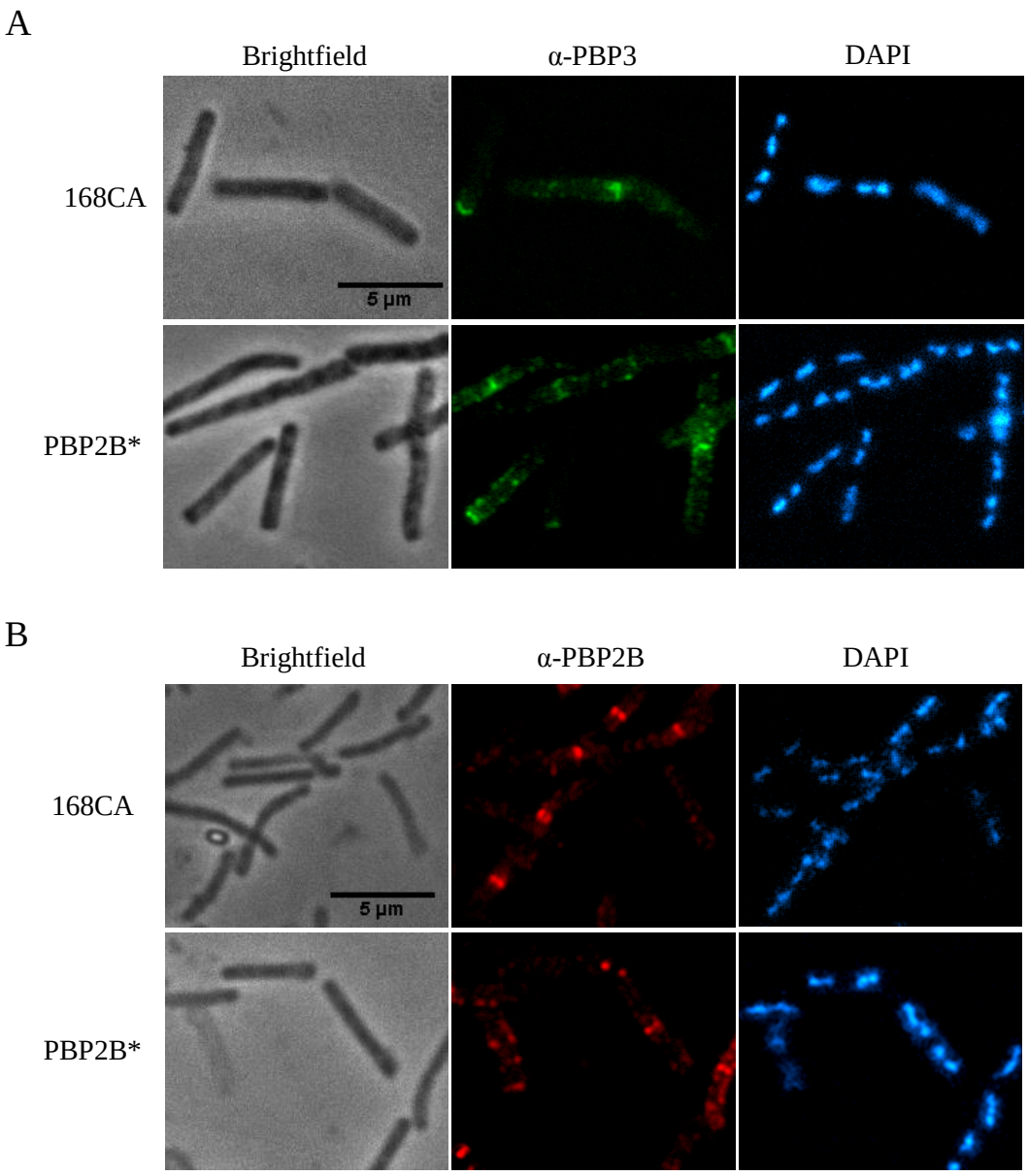

Figure 3.25 Cellular localisation of PBP3 or PBP2B using α-PBP3 or α-PBP2B antibodies, respectively

(A) PBP3 localisation in 168CA and PBP2B* mutant cells was determined by IFM using α-PBP3 antibody and a secondary antibody bound to FITC. PBP3 localised at midcell and occasionally at the lateral cell wall in foci. The DNA was stained with DAPI. Scale bar: 5 µm.

(B) PBP2B localisation in 168CA and PBP2B* mutant cells was determined by IFM using α-PBP2B antibody and a secondary antibody bound to a red fluorescent probe (Alexa 594). PBP2B localised at midcell in vegetative cells. The DNA was stained with DAPI. Scale bar: 5 µm.

4.1.3 PBP3 showed enhanced septal localisation in PBP2B* mutant cells

IFM images were not sufficient to visualize the possible changes of PBP3 localisation during the cell cycle in cells with inactive PBP2B (Figure 3.26). To obtain quantitative data on the localisation of PBP3 and PBP2B, profile maps were generated for both PBPs in 168CA and the PBP2B* mutant. The profile maps represent the fluorescence intensity profile of individual cells normalized to the cell average fluorescence and sorted horizontally by cell length. For the PBP2B* mutant cells, the profile maps showed longer cell length than wild type cells at all stages of the cell cycle (Figure 3.26 A). In young 168CA cells PBP3 localised at the cell poles and periphery but later in the cell cycle PBP3 was mostly recruited to midcell with the exception of some PBP3 molecules that showed occasional cell periphery localisation. In the PBP2B* mutant, PBP3 exhibited similar cell pole localisation to young 168CA cells, however, a decrease in the level of fluorescence at the cell periphery was detected at the early and middle stages of the cell-cycle. Moreover, the localisation of PBP3 at midcell was observed earlier in the PBP2B* mutant cell cycle compared to wild-type (Figure 3.26 A). For comparison, the same analysis using α-PBP2B antibodies showed similar localisation of PBP2B at mid-cell in both 168CA and PBP2B* cells (Figure 3.26 B). This localisation pattern was observed at early stages of the cell cycle in both 168CA or in PBP2B* cells suggesting early recruitment of PBP2B to the septum. These results suggests that the early and enhanced localisation of PBP3 at midcell in the PBP2B* mutant is presumably to complement the lack of PBP2B TPase activity.

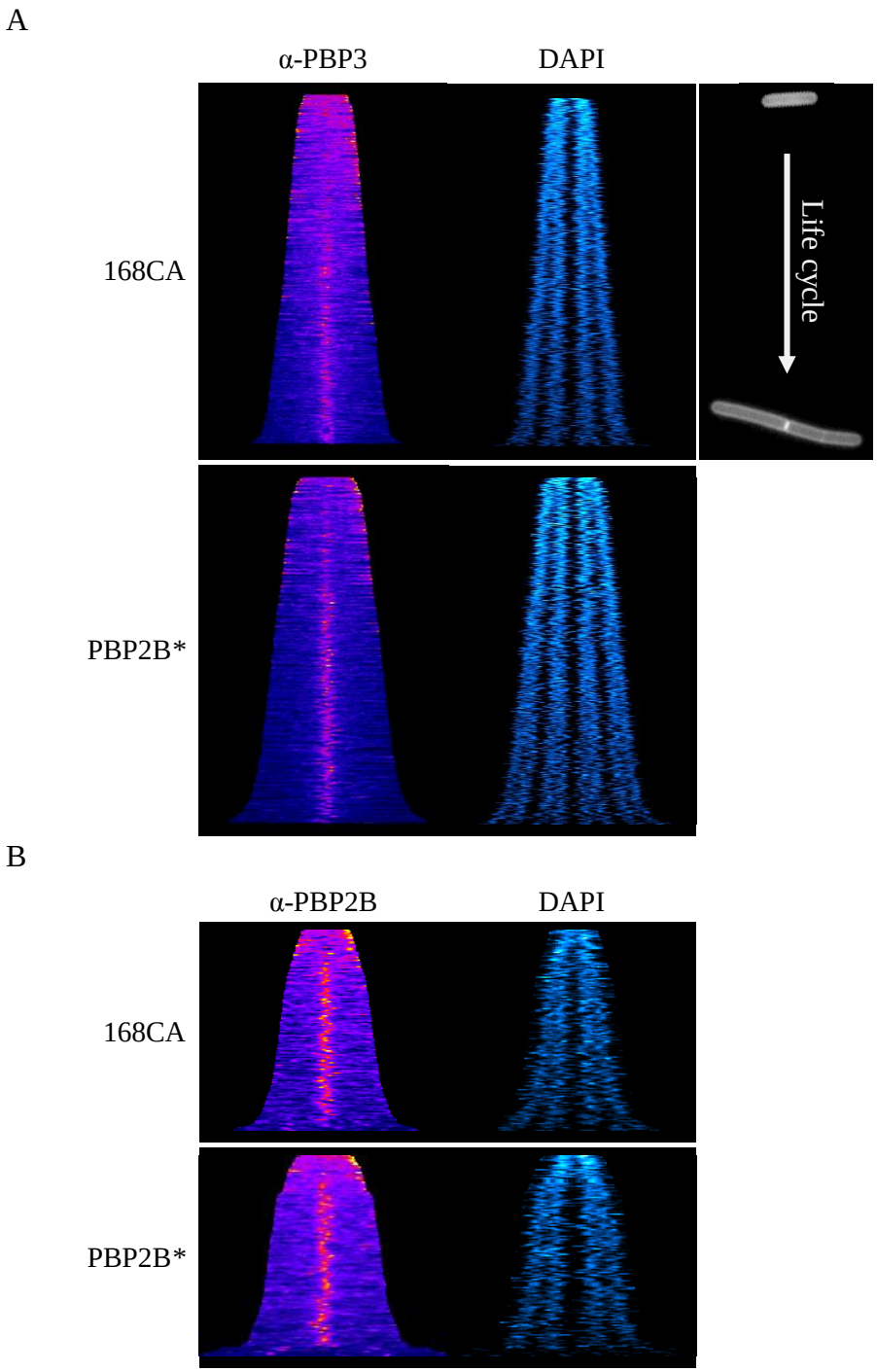

Figure 3.26 Profile maps for the localisation of PBP3 and PBP2B in 168CA and the PBP2B* mutant

(A) Profile maps representing the localisation of PBP3 by IFM using α-PBP3 antibody (n=450 cells). (B) Profile maps representing the localisation of PBP2B using α-PBP2B antibody (n=150 cells). The level of fluorescence was normalized to the mean cell fluorescence. The data was sorted using Python7 and the profile maps were created with ImageJ. PBP3 showed early and enhanced midcell localisation in the PBP2B* mutant compared to 168CA. The DNA was stained with DAPI.

4.1.4 PBP2B* cells have aberrant septum morphology

Microscopic images of the PBP2B* mutant showed an increase in cell length compared to 168CA. We proposed that cells with inactive PBP2B have a delay in building the septal PG which is causing an increase in cell length. However, fluorescence microscopy was insufficient to observe any changes in the septum morphology. Thus, we analysed 168CA, ΔPBP3 or PBP2B* cells by TEM to obtain high resolution images which gave us more insight into septum morphology. Most of the PBP2B* mutant cells (83%) exhibited aberrant septum (n=50) (Figure 3.27). The ΔPBP3 mutant had a similar septum morphology to 168CA cells suggesting a dispensable role for PBP3 in septal PG synthesis. These results suggest that although cells with active PBP3 TPase domain can compensate for the lack of TPase activity of PBP2B, the latter has a more important role in cell division.

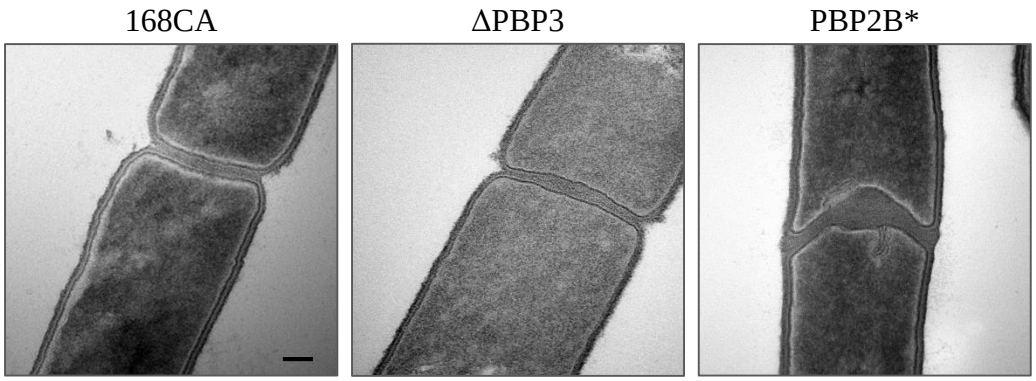

Figure 3.27 TEM images of 168CA, ΔPBP3 or PBP2B* mutant cells

The absence of PBP3 had no effect on the cell morphology whereas the inactivation of the TPase domain of PBP2B caused aberrant septa. Scale bar: 100 nm.

4.1.5 HPLC analysis of muropeptides from 168CA, ΔPBP3 and PBP2B* cells

B. subtilis has 16 PBPs that have redundant roles in PG synthesis, however, the inactivation of PBP2B alone distorted the septum of the cell. Next we analysed muropeptides isolated from ΔPBP3 or PBP2B* mutant cells to study the effect of such mutations on the PG composition. Cell wall material was harvested from exponentially growing cells (Section 2.11.1). The cell wall was purified from cell lysate followed by the PG purification (Section 2.11.2). The PG was digested with cellosyl to muropeptides by cutting the β-1,4-glycosidic bond between the *N*-acetylmuramic acid and the *N*-acetylglucosamine. Muropeptides were reduced and analysed by HPLC using a reversed-phase column. The RP-HPLC muropeptide elution patterns of PGs from 168CA, ΔPBP3 and PBP2B* mutants showed comparable muropeptide profiles with only two minor differences for the PBP2B* mutant (Figure 3.28). First, a small unknown peak, observed in one of the experiments, had a retention time of 96 min and appeared in 168CA and ΔPBP3 muropeptide profiles but not in the PBP2B* muropeptide profile. Second, a mild reduction in the peak area for the muropeptide number 15 for the PBP2B* mutant was observed compared to wild-type. The relative quantification of the muropeptides identified a 2% decrease in the TriTetra(NH_2) for the PBP2B* mutant compared to wild-type (Table 3.2). The lower levels of TriTetra(NH_2) correlated with a 3.1% decrease in percentage of peptides in crosslinks and a 3.1% increase in the sum of monomeric muropeptides from PBP2B* compared to 168CA cells. The changes in muropeptide levels are probably caused by the expression of inactive PBP2B in the cell (Table 3.2). No changes were identified between muropeptides from 168CA or ΔPBP3 cells. To get more insights about the function of these PBPs, biochemical assays were used to characterize the activities and interactions of PBP2B, PBP3 and the class A PBP1.

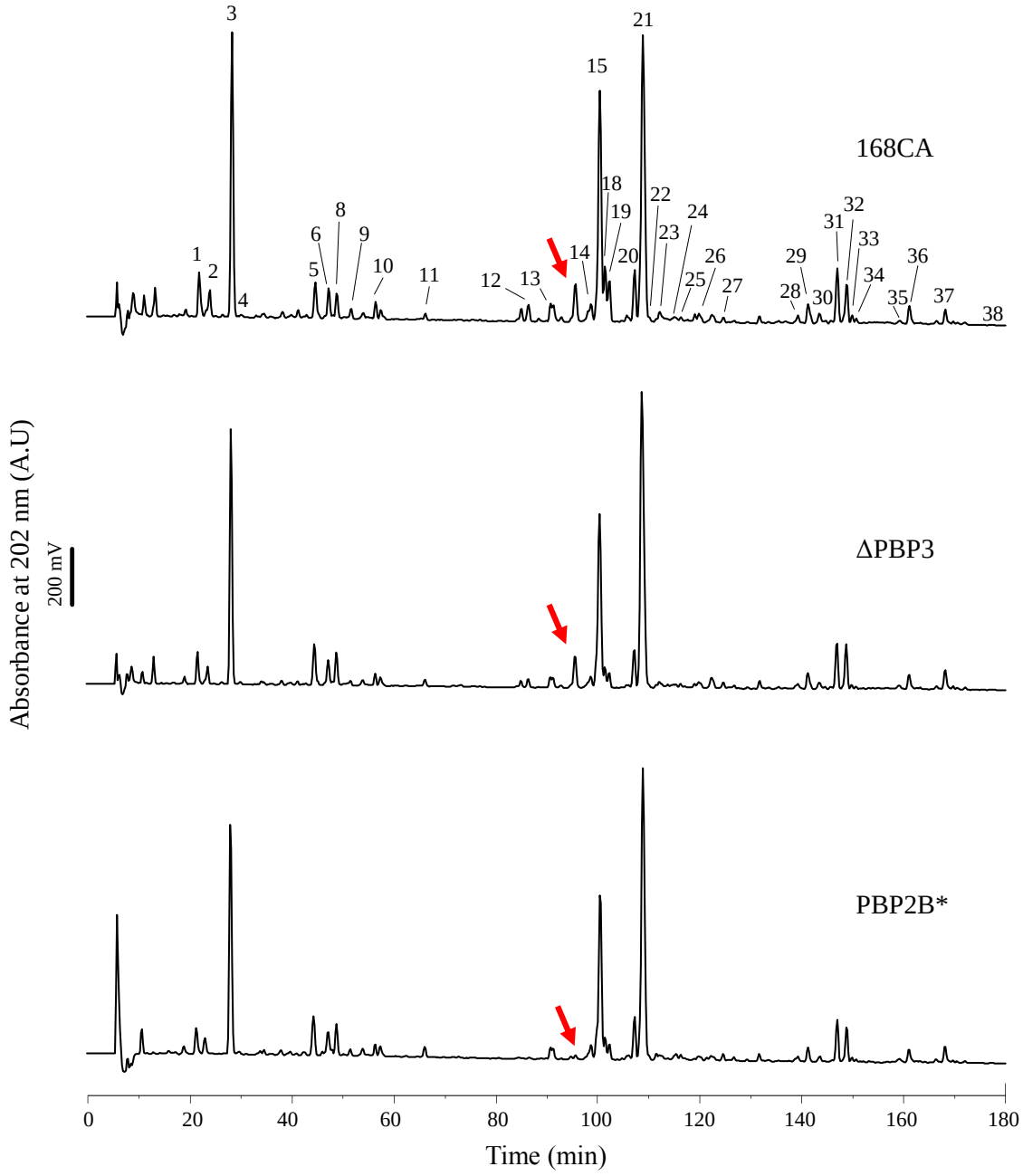

Figure 3.28 RP-HPLC analysis of muropeptides from 168CA, ΔPBP3 and PBP2B* cells

Muropeptide profiles for 168CA, ΔPBP3 and PBP2B* cells. The peaks 1-38 have been assigned according to Bisicchia *et al.*, 2011. 168CA, ΔPBP3 or PBP2B* mutant cells have similar muropeptide profiles except two minor differences, the mild decreased peak area for the muropeptide number 15 in the PBP2B* mutant and the unknown peak (red arrow) detected in only one of the experiments for 168CA and ΔPBP3.

Muropeptides [1]	Peak no	Peak area (%) 168CA	ΔPBP3	PBP2B*
Tri	1	2.0 ± 0.1	1.7 ± 0.2	1.9 ± 0.1
Tri (NH_2) (PO_4)	2	1.4 ± 0.3	1.3 ± 0.2	1.3 ± 0.0
Tri (NH_2)	3	14.1 ± 0.1	14.1 ± 0.1	14.1 ± 0.1
Tri (NH_2) (deAc)	4	0.1 ± 0.1	0.1 ± 0.1	0.1 ± 0.1
Di	5	2.2 ± 0.1	2.3 ± 0.4	2.3 ± 0.4
Tri-Ala-mDap (NH_2)	6	1.3 ± 0.3	1.3 ± 0.2	1.3 ± 0.4
tetra (NH_2)	7	0.2 ± 0.1	0.4 ± 0.2	0.4 ± 0.1
Tri-Ala-mDap (NH_2)$_2$	8	1.2 ± 0.0	1.5 ± 0.3	1.4 ± 0.4
penta (Gly5) (NH_2)	9	0.4 ± 0.0	0.3 ± 0.0	0.4 ± 0.1
TriTetra (-GM) (NH_2)$_2$	10	0.8 ± 0.1	0.7 ± 0.1	0.7 ± 0.0
penta (NH_2)	11	0.4 ± 0.1	0.4 ± 0.0	0.6 ± 0.0
TriTetra (-G)	12	0.6 ± 0.1	0.6 ± 0.0	0.6 ± 0.1
TriTetra (NH_2) (PO_4)	13	1.6 ± 0.8	1.7 ± 0.5	0.6 ± 0.3
TetraTetra (-GM) (NH_2)$_2$	14	1.2 ± 0.3	1.0 ± 0.0	1.0 ± 0.1
TriTetra (NH_2)	15	14.0 ± 1.7	13.1 ± 1.4	12.0 ± 1.3
TriTetra (NH_2) (deAc)	18	2.1 ± 0.5	1.3 ± 0.2	1.4 ± 0.2
TriTetra (NH_2) (deAc)	19	1.8 ± 0.5	1.0 ± 0.2	1.1 ± 0.2
TriTetra (NH_2)	20	2.8 ± 0.0	2.4 ± 0.0	2.5 ± 0.2
TriTetra (NH_2)$_2$	21	25.6 ± 3.1	27.7 ± 0.6	24.2 ± 1.0
TriTetra (NH_2)$_2$ (deAc)	22	0.1 ± 0.1	0.1 ± 0.1	0.1 ± 0.1
TriTetra (NH_2)$_2$ (deAc)	23	0.3 ± 0.1	0.3 ± 0.1	0.4 ± 0.0
Penta (Gly5) Tetra	24	0.5 ± 0.1	0.4 ± 0.2	0.4 ± 0.1
Penta (Gly5) Tetra (NH_2)$_2$	25	0.4 ± 0.2	0.6 ± 0.4	0.5 ± 0.1
TetraTetra (NH_2)$_2$	26	1.1 ± 0.4	0.9 ± 0.1	0.7 ± 0.3
PentaTetra (NH_2)$_2$	27	0.5 ± 0.2	0.5 ± 0.1	0.5 ± 0.0
TriTetraTetra (NH_2)$_2$	28	0.4 ± 0.2	0.4 ± 0.1	0.6 ± 0.4
TriTetraTetra (-G)	29	1.2 ± 0.1	1.1 ± 0.2	0.7 ± 0.3
TriTetraTetra (NH_2)$_2$	30	0.6 ± 0.1	0.5 ± 0.1	1.5 ± 1.1
TriTetraTetra (NH_2)$_3$	31	2.7 ± 0.3	2.5 ± 0.4	2.1 ± 0.1
TriTetraTetra (NH_2)$_3$ (deAc)	32	2.7 ± 0.3	2.6 ± 0.2	1.2 ± 1.0
TriTetraTetra (NH_2)$_3$ (deAc)	33	0.5 ± 0.1	0.4 ± 0.1	0.3 ± 0.2
Penta(Gly5)TetraTetra (NH_2)$_{2-3}$	34	0.3 ± 0.1	0.2 ± 0.1	0.3 ± 0.0
TriTetraTetraTetra (NH_2)$_{2-3}$	35	0.2 ± 0.0	0.3 ± 0.1	0.5 ± 0.3
TriTetra(Anh) (NH_2)$_2$	36	0.8 ± 0.2	0.8 ± 0.1	0.5 ± 0.1
TriTetraTetraTetra (NH_2)$_4$	37	0.9 ± 0.2	1.2 ± 0.2	1.0 ± 0.1
TriTetraTetra(Anh) (NH_2)$_2$	38	0.1 ± 0.1	0.0 ± 0.0	0.0 ± 0.0
Sum monomers		25.3 ± 0.0	25.7 ± 0.9	28.4 ± 0.3
Sum dimers		62.2 ± 0.0	61.9 ± 0.2	59.5 ± 0.4
Sum trimers		9.8 ± 0.2	8.9 ± 0.6	8.6 ± 0.2
Sum tetramers		1.4 ± 0.1	1.7 ± 0.3	1.8 ± 0.5
Sum dipeptides		2.5 ± 0.1	2.7 ± 0.3	2.9 ± 0.3
Sum tripeptides		55.8 ± 0.6	56.2 ± 0.3	57.0 ± 0.2
Sum tetrapeptides		39.7 ± 0.1	39.2 ± 0.3	37.9 ± 0.2
Sum pentapeptides		1.9 ± 0.3	1.8 ± 0.3	2.2 ± 0.2
Degree of Crosslinkage [2]		38.7 ± 0.0	38.2 ± 0.5	36.8 ± 0.0
% Peptides in Crosslinkage [3]		74.7 ± 0.0	74.3 ± 0.9	71.6 ± 0.3

Table 3.2 Muropeptide identities and quantification from 168CA, ΔPBP3 and PBP2B* cells

BSB1, ΔPBP3 or PBP2B* mutants showed similar levels of muropeptides except for a 3.1% decrease in muropeptides in crosslink from the PBP2B* mutant compared to 168CA. Peak areas shown represent the mean ± standard deviation of two independent PG preparations.

[1] Nomenclature of muropeptides according to Glauner *et al.*, (1988)

[2] calculated according to Glauner *et al.*, (1988)

[3] calculated as 100% - % monomers.

4.1.6 Purification of full length PBPs

In vivo work performed in Richard Daniel's lab showed that the activity of PBP3 is essential to complement the lack of PBP2B TPase activity in the cell suggesting partial functional redundancy. The deletion of PBP2B is lethal suggesting that the protein has a non-catalytic role that cannot be replaced even by the overexpression of PBP3 in the cell. To test if PBP3 interacts with PBP2B, we adopted an *in vitro* approach using affinity chromatography and SPR. Thus, we first established the purification of PBP2B and PBP3 and we characterized their enzymatic activities in the presence of PBP1. PBP2B* and PBP3* featuring substitutions in the active site serine residues to alanine were also purified for control experiments.

4.1.6.1 Purification of PBP2B

PBP2B was purified using affinity chromatography and ion exchange chromatography (section 2.9.2). *PbpB* (PBP2B gene) was cloned into pET28(a)+ (section 2.6.2). *E. coli* BL21(DE3) cells were used for the expression of PBP2B with an N-terminal hexahistidine tag (His-PBP2B). Cells were harvested and PBP2B was purified from the solubilised membrane fraction. Affinity chromatography was first performed to purify His-PBP2B from the membrane fraction (Figure 3.29 A). The hexahistidine tag was removed using thrombin. The second purification step consisted of ion exchange chromatography. Using the protein calculator software (http://protcalc.sourceforge.net/), His-PBP2B was predicted to have a positive charge +19 at pH 6.0. Thus, a HiTrap SP HP column was used to further purify PBP2B. Samples containing PBP2B were dialysed to pH 6 which promoted the binding of the protein to the column followed by elution of PBP2B using a gradient of elution buffer with 1 M NaCl and pH 7.5. Collected fractions from the two chromatography experiments were analysed by SDS-PAGE (Figure 3.29 A and B). Typically, 1.46 mg of PBP2B per litre of culture was obtained.

A

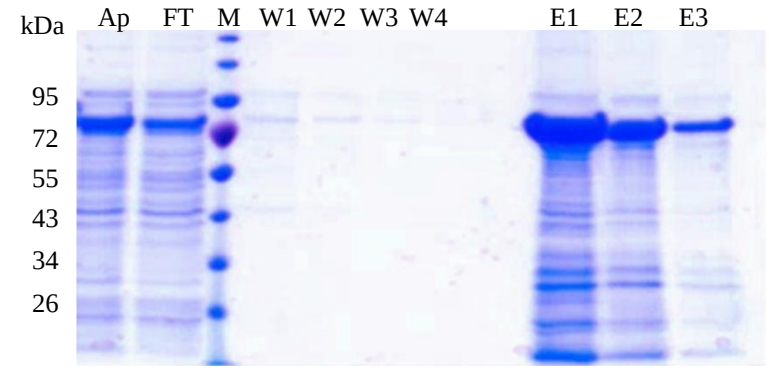

B

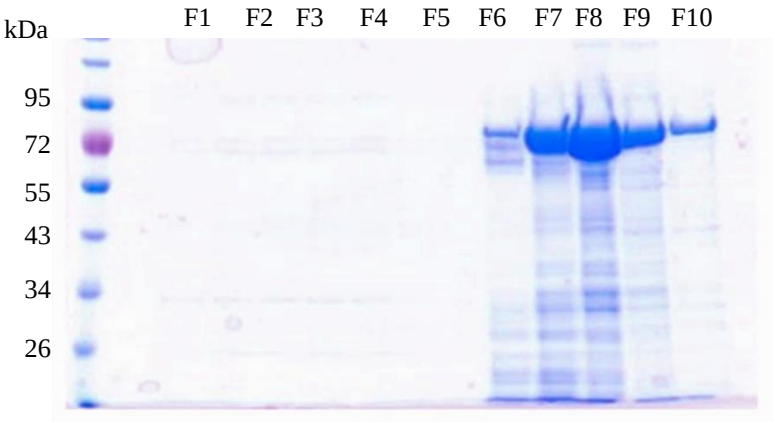

Figure 3.29 Purification of PBP2B

SDS-PAGE analysis shows the fractions of the PBP2B purification steps. Gels were stained with Coomassie blue.

(A) IMAC purification of His-PBP2B. App, applied fraction; FT, flow-through; M, Protein size marker (Fermentas PageRuler); W1-W4, wash fractions; E1-E3, elution fractions. The theoretical molecular weight of His-PBP2B is 81 kDa.

(B) IEX of the purified PBP2B after thrombin cleavage. M, Protein size marker; the bands in F7, F8, F9 and F10 fractions with an apparent molecular weight of 79 kDa correspond to PBP2B.

4.1.6.2 Optimization of PBP2B* purification

*PbpB** gene, encoding PBP2B*, was cloned into pET28(a)+ expression plasmid using ligase free cloning (section 2.6.2). PBP2B* was expressed and solubilized in a similar way to PBP2B (section 4.1.6.2). Affinity chromatography was first performed to purify His-PBP2B* (section 2.9.3) (Figure 3.30 A). Despite the correct DNA sequence for the thrombin recognition site, the enzyme did not cleave of the hexahistidine tag due to an unknown reason (Figure 3.30 C). Although the tag was still attached to PBP2B*, we proceeded to the second purification step to improve protein purity. Ion exchange chromatography was performed with a HiTrap SP HP column. PBP2B* was dialysed to pH 6.0, which promoted the binding of the protein to the column, followed by the elution of PBP2B* using elution buffer with 1 M NaCl and pH 7.5. Fractions collected from the two chromatography experiments were analysed by SDS-PAGE (Figure 3.30 A and B). Typically, 0.24 mg of PBP2B* per litre of culture was obtained. Western blot experiment using α-PBP2B antibody confirmed that the purified protein is PBP2B (Figure 3.31 A). Several bands with smaller sizes than PBP2B were detected by SDS-PAGE and were also identified by the α-PBP2B antibody suggesting that these bands correspond to PBP2B degradation products. The bocillin-binding assay for PBP2B* showed no fluorescence when PBP2B* was incubated with bocillin or with both bocillin and PenG suggesting the inactivation of the TPase domain (Figure 3.31 C).

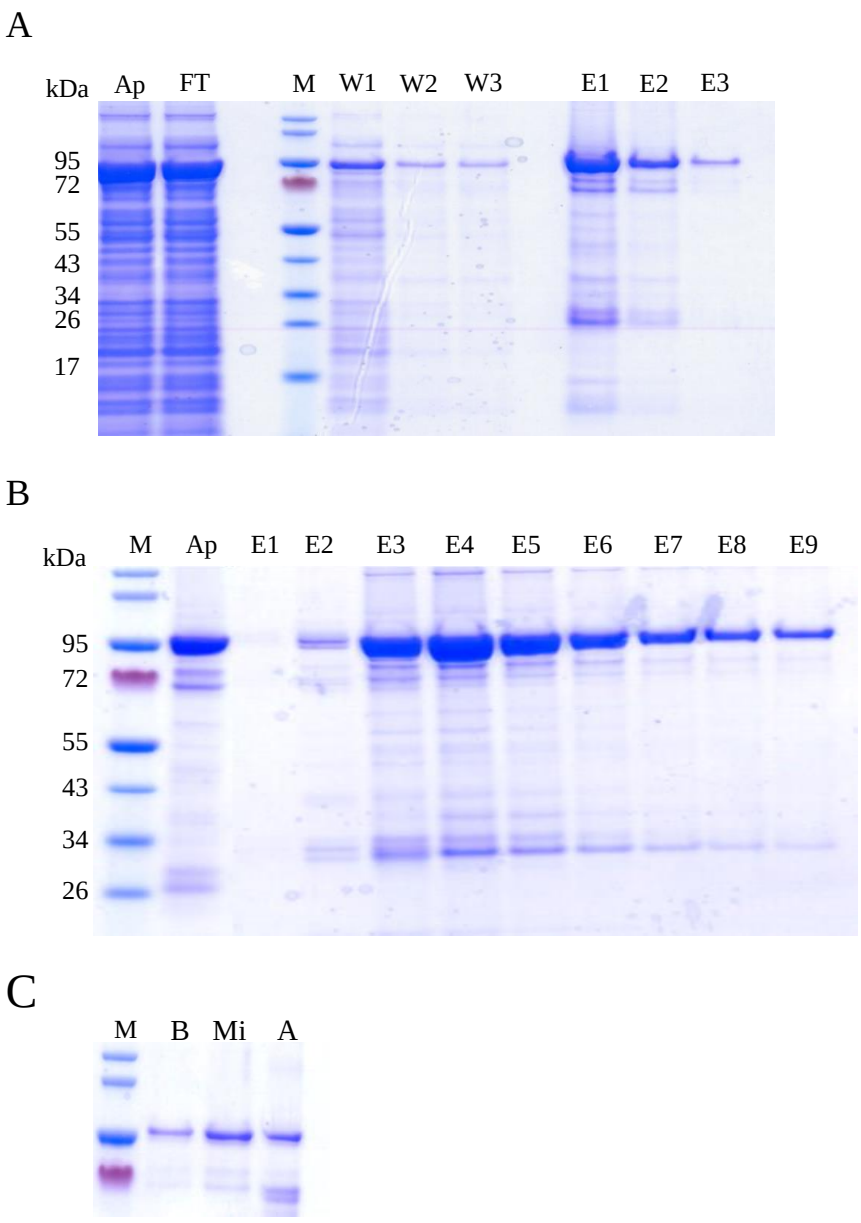

Figure 3.30 Purification of PBP2B*

SDS-PAGE analysis showing the fractions of PBP2B* purification steps. Gels were stained with Coomassie blue.

(A) IMAC purification of His-PBP2B*. Ap, applied fraction; FT, flow-through; M, protein size marker (Fermentas PageRuler); W1-W3, wash fractions; E1-E3, elution fractions. The theoretical molecular weight of His-PBP2B* is 81 kDa.

(B) IEX of the purified PBP2B* after thrombin digest. M, protein size marker; the bands in E2-E9 fractions with an apparent molecular weight of 79 kDa correspond to His-PBP2B*.

(C) Hexahistidine-tag removal using Thrombin. M, protein size marker; B, before thrombin digest; Mi, a mixture of samples containing His-PBP2B with and without thrombin digest; A, after thrombin digest. No decrease in the apparent molecular weight of His-PBP2B* was observed suggesting that the Hexahistidine tag is still attached to PBP2B*.

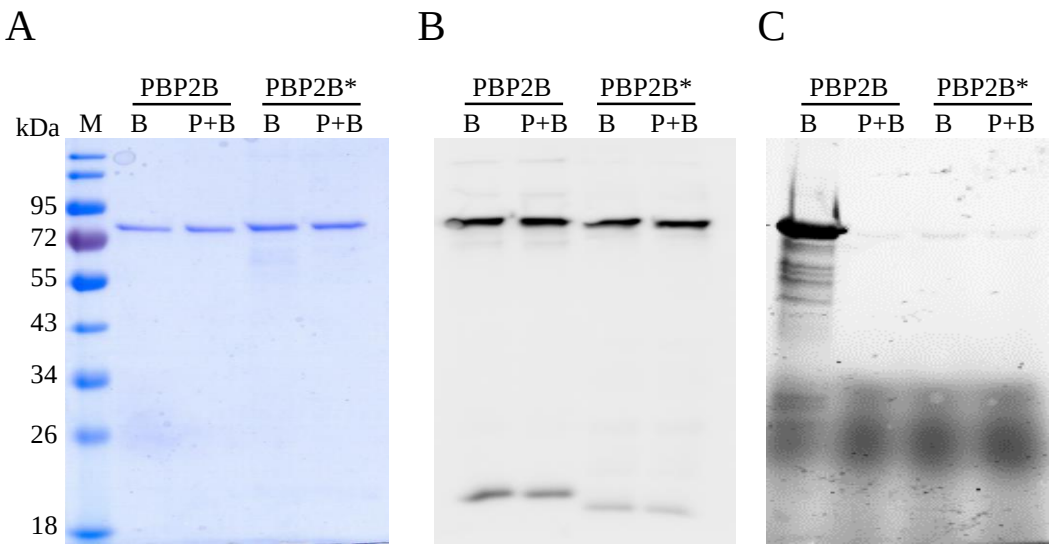

Figure 3.31 Western blot and bocillin-binding assay for PBP2B and PBP2B*

(A) SDS-PAGE, (B) Western blot (using α-PBP2B antibody) and (C) bocillin binding assay for purified PBP2B and PBP2B*. M, Protein size marker (NEB); B, proteins incubated with bocillin; P+B, proteins incubated with PenG then bocillin. The bands in (A) and (B) with an apparent molecular weight of 79 kDa correspond to PBP2B or PBP2B*. (C) Only PBP2B molecules treated with bocillin showed fluorescence suggesting inability of PBP2B* to bind bocillin. PBP2B samples treated with PenG then bocillin showed no fluorescence suggesting a specific binding of bocillin to the TPase domain of PBP2B.

4.1.6.3 Purification of PBP3

PBP3 was purified using affinity and ion exchange chromatography (section 2.9.4). *E. coli* BL21(DE3) cells were used for the expression of PBP3 with an N-terminal Hexahistidine tag (His-PBP3). His-PBP3 was purified from the solubilised membrane fraction. Affinity chromatography was performed to purify His-PBP3 (Figure 3.32 A) and the hexahistidine tag was removed by thrombin. A second purification experiment was performed using ion exchange chromatography. PBP3 was predicted to have negative charge -7.0 at pH 8.3. Therefore, a HiTrap monoQ column was used to further purify PBP3. Samples containing PBP3 were dialysed to pH 8.3 and injected into the column. PBP3 was eluted using a gradient of elution buffer with 1 M NaCl and pH 7.5. Collected samples from the two purification experiments were analysed by SDS-PAGE (Figure 3.32 A and B). Typically, 1 mg of PBP3 per litre of culture was obtained.

PBP3* was purified in a similar way to PBP3 except that PBP3* was dialysed to pH 8.5 permitting the binding of the protein to the HiTrap monoQ column followed by the elution of PBP3* (section 2.9.6) (Figure 3.33 A and B). Typically, 1.33 mg of PBP3* per litre of culture

was obtained. Bocillin-binding assay for the purified PBP3* showed no fluorescence suggesting that the TPase domain of PBP3 is inactive (Figure 3.34).

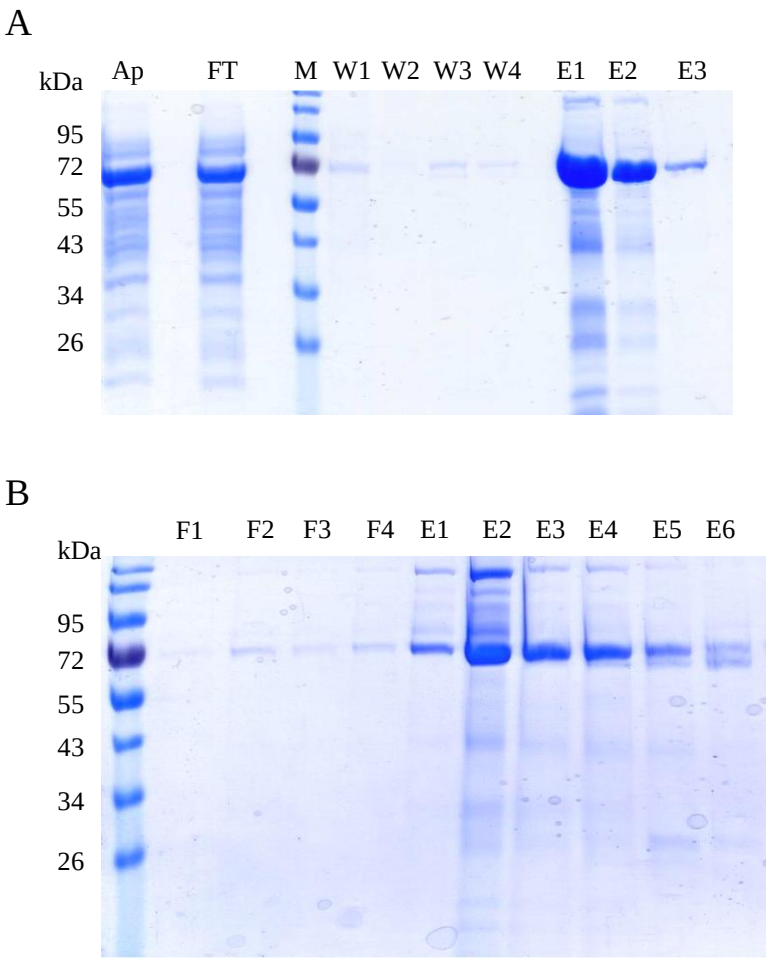

Figure 3.32 Purification PBP3

SDS-PAGE analysis shows fractions from PBP3 purification steps. Gels were stained with Coomassie blue.

(A) IMAC purification of His-tagged PBP3. App, applied fraction; FT, flow-through; M, Protein size marker (Fermentas PageRuler); W1-W4, wash fractions; E1-E3, elution fractions. The theoretical molecular weight of His-PBP3 is 74 kDa.

(B) IEX of the purified PBP3 after thrombin cleavage. Collected samples were diluted four-fold to avoid overloading the gel. M, Protein size marker; the bands in E1, E2, F3 and F4 fractions with an apparent molecular weight of 73 kDa correspond to PBP3.

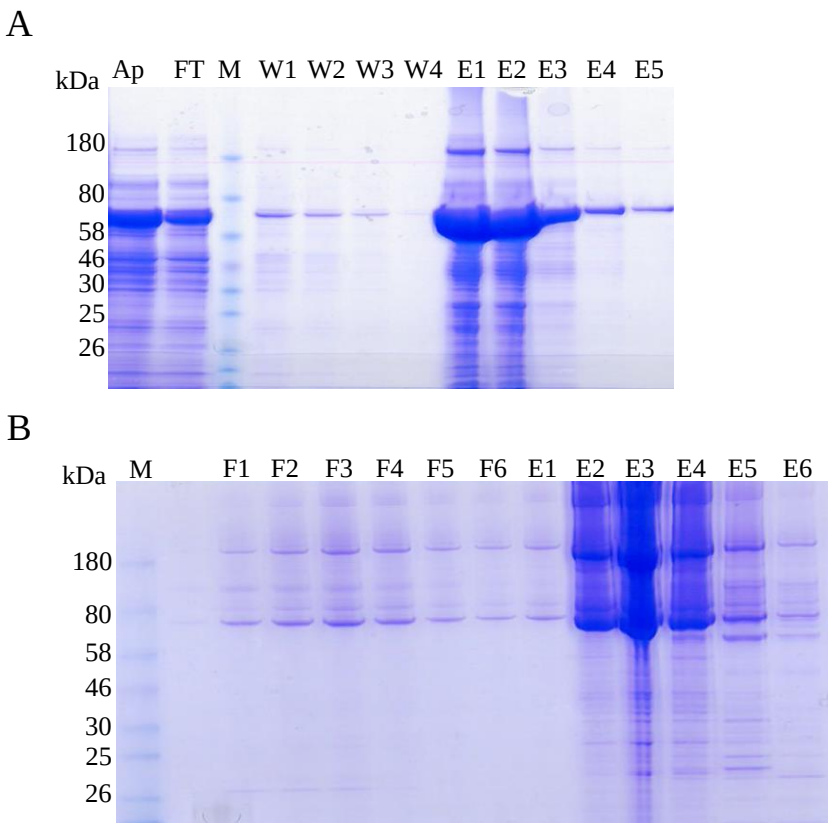

Figure 3.33 Purification of PBP3*

SDS-PAGE analysis shows fractions from PBP3* purification steps. Gels were stained with Coomassie blue.

(A) IMAC purification of His-tagged PBP3*. App, applied fraction; FT, flow-through; M, Protein size marker (NEB); W1-W4, wash fractions; E1-E5, elution fractions. The theoretical molecular weight of His-PBP3* is 74 kDa.

(B) IEX of the purified PBP3* after thrombin cleavage. M, Protein size marker; the bands in E2-E4 fractions with apparent molecular weight 73 KDa correspond to PBP3 however overloading the gel caused this smearing.

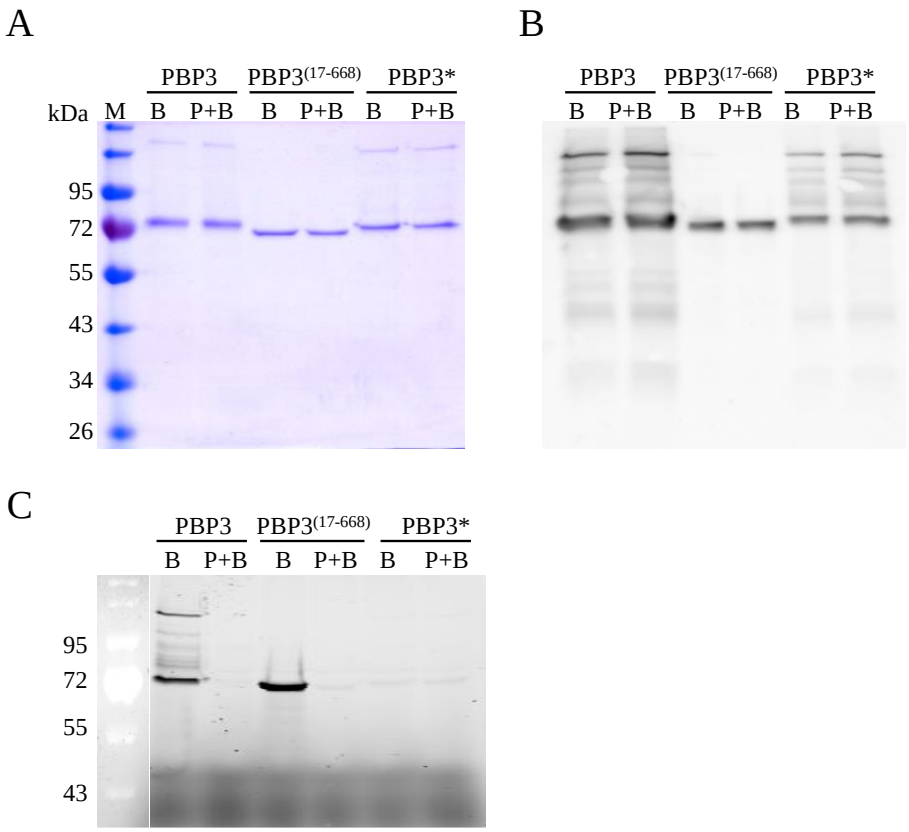

Figure 3.34 Western blot and bocillin-binding assay for PBP3, PBP3(17-668) and PBP3*

(A) SDS-PAGE, (B) Western blot (using α-PBP3 antibody) and (C) bocillin binding assay for purified PBP3, PBP3(17-668) and PBP3*. M, Protein size marker (NEB); B, proteins incubated with bocillin; P+B, proteins incubated with PenG then bocillin. The bands in (A) and (B) with an apparent molecular weight of 72 kDa correspond to PBP3, PBP3(17-668) or PBP3*. (C) Only PBP3 and PBP3(17-668) molecules treated with bocillin showed fluorescence suggesting the inability of PBP3* to bind bocillin. PBP3 and PBP3(17-668) samples treated with PenG then bocillin didn't show a band suggesting a specific binding of bocillin to the TPase domain of PBP3.

4.1.6.4 Purification of PBP3(17-668)

PbpC gene (encoding PBP3) without the transmembrane coding sequence [PBP3(17-668)] was introduced into the expression plasmid pET28(a)+. *E. coli* BL21(DE3) cells were transformed with the latter plasmid and used for the expression of PBP3(17-668) with a hexahistidine-tag (Section 2.9.5). Affinity chromatography was first performed to purify His-PBP3(17-668) (Figure 3.35 A) and the hexahistidine tag was removed using thrombin. Second, ion exchange chromatography was performed using a HiTrap monoQ column to separate PBP3 from the hexahistidine -tag and to obtain a purer PBP3 product. The IEX was performed as described previously for full length PBP3. However, PBP3 did not bind to the column and was eluted in the flow through fractions (Figure 3.35 B). The third step was a gel filtration chromatography to further purify the protein by using a Superdex size exclusion column (Figure 3.35 C).

Collected samples from all purification experiments were analysed by SDS-PAGE (Figure 3. 35 A and B). Typically, 1.5 mg of PBP3 per litre of culture was obtained.

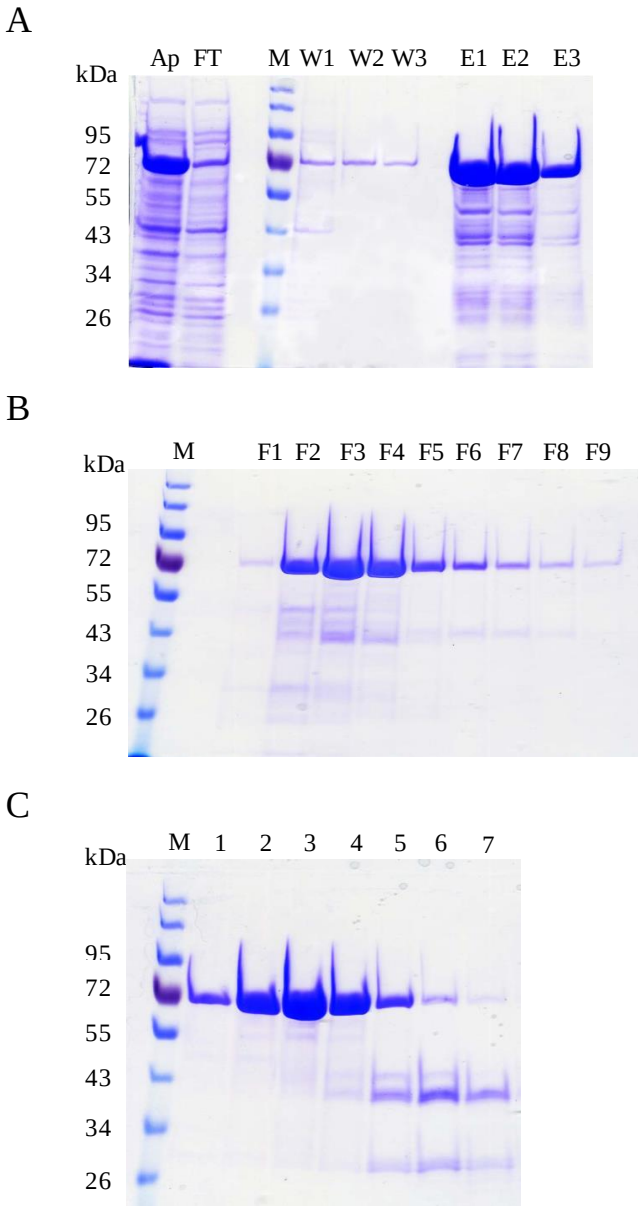

Figure 3.35 Purification of PBP3(17-668)

SDS-PAGE analysis shows the fraction of PBP3(17-668) purification steps. Gels were stained with Coomassie blue.

(A) IMAC purification of His-tagged PBP3(17-668). Ap, applied fraction; FT, flow-through; M, Protein size marker (Fermentas PageRuler); W1-W3, wash fractions; E1-E3, elution fraction. The theoretical molecular weight of His-PBP3(17-668) is 74 kDa.

(B) IEX of the purified PBP3(17-668). F1-F9, flow-through; M, Protein size marker; the bands in F2, F3, F4 and F5 fractions with a size of 72 kDa correspond to PBP3(17-668).

(C) SEC of the protein. The bands with an apparent molecular weight of 72 kDa in all fractions correspond to PBP3(17-668).

4.1.7 PBP3 interacts with PBP2B

The interaction between PBP2B and PBP3 was studied using pull-down assay and Surface Plasmon Resonance (SPR). In a pull-down assay we tested if PBP2B interacts with a hexahistidine-tagged PBP3 (His-PBP3) (section 2.10.1). His-PBP3 and PBP2B were mixed with Ni-NTA beads in an interaction buffer. His-PBP3 had a hexahistidine tag which promoted the binding of PBP3 to the beads. SDS–PAGE analysis of the applied and bound fractions shows whether His-PBP3 was able to pull-down PBP2B (Figure 3.36 A). Both the applied and bound fractions for His-PBP3 showed a band with an apparent molecular weight corresponding to His-PBP3 showing that it was successfully pulled down by the Ni-NTA. PBP2B in the absence of His-PBP3 only appeared in the applied fraction suggesting that PBP2B was not pulled down by the beads. PBP2B in the presence of His-PBP3 appeared in both the applied and bound fractions suggesting that His-PBP3 was able to pull down some of the PBP2B molecules indicating an interaction between the two proteins.

SPR was used to further analyse the interaction between PBP3 and PBP2B and to determine the dissociation constant (K_D) of this interaction (section 2.10.2). First, ampicillin was immobilized to the sensor chip followed by the binding of PBP2B via its TPase domain. This method allows a homogeneous orientation of PBP2B proteins with their N-terminus accessible for interaction. The remaining free ampicillin was digested with β-lactamase. The chip was washed with NaCl buffer (1 M) to remove non-covalent bound protein. In parallel, the control surface was prepared in a similar way without the immobilized PBP2B. PBP3 was injected over the PBP2B surface and the control surface at concentration 400, 200, 100, 50 and 25 nM (Figure 3.36 B). The binding of the injected protein (analyte) to the chip surface or the immobilized protein causes an increase in the SPR curves (Bravman *et al.*, 2006). These SPR curves are called sensorgrams and represent the changes in response unite (RU) plotted against time (s). PBP3 was injected at a flow rate of 75 µl/min. The surface with immobilized PBP2B showed an increase in signal during association (from 0 to 300 s) compared to the control surface (Figure 3.36 B). The response almost reached saturation or equilibrium towards the end of the association (from 200 to 300 s). Subsequently, running buffer was injected after 300 s causing the dissociation of analytes. The increase in response unit for the control surface indicates unspecific binding of the analyte (PBP3) to the chip surface. A higher signal for the PBP2B-surface compared to the control surface during association and equilibrium indicates a specific interaction between PBP2B and PBP3. The subtraction of the control signal from the PBP2B-surface signal is represented in figure 3.36 C. The signal corresponding to analytes with concentration of 100 nM or higher overlapped suggesting a saturation of binding (Figure 3.36

C). The K_D of the interaction was calculated using Sigma Plot software, based on a one site interaction with PBP3. The average response of PBP3 during equilibrium was calculated for every concentration and used for K_D determination. The binding curve was generated by plotting the response in (RU) against analyte concentration in nM (Figure 3.36 D). The K_D of the interaction of PBP2B with PBP3 was 8.7 ± 1.2 nM calculated from three independent experiments.

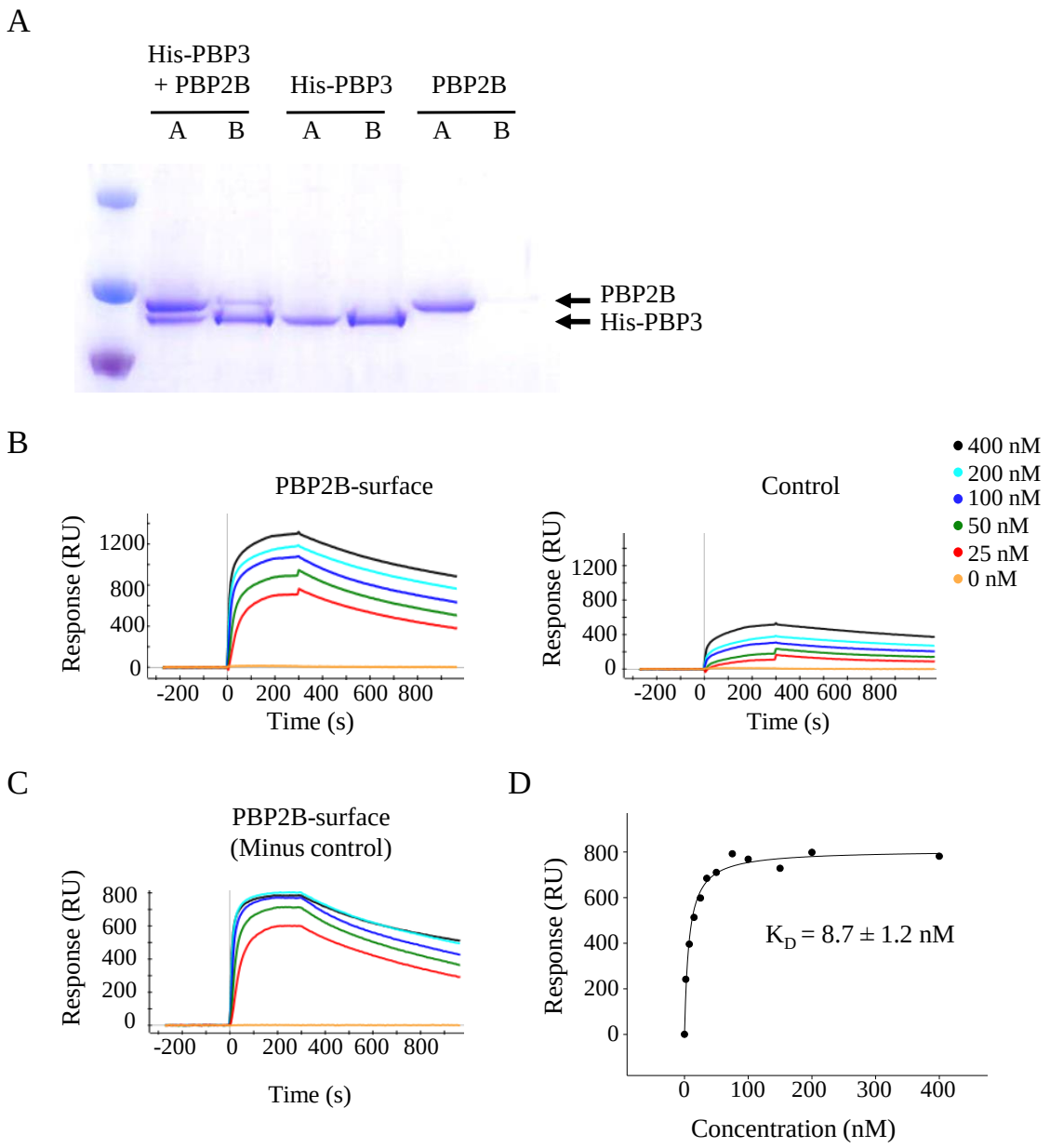

Figure 3.36 Interaction of PBP2B with PBP3 by in vitro pull-down and SPR

(A) Pull-down assay performed to test if PBP2B and PBP3 interact. Coomassie stained SDS-PAGE analysis showing His-PBP3 and PBP2B. His-PBP3 and PBP2B were detected in both the applied and the bound fractions suggesting that His-PBP3 pull-down PBP2B. A, Applied; B, bound fractions.

(B) SPR sensorgrams showing the response for PBP3 when injected over a surface with immobilized PBP2B or a control surface at concentration 20, 50, 100, 200 and 400 nM plotted against time (s). The signal for the PBP2B-surface was higher than the control surface upon PBP3 injection.

(C) SPR sensorgram showing the response for the PBP2B-surface minus control. The signals corresponding to 100, 200 and 400 nM PBP3 overlapped suggesting ligand saturation.

(D) The response values during equilibrium were plotted against the injected PBP3 concentrations. The K_D of the PBP2B-PBP3 interaction was determined by non-linear regression using Sigma Plot software. The K_D value is the mean ± standard deviation of three independent experiments.

A similar SPR experiment was performed with PBP2B immobilised to the chip surface as above except that PBP3 lacking its transmembrane domain (PBP3(17-668)) was injected as an analyte over the PBP2B-surface and a control surface at concentrations 1000, 500, 250, 125 and 62.5 nM. The response over the PBP2B-surface was similar to the control surface upon the injection of PBP3(17-668) suggesting the absence of specific binding between the two proteins (Figure 3.37 A). The subtraction of the control response from the PBP2B-surface response showed no saturation of signal upon increasing the concentration of the analyte supporting the premise of the absence of interaction between the two proteins (Figure 3.37 B).

These results suggest that the interaction between PBP2B and PBP3 is specific and the N-terminal region of PBP3 is required for interaction with PBP2B.

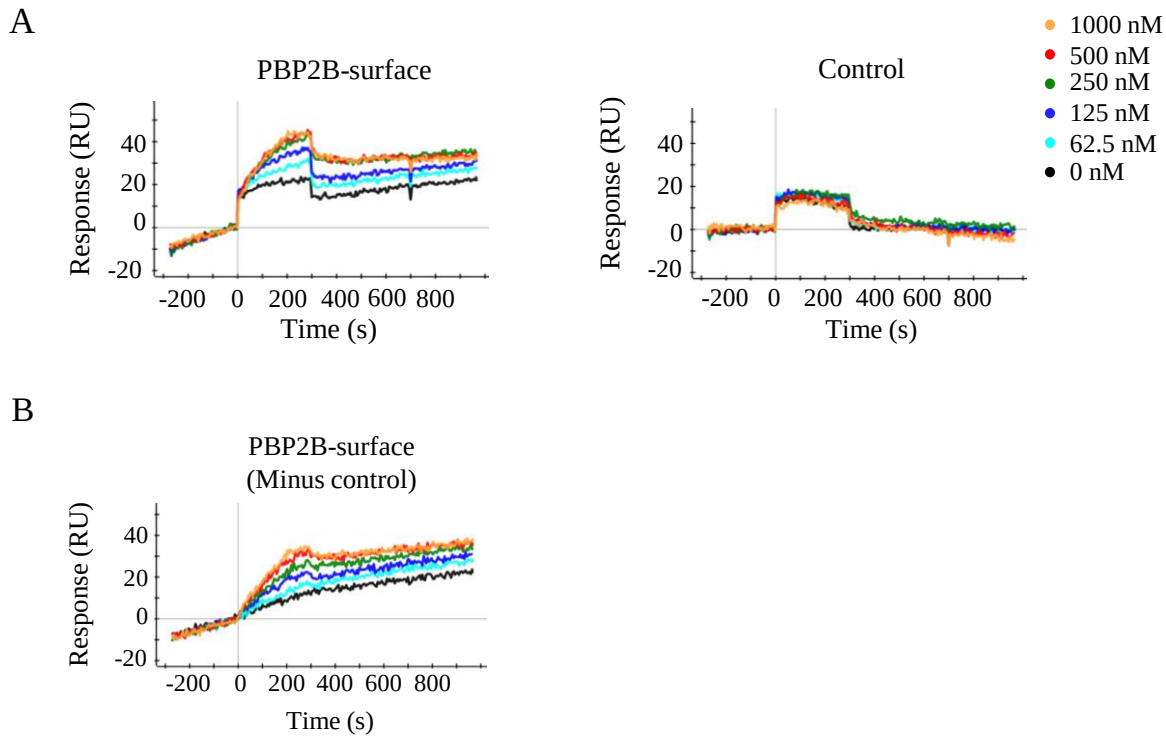

Figure 3.37 PBP2B does not interact with PBP3(17-668) by SPR

(A) SPR sensorgrams showing the response for PBP3(17-668) when injected over a surface with immobilized PBP2B or a control surface at concentration 62.5, 125, 250, 500 and 1000 nM plotted against time (s). The signal for the PBP2B-surface was similar to the control surface upon analyte injection.

(B) SPR sensorgram showing the response for PBP3(17-668) minus the control response. The response for PBP3(17-668) at various concentrations was similar and did not result in a binding curve or signal saturation suggesting absence of interaction between the two proteins.

4.1.8 Interaction between PBP3 and PBP1

B. subtilis has four bi-functional class A PBPs with PBP1, encoded by the *ponA* gene, involved in septal PG synthesis (Scheffers and Errington, 2004). PBP1 was purified (Section 2.10.1) and tested for interaction with PBP3 using *in vitro* pull-down assay and surface plasmon resonance. First, we used Ni^{2+}-NTA pull down to test whether His-PBP3 would retain PBP1. SDS–PAGE analysis for the applied and bound fractions of His-PBP3 showed a band with an apparent molecular weight corresponding to His-PBP3 showing that it was successfully pulled down by the Ni-NTA (Figure 3.38 A). PBP1 in the absence of His-PBP3 only appeared in the applied fraction suggesting that PBP1 was not pulled down by the beads. PBP1 in the presence of His-PBP3 appeared only in the applied fraction suggesting that His-PBP3 did not retain PBP1. To stabilize a possible weak interaction, formaldehyde (0.2%) was used to crosslink interacting proteins. Nevertheless, His-PBP3 did not retain PBP1 suggesting that PBP1 and PBP3 do not interact by pull-down assay.

SPR was also used to test if PBP1 and PBP3 directly interact. Ampicillin was first immobilized to the sensor chip followed by the covalent binding of PBP1 via its TPase domain. A control surface was prepared in the same way without PBP1. The remaining free ampicillin was digested with β-lactamase. The chip was washed with NaCl buffer (1 M) followed by the injection of PBP3 at concentration 200, 100, 50, 25 and 12.5 nM. The sensorgram for the PBP1-surface showed a higher signal during association and equilibrium compared to the control surface followed by a decrease in the signal for both surfaces during dissociation. To test if the PBP1-surface was saturated upon the injection of PBP3, the control signal was subtracted from the PBP1-surface (Figure 3.38 C). The binding levels saturated at 50 nM injected PBP3. This result suggests that PBP1 and PBP3 interact. Whilst three independent experiments have been performed for the interaction of PBP1 and PBP3, only 2 showed an increase in signal suggesting an interaction between PBP1 and PBP3.

A similar experiment was performed with PBP3 being immobilized to the chip surface and PBP1 being injected as an analyte. However, the signal for the control surface when PBP1 was injected as an analyte was high suggesting unspecific binding of PBP1 to the chip surface. These results suggest that PBP3 is presumably interacting with PBP1 but additional experiments are required to confirm such interaction. Next, we proceeded to characterize the enzymatic activities of PBP3 or PBP3* in the presence of PBP1 *in vitro* using established methods in our lab.

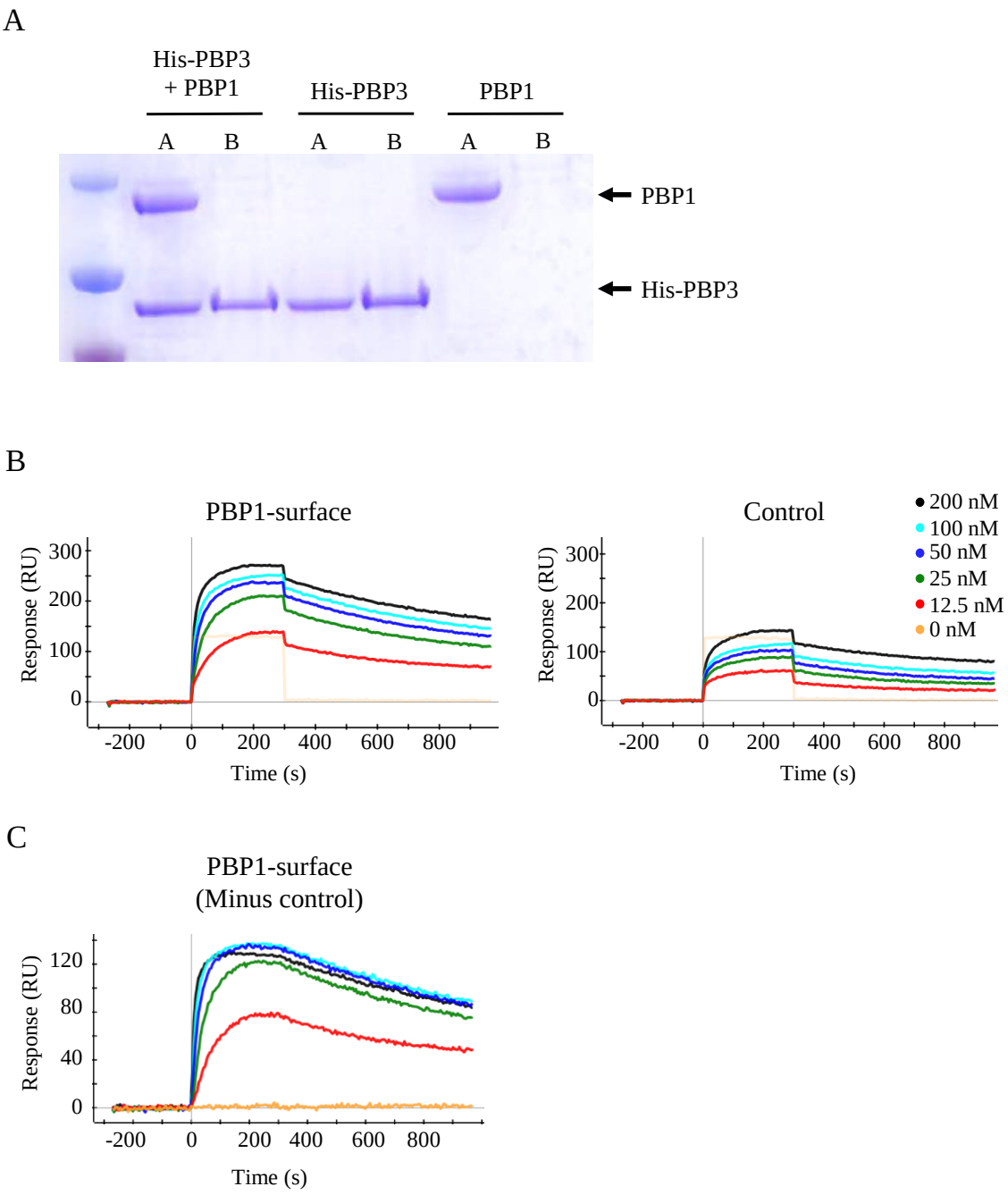

Figure 3.38 Interaction of PBP1 with PBP3 by *in vitro* crosslink / pull-down and SPR

(A) Ni-NTA affinity chromatography used to test if PBP1 and PBP3 directly interact. Coomassie stained SDS-PAGE analysis showing His-PBP3 and PBP1. PBP1 in the presence of His-PBP3 appeared only in the applied fraction suggesting that His-PBP3 did not retain PBP1. A, Applied; B, bound fractions.

(B) SPR sensorgrams showing the response for PBP3 when injected over a surface with immobilized PBP1 or a control surface at concentration 12.5, 25, 50, 100 and 200 nM. The signal for the PBP1-surface was higher than the control surface during association suggesting that PBP1 interacts with PBP3.

(C) SPR sensorgram showing the response for the PBP1-surface minus control. The binding levels saturated at 50 nM injected PBP2B.

4.1.9 PBP3 has DD-transpeptidase and DD-carboxypeptidase activities

The enzymatic activities of the class B PBP3 alone or together with the bifunctional synthase PBP1, were tested using radioactive Lipid II, which is the precursor for peptidoglycan synthesis. To test whether PBP3 contributes to the synthesis of peptides in cross-link, PBP3 with an inactive TPase domain (PBP3*) was also purified (section 2.10.6) and tested. The detection of monomeric muropeptides suggest that lipid was polymerized into a glycan chain by the GTase activity of PBPs and the levels of oligomeric muropeptides (peptides in crosslink) correlate with the TPase activity of the synthases. PBP3 alone had no activity against lipid II (Figure S1). PBP1 alone has GTase and TPase activities, consequently PBP1 polymerised lipid II into glycan strands with crosslinked peptides (Cleverley *et al.*, 2016; Lebar *et al.*, 2014). PBP3 and PBP3* tested together with PBP1 had similar levels of peptides in crosslinks suggesting that PBP3 did not contribute to this activity (Figure 3.39). A mild but significant (4.8%) decrease in levels of peptides in crosslinks was detected for PBP1 with PBP3 compared to PBP1 alone. A similar decrease (6.0%) was noticed for PBP1 with PBP3* suggesting that PBP3 caused a mild reduction in the TPase activity of PBP1 (Figure 3.39). The activity of PBPs was also tested in the presence of sacculi isolated from wild type *B. subtilis* (tripeptide rich) or Δ*dacA* mutant (pentapeptide rich). Samples were incubated for 1 h at 37˚C then the reaction was stopped by boiling the samples for 5 min. The mixture of old and newly synthesised PG was digested with cellosyl overnight, reduced and analysed by HPLC. Muropeptides identified by the HPLC radioactivity detector represented the newly synthesised PG material. An insignificant decrease in the levels of peptides in cross-link was identified for PBP1 with PG compared to PBP1 alone (figure 3.39). PBP1 alone or together with PBP3 in the presence of 168CA or Δ*dacA* PG had similar levels of peptides in crosslink. However, PBP3* with PBP1 had a significant decrease in levels of peptides in crosslink when tested in the presence of 168CA or Δ*dacA* PG (Figure 3.39). These results suggest that PBP3 contributes to the level of peptides in crosslink and has a transpeptidase activity. The decrease in the level of peptides in crosslink for PBP1 with PBP3* compared to PBP1 alone in presence of 168CA or Δ*dacA* PG suggested that PBP3 inhibits the TPase activity of PBP1 in presence of PG.

DD-carboxypeptidase (CPase) activity causes the removal of the fifth D-Ala residue from the Glc*N*Ac-Mur*N*Ac-pentapeptide. Thus, the CPase activity of PBPs is quantified by measuring the levels of Glc*N*Ac-Mur*N*Ac-tetrapeptide (Tetra) and of the crosslinked bis-Glc*N*Ac-Mur*N*Ac-tetrapeptide (TetraTetra) muropeptides. PBP1 alone had 18.7% of CPase products suggesting that PBP1 has a CPase activity which is consistent with previously publish data (Figure 3.40) (Cleverley *et al.*, 2016). PBP3 and not PBP3* together with PBP1 showed 15.8%

increase in the levels of CPase products suggesting that PBP3 has a CPase activity. PBP1 alone had similar levels of CPase products when tested in the presence of 168CA or Δ*dacA* PG suggesting that PBP1 has a CPase activity independent of the presence or absence of PG. PBP3 with PBP1 had 14.5% and 10.3% increase in CPase products when tested in the presence of 168CA or Δ*dacA* PG, respectively. The decrease in CPase products for PBP1 with PBP3 in the presence of PG was complemented by an increase in levels of peptides in crosslink. These results suggest that PBP3 has a CPase activity in the absence of PG and a TPase and a CPase activity in the presence of PG.

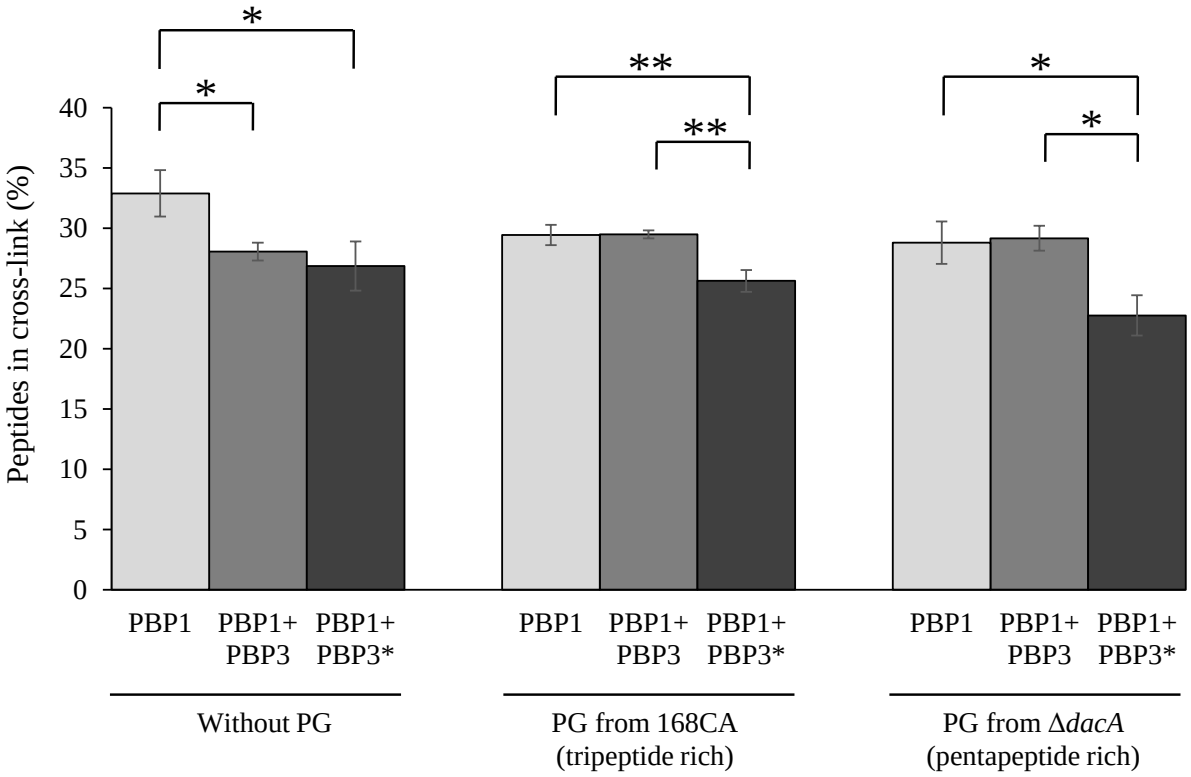

Figure 3.39 TPase activities of PBP1 and PBP3

The percentage of cross-linked peptides in PG produced by PBP1 alone, PBP1 and PBP3 or PBP1 and PBP3*, with or without PG. In the absence of PG, PBP1 with PBP3 or PBP3* had similar levels of peptides in crosslink. In samples containing PG, PBP3 and not PBP3* contributed to the levels of peptides in crosslink. PBP3* caused a mild decrease in the levels of peptides in crosslink produced by PBP1 in presence of 168CA or ΔdacA PG. *, $P<0.05$; **, $P<0.01$

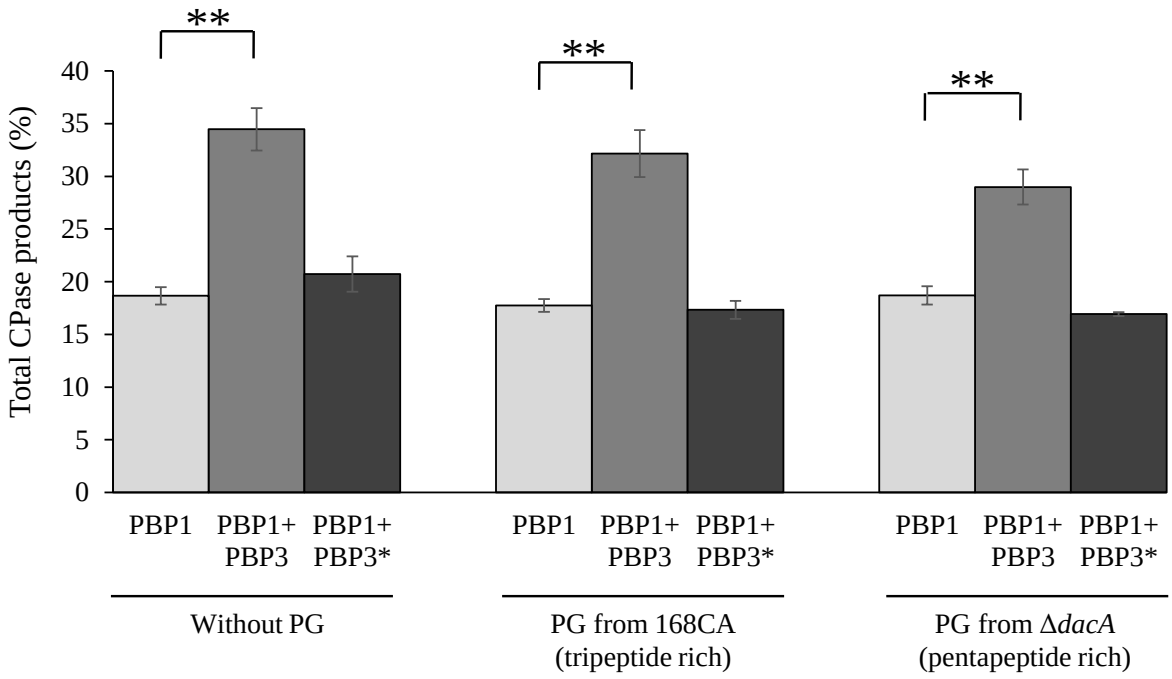

Figure 3.40 DD-Carboxypeptidase activity of PBP1 and PBP3

The percentage of CPase products (Tetra and TetraTetra) produced by PBP1 alone, PBP1 and PBP3 or PBP1 and inactive PBP3*, with or without PG. PBP1 alone with or without PG exhibited an increase in the levels of CPase products suggesting a CPase activity. PBP3 and not PBP3* together with PBP1 showed a significant increase in the levels of CPase products compared to PBP1 alone suggesting that PBP3 has CPase activity. *, P<0.05; **, P<0.01

4.1.10 PBP3 has no effect on the GTase activity of PBP1

The effect of PBP3 on the GTase activity of PBP1 was tested *in vitro* using fluorescently labelled dansyl-lipid II (Section 2.10.3). Class A PBPs have a GTase activity that polymerizes dansyl-lipid II into glycan strands. This polymerization causes a decrease in the fluorescence signal, which is detected by a spectrophotometer and recorded over time. Figure 3.41 shows the mean florescence presented as a percentage of initial fluorescence at a given time-point. Consistent with the TPase assay shown in section 4.1.9, PBP3 showed no decrease in fluorescence detected over time suggesting that PBP3 has no activity against dansyl-lipid II (Figure 3.41). The fluorescence signal detected for PBP1 alone decrease over time suggesting that the dansyl-lipid is polymerised into a glycan chain by a GTase activity which is consistent with previously published data (Cleverley *et al.,* 2016). PBP3 together with PBP1 showed a

similar decrease in the fluorescence signal over time compared to PBP1 alone suggesting that PBP3 has no effect of the GTase activity of PBP1.

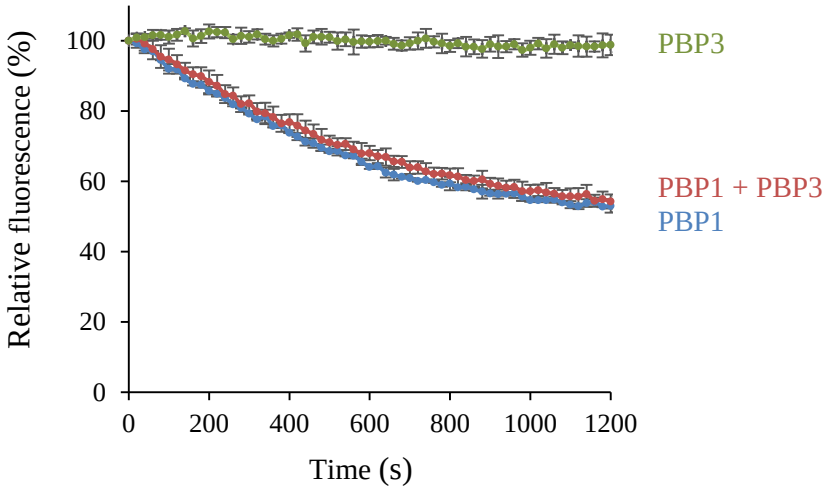

Figure 3.41 The effect of PBP3 on the GTase activity of PBP1

The diagram represent the GTase activity of PBP1 and PBP3. A decrease in relative fluorescence suggests the presence of a GTase activity. PBP3 alone had no activity against dansyl-lipid II. PBP3 had no effect on the GTase activity of PBP1. Values represent the mean ± standard deviation of three independent experiments.

4.2 Characterization of PBP2B *in vitro*

4.2.1 Introduction

PbpB (encoding PBP2B) is the only essential PBP gene in *B. subtilis* (Yanouri *et al.,* 1993). PBP2B is highly conserved across bacterial species and plays a crucial role in cell division (Daniel *et al.,* 1996, 2000; Yanouri *et al.,* 1993). PBP2B is recruited to the septum at the early stages of cell division followed by other PG synthases and hydrolases. PBP2B is the first PBP to be recruited to midcell during cell division and the depletion of PBP2B caused mislocalisation of GFP-PBP1 (Scheffers and Errington, 2004). To further characterise the interaction and biochemical roles of PBP1 and PBP2B in cell division, both proteins were purified and tested *in vitro*.

4.2.2 Dimerization of PBP2B

Bacterial two-hybrid experiments suggested that PBP2B dimerizes *in vivo* (Daniel *et al.,* 2006). In this work, we studied the dimerization of PBP2B by SPR. First, ampicillin was immobilized to the sensor chip followed by the binding of PBP2B via its TPase domain. The remaining free ampicillin was digested with β-lactamase. The chip was washed with NaCl buffer (1 M) to remove non-covalently bound protein. A control surface was prepared in the same way without PBP2B. PBP2B molecules were injected over the PBP2B surface and the control surface at ten different concentrations ranging from 0 to 350 nM. The sensorgrams in figure 3.42 A and B for the PBP2B-surface showed an increase in signal during association compared to the control surfaces. The signal almost reached equilibrium for all PBP2B injected concentrations during association followed by a continuous decrease during the dissociation phase (Figure 3.42 A). The signal for the PBP2B-surface minus the control showed saturation of binding at 80 nM injected PBP2B (Figure 3.42 B). These results suggest that PBP2B dimerises under the tested conditions. The K_D of the interaction was calculated using SigmaPlot software, based on a one site interaction with PBP2B. The average response of PBP2B during equilibrium was calculated for every concentration and used for K_D determination. The binding curve was generated by plotting the response in (RU) against analyte concentration in nM (Figure 3.42 C). The K_D of the dimerization of PBP2B was 21.7 ± 11.4 nM calculated from three independent experiments.

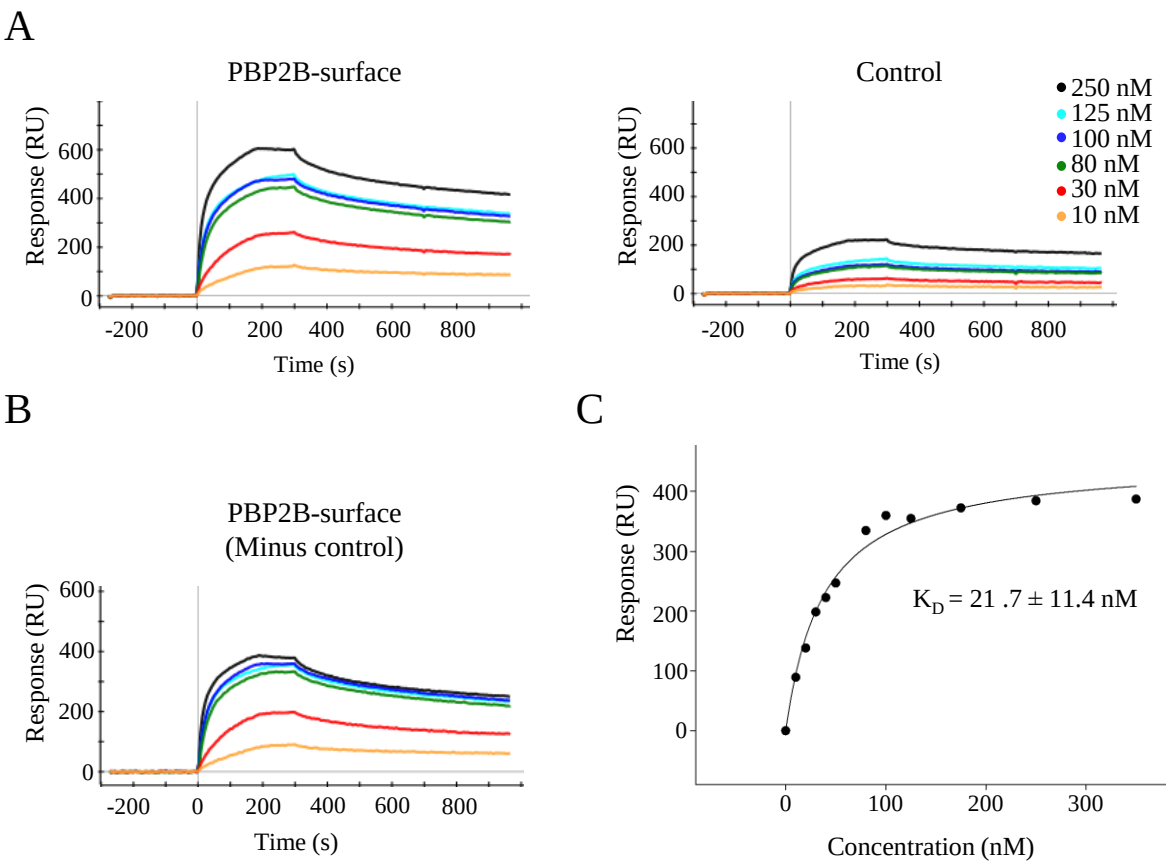

Figure 3.42 Dimerization of PBP2B by SPR

(A) SPR sensorgrams showing the response for PBP2B when injected over the PBP2B-surface and the control surface. The interaction was tested using ten different concentrations of PBP2B and the sensorgrams suggest dimerization of PBP2B.

(B) SPR sensorgram showing the response for the PBP2B-surface minus the control response. The binding levels saturated at 80 nM injected PBP2B.

(C) The response values during equilibrium were plotted against injected PBP2B concentrations. The K_D of the dimerization of PBP2B was determined by non-linear regression using Sigma Plot. The value shown is the mean K_D ± standard deviation of three independent experiments.

4.2.3 Interaction of PBP2B and PBP1 by SPR

PBP1 was tested for interaction with PBP2B using SPR. PBP1 showed substantial unspecific binding to the chip surface when it was injected as an analyte in previous SPR experiments. Thus, PBP1 was immobilized to the surface and PBP2B was injected as an analyte. First, ampicillin was immobilized to the sensor chip followed by the binding of PBP1. The remaining free ampicillin was digested with β-lactamase and the chip was washed with NaCl buffer (1 M). A control surface was prepared in a similar way without the immobilized PBP1. PBP2B was

injected over the control surface and the PBP1-immobilized surface at concentrations 500, 250, 125, 62.5 and 31.25 nM. The sensorgrams showed higher signal for the PBP1-surface compared to the control surface during association (Figure 3.43 A). The SPR signals reached equilibrium towards the end of the association phase followed by a decrease in signal during dissociation phase upon the injection of running buffer (Figure 3.43 A). The curves for the PBP1-surface minus the control overlapped upon the injection of PBP2B at 250 nM concentration and above suggesting a saturation of binding (Figure 3.43 B). This result suggests that PBP2B directly interacts with PBP1. This interaction has been observed in two independent experiments for five PBP2B concentrations however, more experiments are required for the calculation of the interaction K_D of PBP1 with PBP2B. Following the observed interaction between PBP1 and PBP2B, we characterized the enzymatic activities of PBP1 and PBP2B using radioactive or fluorescently labelled lipid II

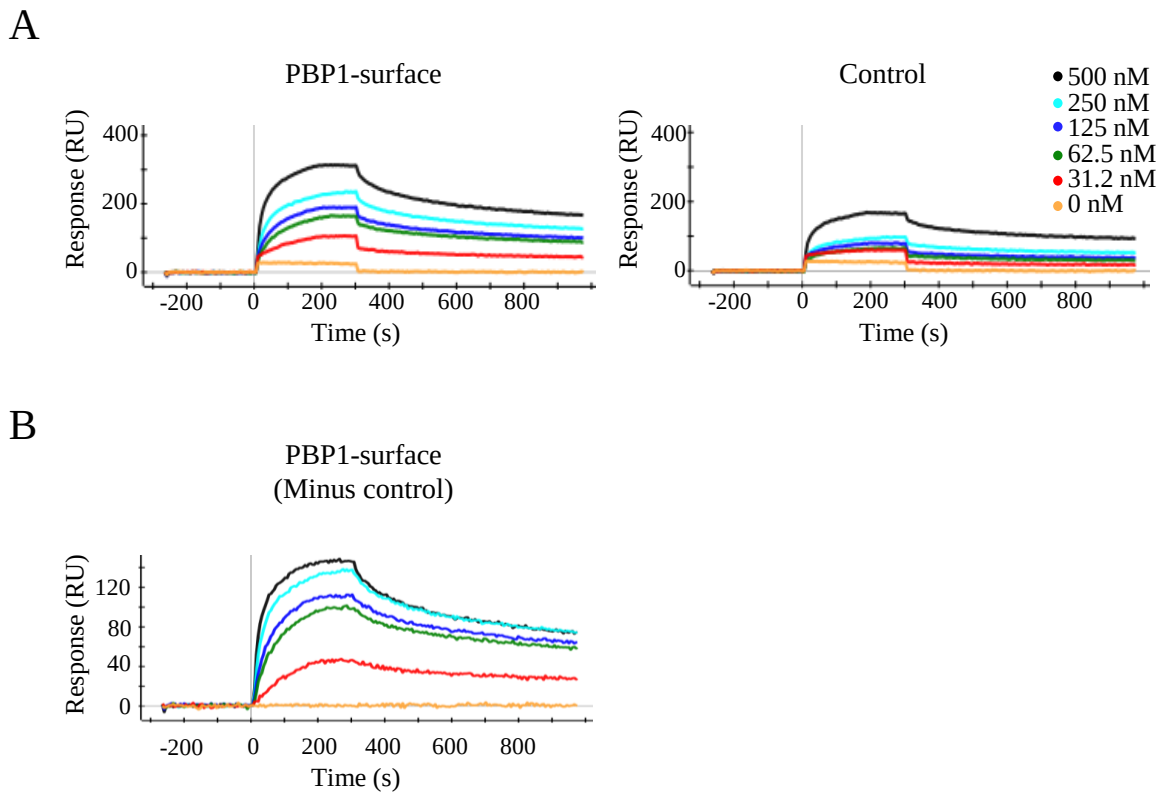

Figure 3.43 Interaction of PBP1 with PBP2B by SPR

(A) SPR sensorgrams showing the response for PBP2B when injected over a surface with immobilized PBP1 or a control surface at concentration 31.2 , 62.5, 125, 250 and 500 nM. The signal for the PBP1-surface was higher than the control surface during association suggesting that PBP1 interacts with PBP2B.

(B) SPR sensorgram showing the response for the PBP1-surface minus control. The binding levels saturated at 250 nM injected PBP2B.

4.2.4 PBP2B has DD-transpeptidase and DD-carboxypeptidase activities

The GTase and TPase activities of PBP1 and PBP2B were tested using *in vitro* PG synthesis assay (section 2.10.4). To test whether PBP2B contributes to the synthesis of peptides in cross-link, PBP2B with an inactive TPase domain (PBP2B*) was also purified (section 2.9.3) and tested with PBP1. PBP2B* featured a substitution of the active site serine residue to alanine making the TPase domain non-functional. PBP2B alone had no activity against lipid II (Figure S3). The TPase and GTase activity of PBP1 was previously described in section 4.1.9. PBP2B together with PBP1 had a mild increase of 4.6% in the levels of peptides in crosslinks compared to PBP1 alone (Figure 3.44 A) and an increase of 8.5% compared to PBP1 with PBP2B*. This suggested that PBP2B contributed to the formation of peptides in crosslinks and has TPase activity. PBP1 and PBP2 were also tested in the presence of 168CA and Δ*dacA* PG. In the presence of 168CA PG, no significant changes were observed for PBP1 alone, PBP1 with PBP2B or PBP1 with PBP2*. In presence of Δ*dacA* PG, PBP1 with PBP2B showed an mild but significant increase in the levels of peptides in crosslink compared to PBP1 alone or PBP1 with PBP2B*, supporting previous results about the TPase activity of PBP2B.

The CPase activity of PBP1 alone in the presence or absence of PG was previously described in section 4.1.9. PBP1 with PBP2B showed a significant increase of 7.1 and 6.5% in the levels of CPase products compared to PBP1 alone or PBP1 with PBP2B*, respectively. These results suggests that PBP2B contributed to the levels of CPase products and has a CPase activity (Figure 3.44 B). In the presence of 168CA or Δ*dacA* PG, no significant differences were detected in the levels of CPase products for PBP1 alone, with PBP2B or with PBP2* suggesting that PBP2B has a CPase activity only in the absence of PG. Taken together, these results suggested that PBP2B has DD-carboxypeptidase and DD-transpeptidase activities. The levels of peptides in crosslink for PBP1 alone or with PBP2B* were similar suggesting that PBP2B* has no effect on the TPase activity of PBP1.

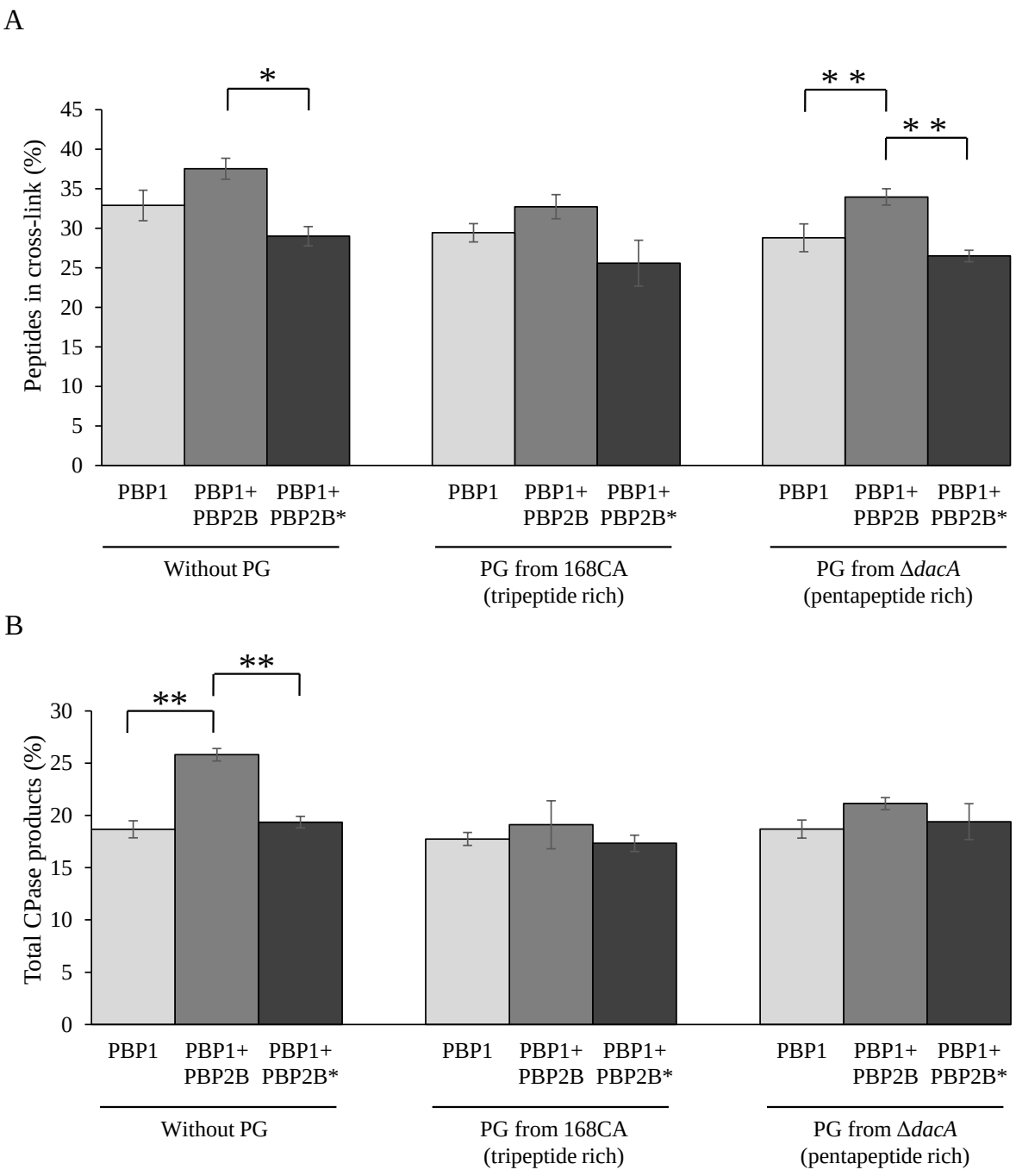

Figure 3.44 Enzymatic activities of PBP1 and PBP2B

(A) The percentage of cross-linked peptides in PG produced by PBP1 alone, PBP1 and PBP2B or PBP1 and inactive PBP2B*, with or without PG. PBP1 with PBP2B had higher levels of peptides in crosslinks compared to PBP1 alone or PBP1 with PBP2B* in the absence of PG or in the presence of Δ*dacA* PG. PBP2B and not PBP2B*, contributed to the levels of peptides in crosslinks suggesting a TPase activity.

(B) The percentage of CPase products produced by PBP1 alone, PBP1 and PBP2B or PBP1 and PBP2B*, with or without PG. PBP1 with PBP2B and not PBP2B* showed increased levels of CPase products only in the absence of PG suggesting that PBP2B has CPase activity.

4.2.5 PBP2B stimulates the GTase activity of PBP1

The *In vitro* PG synthesis assay showed that PBP2B had no GTase activity and no effect on the TPase activity of PBP1. Here, PBP1 and PBP2B were tested for activity against dansyl-lipid II by an *in vitro* glycosyltransferase assay. Supporting previous results (section 4.2.4), there was no decrease in fluorescence for samples with PBP2B alone suggesting that PBP2B has no activity against lipid II (Figure 3.45). PBP1 with PBP2B had a moderately faster decrease in the fluorescence signal compared to PBP1 alone. This suggests that the polymerization of lipid II into glycan strands is occurring at a faster rate when PBP2B is added to PBP1. The GTase rate was 2.0 ± 0.02 fold higher in the presence of PBP2B compared to PBP1 alone, suggesting that PBP2B stimulates the GTase activity of PBP1.

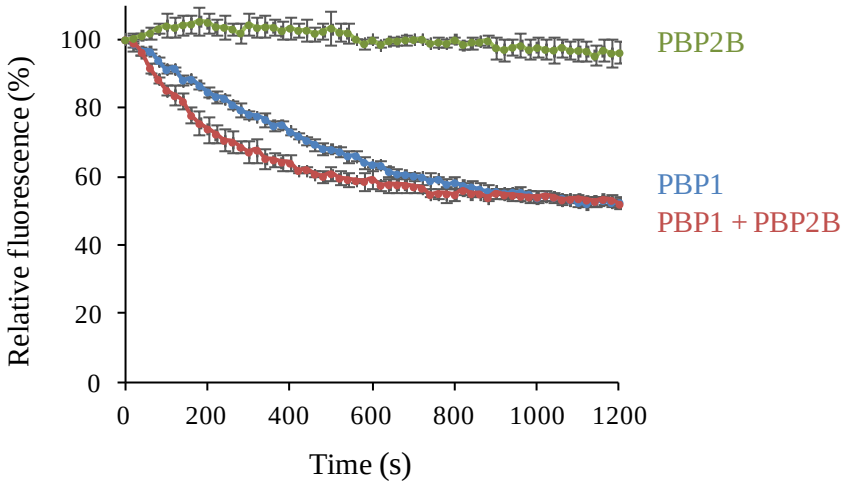

Figure 3.45 PBP2B stimulates the GTase activity of PBP1

In vitro glycosyltransferase assay performed for PBP1, PBP2B or PBP1 with PBP2B. PBP2B alone had no effect on the substrate. PBP1 with PBP2B had a faster decrease in fluorescence compared to PBP1 alone. The rate of the GTase reaction for PBP1 increased by 2.0 ± 0.02 fold in presence of PBP2B. Values represent the mean ± standard deviation of three independent experiments.

4.2.6 *In vitro* pull-down for His-PBP3, PBP1 and PBP2B

The interactions of PBP1, PBP2B and PBP3 were characterized previously using various interaction assays. The formation of multi-protein complexes during cell division is well established in other bacterial species such as *E. coli* (Egan *et al.*, 2015). Therefore, to test whether PBP1, PBP2B and PBP3 form a ternary complex, Ni-NTA crosslink/pull down assay was performed with His-PBP3, PBP1 and PBP2B. Formaldehyde was used as a crosslinker to stabilise possible weak interactions. SDS–PAGE analysis for the applied and bound fractions of His-PBP3 showed a band with an apparent molecular weight corresponding to His-PBP3 showing that it was successfully pulled down by the beads (Figure 3.46). PBP2B and PBP1 in the absence of His-PBP3 appeared only in the applied fraction suggesting that PBP1 and PBP2B were not pulled down by Ni-NTA. The elution fraction of the mixture PBP1, PBP2B and His-PBP3 showed only two bands in the elution fraction corresponding to PBP2B and His-PBP3 suggesting that His-PBP3 was able to pull down PBP2B but not PBP1. These results suggest that the formation of a ternary complex between PBP1, PBP2 and His-PBP3 is doubtful. The K_D of the interaction between PBP2B and PBP3 was 8.7 nM suggesting a strong interaction between the two proteins. Thus, we hypothesised that the presence of PBP3 destabilises the interaction of PBP2B with PBP1. To test this hypothesis we used the *in vitro* GTase assay to monitor the activity of PBP1 in the presence of PBP2B and PBP3.

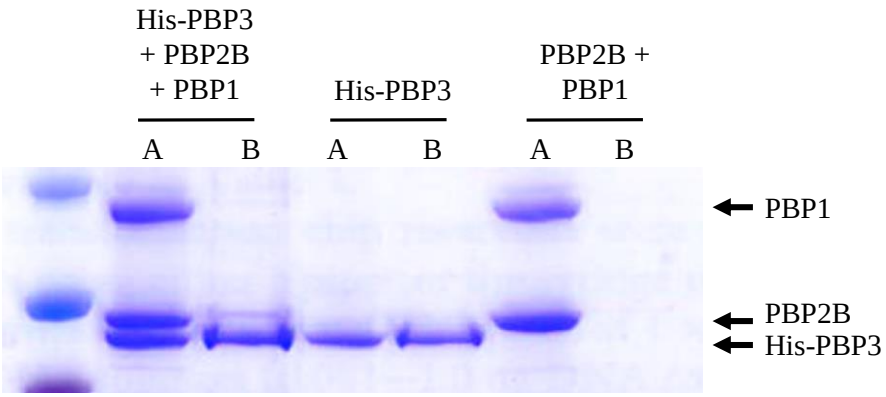

Figure 3.46 *In vitro* crosslink / pull-down assay of His-PBP3 with PBP1 and PBP2B

Ni-NTA pull-down for His-PBP3, PBP1 and PBP2B. Coomassie stained SDS-PAGE analysis showing His-PBP3 and PBP2B but not PBP1 in the bound fraction suggesting that His-PBP3 pulled down PBP2B but not PBP1. A, Applied; B, bound fractions.

4.2.7 GTase activity of PBP1 in the presence of PBP2B and PBP3

The pull-down experiment proposed that PBP1, PBP2B and PBP3 do not form a ternary complex. PBP2B, unlike PBP3, stimulated the GTase activity of PBP1 (Sections 4.1.10 and 4.2.5). The GTase activity of PBP1 was tested in the presence of both PBP2B and PBP3. PBP1 in the presence of both PBP2B and PBP3 had a similar decrease in fluorescence to PBP1 alone (Figure 3.47), suggesting that the stimulation of the GTase activity of PBP1 by PBP2B was diminished upon the addition of PBP3. This effect was probably caused by the destabilization of the interaction between PBP1 and PBP2B.

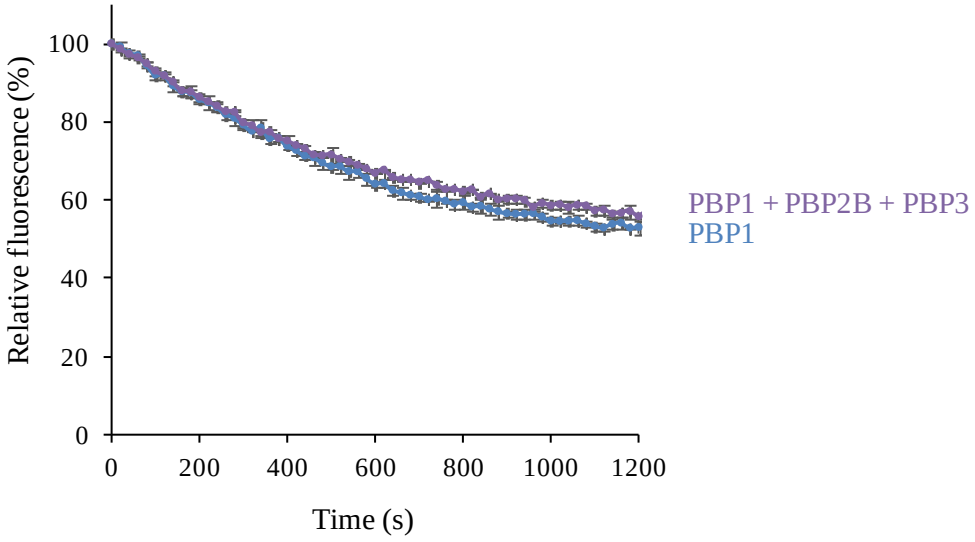

Figure 3.47 The GTase activity of PBP1 in the presence of PBP2B and PBP3

In vitro glycosyltransferase assay for PBP1 alone or PBP1 with PBP2B and PBP3. PBP1 with PBP2B and PBP3 had a similar decrease in the fluorescence signal to PBP1 alone. Values represent the mean ± standard deviation of three independent experiments.

4.3 Conclusions and discussion

The depletion of the essential PBP2B (*Bs*PBP2B) resulted in a block in cell division followed by lysis (Daniel *et al.,* 2000). Work done by Meizhu Xu showed that cells expressing a catalytically inactive *Bs*PBP2B were viable, but they required functional PBP3 (*Bs*PBP3), a homologue of *Bs*PBP2B that is dispensable in wild-type cells (Unpublished data). These results suggests that *Bs*PBP2B has a crucial non-catalytic and a dispensable catalytic roles. In young wild-type cells *Bs*PBP3 localised at the cell poles or in foci at the cell periphery (Scheffers *et al.,* 2004). At later stages of the cell cycle most *Bs*PBP3 molecules were recruited to mid-cell, however distinct foci along the cell periphery were still detected. The depletion of *Bs*PBP2B or FtsZ in the cell resulted in a scattered localisation of *Bs*PBP3 along the cell periphery, suggesting that *Bs*PBP3 is part of the septal PG synthesis machinery and requires the presence of *Bs*PBP2B to find the mid-cell (Richard Daniel, unpublished). Moreover, *Bs*PBP2B and *Bs*PBP3 interact, which supports that the physical presence of PBP2B is essential for PBP3 to find the divisome. Why two class B PBP homologues are needed together for septal PG synthesis is not known. The absence of *Bs*PBP3 had no effect on cell growth, morphology or sporulation (Murray et al., 1996). The amino acid sequence analysis and the crystal structure of *Bs*PBP3 revealed the presence of a MecA domain, which is also present in the *Sa*PBP2a from *S. aureus* (Unpublished data) (Wei Wu *et al.,* 2001). *Sa*PBP2a is responsible for the methicillin-resistance phenotype in *S. aureus* however, since *B. subtilis* cells are sensitive to methicillin, the role of *Bs*PBP3 remains unclear (Matsuhashi *et al.,* 1986). Cells expressing *Bs*PBP2B* exhibited an earlier and enhanced recruitment of PBP3 to mid-cell possibly to complement the lack of TPase activity. However, the *Bs*PBP2B* mutant exhibited longer cell morphology and aberrant septa suggesting a lower efficiency in septal PG synthesis despite the enhanced presence of *Bs*PBP3.

*Bs*PBP2B is a monofunctional transpeptidase presumably catalysing cross-links in the murein (Daniel *et al.,* 1996; Yanouri *et al.,* 1993). However, *Bs*PBP2B alone cannot synthesize the murein net during cell division and requires a synthetic glycosyltransferase activity to polymerize the murein glycan strands. *Bs*PBP2B is the first PBP recruited to the assembling divisome and the depletion of *Bs*PBP2B resulted in the loss of the class A *Bs*PBP1 septal localisation (Scheffers and Errington, 2004). Moreover, *Bs*PBP2B interacts with *Bs*PBP1 by bacterial two-hybrid (Richard Daniel, unpublished) and by SPR suggesting that *Bs*PBP1 is recruited to midcell through its interaction with *Bs*PBP2B. The interaction between class A and B PBPs have been studied previously in *E. coli* where the essential cell division class B PBP3 (*Ec*PBP3) interacts with the class A synthase PBP1B (Bertsche *et al.,* 2006). These results

support a consistent model of murein synthesis between *E. coli* and *B. subtilis* rods where class A PBPs are recruited by class B PBPs for septal PG synthesis.

An interaction between *Bs*PBP3 and *Bs*PBP1 was also detected *in vitro* and *in vivo* (this work and Richard Daniel, unpublished), however the loss of *Bs*PBP3 in cells lacking *Bs*PBP1 didn't not have any additional effect on cell growth or morphology (Murray et al., 1996). This is an evidence of a redundancy between PBPs in *B. subtilis* which produces a robust system for cell wall synthesis. Furthermore, since the cooperation between class A and B PBPs is important for PG synthesis, perhaps the interaction of the class B *Bs*PBP3 with *Bs*PBP1 is important for murein synthesis and it is one on the reasons why *Bs*PBP3 was able to complement the inactive *Bs*PBP2B*.

Purified *Bs*PBP2B and *Bs*PBP3 bound the β-lactam antibiotic bocillin indicating that the TPase domain was folded and potentially active. *Bs*PBP2B and *Bs*PBP3 both had mild transpeptidase and carboxypeptidase activities in assays with *Bs*PBP1. Consequently, both *Bs*PBP2B and *Bs*PBP3 require ongoing PG synthesis by *Bs*PBP1 for activity. The cell division class B *Sp*PBP2x from *S. pneumoniae* is also required for the GTase activity of the class A *Sp*PBP2A to produce PG (Zapun *et al.,* 2013). However, *Ec*PBP3 showed no TPase activity despite the presence of *Ec*PBP1B, FtsN, and/or PG (Waldemar Vollmer, unpublished). The presence of a tripeptide rich PG or a pentapeptide rich PG had no effect on the activity of *Bs*PBP2B, similar to *Sp*PBP2x, which did not require the presence of PG from *S. pneumoniae* for activity (Zapun *et al.,* 2013). In contrast, *Bs*PBP3 from *B. subtilis* showed a TPase activity only in the presence of PG similar to the class B PBP2 from *E. coli* (*Ec*PBP2), which is involved in cell elongation (Banzhaf *et al.,* 2012). These results suggests that *Bs*PBP2B is able to crosslink two nascent glycan strands synthesised by *Bs*PBP1 while *Bs*PBP3 is more involved in attaching newly synthesised PG to the sacculi. The subtle differences between the activities of *Bs*PBP2B and *Bs*PBP3 could be a reason for the partial complementation of the *Bs*PBP2B* mutant by *Bs*PBP3.

PBP2B moderately stimulated the GTase activity of *Bs*PBP1. Since the N-terminals of both synthases are anchored in the membrane, it is possible that the non-catalytic domain of *Bs*PBP2B interacts with the GTase domain of *Bs*PBP1 near to the cytoplasmic membrane resulting in the stimulation of the GTase activity (see section 1.3.1). On the other hand, *Ec*PBP3 had no effect on the GTase or TPase activity of its cognate *Ec*PBP1B [(Egan *et al.,* 2015) and Khai Bui, unpublished]. Despite the homology between *Bs*PBP2B and *Bs*PBP3, the latter modulated the activity of *Bs*PBP1 differently *in vitro*, where *Bs*PBP3 had no effect on the GTase activity but reduced the TPase activity of *Bs*PBP1. Taken together, class B PBPs may have

dissimilar roles in the PG synthesis process by differentially modulating the activity of the class A *Bs*PBP1.

The formation of a multi-protein complex in *E. coli* was previously described between cell division proteins (Egan *et al.,* 2015; Trip and Scheffers, 2015). Thus, we tested if a ternary complex exists in *B. subtilis* between PBP1, PBP2B and PBP3 since binary interactions between each protein was observed. Pull down experiments suggested that His-PBP3 only interacted with PBP2B despite the presence of PBP1 in the mixture. Moreover, the GTase activity of PBP1 increased 2 fold in the presence of PBP2B. However, the GTase activity of the synthase with PBP2B and PBP3 together was similar to that of PBP1 alone suggesting that stimulatory effect of PBP2B on the activity of PBP1 is blocked in the presence of PBP3. The loss of the stimulation could be caused by the destabilization of the PBP1-PBP2B interaction by PBP3 supported by the pull-down experiment, or by a direct effect of the PBP3 interaction on PBP1. However, more experiments are required to verify these suggestions.

PG synthesis in B. subtilis

Cells lacking the FtsZ regulators SepF and EzrA do not recruit the essential PG synthase *Bs*PBP2B to the divisome, resulting in cell death (Hamoen *et al.,* 2006). Moreover, EzrA interacts with GpsB and *Bs*PBP1 and coordinates the recruitment of the synthase to the division site (Claessen *et al.,* 2008; Cleverley *et al.,* 2014; Tavares *et al.,* 2008). Therefore, the recruitment of cell wall synthase seems to be regulated by cytosolic proteins that act as a scaffold to assemble the cell division machinery. In this work, we have shown an interaction between *Bs*PBP1 and *Bs*PBP2B *in vitro* suggesting that the recruitment of *Bs*PBP1 to mid-cell is dependent on the physical presence and interaction of *Bs*PBP1with the class B *Bs*PBP2B, a model that has been observed as well in *E. coli* cells between *Ec*PBP3 and its cognate *Ec*PBP1B (Bertsche et al., 2006; Scheffers and Errington, 2004). *Bs*PBP3 was recruited at later stages in the cell cycle and its recruitment was dependent on *Bs*PBP2B. However, the biochemical characterization of *Bs*PBP3 *in vitro* suggests three criteria for *Bs*PBP3. First, *Bs*PBP3 showed a significantly higher CPase than TPase activity in assays with *Bs*PBP1. CPases are thought to have a role in the regulation of cell shape by limiting the availability of pentapeptides as donor substrates for TPase reactions, hence regulating the extent of cross-linking in PG (Potluri *et al.,* 2010). Second, PBP3 reduced the TPase activity of *Bs*PBP1. Third, *Bs*PBP3 diminished the stimulatory effect of *Bs*PBP2B on the GTase activity of *Bs*PBP1. Taken together, we propose that *Bs*PBP3 is recruited late to mid-cell to finalise the septal PG synthesis by reducing the

activity of the main synthase and dissociating the *Bs*PBP2B-PBP1 complex. This hypothesis correlates with partial complementation of *Bs*PBP3 to the *Bs*PBP2B*, however, it does not take into account the presence of other proteins in the divisome complex that might be modulate PG synthesis. Therefore, for future work, if *Bs*PBP3 is indeed playing a role in the termination of the septal PG synthesis then the overexpression of *Bs*PBP3 should cause a delay or a block in cell division leading to the formation of longer cells.

The lipid II flippase *Ec*FtsW interacts with *Ec*PBP3 and recruits it to mid-cell during cell division (Derouaux *et al.,* 2008; Fraipont *et al.,* 2011; Mohammadi *et al.,* 2014). *Ec*PBP3 also interacts with *Ec*PBP1B and recruits it (Bertsche *et al.,* 2006). Therefore, *Ec*PBP3 is possibly recruiting the synthase *Ec*PBP1B to the lipid II substrate at midcell by interacting with *Ec*FtsW and *Ec*PBP1B. The interaction between *Mt*PBP3 and *Mt*FtsW in *Mycobacterium tuberculosis* was also observed suggesting that the interaction of the lipid II flippase with a cognate PBP is conserved across several bacterial species. In *B subtilis,* the recruitment of *Bs*FtsW to midcell is interdependent on the localisation of *Bs*PBP2B and FtsL (Gamba *et al.,* 2016). Moreover, *Bs*PBP2B interacts with *Bs*FtsW (Richard Daniel, unpublished). Therefore, perhaps the non-catalytic domain of *Bs*PBP2B is essential in *B. subtilis* due to its role in the recruitment of cell division proteins to midcell where the lipid II is being delivered by *Bs*FtsW. Hence, the inability of *Bs*PBP3 to complement the loss of *Bs*PBP2B may be caused by the absence of interaction with the flippase *Bs*FtsW or other essential cell division proteins such as FtsL or DivIC.

B. subtilis has four class A PBPs, PBP1, PBP2c, PBP4 and PBP2d (Section 1.3.1). Cells lacking the four class A PBP were viable and an unknown GTase activity in this quadruple mutant was detected (McPherson and Popham, 2003). Recently, RodA, a presumed lipid II flippase, was suggested to be the missing GTase and responsible for PG synthesis in the quadruple mutant (Meeske *et al.,* 2016). This hypothesis was based on the ability of the RodA overexpression to alleviate the growth and morphology defects of the quadruple mutant. Partially purified RodA showed weak PG polymerization activity, however, the purity of the protein was low which makes it unclear whether the detected activity was from RodA or a contaminant. Another paper by the same group suggested that *Ec*FtsW has a similar GTase activity to RodA and proposed the cytoskeleton-directed SEDS/bPBP (class B PBPs) model for PG synthesis highlighting the separation of labour between the class A PBP system and the SEDS/bPBP system in *E. coli* (Cho *et al.,* 2016). In *B. subtilis,* the localisation of *Bs*PBP1 is dependent on the presence of *Bs*PBP2B and our results shows that class A *Bs*PBP1 interacts with two class B *Bs*PBP2B and *Bs*PBP3 (Scheffers and Errington, 2004). Therefore, these results suggest a collaboration

between class A and B PBPs and SEDS proteins to synthesise the PG regardless of being SEDS being glycosyltransferases or not.

5 Characterization of the role of YrrL

5.1 Introduction

A synthetic lethal screen for regulators of the PG synthase PBP1B in *E. coli* identified a membrane bound potential lytic transglycosylase, MltG (Yunck *et al.,* 2016). MltG interacted with PBP1B by bacterial two-hybrid assay and was described as a terminase for peptidoglycan polymerization in *E. coli* (Yunck *et al.,* 2016). Since MltG is suggested to be part of a conserved lytic transglycosylase enzyme family, a sequence comparison was conducted using the SubtiList web address (http://genolist.pasteur.fr/SubtiList/) in search for a *B. subtilis* homologue. A hypothetical protein, named YrrL, with a YceG-like superfamily domain was identified with 32% amino acid sequence identity and 50% similarity to MltG (Figure 3.53). To characterize the role of YrrL the corresponding gene was deleted and the effect of such deletion on cell morphology was studied using fluorescence microscopy. A homologue for YrrL, YocA, was also identified within the *B. subtilis* proteome and was suggested to have the YceG-like superfamily domain. YocA showed 23.8% amino acid sequence identity and 55.8% similarity to YrrL. To characterise the potential role of YrrL in PG synthesis or hydrolysis, the full length protein was purified and tested *in vitro*. YrrL was tested for interaction with PBP1 or PBP2B using *in vitro* crosslink/pull-down assays and SPR. The effects of such interactions on the GTase and TPase activities of PBP1 were also characterised using various enzymatic assays.

5.2 The effect of *yrrL* or *yocA* deletions on cell morphology

To study the effect of the absence of YrrL on cell morphology, the *yrrL* gene was replaced with an erythromycin resistance cassette in the 168CA strain, and the morphology of the mutant was characterised using fluorescence microscopy. The loss of YrrL had no effect on the cell morphology during vegetative growth when grown in nutrient rich media at 37˚C (Figure 3.48). The effect of *yocA* deletion on cell morphology was also studied using florescence microscopy. The Δ*yocA* mutant had a similar morphology to 168CA with an occasional mild chaining phenotype during exponential phase suggesting a delay in cell separation (Figure 3.48).

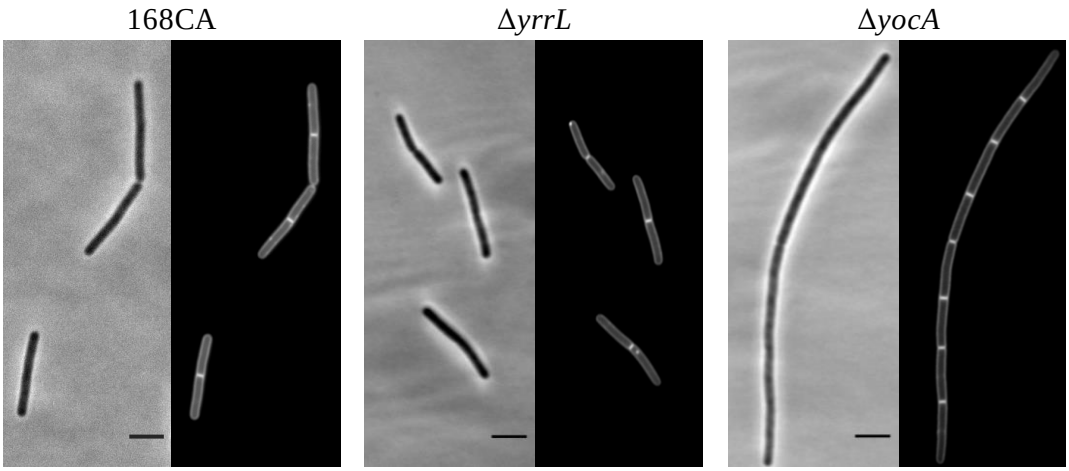

Figure 3.48 Morphology of 168CA, Δ*yrrL* or Δ*yocA* mutants

Phase contrast and cell membrane stained images of 168CA, Δ*yrrL* or Δ*yocA* mutants. Δ*yrrL* or Δ*yocA* cells had similar morphology to wild type cells, with Δ*yocA* having a mild chain morphology. Scale bars: 4 µm.

5.3 The effect of the double deletion of *yrrL* and *yocA* on the cell morphology

Cells lacking either *yrrL* or *yocA* had similar morphology to wild type cells. Thus, a strain lacking both genes, *yrrL* and *yocA*, was constructed and morphologically characterised using fluorescence microscopy. Cells lacking both genes were viable and the majority of the cells had a similar morphology to wild type cells (Figure 3.49 A). However, a few cells (10% of cells) were bloated or wider than 168CA cells (Figure 3.49 B). Bulges were also observed at the cell periphery and sometimes even lysis. Using fluorescence microscopy with a membrane stain showed white foci along the periphery of the cell (Figure 3.49 B). These results suggest that the deletion of *yrrL* and *yocA* causes alterations in the membrane integrity which occasionally leads to cell lysis.

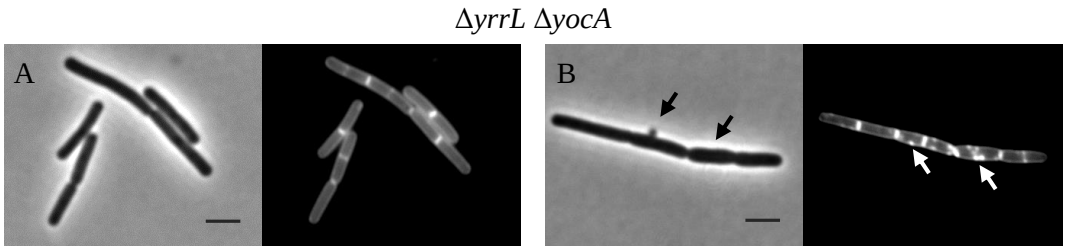

Figure 3.49 Morphology of 168CA Δ*yrrl* Δ*yocA* cells

Phase contrast and cell membrane stained images of 168CAΔ*yrrl* Δ*yocA* mutant. The majority of cells had similar morphology to 168CA (A). However, we observed few cells to have a mildly bloated shape (B). Membrane stain showed white foci along the periphery suggesting cell lysis. Scale bars: 4 µm.

5.4 Purification of YrrL

The TMHMM server (http://www.cbs.dtu.dk/services/TMHMM-2.0/) predicted that YrrL, similar to MltG, has a transmembrane helix (Sonnhammer *et al.,* 1998). The use of the SignalP prediction server (http://www.cbs.dtu.dk/services/SignalP/) did not identify an amino acid sequence recognised by peptidases suggesting that YrrL, like MltG, is a membrane bound protein (Petersen *et al.,* 2011). Based on this prediction, *yrrL* was cloned into an expression plasmid pET28(a)+ using ligase free cloning (sections 2.6.2). *E. coli* BL21(DE3) cells were used for the expression of YrrL with an N-terminal hexahistidine tag (His-YrrL). Cells were harvested and YrrL was purified from the solubilised membrane fraction using affinity chromatography and ion exchange chromatography (section 2.10.7). Affinity chromatography using Ni-NTA was first performed to purify His-YrrL (Figure 3.50 A). The hexahistidine tag was removed using thrombin. The second purification step consisted of ion exchange chromatography. Protein Calculator v3.4 predicted YrrL to have a positive charged of +18.3 at pH 6.0. Thus, a HiTrap SP HP column was used to further purify YrrL. Samples were dialysed to pH 6.0 which promoted the binding of YrrL to the column followed by the elution of the protein using a gradient of elution buffer with 1 M NaCl and pH 7.5. Collected fractions from the two chromatography steps were analysed by SDS-PAGE (Figure 2.50 A and B). Typically, 2.3 mg of YrrL per litre of culture was obtained.

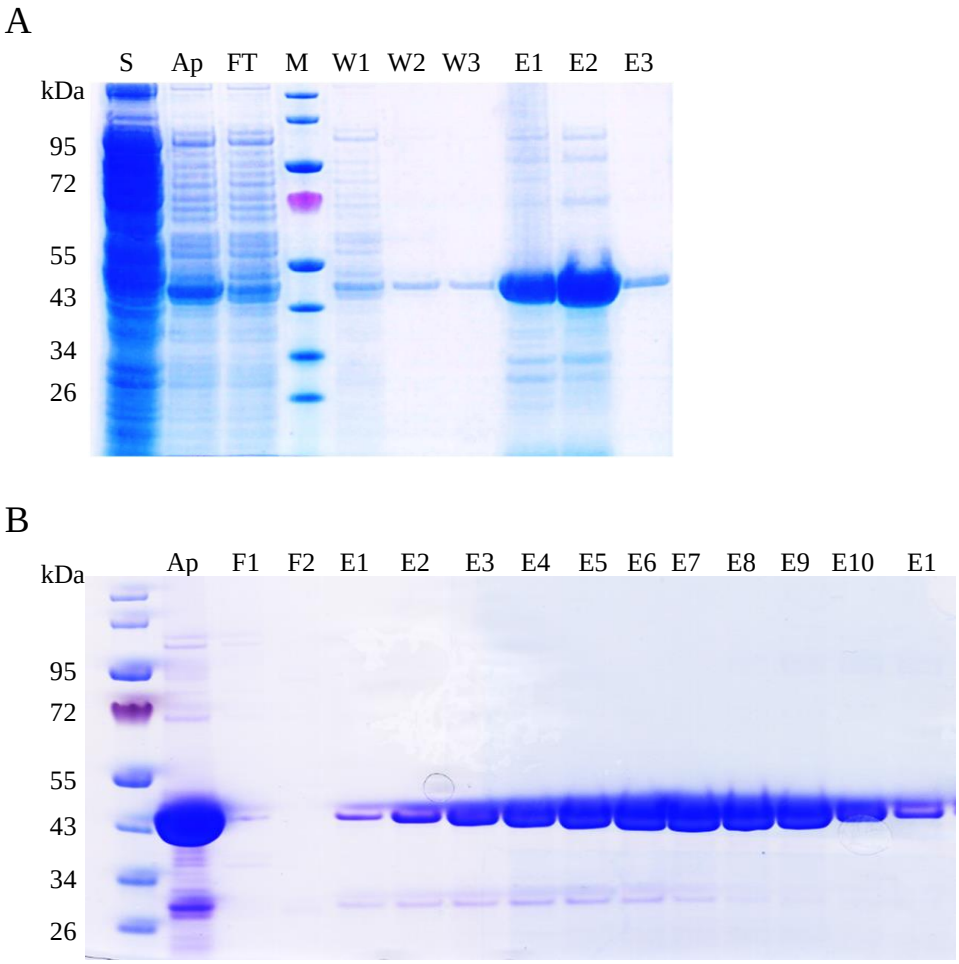

Figure 3.50 Purification of YrrL

SDS-PAGE analysis shows the fractions of YrrL purification steps. Gels were stained with Coomassie blue

(A) IMAC purification of His-YrrL. S, soluble fraction; Ap, applied fraction; FT, flow-through; M, Protein size marker (Fermentas PageRuler); W1-W3, wash fractions; E1-E3, elution fractions. The theoretical molecular weight of His-YrrL is 46 kDa.

(B) IEX of the purified YrrL after thrombin cleavage. M, Protein size marker; the bands in E3 to E10 fractions with an apparent molecular weight of 44 kDa correspond to YrrL. The bands above the marker and YrrL are gel artefacts due to unknown reasons.

5.5 YrrL had no activity against PG

MltG is a potential lytic transglycosylase with a weak endoglycosidase activity (Yunck *et al.*, 2016). The activity of YrrL was tested against PG from *B. subtilis* cells at pH 7.5 or 5, in the presence of 20 or 150 mM NaCl, and with or without $MgCl_2$ and $CaCl_2$. After overnight incubation with PG at 30 or 37˚C, samples were pelleted and the supernatant was reduced and analysed by HPLC. However, no muropeptides were detected suggesting that YrrL has no

activity on PG under the conditions tested. Since MltG is potentially interacting with the cell division synthase PBP1B in *E. coli*, the activity of YrrL was tested in the presence of *B. subtilis* PBP1, PBP2B and PBP3. As before, the supernatant from samples containing YrrL and one or multiple PBPs with *B. subtilis* PG were analysed by HPLC. However, no muropeptides were detected in all samples tested suggesting the absence of muropeptides released into the supernatant. Hence, YrrL showed no activity against tripeptide-rich PG isolated from 168CA cells. The activity of YrrL was also tested against pentapeptide rich PG isolated from 168CA Δ*dacA* mutant cells, but no activity was observed. These results suggest that YrrL is inactive *in vitro* against *B. subtilis* PG under the conditions tested.

5.6 YrrL interacts with PBP1

MltG presumably interacts with the PG synthase PBP1B in *E.coli* (Yunck *et al.,* 2016). YrrL was tested for interaction with the cell division PG synthase, PBP1, by SPR and pull-down experiments using purified PBP1 and YrrL. First, an *in vitro* pull-down experiment was performed using Ni-NTA to test if a hexahistidine-tagged YrrL (His-YrrL) retains PBP1 (section 2.10.1) and formaldehyde was used to stabilize possible weak interactions. SDS-PAGE analysis shows that His-YrrL bound to Ni-NTA and PBP1 was not retained by the beads in the absence of His-YrrL (Figure 3.51 A). PBP1 in the presence of His-YrrL appeared in both the applied and bound fractions suggesting that His-YrrL was able to pull down PBP1 indicating an interaction between the two proteins.

The interaction between PBP1 and YrrL was investigated using SPR as a second method (section 2.10.2). First, ampicillin was immobilized to the sensor chip followed by the covalent binding of PBP1 via its TPase domain. The remaining free ampicillin was digested with β-lactamase followed by a 1 M NaCl buffer wash of the chip surface. A surface without PBP1 was prepared in the same way as a control. YrrL molecules were injected over the PBP1-surface and the control surface at concentration 500, 250, 125, 62.5 and 31.2 nM. Sensorgrams representing both surfaces showed a strong increase in signal during association upon YrrL injection. The PBP1-surface showed slightly higher signal than the control surface (Figure 3.51 B). The signals for the PBP1-surface minus the control for YrrL injected at 250 and 500 nM overlapped suggesting a saturation of binding (Figure 3.51 C). The high signal over the control surface is caused by the unspecific binding of YrrL to the chip surface. Thus, further optimization of the condition is essential to decrease the signal generated by YrrL over the

control surface. Otherwise, an alternative method need to be used to confirm the interaction between the two proteins.

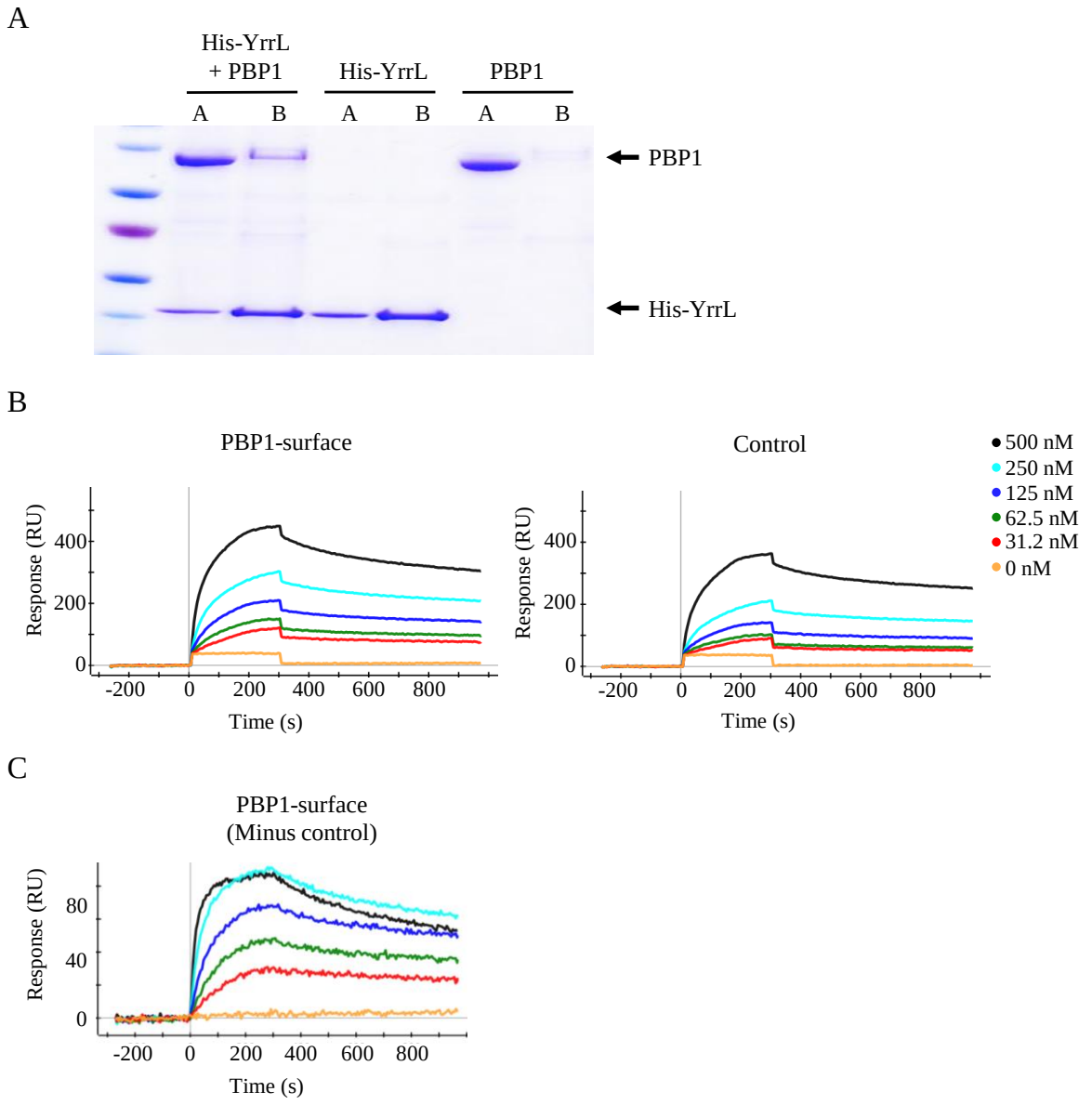

Figure 3.51 Interaction of PBP1 with YrrL by *in vitro* crosslink / pull-down and SPR

(A) Ni-NTA pull-down used to test if PBP1 and YrrL directly interact. Coomassie stained SDS-PAGE analysis for the His-YrrL and PBP1 sample shows both proteins in the applied and bound fractions suggesting that His-YrrL retained PBP1. His-YrrL efficiently bound to the bead and PBP1 was not pulled down in the absence of His-YrrL. A, Applied; B, bound fractions.

(B) SPR sensorgrams showing the signal generated by the injection of Yrrl over the PBP1-surface or the control surface at concentration 31.2, 62.5, 125, 250 and 500 nM. The high signal on the control surface is caused by the unspecific binding of YrrL to the chip surface.

(C) SPR sensorgram showing the response for the PBP1-surface minus control. The binding levels saturated at 250 nM injected YrrL concentration.

5.7 YrrL had no effect on the GTase activity of PBP1

A GTase assay was used to study the activity of YrrL against dansyl-lipid II and the effect of YrrL on the GTase activity of PBP1. The fluorescence signal was monitored using a spectrophotometer. Based on DNA sequence analysis, YrrL is a lytic-transglycosylase and lacks a GTase domain. Consistent with this, no decrease in fluorescence was observed for YrrL alone, suggesting the absence of activity against lipid II (Figure 3.52). PBP1 with YrrL showed a similar decrease in fluorescence to PBP1 alone suggesting that YrrL has no effect on the GTase activity of PBP1.

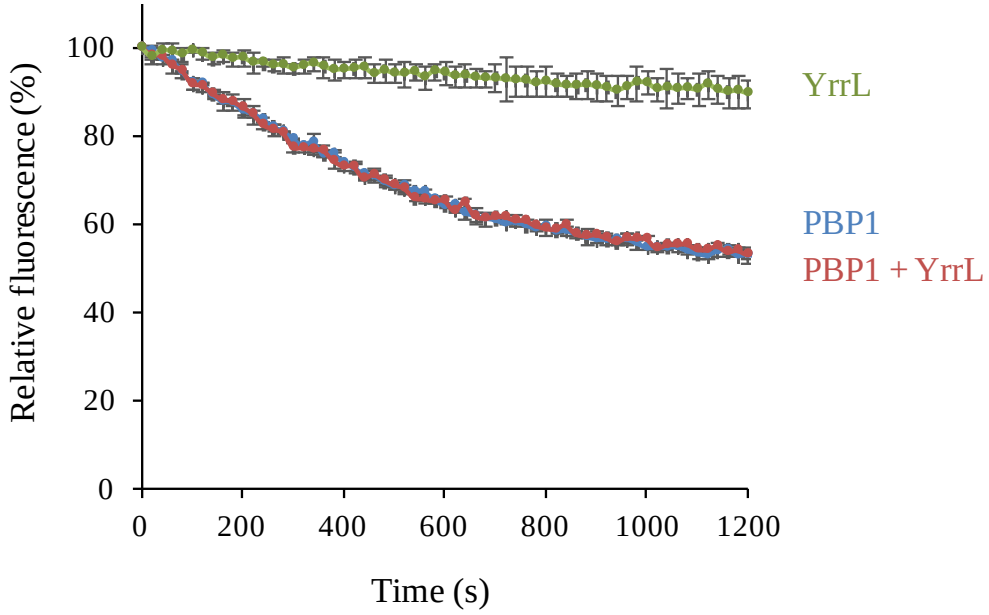

Figure 3.52 The effect of YrrL on the GTase activity of PBP1

The diagram represents the GTase activity of PBP1, PBP1 with YrrL or YrrL alone. A decrease in fluorescence suggests the presence of a GTase activity. YrrL alone has no activity against lipid II and has no effect of the GTase activity of PBP1. Values represent the mean ± standard deviation of three independent experiments.

5.8 YrrL reduces the TPase activity of PBP1

The activity of YrrL against radio-labelled lipid II and the effect of YrrL on the TPase activity of PBP1 was studied using the *in vitro* PG synthesis assay (section 2.11.4). YrrL alone had no activity against lipid II (Figure S5). The relative percentage of peptides in crosslinks decreased 10.9% in samples containing YrrL and PBP1 compared to samples with PBP1 alone (Figure 3.53). The activity of PBP1 and YrrL was also studied in the presence of 168CA PG or Δ*dacA* PG. A decrease of 7.5 and 5.0% in levels of peptides in crosslinks was identified for PBP1 with

YrrL compared to PBP1 alone in the presence of 168CA or Δ*dacA* PG, respectively. These results suggest that YrrL reduces the TPase activity of PBP1 in the presence or absence of PG. Moreover, the HPLC chromatogram representing the radioactive signal for muropeptides produced by PBP1with YrrL showed a small unknown peak (Figure S5). The peak eluted at 64 min on a reversed phase column and represented 9.6% ± 0.5 of the total muropeptides. A similar peak was identified for PBP1 with YrrL in the presence of 168CA or Δ*dacA* PG. Due to the low levels of the unknown product in the aforementioned reactions, we were not able to identify the chemical structure of this component by mass spectrometry.

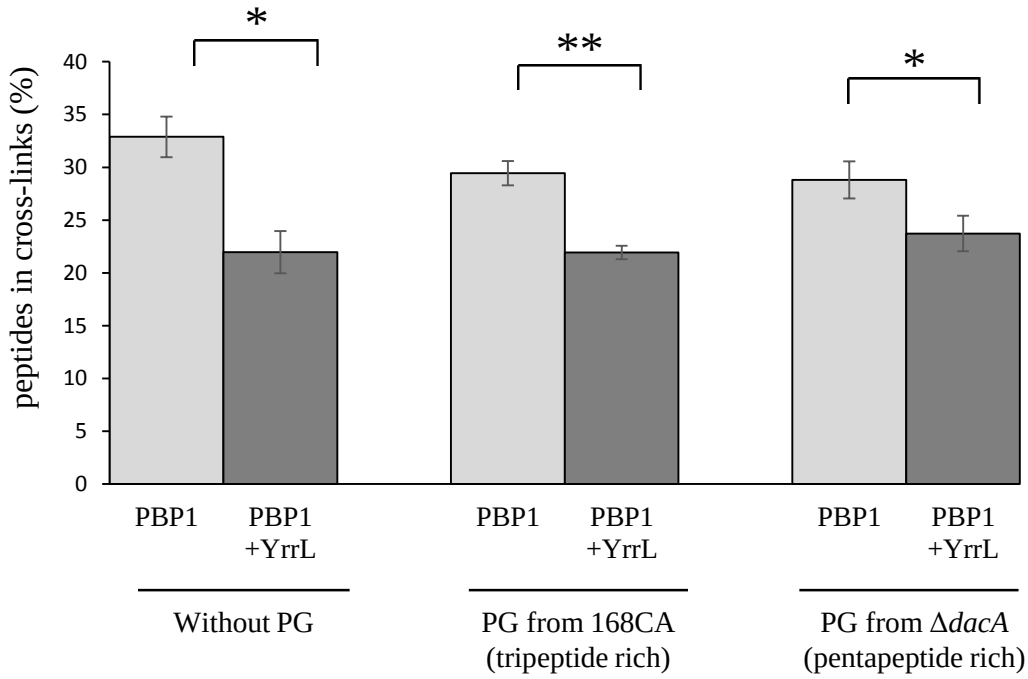

Figure 3.53 YrrL reduces the TPase activity of PBP1

The level of cross-linked peptides in PG produced by PBP1 alone or PBP1 with YrrL in the presence or absence of 168CA or ΔdacA PG. The levels of muropeptides in crosslinks for PBP1 with YrrL significantly decreased compared to PBP1 alone suggesting that YrrL reduces the TPase activity of PBP1 in the presence or absence of PG. *, P<0.05; **, P<0.01

5.9 PBP2B interacts with YrrL

To test if YrrL interacts with the class B PBP2B, pull-down assays and SPR were performed using purified YrrL and PBP2B. First, *in vitro* pull-down assays were used with Ni-NTA to test if His-YrrL retains PBP2B. Formaldehyde (0.2%) was used to stabilise possible weak interactions. For controls, beads were incubated with His-YrrL or PBP2B alone. SDS-PAGE analysis shows that His-YrrL bound to Ni-NTA and PBP2B was not pulled down by the beads in the absence of His-YrrL (Figure 3.54 A). PBP2B in the presence of His-YrrL appeared in both the applied and bound fractions suggesting that His-YrrL pulled down PBP2B. These results indicate that PBP2B interacts with YrrL.

SPR was used as a second method to study the interaction between YrrL and PBP2B and determine the interaction K_D. Ampicillin was immobilized to the sensor chip, followed by the covalent binding of PBP2B. The remaining free ampicillin was digested with β-lactamase, followed by a 1 M NaCl buffer wash of the chip surface. As a control, a surface without PBP2B was prepared in the same way. YrrL was injected at concentration 500, 250, 125, 62.5 and 31.2 nM and the responses were recorded. An increase in the signal was observed upon the injection of YrrL over both surfaces during association (Figure 3.54 B). However, at equilibrium, the signal for the PBP2B surface was significantly higher than the control surface followed by a decrease in both signals during dissociation. The signal for the PBP2B-surface minus the control did not show saturation of binding at the injected PBP2B concentrations (Figure 3.54 C). Although higher concentrations of injected YrrL are required to reach saturation, the SPR and the binding curves suggests that YrrL interacts with PBP2B.

The K_D of the interaction was calculated using SigmaPlot software based on the assumption of one interaction site with YrrL. The response values (RU) at equilibrium during the association phase were plotted against analyte concentrations (nM) to generate the binding curve (Figure 3.54 D). The K_D of the interaction of PBP2B with PBP3 was 101.6 ± 11.6 nM calculated from three independent experiments.

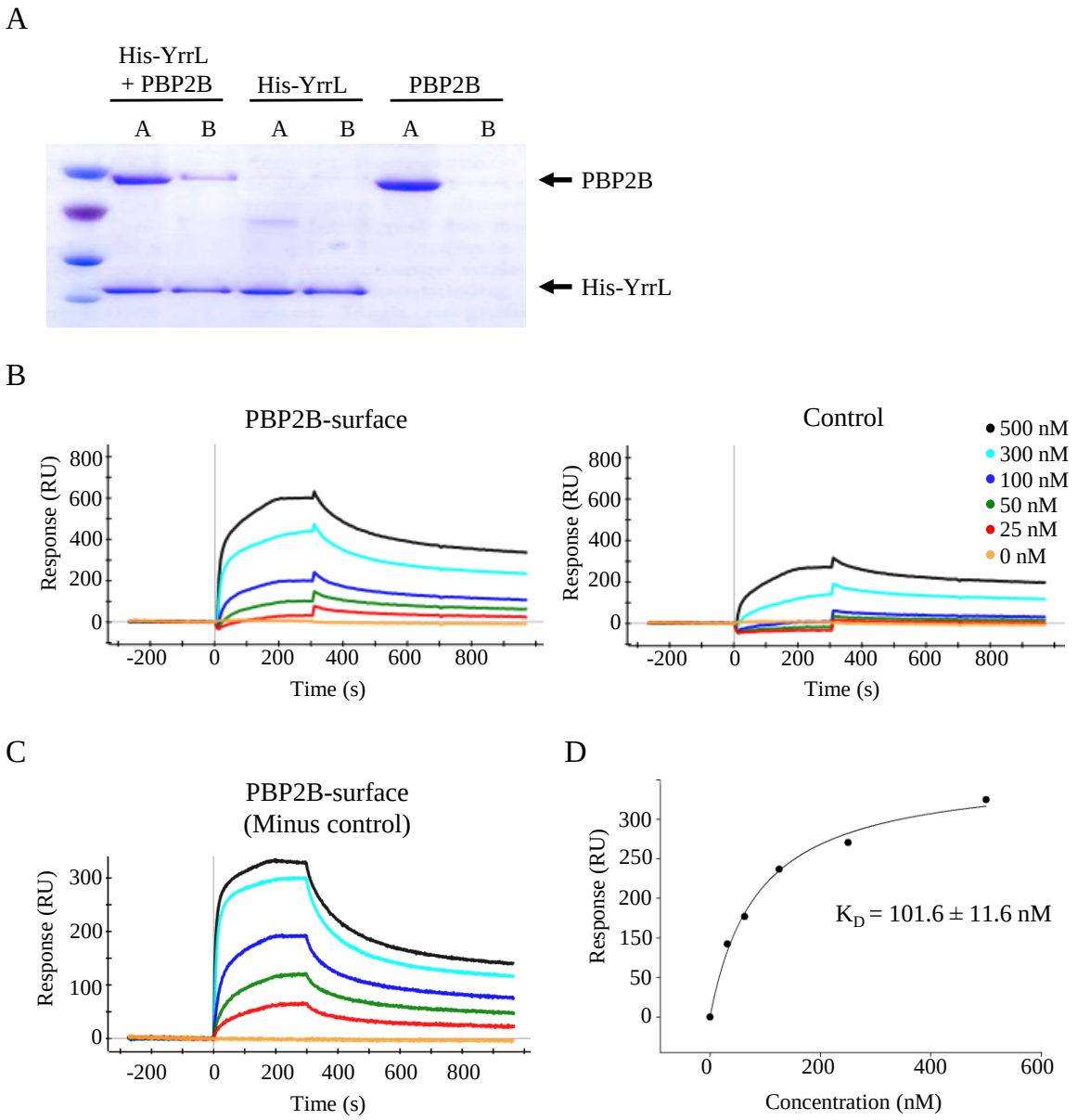

Figure 3.54 Interaction of PBP2B with YrrL by SPR and *in vitro* crosslink/pull-down

(A) Pull down experiment performed to test if PBP2B and His-YrrL interact. Coomassie stained SDS-PAGE analysis for the His-YrrL and PBP2B sample shows both proteins in the applied and bound fractions suggesting that His-YrrL retained PBP2B. His-YrrL efficiently bound to the bead and PBP2B was not pulled down in the absence of His-YrrL. A, Applied; B, bound fractions.

(B) SPR sensorgrams showing the response for YrrL when injected over a surface with immobilized PBP2B or a control surface at concentrations 25, 50, 100, 300 and 500 nM. The PBP2B-surface exhibited a higher signal than the control surface during association suggesting an interaction between PBP2B and YrrL.

(C) SPR sensorgram showing the response for the PBP2B-surface minus control. The saturation of binding was not achieved at the injected YrrL concentrations.

The response values during equilibrium were plotted against the injected YrrL concentrations. The K_D of the PBP2B-YrrL interaction was determined by non-linear regression using Sigma Plot software. The value is the average K_D ± standard deviation of three independent experiments.

5.10 Conclusions and discussion

MltG from *E. coli* (*Ec*MltG) was proposed to be have an endolytic transglycosylase activity based on its ability to hydrolyse bonds at internal positions within the glycan polymer (Yunck *et al.,* 2016). YrrL is the *B. subtilis* homologue of the lytic transglycosylase (LT) *Ec*MltG, however, YrrL showed no activity against PG from wild-type cells or the Δ*dacA* mutant irrespective of the presence or absence of cell division PBPs. Therefore, it remains a conundrum what the activity of YrrL is and/or what activates it in the cell. The comparison of the amino acid sequence of YrrL and Lmo1499, a membrane bound lytic transglycosylase from *Listeria monocytogenes* (*Lm*MltG), showed 67% similarity and 50% identity between the two proteins (Figure 3.55). *Ec*MltG was also described to have high similarity with *Lm*MltG, and both proteins featured a LysM domain, which is known to be involved in PG binding, and a catalytic domain close to the C-terminus of the protein (Figure 3.56) (Buist *et al.,* 2008). Moreover, the LysM domain of YrrL had 49% sequence identity to the LysM domain of *Lm*MltG. This sequence homology appears at the N-termini of both LTs close to the transmembrane domain region of the protein (Figure 3.55 and 3.56). These results suggest that the LysM domain of YrrL perhaps binds to the newly synthesised glycan strand in close proximity to the cytoplasmic membrane.

Pulse chase studies indicated that the formation of the anhydroMurNAc sugar by LT enzymes occurs shortly after lipid II polymerization (Burmant and Park, 1983; Glauner and Höltje, 1990). This result suggests that LT enzymes exist in close proximity to PG synthases or as part of the PG synthesis machinery. Moreover, *Ec*MltG interacts with PBP1B by bacterial two-hybrid (Yunck *et al.,* 2016). Consistent with these results, YrrL interacts with two cell division synthases PBP1 and PBP2B. Moreover, the interaction between YrrL and PBP1 had no effect on the GTase activity of the synthase, however, YrrL significantly reduced the TPase activity of PBP1. These results suggest that lytic transglycosylases like YrrL and MltG might modulate PG synthesis not only through their catalytic activities but also by regulating the activities of PG synthases.

The absence of MltG from *S. pneumoniae* cells caused a round cell morphology, suggesting a role in cell elongation (Tsui *et al.,* 2016). Conversely, the interaction of *Ec*MltG with the cell division synthase *Ec*PBP1B suggests that MltG is part of the cell division machinery. In *B. subtilis*, YrrL interacted with the cell division synthase *Bs*PBP2B, however, the absence of both YrrL and YocA resulted in occasionally bloated cells and bulges at the lateral cell wall. Therefore, based on the existing results it is not clear what role YrrL plays in *B. subtilis*.

```
MltG  1    M------KNTKGKKITIIISIIILILVIATFSGYYYVKSQLEPKDEASKEKITVEIPAGSSISDISTILEDKKVINNASI  74
Yrrl  1    MYINQQKKSFFNKKRIILSSIVVLFLIIG--GAFLYGKSLLEPVEKDSKTTVNINIPSGSSVSAIASILKKNDVIKSEKA  78

MltG  75   FSFYVKYNNDTNLKAGNYELSPAMNTDQIVKKMQEGKTVAPAKLVIPEGYTLDQIADRIVAYQPKLKKADVLKTMDDPEF  154
Yrrl  79   FQYYVKYKGASGFQAGFYHLNKGMDLDAIIQKLTSGATGYAFQITVTEGAQLTQIAAAIAD-ETKYSKKQVIAKLDDETF  157

MltG  155  VASMIKAYPETVTNDVLNKSIKHPLEGYLYPATYTFKGTDVSAEQIITEMVKATDVNIAKYRDELTKQKMSVHKFLTMSS  234
Yrrl  158  INQLKKEFPDTVTNDVFNKNIKHPLEGYLFPATYPFNDPDTSLEDIIKAMIKQTNSYVETYKSEMKKNKVSVHKLLTMAS  237

MltG  235  IIEKEATENVDRKMIASVFYNRLAKDMRLQTDPTVLYALGEHKSKTTYKDLEVDSPYNTYKNNGLPPGPISNSGDSSMEA  314
Yrrl  238  LIEEEATEKADRHKIASVFYNRLKKKMPLQTDPTVLYAAGKHKDRVLYKDLEIDSPYNTYKNTGLTPGPIANAGMSSWEA  317

MltG  315  ALYPEKSDYLYFLANTKTGKVYFSKTLEEHNKLKEEHITKNN--  356
Yrrl  318  ALHPDKTDYLYFLAKSN-GEVVFTKTLKEHNKAKEKYISSKNEK  360
```

∗ Highly conserved amino acid

□ LysM domain of MltG

Figure 3.55 Amino acid sequence alignment for *L. monocytogenes* MltG and YrrL

The amino acid sequence analysis for *Lm*MltG and YrrL showed 67% similarity and 50% identity between the two proteins. The amino acid sequence analysis of the LysM domain (Black Square) of YrrL and *Lm*MltG identified 41% identity and 63% similarity. *, highly conserved residues within the LysM domain. †, MltG active site

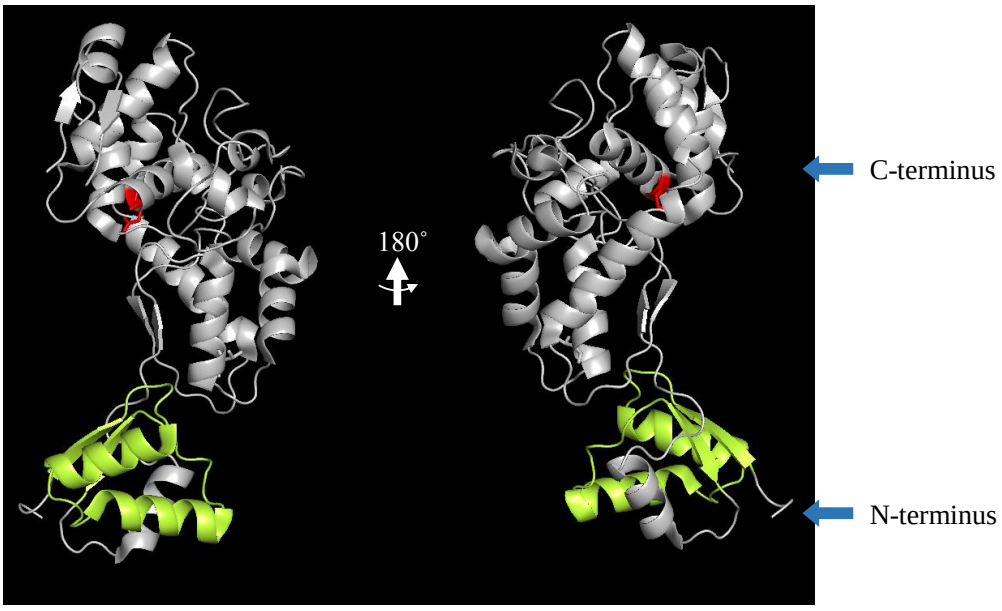

Figure 3.56 The crystal structure of MltG from *L. monocytogenes*

Cartoon representation of the structure of *Lm*MltG (Lmo1499) from the PDB data base (PDB ID: 4IIW) (http://www.rcsb.org/pdb/home/home.do). 180˚ rotation of *Lm*MltG structure along the Y axis. The active site is in red and the LysM domain is in green. Blue arrows indicate the N- or C-terminus of the protein.

Association between PG synthases and lytic transglycosylases

Koch and Doyle proposed the inside-to-outside model for PG growth in Gram-positive cells (Koch and Doyle, 1985). In their model, the synthesis of new PG material occurs at the innermost layer of the sacculus close to the cytoplasmic membrane whereas the hydrolysis of the PG happens at the outermost layer. The PG protects the cell from rupture and maintains cell shape hence, its enlargement must occur by a safe mechanism to avoid defects that could lead to lysis. Despite progress made in the understanding of PG growth, the molecular mechanisms of cell wall growth are largely unknown particularly in Gram-positive bacteria. *B. subtilis* has at least five hypothetical lytic transglycosylases (YomI, SleB, CwlQ, YuiC and SleC) only known to play roles in the lysis of the spore cortex for germination (Kumazawa *et al.,* 2007; Quay *et al.,* 2015; Smith *et al.,* 2000; Sudiarta *et al.,* 2010). Recently, Bernhardt and colleagues identified a potential membrane bound LT with endo-lytic activity in *E. coli* named MltG that interacts with the PG synthase *Ec*PBP1B (Yunck *et al.,* 2016). The absence of MltG resulted in increased average length of the glycan strand suggesting a role in chain length determination. Moreover, *Ec*PBP1B interacts with the lytic transglycosylase MltA via the scaffold protein MipA (Vollmer *et al.,* 1999). Slt, another LT from *E. coli*, selectively interacted with PBP3 and PBP7/8 supporting a multi-protein model that includes both synthases and hydrolases (Romeis and Höltje, 1994). As shown in this work, the lytic transglycosylase homologue from *B. subtilis* YrrL interacted with the class A and B PG synthases PBP1 and PBP2B. Moreover, YrrL modulated the TPase activity of the synthase PBP1 in the presence or absence of PG. The lack of enzymatic activity and the limited knowledge about YrrL made it challenging to understand the role of such a protein in PG synthesis. However, based on our current knowledge, we propose that hypothetical LT enzymes in *B. subtilis* may not only be associated with lysis of the spore cortex but also with PG synthesis complexes. However, more experimental evidences are required to characterize the function of YrrL in the cell.

6 References

Abhayawardhane, Y., and Stewart, G.C. (1995). *Bacillus subtilis* possesses a second determinant with extensive sequence similarity to the *Escherichia coli mreB* morphogene. J. Bacteriol. *177*, 765–773.

Adams, D.W., and Errington, J. (2009). Bacterial cell division: assembly, maintenance and disassembly of the Z ring. Nature *7*, 642–653.

Adams, D.W., Wu, L.J., and Errington, J. (2015). Nucleoid occlusion protein Noc recruits DNA to the bacterial cell membrane. EMBO J. *34*, 491–501.

Adler, H.I., Fisher, W.D., Cohen, A., and Hardigree, A.A. (1967). Miniature *Escherichia coli* cells deficient in DNA. Proc. Natl. Acad. Sci. U. S. A. *57*, 321.

Akio, M., Atsuko, Y., Tsutomu, S., Tatsuo, Y., Gunjana, T., and Yasuo, K. (1992). Sequence of the *Bacillus subtilis* homolog of the *Escherichia coli* cell-division gene *murG*. Gene *118*, 147–148.

Anagnostopoulos, C., and Spizizen, J. (1961). Requirements for transformation in *Bacillus subtilis*. J. Bacteriol. *81*, 741–746.

Araki, Y., and Ito, E. (1989). Linkage units in cell walls of Gram-positive bacteria. Crit Rev Microbiol *17*, 121–135.

Atrih, A., Bacher, G., Williamson, M.P., and Foster, S.J. (1999). Analysis of peptidoglycan structure from vegetative cells of *Bacillus subtilis* 168 and role of PBP5 in peptidoglycan maturation. J. Bacteriol. *181*, 3956–3966.

Azam, M.A., and Jayaram, U. (2016). Inhibitors of alanine racemase enzyme: a review. J Enzym. Inhib Med Chem *31*, 1475–6366.

Van Baarle, S., and Bramkamp, M. (2010). The MinCDJ system in *Bacillus subtilis* prevents minicell formation by promoting divisome disassembly. PLoS One *5*, e9850

Bach, J.N., Albrecht, N., and Bramkamp, M. (2014). Imaging DivIVA dynamics using photo-convertible and activatable fluorophores in Bacillus subtilis. Front. Microbiol. *5*, 59.

Banzhaf, M., van den Berg van Saparoea, B., Terrak, M., Fraipont, C., Egan, A., Philippe, J., Zapun, A., Breukink, E., Nguyen-Distèche, M., den Blaauwen, T., et al. (2012). Cooperativity of peptidoglycan synthases active in bacterial cell elongation. Mol. Microbiol. *85*, 179–194.

Barreteau, H., Kovač, A., Boniface, A., Sova, M., Gobec, S., and Blanot, D. (2008). Cytoplasmic steps of peptidoglycan biosynthesis. FEMS Microbiol. Rev. *32*, 168–207.

Barrett, D., Andrew Wang, T.S., Yuan, Y., Zhang, Y., Kahne, D., and Walker, S. (2007). Analysis of glycan polymers produced by peptidoglycan glycosyltransferases. J. Biol. Chermistry *282*, 31964–31971.

Beall, B., and Lutkenhaus, J. (1989). Nucleotide sequence and insertional inactivation of a *Bacillus subtilis* gene that affects cell division, sporulation, and temperature sensitivity. J. Bacteriol. *171*, 6821–6834.

Beall, B., and Lutkenhaus, J. (1992). Impaired cell division and sporulation of a *Bacillus subtilis* strain with the *ftsA* gene deleted. J. Bacteriol. *174*, 2398–2403.

Beeby, M., Gumbart, J.C., Roux, B., and Jensen, G.J. (2013). Architecture and assembly of the Gram-positive cell wall. Mol. Microbiol. *88*, 664–672.

Behrends, V., Tredwell, G.D., and Bundy, J.G. (2011). A software complement to AMDIS for processing GC-MS metabolomic data. Anal. Biochem. *415*, 206–208.

Bertsche, U., Breukink, E., Kast, T., and Vollmer, W. (2005). *In vitro* murein (peptidoglycan) synthesis by dimers of the bifunctional transglycosylase-transpeptidase PBP1B from *Escherichia coli*. J. Biol. Chem. *280*, 38096–38101.

Bertsche, U., Kast, T., Wolf, B., Fraipont, C., Aarsman, M.E.G., Kannenberg, K., Von Rechenberg, M., Nguyen-Distèche, M., Den Blaauwen, T., Höltje, J.V., et al. (2006). Interaction between two murein (peptidoglycan) synthases, PBP3 and PBP1B, in *Escherichia coli*. Mol. Microbiol. *61*, 675–690.

Bhavsar, A.P., and Brown, E.D. (2006). Cell wall assembly in *Bacillus subtilis*: how spirals and spaces challenge paradigms. Mol. Microbiol. *60*, 1077–1090.

Bhavsar, A.P., Truant, R., and Brown, E.D. (2005). The TagB protein in *Bacillus subtilis* 168 is an intracellular peripheral membrane protein that can incorporate glycerol phosphate onto a membrane-bound acceptor in vitro. J. Biol. Chem. *280*, 36691–36700.

Bi, E., and Lutkenhaus, J. (1991). FtsZ ring structure associated with division in *Escherichia coli*. Nature *354*, 161–164.

Bisicchia, P., Noone, D., Lioliou, E., Howell, A., Quigley, S., Jensen, T., Jarmer, H., and Devine, K.M. (2007). The essential YycFG two-component system controls cell wall metabolism in *Bacillus subtilis*. Mol Microbiol *65*, 180–200.

Bisicchia, P., Bui, N.K., Aldridge, C., Vollmer, W., and Devine, K.M. (2011). Acquisition of VanB-type vancomycin resistance by *Bacillus subtilis*: The impact on gene expression, cell wall composition and morphology. Mol. Microbiol. *81*, 157–178.

den Blaauwen, T.D., de Pedro, M.A., Nguyen-Distè che, M., and Ayala, J.A. (2008). Morphogenesis of rod-shaped sacculi. FEMS Microbiol Rev *32*, 321–344.

Blackman, S.A., Smith, T.J., and Foster, S.J. (1998). The role of autolysins during vegetative growth of *Bacillus subtilis* 168. Microbiology *144*, 73–82.

de Boer, P., Crossley, R., and Rothfield, L. (1992). The essential bacterial cell-division protein FtsZ is a GTPase. Nature *359*, 254–256.

Born, P., Breukink, E., and Vollmer, W. (2006). *In vitro* synthesis of cross-linked murein and its attachment to sacculi by PBP1A from *Escherichia coli*. J. Biol. Chem. *281*, 26985–26993.

Bouhss, A., Trunkfield, A.E., Bugg, T.D.H., and Mengin-Lecreulx, D. (2008). The biosynthesis of peptidoglycan lipid-linked intermediates. FEMS Microbiol. Rev. *32*, 208–233.

Boylan, R.J., and Mendelson, N.H. (1969). Initial characterization of a temperature-sensitive rod-mutant of *Bacillus subtilis*. J. Bacteriol. *100*, 1316–1321.

Boyle, D.S., Khattar, M.M., Addinall, S.G., Lutkenhaus, J., and Donachie, W.D. (1997). *ftsW* is an essential cell-division gene in *Escherichia coli*. Mol. Microbiol. *24*, 1263–1273.

Bramkamp, M., and Van Baarle, S. (2009). Division site selection in rod-shaped bacteria. Curr. Opin. Microbiol. *12*, 683–688.

Bramkamp, M., Weston, L., Daniel, R.A., and Errington, J. (2006). Regulated intramembrane proteolysis of FtsL protein and the control of cell division in *Bacillus subtilis*. Mol. Microbiol. *62*, 580–591.

Bramkamp, M., Emmins, R., Weston, L., Donovan, C., Daniel, R.A., and Errington, J. (2008). A novel component of the division-site selection system of *Bacillus subtilis* and a new mode of action for the division inhibitor MinCD. Mol. Microbiol. *70*, 1556–1569.

Bravman, T., Bronner, V., Lavie, K., Notcovich, A., Papalia, G.A., and Myszka, D.G. (2006). Exploring “one-shot” kinetics and small molecule analysis using the ProteOn XPR36 array biosensor. Anal. Biochem. *358*, 281–288.

Brown, S., Santa Maria, J.P., and Walker, S. (2013). Wall teichoic acids of Gram-Positive bacteria. Annu. Rev. Microbiol. *67*, 313–336.

Buchanan, C.E., and Ling, M.L. (1992). Isolation and sequence-analysis of *dacB*, which encodes a sporulation-specific penicillin-binding protein in *Bacillus subtilis*. J. Bacteriol. *174*, 1717–1725.

Buist, G., Steen, A., Kok, J., and Kuipers, O.P. (2008). LysM, a widely distributed protein motif for binding to peptidoglycans. Mol. Microbiol. *68*, 838–847.

Burman, L.G., and Park, J.T. (1983). Changes in the composition of *Escherichia coli* murein as it ages during exponential growth. J. Bacteriol. *155*, 447–453.

Cao, M., Wang, T., Ye, R., and Helmann, J.D. (2002). Antibiotics that inhibit cell wall biosynthesis induce expression of the *Bacillus subtilis* sigma(W) and sigma(M) regulons. Mol. Microbiol. *45*, 1267–1276.

Carballido-Lopez, R., Formstone, A., Li, Y., Ehrlich, S.D., Noirot, P., Errington, J., Carballido-López, R., Formstone, A., Li, Y., Ehrlich, S.D., et al. (2006). Actin homolog MreBH governs cell morphogenesis by localization of the cell wall hydrolase LytE. Dev. Cell *11*, 399–409.

Carballido-López, R., and Formstone, A. (2007). Shape determination in *Bacillus subtilis*. Curr. Opin. Microbiol. *10*, 611–616.

Chien, A.C., Hill, N.S., and Levin, P.A. (2012a). Cell size control in bacteria. Curr. Biol. *22*, R340–R349.

Chien, A.C., Zareh, S.K.G., Wang, Y.M., and Levin, P.A. (2012b). Changes in the oligomerization potential of the division inhibitor UgtP coordinate *Bacillus subtilis* cell size with nutrient availability. Mol. Microbiol. *86*, 594–610.

Cho, H., Wivagg, C.N., Kapoor, M., Barry, Z., Rohs, P.D.A., Suh, H., Marto, J.A., Garner, E.C., and Bernhardt, T.G. (2016). Bacterial cell wall biogenesis is mediated by SEDS and PBP polymerase families functioning semi-autonomously. Nat. Microbiol. *1*, 16172.

Chung, K.M., Hsu, H.H., Yeh, H.Y., and Chang, B.Y. (2007). Mechanism of regulation of prokaryotic tubulin-like GTPase FtsZ by membrane protein EzrA. J. Biol. Chem. *282*, 14891–14897.

Claessen, D., Emmins, R., Hamoen, L.W., Daniel, R.A., Errington, J., and Edwards, D.H. (2008). Control of the cell elongation-division cycle by shuttling of PBP1 protein in *Bacillus subtilis*. Mol. Microbiol. *68*, 1029–1046.

Cleverley, R.M., Barrett, J.R., Baslé, A., Bui, N.K., Hewitt, L., Solovyova, A., Xu, Z.Q., Daniel, R.A., Dixon, N.E., Harry, E.J., et al. (2014). Structure and function of a spectrin-like regulator of bacterial cytokinesis. Nat. Commun. *5*, 5421.

Cleverley, R.M., Rismondo, J., Lockhart-Cairns, M.P., Van Bentum, P.T., Egan, A.J.F., Vollmer, W., Halbedel, S., Baldock, C., Breukink, E., and Lewis, R.J. (2016). Subunit arrangement in GpsB, a regulator of cell wall biosynthesis. Microb. Drug Resist. *22*, 446–460.

Cole, R.M., Popkin, T.J., Boylan, R.J., and Mendelson, N.H. (1970). Ultrastructure of a temperature-sensitive rod- mutant of *Bacillus subtilis*. J Bacteriol *103*, 793–810.

Coley, J., Tarelli, E., Archibald, A.R., and Baddiley, J. (1978). Linkage between teichoic-acid and peptidoglycan in bacterial cell walls. Febs Lett. *88*, 1–9.

Cordell, S.C., and Löwe, J. (2001). Crystal structure of the bacterial cell division regulator MinD. FEBS Lett. *492*, 160–165.

D'Elia, M.A., Pereira, M.P., Chung, Y.S., Zhao, W., Chau, A., Kenney, T.J., Sulavik, M.C., Black, T.A., and Brown, E.D. (2006). Lesions in teichoic acid biosynthesis in *Staphylococcus aureus* lead to a lethal gain of function in the otherwise dispensable pathway. J Bacteriol *188*, 4183–4189.

Dajkovic, A., Lan, G., Sun, S.X., Wirtz, D., and Lutkenhaus, J. (2008). MinC spatially controls bacterial cytokinesis by antagonizing the scaffolding function of FtsZ. Curr. Biol. *18*, 235–244.

Daniel, R.A., and Errington, J. (2000). Intrinsic instability of the essential cell division protein FtsL of *Bacillus subtilis* and a role for DivlB protein in FtsL turnover. Mol. Microbiol. *36*, 278–289.

Daniel, R.A., and Errington, J. (2003). Control of cell morphogenesis in bacteria: Two distinct ways to make a rod-shaped cell. Cell *113*, 767–776.

Daniel, R.A., Williams, A.M., and Errington, J. (1996). A complex four-gene operon containing essential cell division gene *pbpB* in *Bacillus subtilis*. J. Bacteriol. *178*, 2343–2350.

Daniel, R.A., Harry, E.J., Katis, V.L., Wake, R.G., and Errington, J. (1998). Characterization of the essential cell division gene *ftsL* (*yIID*) of *Bacillus subtilis* and its role in the assembly of the division apparatus. Mol. Microbiol. *29*, 593–604.

Daniel, R.A., Harry, E.J., and Errington, J. (2000). Role of penicillin-binding protein PBP 2B in assembly and functioning of the division machinery of *Bacillus subtilis*. Mol. Microbiol. *35*, 299–311.

Daniel, R.A., Noirot-Gros, M.F., Noirot, P., and Errington, J. (2006). Multiple interactions between the transmembrane division proteins of *Bacillus subtilis* and the role of FtsL instability in divisome assembly. J. Bacteriol. *188*, 7396–7404.

Datta, P., Dasgupta, A., Singh, A.K., Mukherjee, P., Kundu, M., and Basu, J. (2006). Interaction between FtsW and penicillin-binding protein 3 (PBP3) directs PBP3 to mid-cell, controls cell septation and mediates the formation of a trimeric complex involving FtsZ, FtsW and PBP3 in mycobacteria. Mol. Microbiol. *62*, 1655–1673.

Defeu Soufo, H.J., and Graumann, P.L. (2003). Actin-like proteins MreB and Mbl from *Bacillus subtilis* are required for bipolar positioning of replication origins. Curr. Biol. *13*, 1916–1920.

Defeu Soufo, H.J., and Graumann, P.L. (2005). *Bacillus subtilis* actin-like protein MreB influences the positioning of the replication machinery and requires membrane proteins MreC/D and other actin-like proteins for proper localization. BMC Cell Biol. *6*, 1–11.

Derouaux, A., Wolf, B., Fraipont, C., Breukink, E., Nguyen-Distèche, M., and Terrak, M. (2008). The monofunctional glycosyltransferase of *Escherichia coli* localizes to the cell division site and interacts with penicillin-binding protein 3, FtsW, and FtsN. J. Bacteriol. *190*, 1831–1834.

Dmitriev, boris, ehlers, S., and Rietschel, E. (1999). Layered murein revisited: a fundamentally new concept of bacterial cell wall structure, biogenesis and function. Med Microbiol Immunol *187*, 173–181.

Dmitriev, B., Toukach, F., and Ehlers, S. (2005b). Towards a comprehensive view of the bacterial cell wall. Trends Microbiol *13*, 569–574.

Dominguez-Cuevas, P., Porcelli, I., Daniel, R.A., Errington, J., Domínguez-Cuevas, P., Porcelli, I., Daniel, R.A., and Errington, J. (2013). Differentiated roles for MreB-actin isologues and autolytic enzymes in *Bacillus subtilis* morphogenesis. Mol Microbiol *89*, 1084–1098.

Dominguez-Escobar, J., Chastanet, A., Crevenna, A.H., Fromion, V., Wedlich-Soldner, R., Carballido-Lopez, R. (2011). Processive movement of MreB-associated cell wall biosynthetic complexes in bacteria. Science *333*, 225–228.

Dörries, K., Schlueter, R., and Lalk, M. (2014). Impact of antibiotics with various target sites on the metabolome of *Staphylococcus aureus*. Antimicrob. Agents Chemother. *58*, 7151–7163.

Driks, A., and Popham, D.L. (2001). Two class A high-molecular-weight penicillin-binding proteins of *Bacillus subtilis* play redundant roles in sporulation. J. Bacteriol. *183*, 6046–6053.

Duman, R., Ishikawa, S., Celik, I., Strahl, H., Ogasawara, N., Troc, P., Löwe, J., and Hamoen, L.W. (2013). Structural and genetic analyses reveal the protein SepF as a new membrane anchor for the Z ring. Proc. Natl. Acad. Sci. *110*, E4601–E4610.

Edwards, D.H., and Errington, J. (1997). The *Bacillus subtilis* DivIVA protein targets to the division septum and controls the site specificity of cell division. Mol. Microbiol. *24*, 905–915.

Egan, A.J.F., Biboy, J., Van 't Veer, I., Breukink, E., Vollmer, W., van't Veer, I., Breukink, E., and Vollmer, W. (2015). Activities and regulation of peptidoglycan synthases. Phil. Trans. R. Soc. B *370*, 20150031.

Eiamphungporn, W., and Helmann, J.D. (2008a). The *Bacillus subtilis sigM* regulon and its contribution to cell envelope stress responses. Mol Microbiol *67*, 830–848.

Ellwood, D.C. (1970). Wall content and composition of *Bacillus subtilis* var. niger grown in a chemostat. Biochem. J. *118*, 367–373.

Ent, F.V.D., Leaver, M., Bendezu, F., Errington, J., De Boer, P., and Löwe, J. (2006). Dimeric structure of the cell shape protein MreC and its functional implications. Mol. Microbiol. *62*, 1631–1642.

van den Ent, F., and Löwe, J. (2000). Crystal structure of the cell division protein FtsA from *Thermotoga maritima*. EMBO J. *19*, 5300–5307.

Erickson, H.P., Taylor, D.W., Taylor, K.A., and Bramhill, D. (1996). Bacterial cell division protein FtsZ assembles into protofilament sheets and minirings, structural homologs of tubulin polymers. Proc. Natl. Acad. Sci. U. S. A. *93*, 519–523.

Erickson, H.P., Anderson, D.E., and Osawa, M. (2010). FtsZ in bacterial cytokinesis: cytoskeleton and force generator all in one. Microbiol. Mol. Biol. Rev. *74*, 504–528.

Errington, J. (2003). Regulation of endospore formation in *Bacillus subtilis*. Nat Rev Microbiol *1*, 117–126.

Errington, J., Daniel, R.A., and Scheffers, D.J. (2003). Cytokinesis in bacteria. Microbiol. Mol. Biol. Rev. *67*, 52–65.

Estrela, A.I., Pooley, H.M., de Lencastre, H., and Karamata, D. (1991). Genetic and biochemical characterization of *Bacillus subtilis* 168 mutants specifically blocked in the synthesis of the teichoic acid poly(3-O-beta-D-glucopyranosyl-N-acetylgalactosamine 1-phosphate): *gneA*, a new locus, is associated with UDP-N-acetylglucosamine 4-epimerase activity. J. Gen. Microbiol. *137*, 943–950.

Fabret, C., Ehrlich, S.D., and Noirot, P. (2002). A new mutation delivery system for genome-scale approaches in *Bacillus subtilis*. Mol. Microbiol. *46*, 25–36.

Fay, A., and Dworkin, J. (2009). *Bacillus subtilis* Homologs of MviN (MurJ), the putative *Escherichia coli* Lipid II Flippase, Are Not Essential for Growth. J. Bacteriol. *191*, 6020–6028.

Fedtke, I., Mader, D., Kohler, T., Moll, H., Nicholson, G., Biswas, R., Henseler, K., Götz, F., Zähringer, U., and Peschel, A. (2007). A *Staphylococcus aureus ypfP* mutant with strongly reduced lipoteichoic acid (LTA) content: LTA governs bacterial surface properties and autolysin activity. Mol. Microbiol. *65*, 1078–1091.

Feucht, A., Lucet, I., Yudkin, M.D., and Errington, J. (2001). Cytological and biochemical characterization of the FtsA cell division protein of *Bacillus subtilis*. Mol. Microbiol. *40*, 115–125.

Formstone, A., and Errington, J. (2005). A magnesium-dependent *mreB* null mutant: implications for the role of *mreB* in *Bacillus subtilis*. Mol. Microbiol. *55*, 1646–1657.

Formstone, A., Carballido-López, R., Noirot, P., Errington, J., and Scheffers, D.J. (2008). Localization and interactions of teichoic acid synthetic enzymes in *Bacillus subtilis*. J. Bacteriol. *190*, 1812–1821.

Foulquier, E., Pompeo, F., Bernadac, A., Espinosa, L., and Galinier, A. (2011). The YvcK protein is required for morphogenesis via localization of PBP1 under gluconeogenic growth conditions in *Bacillus subtilis*. Mol. Microbiol. *80*, 309–318.

Fraipont, C., Alexeeva, S., Wolf, B., Der Ploeg, R., Schloesser, M., Den Blaauwen, T., and Nguyen-Distèche, M. (2011). The integral membrane FtsW protein and peptidoglycan synthase PBP3 form a subcomplex in *Escherichia coli*. Microbiology *157*, 251–259.

Freymond, P.P., Lazarevic, V., Soldo, B., and Karamata, D. (2006). Poly(glucosyl-N-acetylgalactosamine 1-phosphate), a wall teichoic acid of *Bacillus subtilis* 168: its biosynthetic pathway and mode of attachment to peptidoglycan. Microbiology *152*, 1709–1718.

Fukushima, T., Afkham, A., Kurosawa, S.I., Tanabe, T., Yamamoto, H., and Sekiguchi, J. (2006). A new D,L-endopeptidase gene product, YojL (renamed CwlS), plays a role in cell separation with LytE and LytF in *Bacillus subtilis*. J. Bacteriol. *188*, 5541–5550.

Gaillard, J.L., Lubochinsky, B., and Rigomier, D. (1983). Specific inhibition of phosphatidate cytidylyltransferase from *Bacillus subtilis* membranes by cytidine monophosphate. Biochim Biophys Acta *753*, 372–380.

Gamba, P., Veening, J.W., Saunders, N.J., Hamoen, L.W., and Daniel, R.A. (2009). Two-step assembly dynamics of the *Bacillus subtilis* divisome. J. Bacteriol. *191*, 4186–4194.

Gamba, P., Hamoen, L.W., and Daniel, R.A. (2016). Cooperative recruitment of FtsW to the division site of *Bacillus subtilis*. Front. Microbiol. *7*, 1–9.

Garner, E.C., Bernard, R., Wang, W., Zhuang, X., Rudner, D.Z., and Mitchison, T. (2011). Coupled, circumferential motions of the cell wall synthesis machinery and MreB filaments in *B. subtilis*. Science *333*, 222–225.

Garufi, G., Hendrickx, A.P., Beeri, K., Kern, J.W., Sharma, A., Richter, S.G., Schneewind, O., and Missiakas, D. (2012). Synthesis of lipoteichoic acids in *Bacillus anthracis*. J. Bacteriol. *194*, 4312–4321.

Ghuysen, J.M., and Leyh-Bouille, M. (1970). Biochemistry of the bacterial wall peptidoglycan. FEBS symposium. *20*, 59–69.

Giebel, J.D., Carr, K.A., Anderson, E.C., and Hanna, P.C. (2009). The germination-specific lytic enzymes SleB, CwlJ1, and CwlJ2 each contribute to *Bacillus anthracis* spore germination and virulence. J. Bacteriol. 191, 5569–5576.

Ginsberg, C., Zhang, Y.H., Yuan, Y., and Walker, S. (2006). *In vitro* reconstitution of two essential steps in wall teichoic acid biosynthesis. ACS Chem Biol *1*, 25–28.

Glauner, B., and Höltje, J. V. (1990). Growth pattern of the murein sacculus of *Escherichia coli*. J. Biol. Chermistry *265*, 18988–18996.

Glauner, B., Höltje, J. V., and Schwarz, U. (1988). The composition of the murein of *Escherichia coli*. J. Biol. Chem. *263*, 10088–10095.

Goehring, N.W., and Beckwith, J. (2005). Diverse paths to midcell: assembly of the bacterial cell division machinery. Curr Biol *15*, R514-26.

Goehring, N.W., Gonzalez, M.D., and Beckwith, J. (2006). Premature targeting of cell division proteins to midcell reveals hierarchies of protein interactions involved in divisome assembly. Mol. Microbiol. *61*, 33–45.

Gram, H.C. (1884). Gram staining. Fortschritte Der Med. *2*, 185–189.

Gregory, J.A., Becker, E.C., and Pogliano, K. (2008). *Bacillus subtilis* MinC destabilizes FtsZ-rings at new cell poles and contributes to the timing of cell division. Genes Dev. *22*, 3475–3488.

Grundling, A., and Schneewind, O. (2007a). Synthesis of glycerol phosphate lipoteichoic acid in *Staphylococcus aureus*. Proc Natl Acad Sci U S A *104*, 8478–8483.

Grundling, A., and Schneewind, O. (2007b). Genes required for glycolipid synthesis and lipoteichoic acid anchoring in *Staphylococcus aureus*. J Bacteriol *189*, 2521–2530.

Gueiros-Filho, F.J., and Losick, R. (2002). A widely conserved bacterial cell division protein that promotes assembly of the tubulin-like protein FtsZ. Genes Dev. *16*, 2544–2556.

Haeusser, D.P., Schwartz, R.L., Smith, A.M., Oates, M.E., and Levin, P.A. (2004). EzrA prevents aberrant cell division by modulating assembly of the cytoskeletal protein FtsZ. Mol. Microbiol. *52*, 801–814.

Hale, C.A., and de Boer, P.A.J. (1999). Recruitment of ZipA to the septal ring of *Escherichia coli* is dependent on FtsZ and independent of FtsA. J. Bacteriol. *181*, 167–176.

Hamoen, L.W., Smits, W.K., de Jong, A., Holsappel, S., and Kuipers, O.P. (2002). Improving the predictive value of the competence transcription factor (ComK) binding site in *Bacillus subtilis* using a genomic approach. Nucleic Acids Res. *30*, 5517–5528.

Hamoen, L.W., Meile, J.C., De Jong, W., Noirot, P., and Errington, J. (2006). SepF, a novel FtsZ-interacting protein required for a late step in cell division. Mol. Microbiol. *59*, 989–999.

Harry, E.J., and Wake, R.G. (1989). Cloning and expression of a *Bacillus subtilis* division initiation gene for which a homolog has not been identified in another organism. J. Bacteriol. *171*, 6835–6839.

Hashimoto, M., Ooiwa, S., and Sekiguchi, J. (2012). Synthetic lethality of the *lytE cwlO* genotype in *Bacillus subtilis* is caused by lack of D, L-endopeptidase activity at the lateral cell wall. J. Bacteriol. *194*, 796–803.

Hashimoto, M., Seki, T., Matsuoka, S., Hara, H., Asai, K., Sadaie, Y., and Matsumoto, K. (2013). Induction of extracytoplasmic function sigma factors in *Bacillus subtilis* cells with defects in lipoteichoic acid synthesis. Microbiology *159*, 23–35.

Hayhurst, E.J., Kailas, L., Hobbs, J.K., and Foster, S.J. (2008). Cell wall peptidoglycan architecture in *Bacillus subtilis*. Proc. Natl. Acad. Sci. U. S. A. *105*, 14603–14608.

Van Heijenoort, J. (2001). Formation of the glycan chains in the synthesis of bacterial peptidoglycan. Glycobiology 11, 25–36.

Henriques, A.O., Glaser, P., Piggot, P.J., and Moran, C.P. (1998). Control of cell shape and elongation by the *rodA* gene in *Bacillus subtilis*. Mol. Microbiol. *28*, 235–247.

Higgins, D., and Dworkin, J. (2012). Recent progress in *Bacillus subtilis* sporulation. FEMS Microbiol. Rev. *36*, 131–148.

Hill, M. (1984). Purification and properties of autolytic endo-1-*N*-acetylglucosaminidase and the *N*-Acetylmuramyl-L-alanine amidase from *Bacillus subtilis* Strain 168. J. Gen. Microbiol. *130*, 2395–2402.

Höltje, J. V (1998). Growth of the stress-bearing and shape-maintaining murein sacculus of *Escherichia coli*. Microbiol Mol Biol Rev *62*, 181–203.

Höltje, J. V., and Tomasz, A. (1975). Lipoteichoic acid: a specific inhibitor of autolysin activity in *Pneumococcus*. Proc. Natl. Acad. Sci. *72*, 1690–1694.

Höltje, J. V., Mirelman, D., Sharon, N., and Schwarz, U. (1975). Novel type of murein transglycosylase in *Escherichia coli*. J. Bacteriol. *124*, 1067–1076.

Huang, W.Z., Wang, J.J., Chen, H.J., Chen, J.T., and Shaw, G.C. (2013). The heat-inducible essential response regulator WalR positively regulates transcription of *sigI*, *mreBH* and *lytE* in *Bacillus subtilis* under heat stress. Res. Microbiol. *164*, 998–1008.

Ikeda, M., Sato, T., Wachi, M., Jung, H.K., Ishino, F., Kobayashi, Y., and Matsuhashi, M. (1989). Structural similarity among *Escherichia coli* FtsW and RodA proteins and *Bacillus subtilis* SpoVE protein, which function in cell division, cell elongation, and spore formation, respectively. J. Bacteriol. *171*, 6375–6378.

Ishikawa, S., Kawai, Y., Hiramatsu, K., Kuwano, M., and Ogasawara, N. (2006). A new FtsZ-interacting protein, YlmF, complements the activity of FtsA during progression of cell division in *Bacillus subtilis*. Mol. Microbiol. 60, 1364–1380.

Jerga, A., Lu, Y.J., Schujman, G.E., de Mendoza, D., and Rock, C.O. (2007). Identification of a soluble diacylglycerol kinase required for lipoteichoic acid production in *Bacillus subtilis*. J Biol Chem *282*, 21738–21745.

Jervis, A.J., Thackray, P.D., Houston, C.W., Horsburgh, M.J., and Moir, A. (2007). SigM-responsive genes of *Bacillus subtilis* and their promoters. J. Bacteriol. *189*, 4534–4538.

Jones, L.J.F., Carballido-López, R., Errington, J., Carballido-Ló Pez, R., Errington, J., Carballido-Lopez, R., and Errington, J. (2001). Control of cell shape in bacteria: helical, actin-like filaments in *Bacillus subtilis*. Cell *104*, 913–922.

Jorasch, P., Wolter, F.P., Zahringer, U., and Heinz, E. (1998). A UDP glucosyltransferase from *Bacillus subtilis* successively transfers up to four glucose residues to 1,2-diacylglycerol: expression of *ypfP* in *Escherichia coli* and structural analysis of its reaction products. Mol Microbiol *29*, 419–430.

Kasahara, J., Kiriyama, Y., Miyashita, M., Kondo, T., Yamada, T., Yazawa, K., Yoshikawa, R., and Yamamoto, H. (2016). Teichoic acid polymers affect expression and localization of DL-endopeptidase LytE required for lateral cell wall hydrolysis in *Bacillus subtilis*. J. Bacteriol. *198*, 1585–1594.

Katis, V.L., Harry, E.J., and Wake, R.G. (1997). The *Bacillus subtilis* division protein DivIC is a highly abundant membrane-bound protein that localizes to the division site. Mol. Microbiol. *26*, 1047–1055.

Kawai, F., Hara, H., Takamatsu, H., Watabe, K., and Matsumoto, K. (2006). Cardiolipin enrichment in spore membranes and its involvement in germination of *Bacillus subtilis* Marburg. Genes Genet Syst *81*, 69–76.

Kawai, Y., Asai, K., and Errington, J. (2009a). Partial functional redundancy of MreB isoforms, MreB, Mbl and MreBH, in cell morphogenesis of *Bacillus subtilis*. Mol Microbiol *73*, 719–731.

Kawai, Y., Daniel, R.A., and Errington, J. (2009b). Regulation of cell wall morphogenesis in *Bacillus subtilis* by recruitment of PBP1 to the MreB helix. Mol. Microbiol. *71*, 1131–1144.

Kawai, Y., Marles-Wright, J., Cleverley, R.M., Emmins, R., Ishikawa, S., Kuwano, M., Heinz, N., Bui, N.K., Hoyland, C.N., Ogasawara, N., et al. (2011). A widespread family of bacterial cell wall assembly proteins. EMBO J. *30*, 4931–4941.

Kiriyama, Y., Yazawa, K., Tanaka, T., Yoshikawa, R., Yamane, H., Hashimoto, M., Sekiguchi, J., Yamamoto, H., and Hiroki Yamamoto, C. (2014). Localization and expression of the *Bacillus subtilis* DL-endopeptidase LytF are influenced by mutations in LTA synthases and glycolipid anchor synthetic enzymes. Microbiology *160*, 2639–2649.

Kleijn, R.J., Buescher, J.M., Le Chat, L., Jules, M., Aymerich, S., and Sauer, U. (2010). Metabolic fluxes during strong carbon catabolite repression by Malate in *Bacillus subtilis*. J. Biol. Chem. *285*, 1587–1596.

Koch, A.L., and Doyle, R.J. (1985). Inside-to-outside growth and turnover of the wall of gram-positive rods. J. Theor. Biol. *117*, 137–157.

Król, E., van Kessel, S.P., van Bezouwen, L.S., Kumar, N., Boekema, E.J., and Scheffers, D.J. (2012). *Bacillus subtilis* SepF binds to the C-terminus of FtsZ. PLoS One *7*, e43293.

Kruse, T., Mùller-Jensen, J., Lùbner-Olesen, A., and Gerdes, K. (2003). Dysfunctional MreB inhibits chromosome segregation in *Escherichia coli*. EMBO J. *22*, 5283–5292.

Kumazawa, T., Masayama, A., Fukuoka, S., Makino, S., Yoshimura, T., and Moriyama, R. (2007). Mode of action of a germination-specific cortex-lytic enzyme, SleC, of *Clostridium perfringens* S40. Biosci. Biotechnol. Biochem *71*, 884–892.

Land, A.D., Luo, Q., and Levin, P.A. (2014). Functional domain analysis of the cell division inhibitor EzrA. PLoS One *9*, 1–14.

Lazarevic, V., and Karamata, D. (1995). The *tagGH* operon of *Bacillus subtilis* 168 encodes a two-component ABC transporter involved in the metabolism of two wall teichoic acids. Mol Microbiol *16*, 345–355.

Lazarevic, V., Margot, P., Soldo, B., and Karamata, D. (1992). Sequencing and analysis of the *Bacillus subtilis lytRABC* divergon: a regulatory unit encompassing the structural genes of the N-acetylmuramoyl-L-alanine amidase and its modifier. J. Gen. Microbiol. *138*, 1949–1961.

Lazarevic, V., Soldo, B., Médico, N., Pooley, H., Bron, S., and Karamata, D. (2005). *Bacillus subtilis* alpha-phosphoglucomutase is required for normal cell morphology and biofilm formation. Appl. Environ. Microbiol. *71*, 39–45.

Leaver, M., and Errington, J. (2005). Roles for MreC and MreD proteins in helical growth of the cylindrical cell wall in *Bacillus subtilis*. Mol. Microbiol. 57, 1196–1209.

Lebar, M.D., May, J.M., Meeske, A.J., Leiman, S.A., Lupoli, T.J., Tsukamoto, H., Losick, R., Rudner, D.Z., Walker, S., and Kahne, D. (2014). Reconstitution of peptidoglycan cross-Linking leads to improved fluorescent probes of cell wall synthesis. J. Am. Chem. Soc. *136*, 10874–10877.

Lee, T.K., and Huang, K.C. (2013). The role of hydrolases in bacterial cell-wall growth. Curr. Opin. Microbiol. *16*, 760–766.

Lenarcic, R., Halbedel, S., Visser, L., Shaw, M., Wu, L.J., Errington, J., Marenduzzo, D., and Hamoen, L.W. (2009). Localisation of DivIVA by targeting to negatively curved membranes. EMBO J. *28*, 2272–2282.

Levin, P.A., Kurtser, I.G., and Grossman, A.D. (1999). Identification and characterization of a negative regulator of FtsZ ring formation in *Bacillus subtilis*. Proc. Natl. Acad. Sci. U. S. A. *96*, 9642–9647.

Lewis, P.J., and Marston, A.L. (1999). GFP vectors for controlled expression and dual labelling of protein fusions in *Bacillus subtilis*. Gene *227*, 101–110.

Li, Y., Butzin, X.Y., Davis, A., Setlow, B., Korza, G., Üstok, F.I., Christie, G., Setlow, P., and Hao, B. (2013). Activity and regulation of various forms of CwlJ, SleB, and YpeB proteins in degrading cortex peptidoglycan of spores of bacillus species *in vitro* and during spore germination. J. Bacteriol. *195*, 2530–2540.

Li, Z., Trimble, M.J., Brun, Y. V, and Jensen, G.J. (2007). The structure of FtsZ filaments in vivo suggests a force‐generating role in cell division. EMBO J. *26*, 4694‐4708.

Liebeke, M., Pöther, D.C., Van Duy, N., Albrecht, D., Becher, D., Hochgräfe, F., Lalk, M., Hecker, M., and Antelmann, H. (2008). Depletion of thiol-containing proteins in response to quinones in *Bacillus subtilis*. Mol. Microbiol. *69*, 1513–1529.

Liebeke, M., Dörries, K., Zühlke, D., Bernhardt, J., Fuchs, S., Pané-Farré, J., Engelmann, S., Völker, U., Bode, R., Dandekar, T., et al. (2011). A metabolomics and proteomics study of the adaptation of *Staphylococcus aureus* to glucose starvation. Mol.Biosyst. *7*, 1241–1253.

Lim, D., and Strynadka, N.C.J. (2002). Structural basis for the beta lactam resistance of PBP2a from methicillin-resistant *Staphylococcus aureus*. Nat. Struct. Biol. *9*, 870–876.

Lovering, A.L., Safadi, S.S., and Strynadka, N.C.J. (2012). Structural perspective of peptidoglycan biosynthesis and assembly. Annu. Rev. Biochem. *81*, 451–478.

Low, H.H., Moncrieffe, M.C., and Löwe, J. (2004). The crystal structure of ZapA and its modulation of FtsZ polymerisation. J. Mol. Biol. *341*, 839–852.

Löwe, J., and Amos, L.A. (1999). Tubulin-like protofilaments in Ca^{2+}-induced FtsZ sheets. EMBO J. *18*, 2364–2371.

Margot, P., and Karamata, D. (1992). Identification of the structural genes for N-acetylmuramoyl-L-alanine amidase and its modifier in *Bacillus subtilis* 168: inactivation of these genes by insertional mutagenesis has no effect on growth or cell separation. Mol. Gen. Genet. *232*, 359–366.

Margot, P., Wahlen, M., Gholamhuseinian, A., Piggot, P., and Karamata, D. (1998). The *lytE* gene of *Bacillus subtilis* 168 encodes a cell wall hydrolase. J. Bacteriol. *180*, 749–752.

Margot, P., Pagni, M., and Karamata, D. (1999). *Bacillus subtilis* 168 gene *lytF* encodes a 7-D-glutamate-meso-diaminopimelate muropeptidase expressed by the alternative vegetative sigma factor, σ^D. Microbiology *145*, 57–65.

Marston, A.L., and Errington, J. (1999). Selection of the midcell division site in *Bacillus subtilis* through MinD-dependent polar localization and activation of MinC. Mol Microbiol *33*, 84–96.

Matias, V.R.F., and Beveridge, T.J. (2005). Cryo-electron microscopy reveals native polymeric cell wall structure in *Bacillus subtilis* 168 and the existence of a periplasmic space. Mol. Microbiol. *56*, 240–251.

Matias, V.R.F., and Beveridge, T.J. (2008). Lipoteichoic acid is a major component of the *Bacillus subtilis* periplasm. J. Bacteriol. *190*, 7414–7418.

Matsuhashi, M., Song, M.D., Ishino, F., Wachi, M., Doi, M., Inoue, M., Ubukata, K., Yamashita, N., and Konno, M. (1986). Molecular cloning of the gene of a penicillin-binding protein supposed to cause high resistance to beta-lactam antibiotics in *Staphylococcus aureus*. J. Bacteriol. *167*, 975–980.

Matsuoka, S., Chiba, M., Tanimura, Y., Hashimoto, M., Hara, H., and Matsumoto, K. (2011a). Abnormal morphology of *Bacillus subtilis ugtP* mutant cells lacking glucolipids. Genes Genet. Syst. *86*, 295–304.

Matsuoka, S., Hashimoto, M., Kamiya, Y., Miyazawa, T., Ishikawa, K., Hara, H., and Matsumoto, K. (2011b). The *Bacillus subtilis* essential gene *dgkB* is dispensable in mutants with defective lipoteichoic acid synthesis. Genes Genet. Syst. *86*, 365–376.

Mauel, C., Young, M., and Karamata, D. (1991). Genes concerned with synthesis of poly(glycerol phosphate), the essential teichoic acid in *Bacillus subtilis* strain 168, are organized in two divergent transcription units. J Gen Microbiol *137*, 929–941.

McPherson, D.C., and Popham, D.L. (2003). Peptidoglycan synthesis in the absence of class A penicillin-binding proteins in *Bacillus subtilis*. J. Bacteriol. *185*, 1423–1431.

Meeske, A.J., Riley, E.P., Robins, W.P., Uehara, T., Mekalanos, J.J., Kahne, D., Walker, S., Kruse, A.C., Bernhardt, T.G., and Rudner, D.Z. (2016). SEDS proteins are a widespread family of bacterial cell wall polymerases. Nature *537*, 634–638.

Meisner, J., Montero Llopis, P., Sham, L.T., Garner, E., Bernhardt, T.G., and Rudner, D.Z. (2013). FtsEX is required for CwlO peptidoglycan hydrolase activity during cell wall elongation in *Bacillus subtilis*. Mol. Microbiol. *89*, 1069–1083.

Mercer, K.L.N., and Weiss, D.S. (2002). The *Escherichia coli* cell division protein FtsW is required to recruit its cognate transpeptidase, FtsI (PBP3), to the division site. J. Bacteriol. *184*, 904–912.

Miyao, A., Yoshimura, A., Sato, T., Yamamoto, T., Theeragool, G., and Kobayashi, Y. (1992). Sequence of the *Bacillus subtilis* homolog of the *Escherichia coli* cell-division gene *murG*. Gene *118*, 147–148.

Miyazaki, C., Kuroda, M., Ohta, A., and Shibuya, I. (1985). Genetic manipulation of membrane phospholipid composition in *Escherichia coli*: *pgsA* mutants defective in phosphatidylglycerol synthesis. Proc Natl Acad Sci U. S. A. *82*, 7530–7534.

Mohammadi, T., van Dam, V., Sijbrandi, R., Vernet, T., Zapun, A., Bouhss, A., Diepeveen-de Bruin, M., Nguyen-Disteche, M., de Kruijff, B., and Breukink, E. (2011). Identification of FtsW as a transporter of lipid-linked cell wall precursors across the membrane. EMBO J. *30*, 1425–1432.

Mohammadi, T., Sijbrandi, R., Lutters, M., Verheul, J., Martin, N.I., Den Blaauwen, T., De Kruijff, B., and Breukink, E. (2014). Specificity of the transport of lipid II by FtsW in *Escherichia coli*. J. Biol. Chem. *289*, 14707–14718.

Morimoto, T., Loh, P.C., Hirai, T., Asai, K., Konayashi, K., Moriya, S., and Ogasawara, N. (2002). Six GTP-binding proteins of the Era/Obg family are essential for cell growth in *Bacillus subtilis*. Microbiology *148*, 3539–3552.

Muchová, K., Chromiková, Z., and Barák, I. (2013). Control of *Bacillus subtilis* cell shape by RodZ. Environ. Microbiol. *15*, 3259–3271.

Mukherjee, A., and Lutkenhaus, J. (1994). Guanine nucleotide-dependent assembly of FtsZ into filaments. J. Bacteriol. *176*, 2754–2758.

Mukherjee, A., and Lutkenhaus, J. (1998). Dynamic assembly of FtsZ regulated by GTP hydrolysis. EMBO J. *17*, 462–469.

Mukherjee, A., and Lutkenhaus, J. (1999). Analysis of FtsZ assembly by light scattering and determination of the role of divalent metal cations. J Bacteriol *181*, 823–832.

Mukherjee, A., Dai, K., and Lutkenhaus, J. (1993). *Escherichia coli* cell division protein FtsZ is a guanine nucleotide binding protein. Proc. Natl. Acad. Sci. U. S. A. *90*, 1053–1057.

Murray, T., Popham, D.L., and Setlow, P. (1996). Identification and characterization of *pbpC*, the gene encoding *Bacillus subtilis* penicillin-binding protein 3. J. Bacteriol. *178*, 6001–6005.

Murray, T., Popham, D.L., Pearson, C.B., Hand, A.R., and Setlow, P. (1998a). Analysis of outgrowth of *Bacillus subtilis* spores lacking penicillin-binding protein 2a. J. Bacteriol. *180*, 6493–6502.

Murray, T., Popham, D.L., and Setlow, P. (1998b). *Bacillus subtilis* cells lacking penicillin-binding protein 1 require increased levels of divalent cations for growth. J. Bacteriol. *180*, 4555–4563.

Neuhaus, F.C., and Baddiley, J. (2003). A continuum of anionic charge: structures and functions of D-alanyl-teichoic acids in gram-positive bacteria. Microbiol Mol Biol Rev *67*, 686–723.

Nicolas, P., Mäder, U., Dervyn, E., Rochat, T., Leduc, A., Pigeonneau, N., Bidnenko, E., Marchadier, E., Hoebeke, M., Aymerich, S., et al. (2012). Condition-dependent transcriptome reveals high-level regulatory architecture in *Bacillus subtilis*. Science *335*, 1103–1106.

Nishibori, A., Kusaka, J., Hara, H., Umeda, M., and Matsumoto, K. (2005). Phosphatidylethanolamine domains and localization of phospholipid synthases in *Bacillus subtilis* membranes. J. Bacteriol. *187*, 2163–2174.

Offant, J., Terrak, M., Derouaux, A., Breukink, E., Nguyen-Distèche, M., Zapun, A., and Vernet, T. (2010). Optimization of conditions for the glycosyltransferase activity of penicillin-binding protein 1a from *Thermotoga maritima*. FEBS J. *277*, 4290–4298.

Ohnishi, R., Ishikawa, S., and Sekiguchi, J. (1999). Peptidoglycan hydrolase *lytF* plays a role in cell separation with *cwlF* during vegetative growth of *Bacillus subtilis*. J. Bacteriol. *181*, 3178–3184.

Oliva, M.A., Cordell, S.C., and Löwe, J. (2004). Structural insights into FtsZ protofilament formation. Nat. Struct. Mol. Biol. *11*, 1243–1250.

Osawa, M., and Erickson, H.P. (2013). Liposome division by a simple bacterial division machinery. Proc. Natl. Acad. Sci. *110*, 11000–11004.

Ouzounov, N., Nguyen, J.P., Bratton, B.P., Jacobowitz, D., Gitai, Z., and Shaevitz, J.W. (2016). MreB orientation correlates with cell diameter in *Escherichia coli*. Biophys. J. *111*, 1035–1043.

Patrick, J.E., and Kearns, D.B. (2008). MinJ (YvjD) is a topological determinant of cell division in *Bacillus subtilis*. Mol. Microbiol. *70*, 1166–1179.

Pedersen, L.B., Murray, T., Popham, D.L., and Setlow, P. (1998). Characterization of *dacC*, which encodes a new low-molecular weight penicillin-binding protein in *Bacillus subtilis*. J. Bacteriol. *180*, 4967–4973.

Pedersen, L.B., Angert, E.R., and Setlow, P. (1999). Septal localization of penicillin-binding protein 1 in *Bacillus subtilis*. J. Bacteriol. *181*, 3201–3211.

Percy, M.G., and Gründling, A. (2014). Lipoteichoic acid synthesis and function in Gram-positive bacteria. Annu. Rev. Microbiol. *68*, 81–100.

Perego, M., Glaser, P., Minutello, A., Strauch, M.A., Leopold, K., and Fischer, W. (1995). Incorporation of D-alanine into lipoteichoic acid and wall teichoic-acid in *Bacillus subtilis* - identification of genes and regulation. J. Biol. Chem. *270*, 15598–15606.

Perlstein, D.L., Zhang, Y., Wang, T.-S., Kahne, D.E., and Walker, S. (2007). The direction of glycan chain elongation by peptidoglycan glycosyltransferases. J. Am. Chem. Soc. *129*, 12674–12675.

Petersen, T.N., Brunak, S., von Heijne, G., and Nielsen, H. (2011). SignalP 4.0: discriminating signal peptides from transmembrane regions. Nat. Methods *8*, 785–786.

Popham, D.L., and Setlow, P. (1995). Cloning, nucleotide sequence, and mutagenesis of the *Bacillus subtilis ponA* operon, which codes for penicillin-binding protein (PBP) 1 and a PBP-related factor. J. Bacteriol. *177*, 326–335.

Popham, D.L., and Setlow, P. (1996). Phenotypes of *Bacillus subtilis* mutants lacking multiple class A high-molecular-weight penicillin-binding proteins. J Bacteriol *178*, 2079–2085.

Popham, D.L., and Young, K.D. (2003). Role of penicillin-binding proteins in bacterial cell morphogenesis. Curr. Opin. Microbiol. *6*, 594–599.

Potluri, L., Karczmarek, A., Verheul, J., Piette, A., Wilkin, J.M., Werth, N., Banzhaf, M., Vollmer, W., Young, K.D., Nguyen-Distèche, M., et al. (2010). Septal and lateral wall localization of PBP5, the major D,D-carboxypeptidase of *Escherichia coli*, requires substrate recognition and membrane attachment. Mol. Microbiol. *77*, 300–323.

Price, K.D., Roels, S., and Losick, R. (1997). A *Bacillus subtilis* gene encoding a protein similar to nucleotide sugar transferases influences cell shape and viability. J. Bacteriol. *179*, 4959–4961.

Quay, D.H.X., Cole, A.R., Cryar, A., Thalassinos, K., Williams, M. a., Bhakta, S., and Keep, N.H. (2015). Structure of the stationary phase survival protein YuiC from *B. subtilis*. BMC Struct. Biol. *15*, 1–14.

RayChaudhuri, D., and Park, J.T. (1992). *Escherichia coli* cell-division gene *ftsZ* encodes a novel GTP-binding protein. Nature *359*, 251–254.

Reeve, J.N., Mendelson, N.H., Coyne, S.I., Hallock, L.L., and Cole, R.M. (1973). Minicells of *Bacillus subtilis*. J. Bacteriol. *114*, 860–873.

Reichmann, N.T., Piçarra Cassona, C., Monteiro, J.M., Bottomley, A.L., Corrigan, R.M., Foster, S.J., Pinho, M.G., and Gründling, A. (2014). Differential localization of LTA synthesis proteins and their interaction with the cell division machinery in *Staphylococcus aureus*. Mol. Microbiol. *92*, 273–286.

Reith, J., and Mayer, C. (2011). Peptidoglycan turnover and recycling in Gram-positive bacteria. Appl Microbiol Biotechnol *92*, 1–11.

Richardson, T.T., Harran, O., and Murray, H. (2016). The bacterial DnaA-trio replication origin element specifies single-stranded DNA initiator binding. Nature. *534*, 412-416.

Rismondo, J., Cleverley, R.M., Lane, H. V, Großhennig, S., Steglich, A., Möller, L., Mannala, G.K., Hain, T., Lewis, R.J., and Halbedel, S. (2016). Structure of the bacterial cell division determinant GpsB and its interaction with penicillin-binding proteins. Mol. Microbiol. *99*, 978–998.

Robson, S.A., and King, G.F. (2006). Domain architecture and structure of the bacterial cell division protein DivIB. Proc. Natl. Acad. Sci. U. S. A. *103*, 6700–6705.

Rodrigues, C.D.A., and Harry, E.J. (2012). The Min system and nucleoid occlusion are not required for identifying the division site in *Bacillus subtilis* but ensure its efficient utilization. Plos Genet. *8*, 1–20.

Romeis, T., and Höltje, J.V. (1994). Specific interaction of penicillin-binding proteins 3 and 7/8 with soluble lytic transglycosylase in *Escherichia coli*. J. Biol. Chem. *269*, 21603–21607.

Rowland, S.L., Katis, V.L., Partridge, S.R., and Wake, R.G. (1997). DivIB, FtsZ and cell division in *Bacillus subtilis*. Mol Microbiol *23*, 295–302.

Ruiz, N. (2008). Bioinformatics identification of MurJ (MviN) as the peptidoglycan lipid II flippase in *Escherichia coli*. Proc. Natl. Acad. Sci. U. S. A. *105*, 15553–15557.

Salzberg, L.I., and Helmann, J.D. (2008). Phenotypic and transcriptomic characterization of *Bacillus subtilis* mutants with grossly altered membrane composition. J. Bacteriol. *190*, 7797–7807.

Salzberg, L.I., Powell, L., Hokamp, K., Botella, E., Noone, D., and Devine, K.M. (2013). The WalRK (YycFG) and SigI RsgI regulators cooperate to control CwlO and LytE expression in exponentially growing and stressed Bacillus subtilis cells. Mol. Microbiol. *87*, 180–195.

Scheffers, D.J. (2008). The effect of MinC on FtsZ polymerization is pH dependent and can be counteracted by ZapA. FEBS Lett. *582*, 2601–2608.

Scheffers, D.J., and Errington, J. (2004). PBP1 is a component of the *Bacillus subtilis* cell division machinery. J. Bacteriol. *186*, 5153–5156.

Scheffers, D.J., De Wit, J.G., Den Blaauwen, T., and Driessen, A.J.M. (2002). GTP hydrolysis of cell division protein FtsZ: Evidence that the active site is formed by the association of monomers. Biochemistry *41*, 521–529.

Scheffers, D.J., Jones, L.J.F., and Errington, J. (2004). Several distinct localization patterns for penicillin-binding proteins in *Bacillus subtilis*. Mol. Microbiol. *51*, 749–764.

Schertzer, J.W., and Brown, E.D. (2003). Purified, recombinant TagF protein from *Bacillus subtilis* 168 catalyzes the polymerization of glycerol phosphate onto a membrane acceptor *in vitro*. J. Biol. Chem. *278*, 18002–18007.

Schirner, K., and Errington, J. (2009). The cell wall regulator σI specifically suppresses the lethal phenotype of *mbl* mutants in *Bacillus subtilis*. J. Bacteriol. *191*, 1404–1413.

Schirner, K., Marles-Wright, J., Lewis, R.J., and Errington, J. (2009). Distinct and essential morphogenic functions for wall- and lipo-teichoic acids in *Bacillus subtilis*. EMBO J. *28*, 830–842.

Schirner, K., Eun, Y.J., Dion, M., Luo, Y., Helmann, J.D., Garner, E.C., and Walker, S. (2014). Lipid-linked cell wall precursors regulate membrane association of bacterial actin MreB. Nat. Chem. Biol. *11*, 38–45.

Schneewind, O., and Missiakas, D. (2014). Lipoteichoic acids, phosphate-containing polymers in the envelope of Gram-positive bacteria. J Bacteriol *196*, 1133–1142.

Schneider, C. A., Rasband, W.S., and Eliceiri, K.W. (2012). NIH Image to ImageJ: 25 years of image analysis. Nat. Methods *9*, 671–675.

Schwartz, B., Markwalder, J.A., Seitz, S.P., Wang, Y., and Stein, R.L. (2002). A kinetic characterization of the glycosyltransferase activity of *Escherichia coli* PBP1b and development of a continuous fluorescence assay. Biochemistry *41*, 12552–12561.

Seki, T., Mineshima, R., Hashimoto, M., Matsumoto, K., Hara, H., and Matsuoka, S. (2015). Repression of the activities of two extracytoplasmic function σ factors, σM and σV, of *Bacillus subtilis* by glucolipids in *Escherichia coli* cells. Genes Genet. Syst *90*, 109–114.

Sham, L.T., Butler, E.K., Lebar, M.D., Kahne, D., Bernhardt, T.G., and Ruiz, N. (2014). MurJ is the flippase of lipid-linked precursors for peptidoglycan biogenesis. Science. *345*, 220–222.

Shiomi, D., and Margolin, W. (2007). Dimerization or oligomerization of the actin-like FtsA protein enhances the integrity of the cytokinetic Z ring. Mol. Microbiol. *66*, 1396–1415.

Sieger, B., Schubert, K., Donovan, C., and Bramkamp, M. (2013). The lipid II flippase RodA determines morphology and growth in *Corynebacterium glutamicum*. Mol Microbiol *90*, 966–982.

Singh, J.K., Makde, R.D., Kumar, V., and Panda, D. (2007). A membrane protein, EzrA, regulates assembly dynamics of FtsZ by interacting with the C-terminal tail of FtsZ. Biochemistry *46*, 11013–11022.

Singh, J.K., Makde, R.D., Kumar, V., and Panda, D. (2008). SepF increases the assembly and bundling of FtsZ polymers and stabilizes FtsZ protofilaments by binding along its length. J. Biol. Chem. *283*, 31116–31124.

Singh, P., Makde, R.D., Ghosh, S., Asthana, J., Kumar, V., and Panda, D. (2013). Assembly of *Bacillus subtilis* FtsA: Effects of pH, ionic strength and nucleotides on FtsA assembly. Int. J. Biol. Macromol. *52*, 170–176.

Smith, T.J., and Foster, S.J. (1995). Characterization of the involvement of two compensatory autolysins in mother cell lysis during sporulation of *Bacillus subtilis* 168. J. Bacteriol. *177*, 3855–3862.

Smith, T.J., Blackman, S.A., and Foster, S.J. (2000). Autolysins of *Bacillus subtilis*: Multiple enzymes with multiple functions. Microbiology *146*, 249–262.

Smith, T.J., Blackman, S.A., and Foster, S.J. (1996). Peptidoglycan hydrolases of *Bacillus subtilis* 168. Microb. Drug Resist. *2*, 113–118.

Soldo, B., Lazarevic, V., and Karamata, D. (2002). TagO is involved in the synthesis of all anionic cell-wall polymers in *Bacillus subtilis* 168. Microbiology. *148*, 2079–2087.

Sonnhammer, E.L., von Heijne, G., and Krogh, A. (1998). A hidden Markov model for predicting transmembrane helices in protein sequences. Proc. Int. Conf. Intell. Syst. Mol. Biol. *6*, 175–182.

Stricker, J., Maddox, P., Salmon, E.D., and Erickson, H.P. (2002). Rapid assembly dynamics of the *Escherichia coli* FtsZ-ring demonstrated by fluorescence recovery after photobleaching. Proc. Natl. Acad. Sci. U. S. A. *99*, 3171–3175.

Sudiarta, I.P., Fukushima, T., and Sekiguchi, J. (2010). *Bacillus subtilis* CwlQ (previous YjbJ) is a bifunctional enzyme exhibiting muramidase and soluble-lytic transglycosylase activities. Biochem. Biophys. Res. Commun. *398*, 606–612.

Szeto, T.H., Rowland, S.L., Habrukowich, C.L., and King, G.F. (2003). The MinD membrane targeting sequence is a transplantable lipid-binding helix. J. Biol. Chem. *278*, 40050–40056.

Tavares, J.R., De Souza, R.F., Meira, G.L.S., and Gueiros-Filho, F.J. (2008). Cytological characterization of YpsB, a novel component of the *Bacillus subtilis* divisome. J. Bacteriol. *190*, 7096–7107.

van Teeffelen, S., Wang, S., Furchtgott, L., Huang, K.C., Wingreen, N.S., Shaevitz, J.W., and Gitai, Z. (2011). The bacterial actin MreB rotates, and rotation depends on cell-wall assembly. Proc Natl Acad Sci U. S. A. *108*, 15822–15827.

Thompson, L.S., Beech, P.L., Real, G., Henriques, A.O., and Harry, E.J. (2006). Requirement for the cell division protein DivIB in polar cell division and engulfment during sporulation in *Bacillus subtilis*. J. Bacteriol. *188*, 7677–7685.

Todd, J.A., Roberts, A.N., Johnstone, K., Piggot, P.J., Winter, G., and Ellar, D.J. (1986). Reduced heat resistance of mutant spores after cloning and mutagenesis of the *Bacillus subtilis* gene encoding penicillin-binding protein 5. J. Bacteriol. *167*, 257–264.

Trip, E.N., and Scheffers, D.J. (2015). A 1 MDa protein complex containing critical components of the *Escherichia coli* divisome. Sci. Rep. *5*, 1–10.

Tseng, C.L., and Shaw, G.C. (2008). Genetic evidence for the actin homolog gene *mreBH* and the bacitracin resistance gene *bcrC* as targets of the alternative sigma factor SigI of *Bacillus subtilis*. J Bacteriol *190*, 1561–1567.

Tseng, C.L.L., Chen, J.T.T., Lin, J.H.H., Huang, W.Z.Z., and Shaw, G.C.C. (2011). Genetic evidence for involvement of the alternative sigma factor SigI in controlling expression of the cell wall hydrolase gene *lytE* and contribution of LytE to heat survival of *Bacillus subtilis*. Arch. Microbiol. *193*, 677–685.

Tsui, H.C.T.C.T., Zheng, J.J., Magallon, A.N., Ryan, J.D., Yunck, R., Rued, B.E., Bernhardt, T.G., and Winkler, M.E. (2016). Suppression of a deletion mutation in the gene encoding essential PBP2b reveals a new lytic transglycosylase involved in peripheral peptidoglycan synthesis in *Streptococcus pneumoniae* D39. Mol. Microbiol. *100*, 1039–1065.

Vagner, V., Dervyn, E., and Ehrlich, S.D. (1998). A vector for systematic gene inactivation in *Bacillus subtilis*. Microbiology *144*, 3097–3104.

Varley, A.W., and Stewart, G.C. (1992). The *divIVB* region of the *Bacillus subtilis* chromosome encodes homologs of *Escherichia coli* septum placement (MinCD) and cell shape (MreBCD) determinants. J. Bacteriol. *174*, 6729–6742.

Veening, J.W., Kuipers, O.P., Brul, S., Hellingwerf, K.J., and Kort, R. (2006). Effects of phosphorelay perturbations on architecture, sporulation, and spore resistance in biofilms of *Bacillus subtilis*. J. Bacteriol. *188*, 3099–3109.

Vollmer, W. (2008). Structural variation in the glycan strands of bacterial peptidoglycan. FEMS Microbiol. Rev. *32*, 287–306.

Vollmer, W. (2012). Bacterial growth does require peptidoglycan hydrolases. Mol. Microbiol. *86*, 1031–1035.

Vollmer, W., and Seligman, S.J. (2010). Architecture of peptidoglycan: more data and more models. Trends Microbiol. *18*, 59–66.

Vollmer, W., Von Rechenberg, M., and Höltje, J.V. (1999). Demonstration of molecular interactions between the murein polymerase PBP1B, the lytic transglycosylase MltA, and the scaffolding protein MipA of *Escherichia coli*. J. Biol. Chem. *274*, 6726–6734.

Vollmer, W., Blanot, D., and De Pedro, M.A. (2008a). Peptidoglycan structure and architecture. FEMS Microbiol. Rev. *32*, 149–167.

Vollmer, W., Joris, B., Charlier, P., and Foster, S. (2008b). Bacterial peptidoglycan (murein) hydrolases. FEMS Microbiol. Rev. *32*, 259–286.

Wadenpohl, I., and Bramkamp, M. (2010). DivIC stabilizes FtsL against RasP cleavage. J. Bacteriol. *192*, 5260–5263.

Wang, X., Huang, J., Mukherjee, A., Cao, C., and Lutkenhaus, J. (1997). Analysis of the interaction of FtsZ with itself, GTP, and FtsA. J. Bacteriol. *179*, 5551–5559.

Weart, R.B., Lee, A.H., Chien, A.C., Haeusser, D.P., Hill, N.S., and Levin, P.A. (2007). A metabolic sensor governing cell size in bacteria. Cell *130*, 335–347.

Wecke, J., Perego, M., and Fischer, W. (1996). D-alanine deprivation of *Bacillus subtilis* teichoic acids is without effect on cell growth and morphology but affects the autolytic activity. Microb. Drug Resist. Epidemiol. Dis. *2*, 123–129.

Wecke, J., Madela, K., and Fischer, W. (1997). The absence of D-alanine from lipoteichoic acid and wall teichoic acid alters surface charge, enhances autolysis and increases susceptibility to methicillin in *Bacillus subtilis*. Microbiology *143*, 2953–2960.

Wei, Y., Havasy, T., McPherson, D.C., and Popham, D.L. (2003). Rod shape determination by the *Bacillus subtilis* class B penicillin-binding proteins encoded by *pbpA* and *pbpH*. J Bacteriol *185*, 4717–4726.

Wei, W.S., Lencastre, H., and Tomasz, A. (2001). Recruitment of the *mecA* gene homologue of *Staphylococcus sciuri* into a resistance determinant and expression of the resistant phenotype in *Staphylococcus aureus*. Society *183*, 2417–2424.

Wormann, M.E., Corrigan, R.M., Simpson, P.J., Matthews, S.J., and Grundling, A. (2011). Enzymatic activities and functional interdependencies of *Bacillus subtilis* lipoteichoic acid synthesis enzymes. Mol Microbiol *79*, 566–583.

Wu, L.J., and Errington, J. (2004). Coordination of cell division and chromosome segregation by a nucleoid occlusion protein in *Bacillus subtilis*. Cell *117*, 915–925.

Wu, L.J., Ishikawa, S., Kawai, Y., Oshima, T., Ogasawara, N., and Errington, J. (2009). Noc protein binds to specific DNA sequences to coordinate cell division with chromosome segregation. EMBO J. *28*, 1940–1952.

Yamamoto, H., Kurosawa, S.I., and Sekiguchi, J. (2003). Localization of the vegetative cell wall hydrolases LytC, LytE, and LytF on the *Bacillus subtilis* cell surface and stability of these enzymes to cell wall-bound or extracellular proteases. J. Bacteriol. *185*, 6666–6677.

Yanouri, A., Daniel, R.A., Errington, J., and Buchanan, C.E. (1993). Cloning and sequencing of the cell division gene *pbpB*, which encodes penicillin-binding protein 2B in *Bacillus subtilis*. J. Bacteriol. *175*, 7604–7616.

Yasbin, R.E., Maino, V.C., and Young, F.E. (1976). Bacteriophage resistance in *Bacillus subtilis* 168, W23, and interstrain transformants. J Bacteriol *125*, 1120–1126.

Yim, L., Vandenbussche, G., Mingorance, J., Rueda, S., Casanova, M., Ruysschaert, J.M., and Vicente, M. (2000). Role of the carboxy terminus of *Escherichia coli* FtsA in self-interaction and cell division. J. Bacteriol. *182*, 6366–6373.

Yokoyama, K., Miyashita, T., Araki, Y., and Ito, E. (1986). Structure and functions of linkage unit intermediates in the biosynthesis of ribitol teichoic acids in *Staphylococcus aureus* H and *Bacillus subtilis* W23. Eur J Biochem *161*, 479–489.

Yunck, R., Cho, H., and Bernhardt, T.G. (2016). Identification of MltG as a potential terminase for peptidoglycan polymerization in bacteria. Mol. Microbiol. *99*, 700–718.

Zapun, A., Philippe, J., Abrahams, K.A., Signor, L., Roper, D.I., Breukink, E., and Vernet, T. (2013). *In vitro* reconstitution of peptidoglycan assembly from the Gram-positive pathogen *Streptococcus pneumoniae*. ACS Chem. Biol. *8*, 2688–2696.

Zhao, G., Meier, T.I., Kahl, S.D., Gee, K.R., and Blaszczak, L.C. (1999). Bocillin-FL, a sensitive and commercially available reagent for detection of penicillin-binding proteins. Antimicrob. Agents Chemother. *43*, 1124–1128.

Zuber, U., Drzewiecki, K., and Hecker, M. (2001). Putative sigma factor sigI (*ykoZ*) of *Bacillus subtilis* is induced by heat shock. J. Bacteriol. *183*, 1472–1475.

Appendix

Table S1 List of primers used in this study

Name	Restriction site	5'-3' sequence	Reference/comment
AG124	-	CCATCATCTGGTGCGAAAGG	*ponA* seq F
AG125	-	CCGCAAAGCCGATTAATTGG	*ponA* seq R
JS01	-	AAGCACACGCAGGTCATTTG	Check for integration into *aprE*
JS02	-	CCATCCGTCGATCATGGAAC	Check for integration into *aprE*
JS05	SalI	CGGTCGACGCTTGTTGTTGATTACATTGAGGTG	5' *ugtP* (construction of pJS01)
JS06	SphI	CTGCATGCCGTATGCTCTCAAGTACGCC	3' *ugtP* (construction of pJS01)
JS07	BamHI	GTGGATCCGTGACAGAGGCACCCGCTTC	5' *pgcA* (construction of pJS02)
JS8	SacI	GCGAGCTCAGCCGGATCATTTACAATGAC	3' *pgcA* (construction of pJS02)
JS09	SalI	GAGTCGACCGATCATAAGGAAGGTGC	5' *gtaB* (construction of pJS03)
JS10	EcoRI	GTGAATTCGCCGTTGATCAGGTCTTCGCAG	3' *gtaB* (construction of pJS03)
JS17	-	GTGGCGACAGATTACGTGAAGG	5' *ugtP* for sequencing
JS18	-	TTGCTTGGATGAGTGCCGATCTCCAG	3' *ugtP* for sequencing
JS19	-	CTCCACTGTTACATCGCCGAACC	5' *pgcA* for sequencing
JS20	-	TCGCGTTTACCTGCTCAATGAC	3' *pgcA* for sequencing
JS35	-	TCCGTTTCCCGCATCTCAGCCTC	*5' ponA* upstream (construction of JS06)
JS36	-	CCGTTCCCAAGACTGTTAAACC	*3' ponA* downstream (construction of JS06)
JS43		GAAAGCGCCCTTTCCGATATTAC	*5' gtaB* upstream (construction of JS07)
JS46		CCTCTTCCAAAGTAATATCGACACATGC	*3' gtaB* downstream (construction of JS07)
JS49	-	ACCACCAGTGATTATGCC	Check for integration in *amyE* (5')
JS50	-	CCGCTCGCCATGACTTCACTAAC	Check for integration in *amyE* (3')

JS51	XbaI	TCTAGAACGCTAGCACCCATTAGTTCAACAAACG	Amplification of *Cm* cassette from P_{CotC}-*cotC-gfp* (5')
JS53	BsgI	CGTGCAGAATTCGTACAGTCGGCATTATCTC	Amplification of *Cm* cassette from P_{CotC}-*cotC-gfp* (3')
JS56	-	GCTCTAGATTTCGGTAATCAGCTCATCAAG	*5' ponA* downstream (construction of JS06)
JS57	XbaI	GCTCTAGATCACGGCTGTTAAATTGATCTG	*3' ponA* upstream (construction of JS06)
JS59	NdeI	GCGCCATATGTTAAAAAAGTGTATTCTACTAGTATTTCTATGCGTCGGATTG	5' *pbpC* (construction of pJS05)
JS60	BamHI	GCGGATCCTAGTTCATTCGGCCTCAGATCCC	3' *pbpC* (construction of pJS05)
JS63	NdeI	CGCATATGTGGGATCGCATGGAAGCATTCGTGAAAC	5' *pbpC* (construction of pJS06)
JS67	XbaI	CGCTCTAGAAAGACGGTTCGTGTTCGTGCTGAC	Amplification of *erm* cassette from pMUTIN4 (5')
JS68	EcoRI	CGCGAATTCAGCTCCTTGGAAGCTGTCAGTAG	Amplification of *erm* cassette from pMUTIN4 (3')
JS69	XbaI	CGCTCTAGAAGCCTGCTGCTGGAATTATGGCTTTACG	*3' gtaB* upstream (construction of JS07)
JS70	EcoRI	CAGGAATTCGCTCTTCATTATCAACTGCGAAGAC	*5' gtaB* downstream (construction of JS07)
JS79	-	CAAGCAGCTGGCTGACGAC	*pbpC* internal for sequencing
JS80	-	AGGACGGCGAGGATCTTCAC	*pbpC* internal for sequencing
JS81	-	CCCGATCCAGAAATCGTC	*pbpC* internal for sequencing
JS82	-	CCCTACAGTGTTATGGCTTGAACAATC	5' $P_{hy\text{-}spank}$ for pDR111
JS83	-	CCCTACAGTGTTATGGCTTGAACAATC	3' *amyE* for pDR111
JS84	NheI	GCGCTAGCCGCATGATTCAAATGCCAAAAAAG	5' *pbpB* (construction of pJS07)
JS85	BamHI	GGATCCGCGGTAGAACGATGCTCCTCTGAAG	3' *pbpB* (construction of pJS07)
JS88	-	GTCTGTGCTTGAGGATAAGG	*lytE* upstream
JS89	-	GATCCGTTTGCGTGTTTC	*lytE* downstream
JS90	-	CCCGCTCCCGACATTCCAGTTATAATGAC	*cwlO* upstream

JS91	-	GTTAATGGCTTCCCATGGCCTTTACC	*cwlO* downstream
JS93		GGTGATTGTAATGAAGCTCAG	*3' ugtP* downstream
JS94	NheI	CGGCTAGCTGTATTCAAATAACCGGAAAAGCGAACGGCGAAG	5' *pbpB* (construction of pJS08)
JS95	-	AAGCGACAAATCCGGCTGGGAG	*pbpB* internal for sequencing
JS98	-	GTGGCAGCAGCCAACTCAG	5' $P_{T7\text{-promotor}}$ for pET-28a(+)
JS99	-	GCCACGATGCGTCCGGCGTAG	3' $P_{T7\text{-terminator}}$ for pET-28a(+)
JS100	EagI	GAACGGCCGAGCTCCTTGGAAGCTGTCAGTAG	Amplification of *erm* cassette from pMUTIN4 (3')
JS101	-	CTGCGAGAGAACACCTTGAC	*5'* S827 upstream (construction of JS32)
JS102	XbaI	CGTCTAGAACGCCATTACGATAGCAC	*3'* S827 upstream (construction of JS32)
JS103	EagI	CACGGCCGATATTCAGCCATCAATAAAAGCGGTTAC	*5'* S827downstream (construction of JS32)
JS104	SphI	GAGCATGCCCGTCAAGTTGCGAAACGGCTTAT	3' *ugtP* (construction of pJS04)
JS128	-	ATGGCTAGCATGACTGGTGGAC	5' to amplify pET-28a(+) for ligase free cloning
JS129	-	ATGGCTGCCGCGCGGCACCAG	3' to amplify pET-28a(+) for ligase free cloning
JS130	-	CTGGTGCCGCGCGGCAGCCATATGCCAAAAAAGAATAAATTTATGAATAGAG	5' *pbpB** (construction of pJS09)
JS131	-	TGTCCACCAGTCATGCTAGCCATGCCTGCATAACGACGGCTTTC	3' *pbpB** (construction of pJS09)
JS132	-	CTGGTGCCGCGCGGCAGCCATATGTTAAAAAAGTGTATTCTACTA	5' *pbpC** (construction of pJS10)
JS133	-	TGTCCACCAGTCATGCTAGCCATGTTCATTCGGCCTCAGATCCC	3' *pbpC** (construction of pJS10)
JS134	-	CTGGTGCCGCGCGGCAGCCATATGTATATCAATCAGCAAAAAAAATCG	5' *yrrL* (construction of pJS11)

JS135	-	TGTCCACCAGTCATGCTAGCCATGCGGAAAGCGAACAAAAGGAGAG	3’ *yrrL* (construction of pJS11)

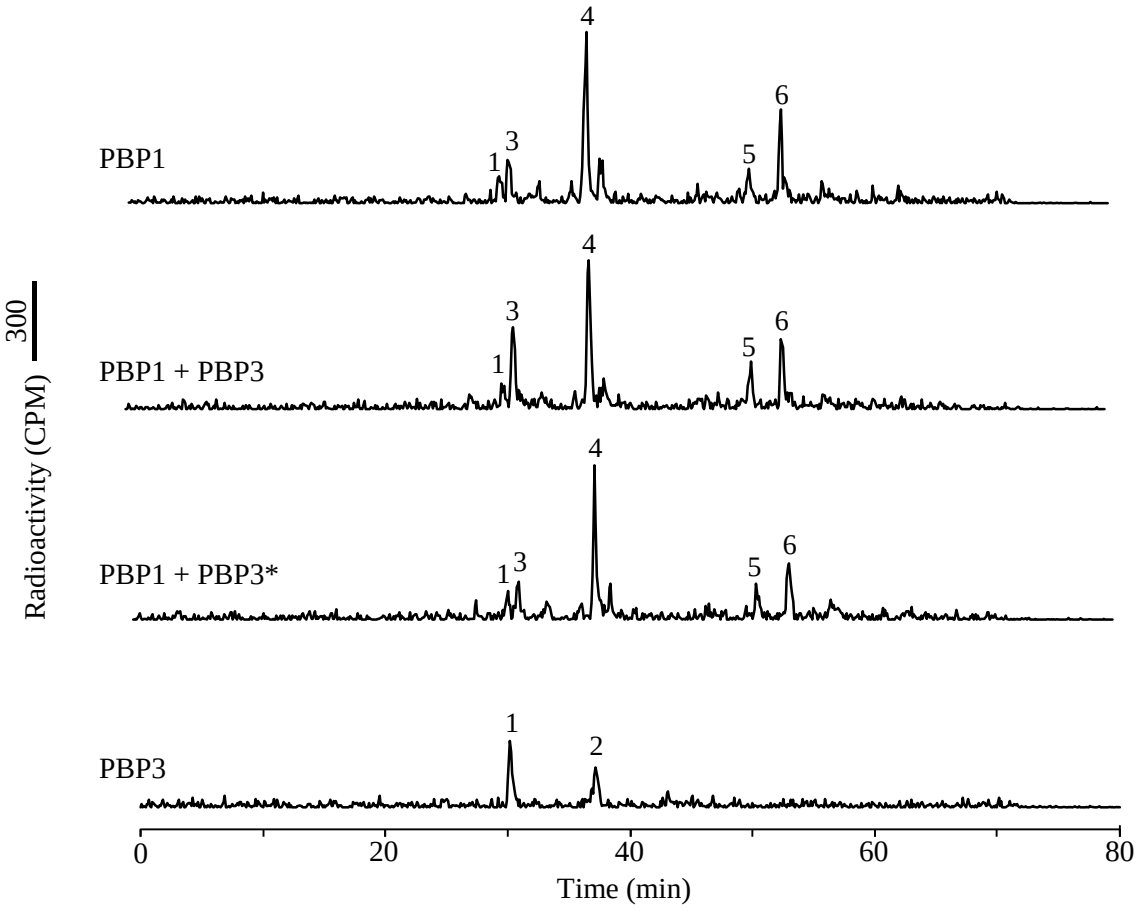

Figure S1 HPLC chromatograms corresponding to Figure 3.39 and 3.40

HPLC analysis of new peptidoglycan synthesised by PBP1 alone, PBP1 with PBP3, PBP1 with PBP3* or PBP3 alone. Muropeptide peaks are annotated as in Figure 2.5.

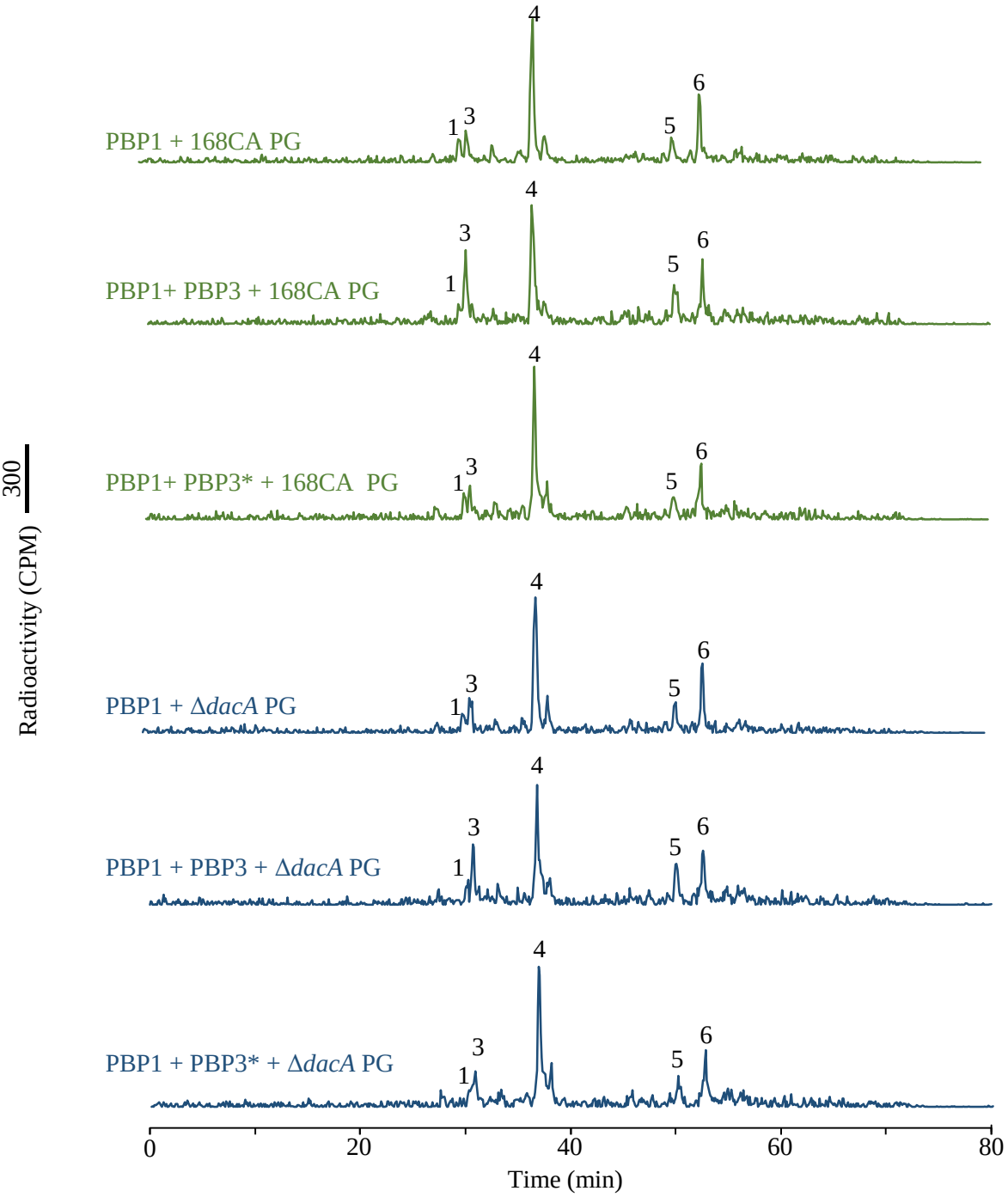

Figure S2 HPLC chromatograms corresponding to Figure 3.39 and 3.40

HPLC analysis of new peptidoglycan synthesised by PBP1 alone, PBP1 with PBP3 or PBP1 with PBP3*, in the presence of PG from 168CA cells or Δ*dacA* mutant. Muropeptide peaks are annotated as in Figure 2.5.

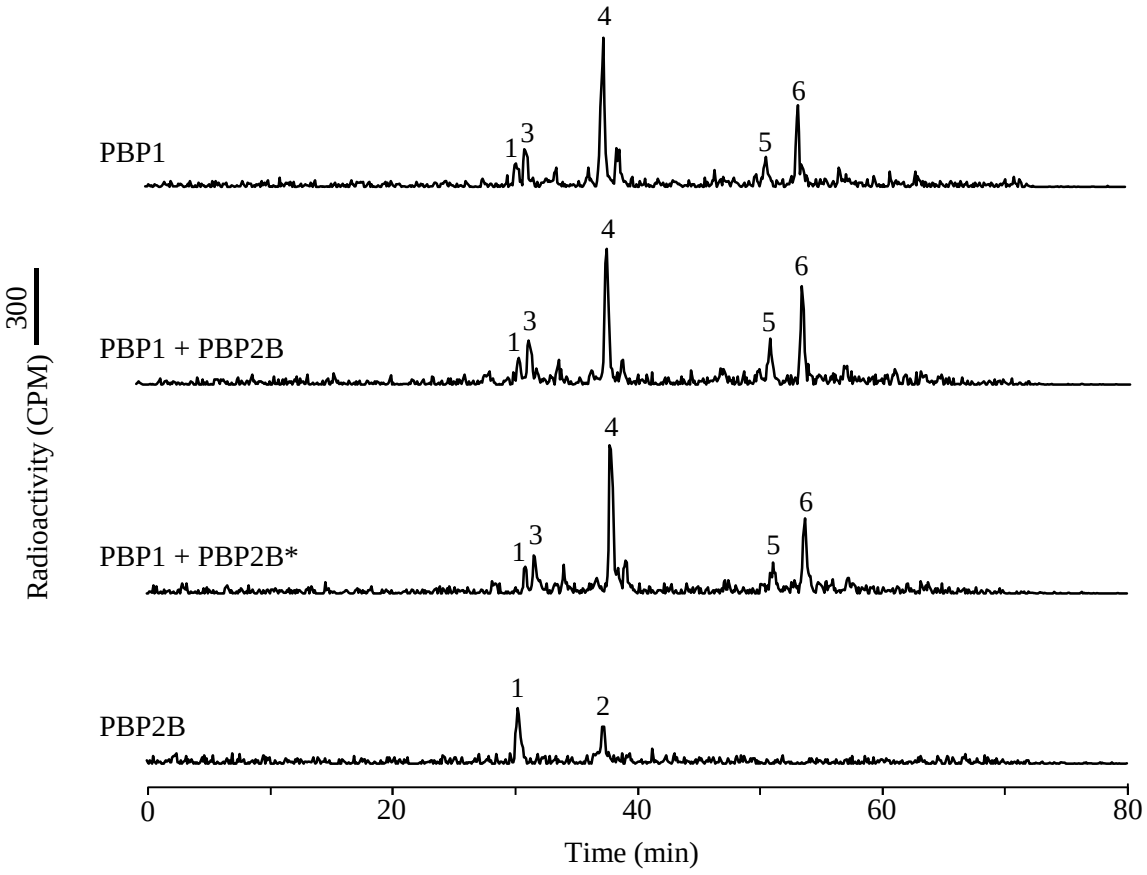

Figure S3 HPLC chromatograms corresponding to Figure 3.44 (A) and (B)

HPLC analysis of new peptidoglycan synthesised by PBP1 alone, PBP1 with PBP2B, PBP1 with PBP2B* or PBP2B alone. Muropeptide peaks are annotated as in Figure 2.5.

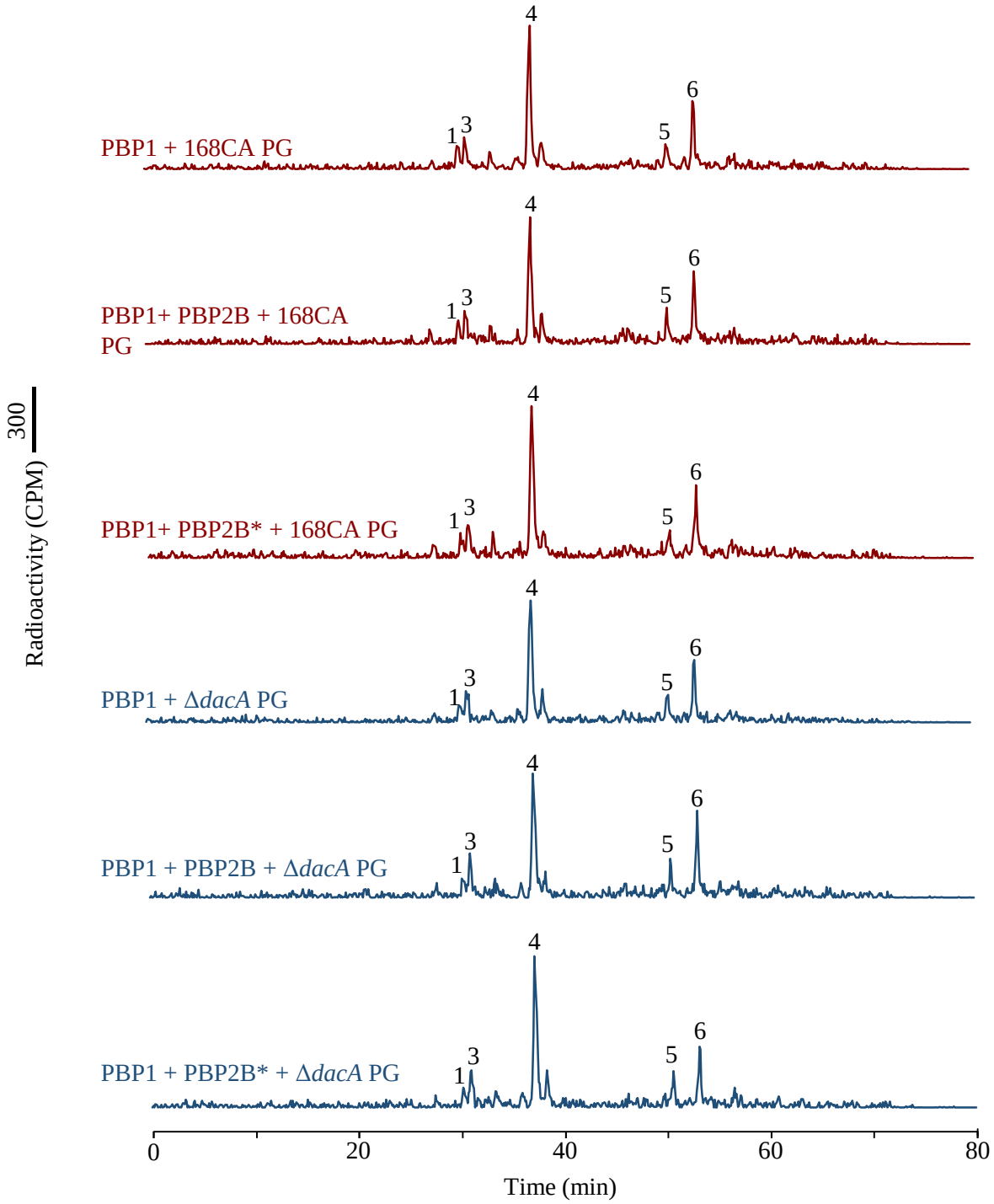

Figure S4 HPLC chromatograms corresponding to Figure 3.44 (A) and (B)

HPLC analysis of new peptidoglycan synthesised by PBP1 alone, PBP1 with PBP2B or PBP1 with PBP2B*, in the presence of PG from 168CA cells or Δ*dacA* mutant. Muropeptide peaks are annotated as in Figure 2.5.

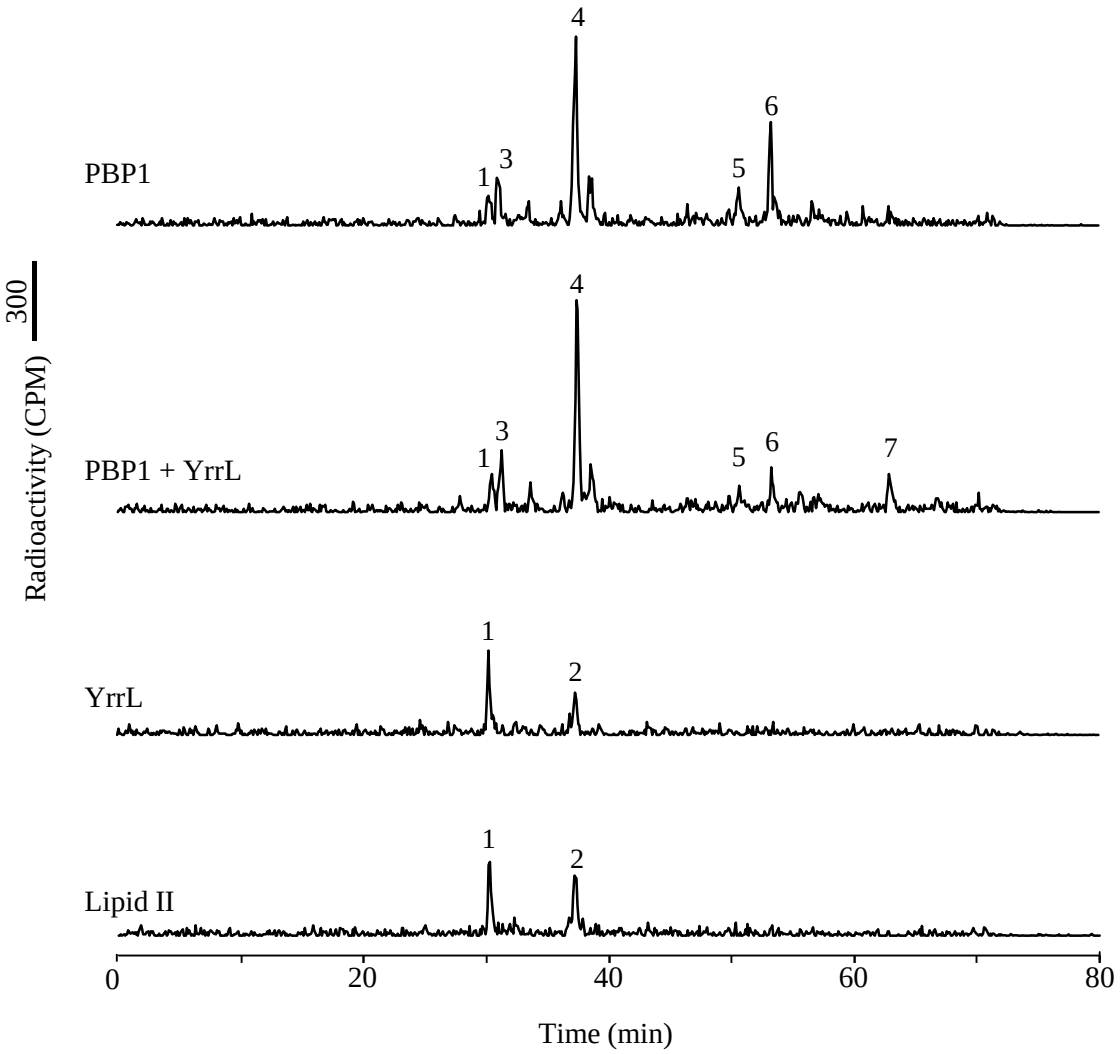

Figure S5 HPLC chromatograms corresponding to Figure 3.53

HPLC analysis of lipid II or of new peptidoglycan synthesised by PBP1 alone, PBP1 with YrrL or YrrL alone. Muropeptide peaks are annotated as in Figure 2.5. The muropeptide of Peak number 7 is unknown.

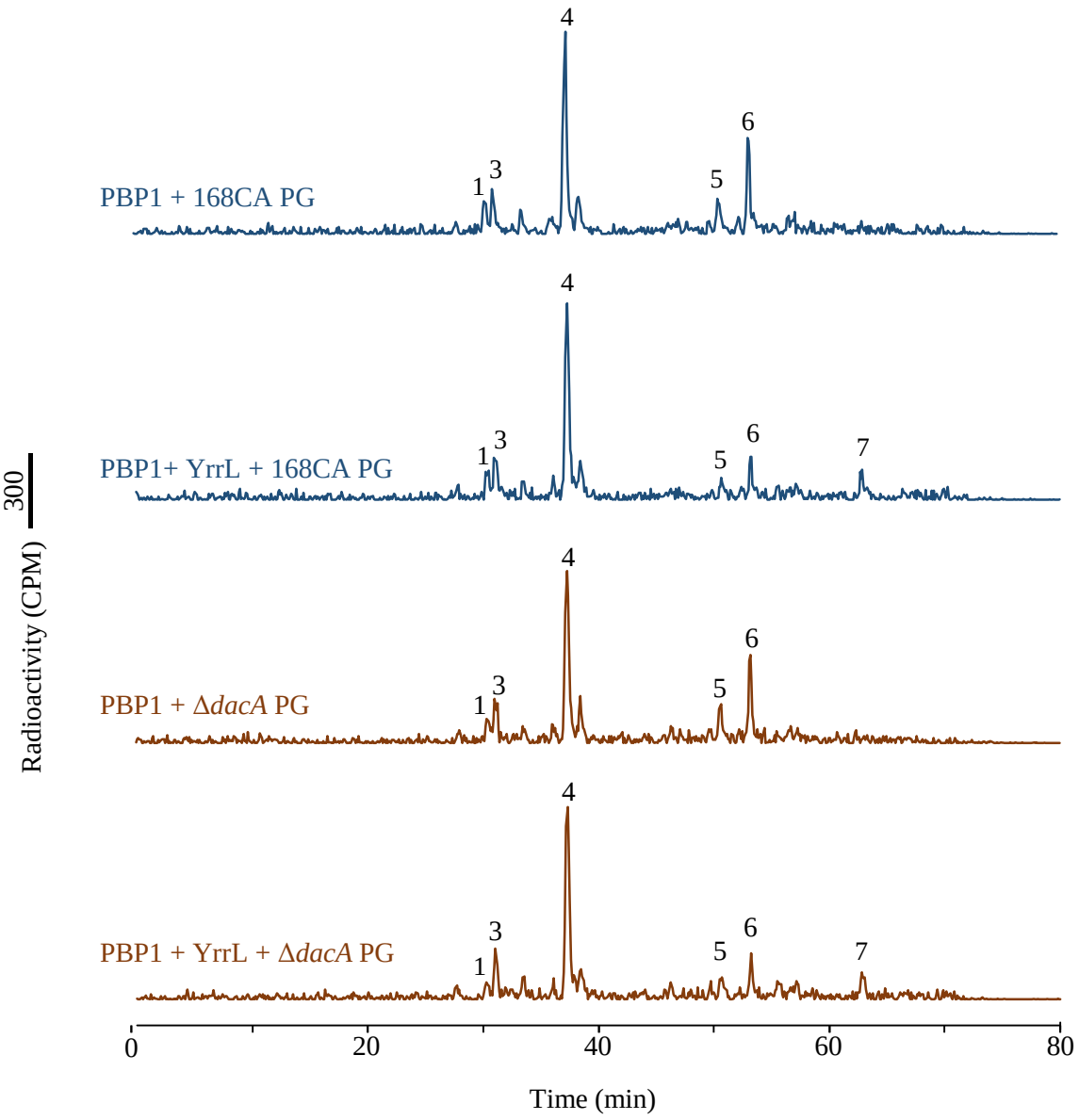

Figure S6 HPLC chromatograms corresponding to Figure 3.53

HPLC analysis of new peptidoglycan synthesised by PBP1 alone or PBP1 with YrrL, in the presence of PG from 168CA cells or Δ*dacA* mutant. Muropeptide peaks 1-6 are annotated as in Figure 2.5. The muropeptide of Peak number 7 is unknown.

Publications or submitted manuscripts

Jad Sassine, Meizhu Xu, Karzan R. Sidiq, Robyn Emmins, Jeff Errington and Richard A. Daniel (2017) Functional redundancy of division specific penicillin-binding proteins in *Bacillus subtilis. Mol Microbiol.* (Manuscript accepted)